The Parallel Seismic detection of defects in pile foundations

PH de Groot

Master thesis Geo Engineering TU Delft

TU Delft

Master Thesis

Evaluation of the Parallel Seismic detection of defects in pile foundations

Main Supervisor:
P Hölscher

TU Delft Supervisors:
A.F. van Tol
H.J. Everts

Deltares Supervisors:
P Hölscher
V Hopman

Author:
Paul H. de Groot
Masters Thesis Geo Engineering

September 2014

Summary

The Parallel Seismic test

This thesis explores the use of the Parallel Seismic (PS) method to detect flaws in in-situ constructed foundation piles as an alternative to existing testing methods. PS is a non destructive test. An acoustic signal is introduced to the head of the pile with a hammer. An elastic wave propagates through the pile, and vibrations are radiated out into the soil. Neighboring the pile, geophones are lowered or pushed into the ground such that the vibrations in the soil can be measured.

Theoretically, the vibrations originating from the pile shaft should provide a blueprint of the pile's condition. Flaws will affect wave arrivals, damping, and cause reflections. However, difficulties arise if the soil should be considered heterogeneous or when vibrations of the shaft are masked by other vibrations originating from the surface or the pile toe.

Methodology

A computer model was made using an analytical approach to determine what vibrations may develop. Pile vibrations are calculated using a 1D pile model. Shaft forces are then transferred to the surrounding soil, and the resulting vibrations are calculated in a 2D domain. Soil heterogeneity is accounted for in the form of horizontal soil layering.

This was followed by two field tests with the PS on an experimental pile field. Artificial flaws were installed in these piles by a third party, allowing for a blind test. From the results an understanding of vibrations in the pile and soil was developed and an attempt was made to detect any flaws. This was then compared to the original design of the artificial flaws to judge how well the flaws can be detected.

Finally, the field test results were used to validate the original model. This was used to improve the model and determine how the PS could be more successful in detecting flaws.

Results

From the results of the field tests it was not possible to detect flaws in the foundation piles using the PS. The procedure did not sufficiently measure the vibrations radiated from the pile shaft while avoiding interference from other vibration sources or soil heterogeneity.

The field test did however provide a better understanding of the vibrations that develop in the soil. This provided improvements on the model, allowing for more extensive simulations.

Based on these, possible improvements on the PS procedure could be suggested.

For the procedure used in the field test, a bar pressed two geophones into the ground. This bar acted as a medium for vertically vibrating waves, thus masking vertical vibrations from the pile. The detection of flaws improves if vertical vibrations originating directly from the shaft can be successfully measured.

Furthermore, the field test proved that heterogeneous soils do affect the propagation of acoustic waves. The effect was however less than the theory suggests. If the properties of the subsurface are well known, the effects of the heterogeneity can be distinguished from flaws.

To further develop the research, a few piles from the field test should be pulled out to verify that the designed flaws are indeed present. Then a few changes on the PS procedure can be tested on the remaining piles to test the improvements suggested in this thesis.

Acknowledgements

I would like to express my gratitude towards Deltares and Victor Hopman for providing me with the means to do this research. Also I appreciate the input I received from my committee members Prof Frits van Tol and Bert Everts.

I am very grateful for the guidance from Paul Holscher during all the stages of my research.

Finally I would like to thank Carel, Annemarieke, Hanneke, Suzanne, and Frederique for their support.

Contents

List of Figures

List of Tables

Abbreviations

Abbreviation	Definition
a.t	arrival time
CPT	Cone Penertration Test
FFT	Fast Fourier Transform
IR	Impact Response
NAP	Normaal Amsterdams Peil
NDT	Non Destructive Testing
NS	Non Symetric
PS	Parallel Seismic
SCPT	Sesimic Cone Penetration Test
SE	Sonic Echo
TUD	Technical University Delft

Symbols

Symbol	Description
A	cross-sectional area
c	dashpot constant or wave speed
c_p	pressure wave speed
c_s	shear wave speed
D_p	local pile diameter
E	Young's modulus
F	force
G_s	shear modulus
K	bulk modulus
k	spring constant
M	oedometer stiffness
n	element number
t	time
t_i	impulse durations
u	displacement in pile
v	speed of pile vibration
w	displacement of wave
x,y	horizontal co-oridantes
z	depth (vertical cooridnates)
Z	impedance
γ	self weight
ν	Poissons ratio
ρ	density
θ	wave angle

Chapter 1

Introduction

1.1 General introduction

Geo Impuls is an initiative of the geo technical engineering community in the Netherlands that aims to reduce ground related failures in construction projects. Experience has thought that building failures caused by unforeseen ground conditions or faulty construction will lead to very high constructions costs, conflicts between shareholders, and ultimately significant delays. Geo Impuls focuses on three main subjects of improvement: building contracts, environment control, and construction techniques for reducing failure risk. The research done in this thesis addresses the third subject.

One common failure is caused by flaws in foundation piles. To reduce the risk of this failure, Geo Impuls is improving on old techniques to detect these flaws after construction. To do this a small field of piles was made to provide different parties with a testing ground for their techniques. One such technique is the Parallel Seismic(PS) method, which measures vibrations in the soil that have been transmitted through the foundation pile. The main topic of this thesis is the use of the PS method to detect flaws in in-situ constructed[1] foundation piles.

In this first chapter the problem for the research is defined. This is followed by the research questions and the research methodology. Finally the structure of the thesis is presented.

1.2 Problem definition

Detecting[2] flaws in piles has been a source of difficulty for many years and as of yet no reliable techniques have been found. Some techniques need to remove or break the pile to detect the flaws which means the pile become useless. To avoid this, non destructive tests are used. These however are not completely successful. For example it is possible to miss a 50% reduction in

[1] In-situ constructed piles are piles that have been constructed in the ground, not pre-fabricated. The construction processes is explained in chapter 2.

[2] Detecting the flaw is to locate and define the shape and size of the flaw.

diameter at $4m$ depth because the flaw is not sudden enough to be noticeable. Therefore improvements are desired.

The concept of the PS method is explained thoroughly in this thesis. Basically vibrations are introduced to the pile with a hammer hit. The vibrations in the soil that are radiated from the pile are then measured and the state of the pile can be established.

The challenge that arises when using this method is to be able to understand the data when the test is done in heterogeneous soil conditions. This means that a good understanding of vibrations and wave propagation in piles and soil needs to be combined with thorough testing and data processing to detect any flaws.

1.3 Research questions

Following the definition of the problem, the main research question is:

Is it possible to use the Parallel Seismic method for detecting flaws in in-situ constructed foundation piles as an alternative to existing testing methods?

To help answer the main questions, the following subquestions are answered in this thesis.

- What is the state of research on the PS?
- What are the physics of sonic wave propagation in concrete piles and heterogeneous soils?
- What vibrations are measured if the PS is modeled on the computer?
- What vibrations are measured if the PS is performed in a field test?
- Is it possible to find the designed flaws from a field test?
- In which conditions is the PS useful and what are its weaknesses?

1.4 Methodology

To ensure a structured research process, the following steps are taken:

1. The main research question and subquestions are formulated.
2. A project proposal is written to organize the research.
3. A literature study is done to develop a thorough understanding of the science involved in the PS.
4. The problem is simulated and a scenario study is done to evaluate how the PS theoretically performs.

5. A field test is performed on multiple piles with pre-designed flaws. This test is done twice, allowing for improvements on the second test based on results from the first. The results are also used to validate the model.

6. Findings from the literature study, simulations, and field tests are reported and the main research question is answered.

The research is done at the research institute Deltares as a master thesis for Geo technical engineering at the TU Delft(TUD). From both institutes guidance is provided by evaluation of the project plan, periodic meetings to discuss progress, and assessment of the report.

The literature study is done using the library at the TUD and Deltares and papers available on-line. The simulations are done using a program written in Matlab. Finally the field test is done on a pile field constructed by Deltares at their own office site in Delft while the PS is done in cooperation with a team from Fugro.

1.4.1 Limitations of the research

The research is focused solely on the PS method for detecting flaws. Other testing techniques are merely mentioned but not evaluated in detail. In addition, the research is only done towards detection of flaws. Any effects of the flaws on pile performance or remediations are not considered.

Furthermore the tests and simulations are done for piles placed in soils that are common in the west of the Netherlands. The pile toe is not founded in hard bed rock.

1.5 Thesis structure

The research has three main stages: the literature study, the simulation of the PS, and the field tests. For each stage multiple chapters are written in this thesis.

Chapter 2 shows the current techniques used for flaw detection and the basics of wave propagations in piles and heterogeneous soils. In chapter 3 the PS is explained in detail. Also the state of the research done by other authors is shown. In chapter 4 the PS model is built and a scenario study is done. Chapter 5 and 6 show the results of the first and second field test. In chapter 7 the results are used to validate the model described in chapter 4. Finally chapter 8 concludes on the research by answering the research questions and discussing the findings. Chapter 8 also proposes possible improvements for the PS and further research topics.

In appendix A the structure of the model is shown in the form of flow charts. Also the results from varying simulations are plotted. Appendix B shows the results of ground investigations

done by Fugro at the pile field site. This is followed by the procedure of the field test in appendix C. In appendix D the results from the first field test are plotted. Per pile the results are evaluated and an attempt is made to detect the flaws. In appendix E the same procedure is repeated for the results of the second field test. Finally a list of literature used for the thesis is given in the bibliography.

Chapter 2

Basics of Defect Detection

2.1 Introduction

In this chapter the basics of defect detection in pile foundations is introduced. First the causes and effects of pile defects are shown. This is followed by the theory on wave propagation in piles and soil. Finally non destructive testing is explained.

2.2 Defects in piles: causes and effects

In the Netherlands, cast in-situ piles are often used when limited vibrations or noise is allowed in construction. One of these pile designs is the *HEKpaal* which is used as the focus of this thesis.

A *HEKpaal* is made using a round casing drilled intro the ground with a loose drill head that displaces the soil while moving downwards. Once the drill is at the desired depth the reinforcement is lowered into the casing and concrete is poured in. Simultaneously, the casing is pulled/vibrated out, leaving the drill behind [van t' Hek, 2014]. While the concrete cures the bore-hole keeps its shape by overcoming the pressure acting on it from the surrounding ground.

This process is however, not flawless and could lead to defects in piles which may have hazardous implications on the final construction [Klingmuller and Kirsch]. Defects can be either bulges, necks, cracks, voids, or areas of weakly formed concrete. A *bulge* is an increase in local diameter and a *neck* is a a decrease.

Defects occur when pressures within the bore-hole are not balanced with the horizontal ground pressure. This often occurs in unexpected ground conditions, where the distributions of pressure may differ from what is expected[Abrabbo and Gaaver, 2012].

Other sources of defects come mainly from the construction process [Klingmuller and Kirsch]. For example the curing process of the concrete could develop unevenly. As the casing is removed

the fluid concrete will penetrate the soil. The rate of spreading and curing of the concrete depends on the porosity of the neighboring soil layer. If this varies a lot, some points in the pile might expand more than others, resulting in bulge and neck forming. Therefore, when trying to avoid defects, it is important to choose experienced contractors with proven installation methods [Abrabbo and Gaaver, 2012].

Defects in piles are considered unwanted construction mistakes. They lead to unexpected performances. One possible effect of a neck is that re-enforcement comes in contact with surrounding soil and starts to rust. In cracks and voids the bearing capacity of the pile could reduce. Even when the diameter increases (bulging) and the bearing capacity of the pile is increased, the situation is considered undesirable [Wakil and Kassim, 2010]. Bulging often implies an uneven distribution of concrete which implies the presence of necks or voids.

2.3 Wave propagation in piles and soil

Sonic waves are very common in the subsurface. The cause can be natural, like earthquakes or wind on trees. Or they can be man made, like vibrations from trains, machinery, or purposely introduced with a hammer. In this section the basics of wave propagation in piles and soil is explained.

The properties of the waves depend on the type of source and the medium through which the wave propagates. For example, a hammer impulse will create very high frequency vibrations when compared to an earthquake. The medium of the wave dictates the amplitude of the vibrations and how fast and far the waves propagate.

First waves in a homogeneous medium are discussed. This is followed by wave propagation in non-homogeneous media and the phenomena that arise when waves pass through piles and layered soils.

2.3.1 Propagation through homogeneous material

When a pile is impacted with a single small temporary load, elastic strains travel through the material like a wave. These vibrations are both lateral and longitudinal, created by two main types of body waves. Longitudinal vibration, parallel to direction of wave propagation, is created by p(pressure)-waves. Lateral vibration is perpendicular to propagation direction and created by s(shear)-waves.

If a medium cannot carry shear loads, the s-wave is not transmitted [Das and Ramana, 2011]. Therefore s-waves do not pass through water.

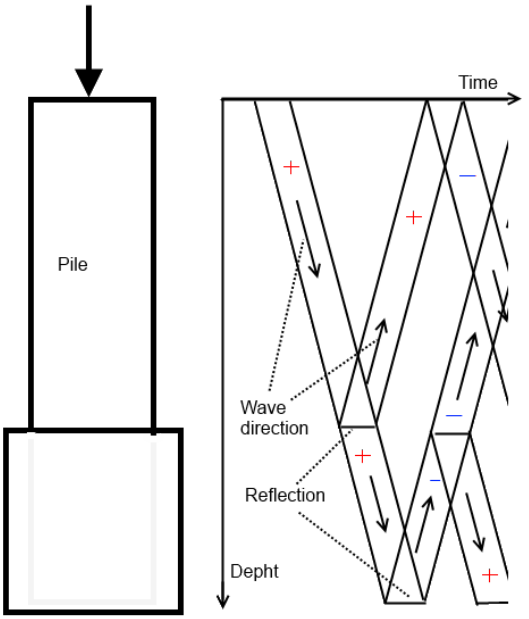

FIGURE 2.1: Propagation of a wave through a pile loaded with a single compressional impulse. The arrows show the direction of the wave moving in time. The plus signs signifie a compressional wave and a minus sign a tensional wave. In this example the pile rests on softer soil than the concrete of the pile, representing a *free* end.

Another distinction can be made between compressional waves and tensional waves. Compression waves causes local shortening of the vibrating medium while tensional waves cause lengthening.

Propagation in a 1D pile

In practice piles are mostly loaded in compression, so compression waves are created. At the end of the pile the wave is partially reflected. If the end is free, a tensional wave is reflected. If the end is not free, like when the pile is embedded in hard rock, the reflected wave will be compressional. The top of the pile is often free so the second reflection is mostly the opposite of the first reflected wave. Figure 2.1 shows the propagation of waves in a pile loaded by only one impulse.

The wave propagation equation

When modeling the propagation, the 1D wave equation is often used, equation 2.1 [Holscher, 2013]. The local displacement of the medium (w) depends on the wave speed (c), time (t), and a spatial variable (z).

$$\frac{\delta^2 w}{\delta z^2} = c^2 \frac{\delta^2 w}{\delta t^2} \tag{2.1}$$

2.3.2 Determining wave velocity

The speed of the wave is based on material properties and varies for each type of wave. Equations 2.2 and 2.3 show the theoretical values for p-wave speed (c_p) and s-wave speed (c_s) respectively where $\nu[-]$is the Poisson's ratio, $E[Pa]$ is the Young's modulus, and $\rho[kgm^{-3}]$ is the density [Liao et al., 2005]. P-waves are faster than s-waves [Holscher, 2013].

$$c_p = \sqrt{\frac{(1-\nu)E}{(1+\nu)(1-2\nu)\rho}}\ [ms^{-1}] \tag{2.2}$$

$$c_s = \sqrt{\frac{E}{\rho}}\ [ms^{-1}] \tag{2.3}$$

The values in equations 2.2 and 2.3 are not always available, which means that other correlations are needed. In the Netherlands, most in-situ investigations are done using the Cone Penetration Test (CPT). Empirical correlation between shear wave speeds and CPT results have been found from numerous field tests in combination with seismic testing [Robertson, 2009],[Tonni and Simonini, 2013]. These are often very site specific and contain large error margins.

It is also possible to determine wave speeds using seismic CPT's (SCPT) in which vibrations from hammer blows are measured in sensors placed in the cone. This test will produce a series of vibrations at varying depths. The arrival time (a.t) of the wave is compared to the arrival 50 *cm* higher or lower to determine the time needed for the wave to propagate through those 50 *cm*. This will lead to the local wave speed. This method is used in this thesis, the procedure for the test is elaborated in appendix C.

2.3.3 Propagation through non-homogeneous material

Propagation through layers of varying material properties is more complicated. When a wave travels into another medium, multiple phenomena might occur.

Reflection in a pile: When a wave travels from one medium into another, it partially reflects. This is due to a change in impedance (Z), defined in equation 2.4 for piles [Holscher, 2013]. Here A is the area of the cross section. Z changes if the material or the shape or size of the cross section changes. Therefore defected or weakened concrete causes reflections.

$$Z = \frac{EA}{c_s} \tag{2.4}$$

If a homogeneous pile is constructed in layered soil, reflections will still occur. Changes in soil stiffness affect the impedance of the pile locally, such that reflections are caused at the depths of changing soil. In addition, at the boundary of the pile, waves are also reflected.

The nature of the reflection depends on whether impedance increases or decreases and by how

much.

Reflection in soil: When waves pass through multiple layers of soil, reflections also occur. Again this is caused by a change in impedance. Equation 2.5 gives the impedance of soil [Holscher, 2013], where M is the oedometer stiffness modulus of the soil. This impedance is based on soil that is expected to be confined perpendicularly to propagation direction.

$$Z = \frac{M}{c_s} \tag{2.5}$$

Transmission: Besides reflection, when a wave travels from one medium to another, some of the vibrations are also transmitted. Due to the change in material, the wave will change speed. Transmission occurs when waves reach the boundary of the pile and energy is transmitted into the surrounding soil. Since the speed changes, if it arrives at an angle towards the normal of the boundary (known as the incidence angle), the direction of the wave changes as well. This occurs according to Snell's law illustrated in figure 2.2 and equation 2.6. The law applies to both p-waves and s-waves.

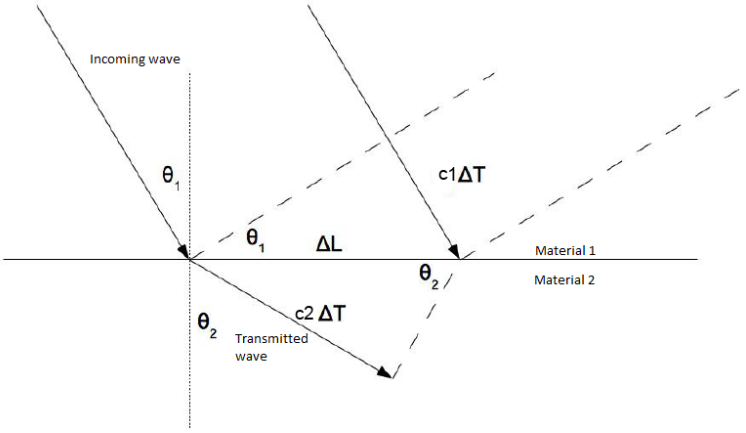

FIGURE 2.2: Incoming wave transmitted due to change in medium. Figure taken and edited from [Holscher, 2013].

$$\frac{\Delta T}{\Delta L} = \frac{sin(\theta_1)}{c_1} = \frac{sin(\theta_2)}{c_2} \tag{2.6}$$

Both angles θ_1 and θ_2 give the orientation between the direction of wave propagation and the material boundary. ΔT is the time it takes for either wave to travel an arbitrary distance $\Delta L sin(\theta_1)$.

θ_1 and θ_2 are limited between 0 and $\pi/2$. This means that when $c_2 > c_1$ and θ_1 is above a certain critical value, θ_2 is limited to $\pi/2$. In this case the wave will propagate along the surface of the boundary, creating surface waves.

Surface waves: When a wave propagates along a boundary surface, surface waves arise [Das

and Ramana, 2011]. The surface could be the top of the pile or a boundary between two different soil types. These waves contain both longitudinal and transversal deformation and by definition the amplitude decreases further away from the surface.

Reflection at an angle: When a wave comes across a boundary at an angle ($\theta_1 \neq 0$), it will be reflected at an angle. The reflected wave has the same incidence angle as the incoming wave since they have the same wave speed.

There is however an extra phenomenon which occurs in this situation. When the equilibrium of stresses is studied, it becomes clear that a second wave needs to be generated at the boundary.

Figure 2.3 shows the direction of stresses of an example. If the incoming wave at a horizontal boundary is a p-wave, a p-wave is reflected. But to maintain horizontal equilibrium, an s-wave is generated. In addition, since s-waves travel at another velocity, it is reflected at another angle which can be found according to Snell's law in equation 2.6.

If the incoming wave is an s-wave, a p-wave and s-wave are reflected. In this case however s-waves are slower than p-waves, which might lead to the formation of surface waves when the incoming wave has an incidence angle higher than the critical angle mentioned above. With the same reasoning, during transmission, a second wave type is formed as well [Holscher, 2013].

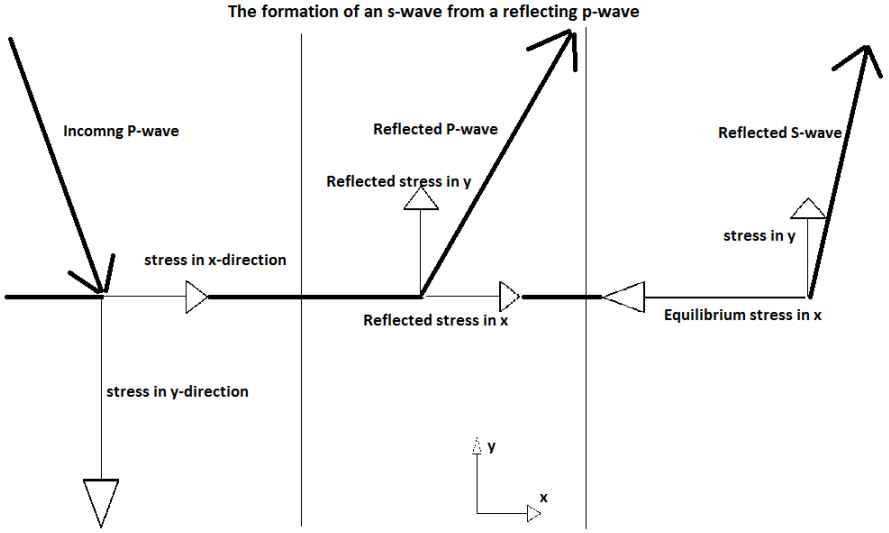

FIGURE 2.3: Incoming wave reflected due to change in medium. The reflected p-wave and s-wave show how stress equilibrium is in equilibrium when an incoming p-wave is reflected at an angle.

2.4 Damping

As acoustic waves pass through the soil and pile the amplitude of vibrations damps. This is the dissipation of energy due to spatial radiation and material nonlinear behavior [Holscher, 2013].

Spatial damping happens due to *spreading* of the wave. For example if a point source excites its surroundings in a 2D environment, a wave will propagate outward in all directions. Since energy is conserved the amplitude of vibrations at any single point from the source is inversely proportional to the distance from the source squared [Holscher, 2013].

The second type of damping is caused by the medium which is a result of nonlinear behavior of the material [Ostadan et al., 2004]. The damping can be modeled as viscous damping which is similar to movement through a liquid where drag is proportional to the square of the velocity [Ostadan et al., 2004]. Damping in soil is a bit more complicated and modeling it as hysteric damping which is based on dissipated energy and maximum strain energy of the material is more realistic[Ostadan et al., 2004].

In any case the properties concerning damping depend on material properties and frequency of vibrations [Ostadan et al., 2004],[Hashash and Park, 2002]. Therefore the amplitude of vibrations depend on the distance from the source, the material of the medium, and the impulse of the source. Equation 2.7 shows how vibration velocity (w) decays away from the source of the vibration[Kim and Lee, 2000]. r_1 and r_2 are the distance from the source. n is a coefficient for spatial damping and depends on the shape of the vibration source and α is the coefficient for material damping.

$$w_1 = w_1 \frac{r_1}{r_2}^n * e^{-\alpha(r_2 - r_1)} \tag{2.7}$$

α depends on the frequency of vibrations and the propagation speed, calculated according to equation 2.8. Here η is a loss factor [Kim and Lee, 2000].

$$\alpha = \frac{\pi \eta f}{c} \tag{2.8}$$

2.5 Non destructive testing

Using the properties of wave propagation, structures may be examined without needing to take them apart. This is known as non destructive testing (NDT) and is used in many fields of engineering. For pile foundations, two types of NDTs can be done to ascertain the state of the pile: reflection and direct transmission [Liao et al., 2005].

Two popular reflection methods are the Impulse Response (IR) and the Sonic Echo (SE). With a simple hammer hit on the pile head, a small strain elastic compression wave is send into the pile. All reflections are picked up at a receiver that is also placed at the pile head. The timing,

amplitude, and nature of the reflection can tell testers the length of the pile and locations of possible defects, material changes, and particular soil layers.

SE measures the velocity waveform in the time domain [Huang and Ni, 2012] and is useful for detecting weaknesses in the concrete [Davis, 2003]. IR measures the ratio between the velocity spectrum and force spectrum in the frequency domain (FD) to give a mobility ratio [Huang and Ni, 2012]. This is useful to find voids, delaminations, density variations, and other anomalies [Davis, 2003].

Reflection NDTs are easy to perform and cheap. They are however not able to give local diameter widths and are weak for very long or deep piles [Liao et al., 2005]. Also the results strongly depend on the interpretation of the engineer who looks at the signals since it is often unclear which signals correspond to which changes in the pile.

In case the pile is very long or the pile needs to be examined in more detail, direction transmission NDTs can be used. One example uses receivers installed in the pile during construction known as deep acoustic. Using the same hammer hit, the wave is directly measured in the pile and any anomalies in the pile are detected. Another option is the PS, in which receivers are installed in the surrounding soil.

Direct transmission NDTs are more expensive and often used for longer piles or in cases where defects are expected and further testing is desired [Liao et al., 2005]. In these tests direct waves, transmission, and reflection is used to examine the pile.

Chapter 3

The Parallel Seismic Method

3.1 Introduction

Currently the PS is mostly in the research stage. In practice the PS is only used in France and the United States of America [Niederleithinger, 2012b]. In these cases, and where most research has been done towards is determination of the length of an installed pile. Much less research has been done towards detection of defects using PS although a few studies have been done on the subject [Huang and Ni, 2012], [Liao et al., 2005], [Niederleithinger, 2012a].

In this section a brief description of the PS is given. First the test process is described. This is followed by an overview of current applications of the PS and the available interpretation methods.

3.2 Basics of the parallel seismic

The concept of the PS is based on elastic waves generated with a given impulse that travel through the concrete pile and surrounding soils and are picked up by receivers in the soil, parallel to the pile. It was originally designed to determine the length of in-situ piles [Olson], [Niederleithinger, 2012a]. Figure 3.1 shows a schematic of the PS.

The first step is to install the impact hammer and receivers and connect to an oscilloscope and computer that collects the data. The receivers are velocity transducers, also known as geophones. These can be installed in a bore hole filled with water or PVC piping. To ensure a good connection between the geophone and the ground, it may be placed in a tight rubber encasing that presses against the wall of the bore-hole [Kim and Lee, 2000]. Another option is to use geophones at the end of a cone that then penetrates the ground. Depending on the number of receivers, the test should be repeated with the receivers at different depths, such that the receivers exceed the depth of the part of the pile that needs to be measured.

The next step is to introduce an impulse with the impact hammer. This should also signal

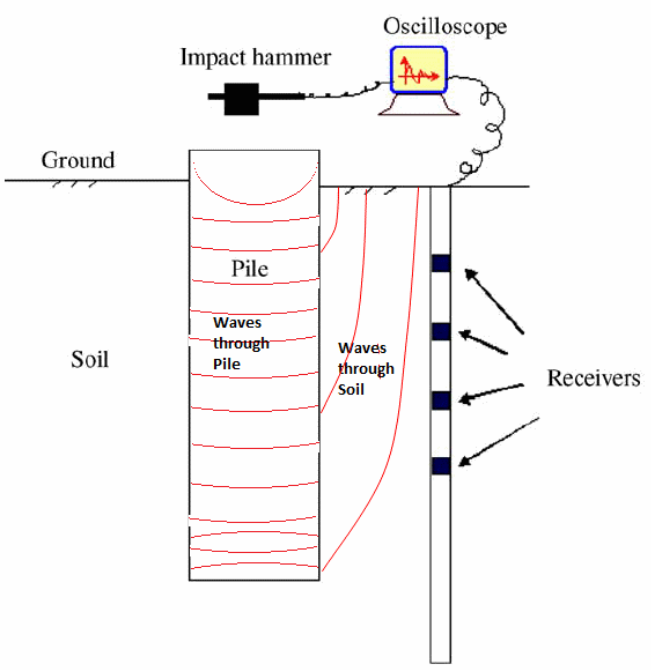

FIGURE 3.1: Systematization of the PS method. The impact hammer introduces acoustic waves in the pile which propagate through the pile and radiate out into the soil. The receivers pick up these radiated waves. Figure taken from [Liao et al., 2005] and edited.

the start of the measurements in the receivers which can be done by completing an electric circuit when the hammer connects with the pile.

When the pile is induced with an impulse the elastic deformation wave will travel downward. Most of the energy will remain in the pile but some will be refracted out into the soil [Niederleithinger, 2012a]. The received signal is affected by the impedance in the pile and the soil so the state of the pile might be deduced. In case of defects, the impedance also changes causing diffractions, reflections, and changes in wave types [Niederleithinger, 2012a]. These phenomena were discussed further in section 2.3 in which the basics of the supporting theory is discussed.

The third step is interpretation of results. This can be done to either determine the length of the pile or two detect flaws in the pile. Interpretation is discussed in the two following sections.

3.3 Determining the length of piles

When using PS to determine the length of installed piles, the change in wave velocity in concrete and soil is used. If a receiver is below the tip of the pile, the arrival of the p-wave is delayed which can be seen when making a seismograph. Figure 3.2 shows an example of a seismograph with a clear change in wave velocity represented by the lines formed by the first arrival of the waves. The length of the pile can then be estimated graphically from the intersection of the lines[Niederleithinger, 2012b], [Ni et al., 2010].

Due to the offset of the bore hole, a correction factor has been proposed and proven to improve results [Liao et al., 2005]. Furthermore, bore holes in which the receivers are placed are known to deviate when made near piles. This is caused by stiffening of the soil during installation of the pile. Another correction factor has been proposed in which this deviation is accounted for. This means that the deviation of the bore hole should be known, which is possible using inclinometers in the bore hole or cone.

Another impression left by the pile are the vibrations of the toe. This can also be seen in figure 3.2 as s-diffraction. The pile toe acts as a new source of vibrations and sends acoustic waves in all directions with relatively high amplitudes.

From numerical and experimental tests, PS has been proven relatively accurate when determining length [Liao et al., 2005]. It can be used on multiple types of foundations, like deep foundations or abutments [Olson]. It is mostly a good choice for foundations that are hard to access, like that of bridges or deep foundations [Olson] or very long piles.

The PS method is however expensive when compared to other NDT's and so not always the favored option. The cost of the PS mostly comes from making the bore-hole and/or installing the receivers in the ground.

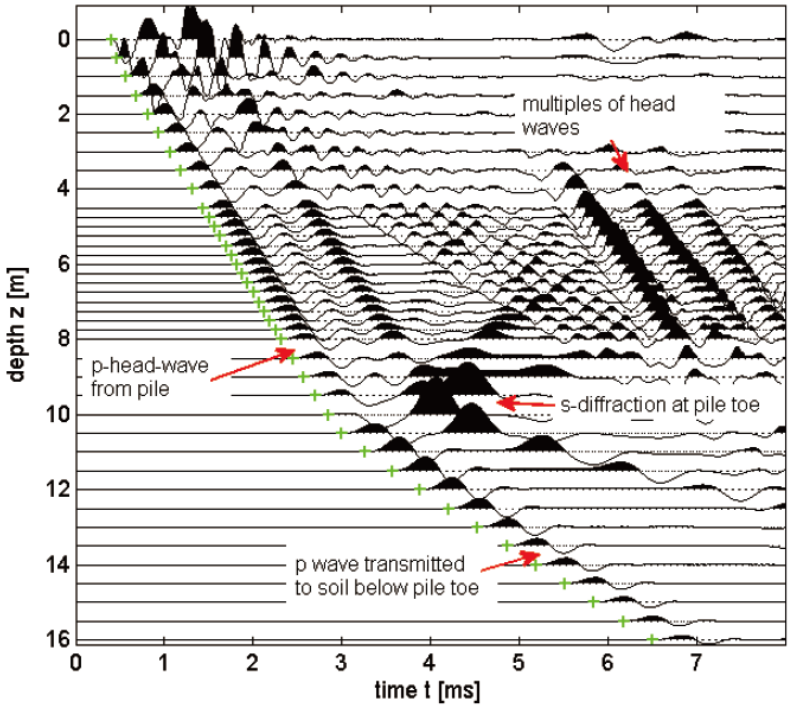

FIGURE 3.2: Example of a typical seismograph showing the length of a flawless pile graphically. On the x-axis is the time and on the z-axis is depth. Each line represents the vibrations of a receiver at the given depth. From the first arrivals at each receiver a slope can be seen which represents the wave speed in the pile. The change in slope shows the change in head wave velocity which indicates the tip of the pile since the wave does not travel through the pile at this depth. Figure taken from the PS modeled [Niederleithinger, 2012a].

3.4 Detection of defects in piles

When looking for defects, the process is more complicated. A seismograph can be used to show the arrival of waves at different depths in time. This will show how waves change speed when impedance changes or how they are reflected, refracted, etc. Figure 3.3 shows the basis of the PS for detection of flaws.

Indications of defects

The first indicator of a defect is the change in a.t of the first p-wave. For example if the pile reduces in diameter, the path through the soil increases. Since the speed of the wave in soil is less than through the pile, the a.t at the receiver near the defect is delayed. In the case that a bulge is present, the opposite can be expected and the a.t is shorter. If vibrations are transfered from the pile to the soil at the location of the defect, this is measurable.

Besides the arrival of the p-wave, the arrival of the s-wave may be of significance. A possible indication of a defect is the amplitude of both wave types. Depending on the type of flaw, either p-waves or s-waves become more prominent [Niederleithinger, 2012a]. In this case the depth of the flaw and receiver is also of importance.

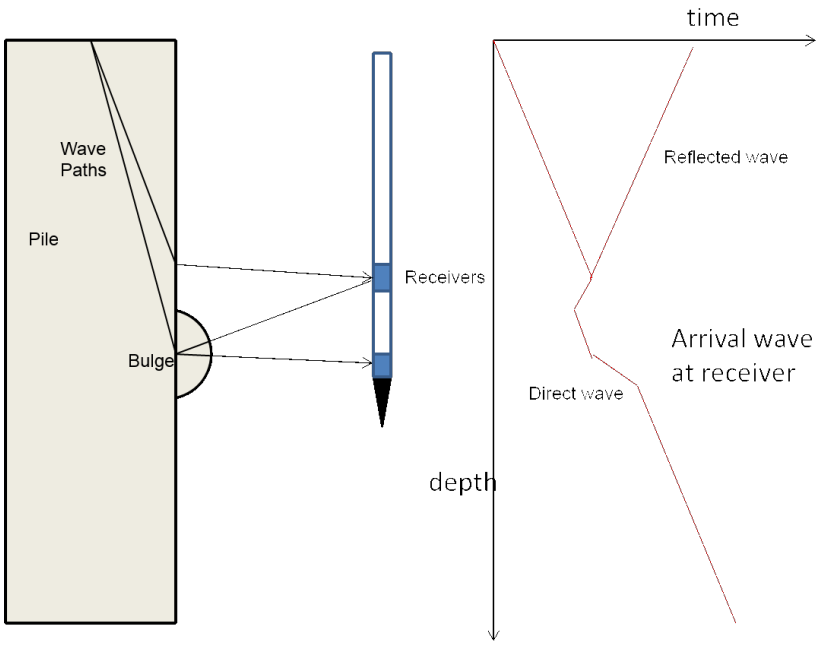

FIGURE 3.3: The figure shows the basis of using the PS to detect piles. On the right the seismographs shows the arrival of waves that are measured by the receivers if the pile on the left were to be tested. Depending on the flaw type, arrival time of the direct wave will change. In addition reflections might be measured.

Another indicator of a defect is the reflection of the wave at the defect, measured above the defect. Again with a clear seismograph, reflections can be seen following head waves [Niederleithinger, 2012a].

Research in the detection of flaws with PS

Research towards the use of PS for detection of defects is much less developed. A few authors have commented on this possibility. It seems that the PS is not too successful in detecting flaws [Huang and Ni, 2012], [Niederleithinger, 2012a].

A comparison study was done between PS and Sonic Echo and Impulse Response in detecting flaws [Huang and Ni, 2012]. The PS is weakest in detecting non-axisymmetric defects since it only measures the deflection of waves at one side (in case only one bore-hole is used). Also, PS is least successful when defects are small. Finally, the presence of inhomogeneities in the soil could give the same results as defects in the pile would, which makes detection less reliable.

However, the potential of the PS has been realized. The setup of the PS allows it to be used in particular situations where other NDTs are less practical, for example it could be useful in detecting earthquake damage [Liao et al., 2005] in existing structures. Furthermore, there is not need for preperations before construction of the pile. For this reasons, it remains interesting to research the PS method.

3.5 Presence of heterogeneity

As might be expected, the interpretation methods mentioned above could be made very difficult when testing in heterogeneous soils. In this case these are a few options to improve detection.

With knowledge of the subsurface, anomalies in the PS results can theoretically either be attributed to soil layering or possible defects. Soil layers have different damping characteristics, soft soils like peat and clay will exhibit large amplitudes in vibration when compared to stiff layers like sand. Furthermore there is the option of looking at the frequency of the vibrations and how this changes due to soil layering. Finally, if a CPT is used to determine the local soil characteristics these could help understand the results of the PS test results.

Chapter 4

Simulation of the Parallel Seismic Test

4.1 Simulating the PS

To assist the study of the PS, a mode is built to determine theoretically how vibrations propagate through the pile and soil, allowing for prediction of what can be expected when doing the PS for real. Furthermore it is useful to compare the model to results from the PS test and conclude on the state of the piles.

In this chapter the model of the PS is explained. First the building of a program is shown, including the program structure, preliminary assumptions, and verification tests. This is followed by a scenario study and finally a simulation of the field test and a discussion on the results.

4.2 Building the simulation

Due to the elastodynamic[1] nature of the problem, an analytical approach and wave theory, as explained in section 2.3, is used. Numerical methods like explicit dynamic solvers are good options but are expected to be too expensive in time and money. Another option could be to use finite integration techniques [Niederleithinger, 2012a] but this is also costly. The program used here is written in Matlab, and applies *ScatMat* written by Tom van der Poel [van der Poel] and *Deep Acoustic Check of piles (D.A.C)* written by Paul Holscher. [Holscher, 2012].

The concept of the program is illustrated in figure 4.1. The pile is discretized into a number of elements n. At each element a source of vibrations from the pile is introduced to the surrounding soil and a receiver is placed at a horizontal distance from the pile. The magnitude of the source depends on the simulated impulse on the pile head, the state of the pile, and the ground conditions. Then, the resulting vibrations at the receiver are calculated.

[1] The stresses and strains of material stay in the elastic domain.

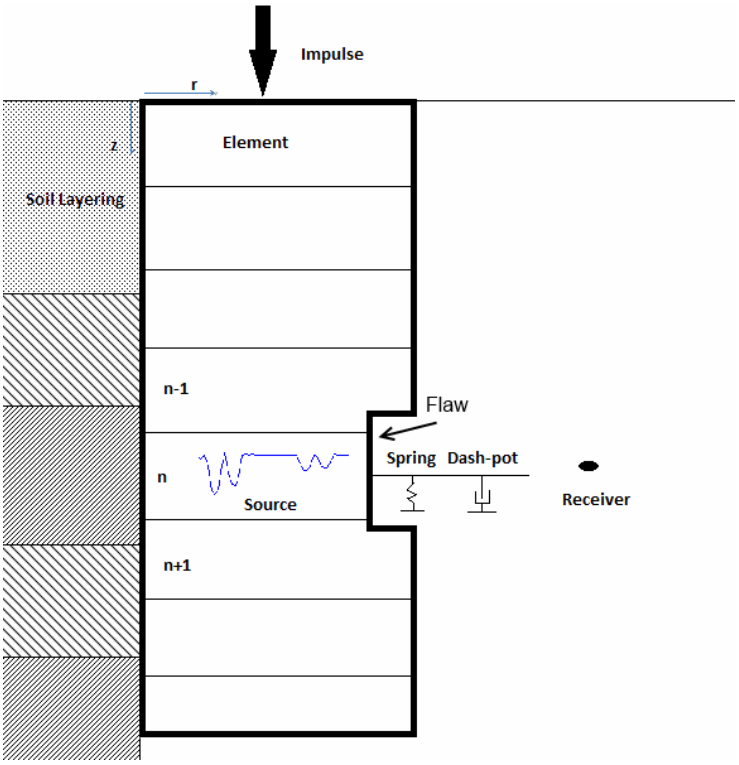

FIGURE 4.1: Concept of the simulated PS with neck flaw at calculation step n. The figure shows half the pile, and assumes the pile is axis-symmetric over the z-axis. Each element, n, in the pile represents a source of vibrations into the soil. Note that the location of the source in each element is on the boundary between the pile and the soil.

The source vibrations are vertical vibrations that will induce mainly vertically oriented s-waves. A vibrating shaft mostly creates this from of vibration [Kim and Lee, 2000].

Figure 4.2 shows the main structure of the program. In appendix A a flow chart shows the structure of functions that define the properties of the source. The inputs for the program are the dimensions of the pile and any flaws and soil conditions.

The first step is to calculate the location of the source in each element, which depends on the local pile diameter. This is followed by calculations of the source signal and vibrations in the soil for each element. Finally, the results are plotted in the time, space, and frequency domain.

4.2.1 Simulating the vibrations in the pile

The vibrations in the pile are simulated as discrete dynamic loading on the surrounding soil. The magnitude of the load is calculated using an edited script written by Paul Holscher that is originally used to simulate a deep acoustic check of piles. D.A.C calculates the force and displacement of pile elements in the frequency domain. An element stiffness matrix is used to model the properties of the pile along the element [Holscher, 2012].

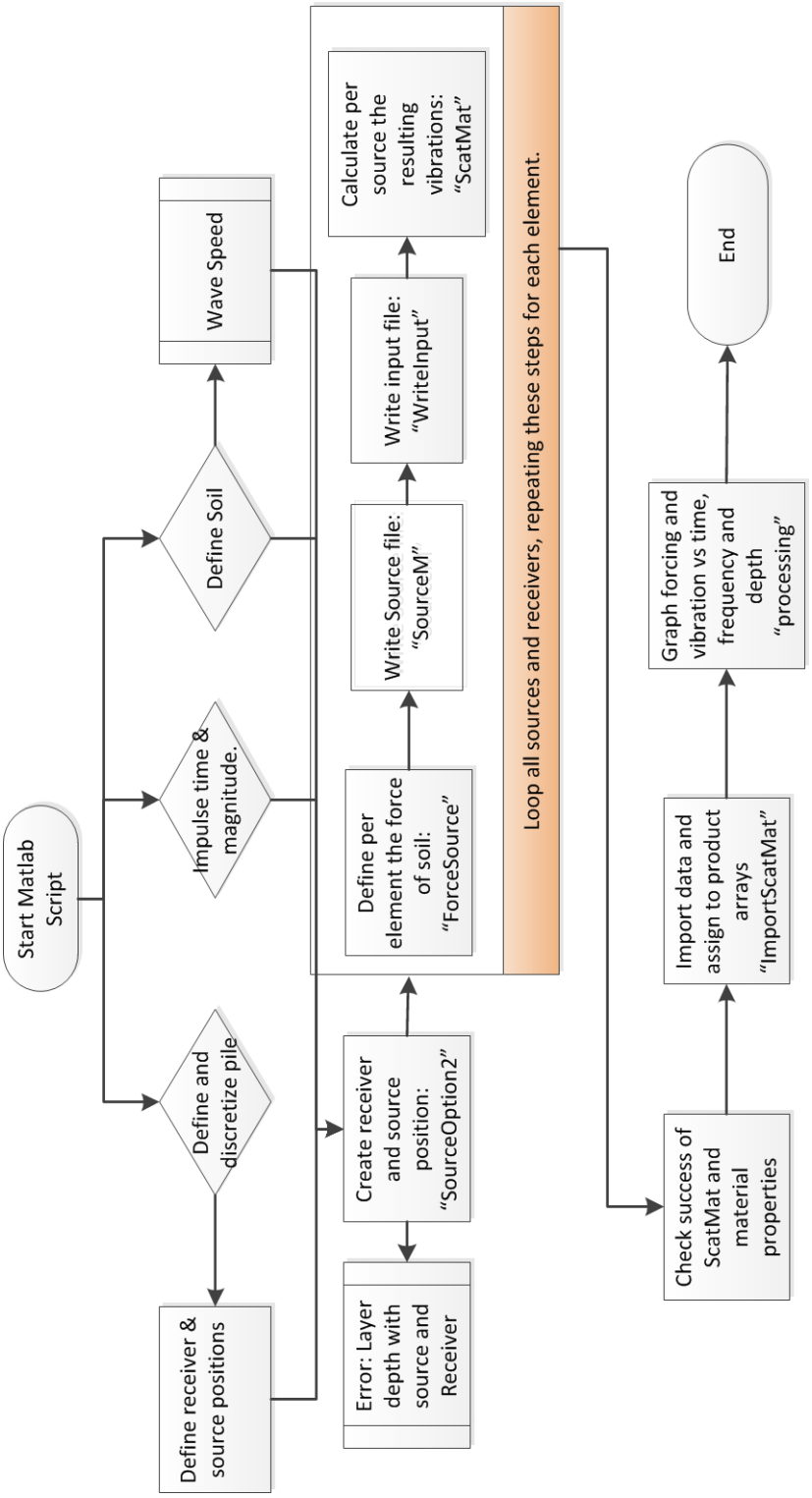

FIGURE 4.2: Structure of the main program.

The speed (v) and displacement (u) of the pile can be calculated in time for each element. The force ($F(t)$) that is translated into the soil is then found using equation 4.1. This method uses a spring & dash-pot system as shown in figure 4.1 to represent the soil. k and c are the spring and damping constants and depend on the soil properties and local pile dimensions as shown in equations 4.2 and 4.3.

$$F = k * u + c * v \tag{4.1}$$

$$k = 2 * G_s \tag{4.2}$$

$$c = 3.5 D_p \sqrt{G_s \rho_s} \tag{4.3}$$

- G_s is the shear modulus of the soil $[Pa]$.
- D_p is the local diameter of the pile $[m]$.
- ρ_s is the mass density of the soil $[kg/m^3]$.

4.2.2 Simulating the vibrations in the soil

Using the force calculated in equation 4.1 [Holscher, 2013], the resulting vibrations are found using ScatMat. Similarly to D.A.C ScatMat numerically implements the scattering matrix method that describes the relation between incoming waves and waves propagating away from soil boundaries, the source, and the receiver [van der Poel]. Calculations are done in the frequency domain. Results are then transformed back to the space-time domain.

ScatMat takes into account reflections at boundary layers, damping, refraction, and formations of surface waves. Figure 4.3 shows the wave paths that are accounted for. For this model, the source is treated as a point source with solely vertical loading.

4.2.3 Preliminary assumptions

To be able to simulate the PS test, a few important simplifications have to be made.

- First, the pile and soil are elastic mediums so analytical calculations may be applied. This assumption implies that all deformations are elastic. This is applicable as long as strains are small. In this problem, dynamic loading has a very small range and short durations so deformations can be assumed elastic.

- A second assumption is that the pile properties are constant and exactly as defined by the user. No random properties are applied to the pile. Realistically, the pile surface will not be smooth and the flaw will not be exactly cornered as implied in figure 4.1. Also the density of the concrete is assumed constant.

- Third, below the pile and problem environment, the waves are adsorbed. This means that reflected waves from possible layers below are ignored.

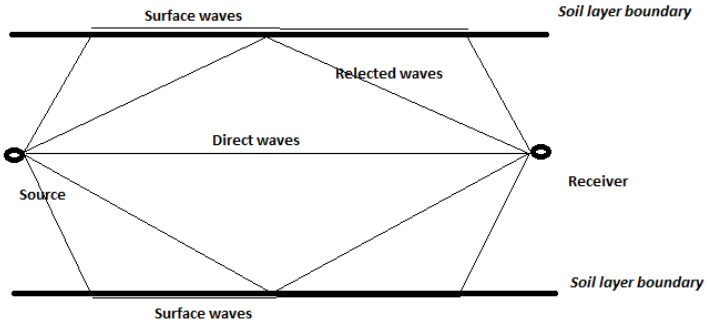

FIGURE 4.3: This figure shows the possible wave paths that ScatMat accounts for. Direct waves travel the shortest route from the source to the receiver. Reflected waves travel via reflections of neighboring soil boundaries. Surface waves travel along the boundaries and radiate back into the soil.

- Another assumption is that the pile is fully embedded in the ground and the layering in the ground is horizontal.

- Finally, an important assumption is that the most prominent vibrations originate directly from the pile at the same height as the receiver. Soft soils tend to damp more than concrete, so waves that travel longer in soil will be less detectable. This greatly speeds up the calculation process since it avoids the need to determine vibrations at all receiver depths from each source element.

4.2.4 Input parameters

When using the program, the following input choices can be made:

- Pile length, radius, and distance from vibration sensors.

- First and second flaw depth, height, and width. A choice can be made between neck and bulge by changing the sign of the flaw's width.

- Ground conditions: Shear modulus, density, damping[2], depth, and bulk modulus. Table 4.2 shows the parameters of the soil used in this model.

- Impulse duration (t_i) and magnitude. $t_i = 0.001[s]$ and magnitude $= 400N$ in this thesis.

- Pile conditions: Concrete density and Young's modulus. Table 4.1 shows the parameters of the pile used in this thesis for any following simulations.

- Element size: The pile is discretized into small elements. When calculating the vibrations on the soil from the pile, the program fits all boundaries of flaws and soil layers to these

[2]Since ScatMat uses purely elastic consitutive methods, material damping is introduced using a damping constant.

elements. Therefore, element size should be sufficiently small to avoid errors. In this thesis element size is $0.25m$.

	$\mathbf{E}[Mpa]$	$\boldsymbol{\gamma}[\boldsymbol{kg/m^3}]$
Concrete	3.47E+04	2400

TABLE 4.1: Material properties used as input for the pile.

Soile Type	$\mathbf{G}[\boldsymbol{Mpa}]$	$\boldsymbol{\gamma}[\boldsymbol{kg/m^3}]$	$\mathbf{K}[\boldsymbol{Mpa}]$	**Damping**
Peat	0.34	0.45	3.3	2.1
Clay	7	0.45	67	1.9
Silt	12	0.45	116	1.7
Sand	30	0.45	300	1.5
Stiff sand	450	0.45	435	1.4

TABLE 4.2: Soil properties used as input for soil in this thesis.

4.2.5 Output

With the input parameters and calculations mentioned above, the program gives the following output in the time and frequency domain:

- Vertical and radial (horizontal) vibration velocity at the receiver positions in time and frequency domain.
- Force vibrations at the source positions (the edge of the pile).

4.3 Verification

To determine if the model is reliable, it can be verified. First the assumptions used to make calculations possible are verified. Finally the results are verified by comparing to results from other simulations.

4.3.1 Validity of assumptions

Ignoring vibration sources at multiple depths: The reliability of the program depends on the assumptions that were made to simplify the problem. The first assumptions verified is, that for each receiver only the source at the same depth is needed.

Table 4.3 shows the input parameters for a simple test. This test is run twice, once where the receivers sum all vibrations from all sources and once where each receiver only records vibrations from the source at the receiver's depth.

Pile Conditions		**Unit**
Pile Length	10	m
Average Diameter	0.6	m
Flaw	none	
Soil Conditions	**Depth**	
Clay	0 to 5.25	m
Stiff Sand	5.25 to 15	m
Impulse Conditions		
Duration	0.001	s

TABLE 4.3: Test conditions to verify that vibrations from other sources can be assumed insignificant.

Figures 4.4 and 4.6 show the response of the soil at $1m$ increments. Figure 4.4 shows the response when only the source at the same depth is accounted for while figure 4.6 shows the response when vibrations from all sources are summed up.

There are a few differences in the results. Figure 4.6 shows that in the upper clay layer there are vibrations that arrive very early. This is incorrect, and can be explained by calculation mistakes that arise when calculating the propagation of waves through multiple soil layers. Also the results around the boundary at $5m$ show incorrect vibrations. Figure 4.4 seems more realistic although the vibrations are very simplified.

Figures 4.5 and 4.7 show that the magnitude of the vibrations are the same for both methods except when close to the soil boundary. Besides the increased model speed, this simplification avoids calculation problems around soil layers which arise in ScatMat.

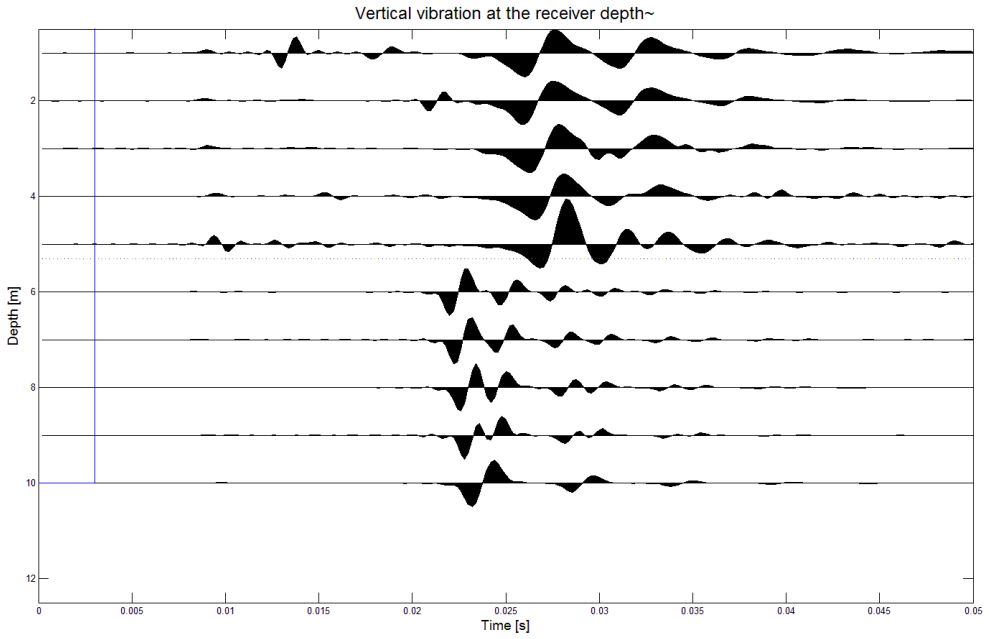

FIGURE 4.4: Vibration and a.t at five depths for an intact pile in two layers soil. The response is calculated in the soil at each receiver depth with the source of vibrations only being the element of the pile at the same depth as the receiver. This ignores pile vibrations above and below the receiver.

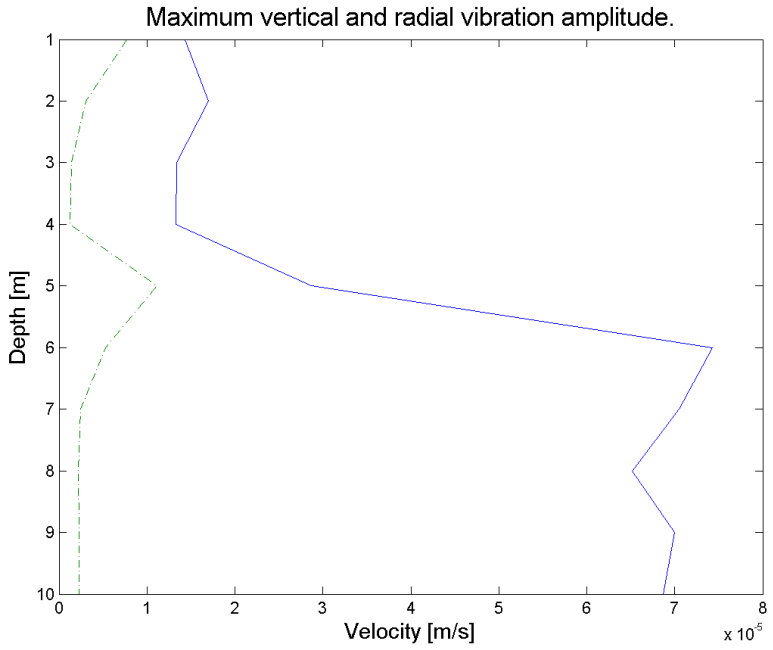

FIGURE 4.5: Magnitude of vibrations. The response is solely based on vibrations of the pile at the same depth.

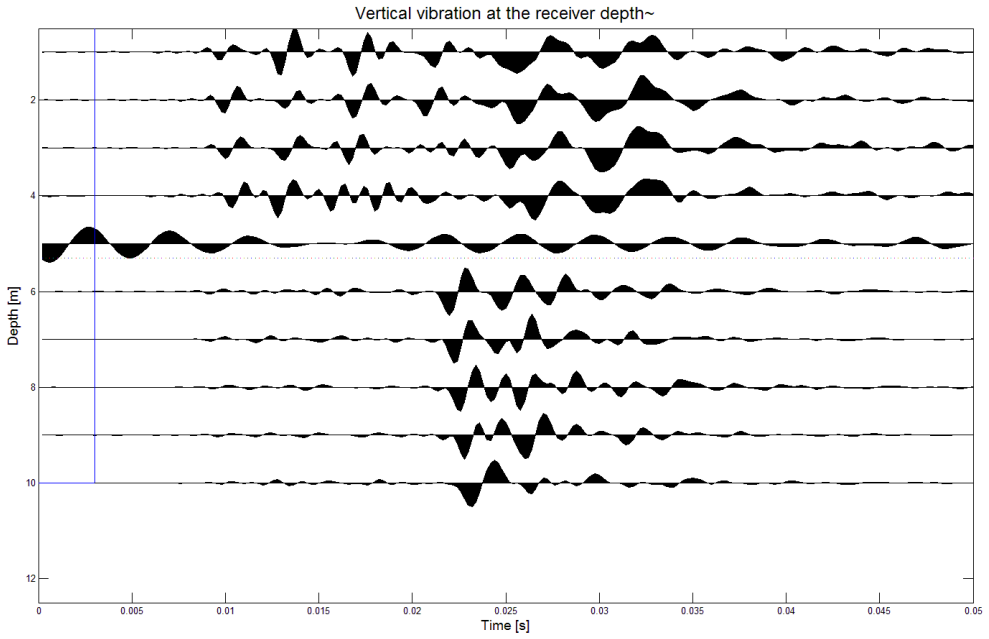

FIGURE 4.6: Vibration and at five depths for an intact pile in two layers soil. The response is based on vibrations of the pile at all depths.

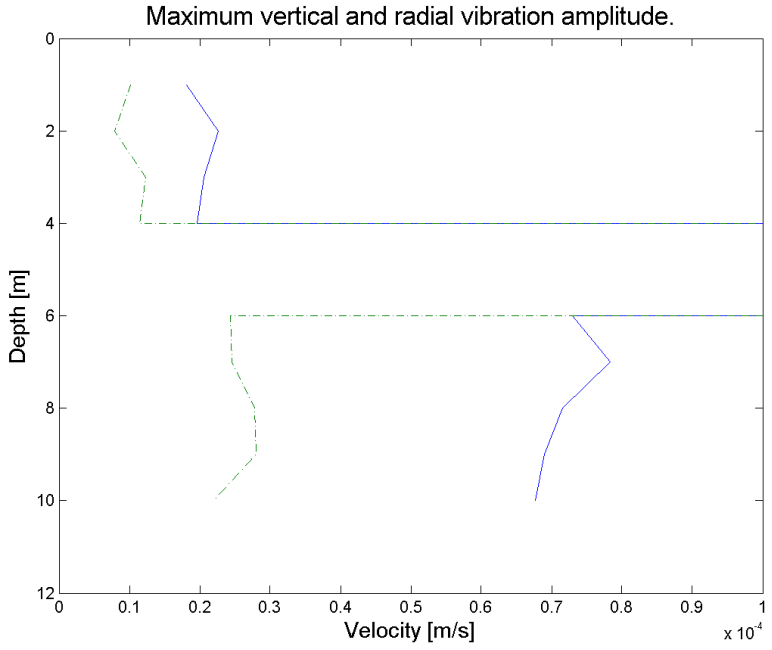

FIGURE 4.7: Magnitude of vibrations. The response is based on vibrations of the pile at all depths.

Verification of damping characteristics: An important process is the development of amplitude of vibrations in the pile. As mentioned above, the model calculates the vibration force that the pile exerts on the soil at each element. Due to damping, in a homogeneous soil, the force is expected to decrease.

The force depends on the diameter of the pile and the soil properties as show in equation 4.1. Figure 4.8 shows the maximum force as a function of depth for a pile in clay. The pile has a neck at 6 m. Figure 4.9 shows the force in a pile in layered soil.

As may be expected, due to spatial dispersion [Holscher, 2013], the magnitude of the vibrations reduce linearly with depth if the pile is flawless and the soil is homogeneous.

If a neck (or bulge) is introduced, the forcing is first increased and then decreased (or vice-versa). The dash-pot constant (c) depends on the local diameter. u and v from equation 4.1 have the inverse relation to the diameter. This explains why a neck would first increase local force and later decrease it. Furthermore the flaw reduces the magnitude below the flaw as well.

Figure 4.9 shows that the force increases if the soil is stiffer. The change in magnitude is in the same order as when there is a flaw.

Finally both figures show that the force at the pile toe increases which is to be expected [Kim and Lee, 2000]. At the boundary the amplitude of vibrations radiated to the ground is expected to be very high. Since the model only accounts for vibrations radiated from the pile at the height of the receiver, this will be missed in the results. In truth the vibrations at the pile toe might be measured by receivers far above the pile toe.

4.3.2 Comparison to other simulations

The second verification is a comparison to results found in literature. A numerical simulation was done with the pile shown in figure 4.10 and the results are shown in figure 4.11 [Niederleithinger, 2012a]. Table 4.4 shows the input used for this verification and the result using the analytical model is shown in figure 4.12.

The arrival of the waves in the simulation done by [Niederleithinger, 2012a] are much quicker. This is probably due to a small difference in concrete properties which changes the wave speed and has a large affect on the a.t. The flaw causes a similarly small delay in a.t. The biggest difference is the presence of reflections. The model from [Niederleithinger, 2012a] predicts larger reflections than can be seen in figure 4.12. Finally the shape of the wave in figure 4.12 are idealized as Ricker wavelets [van der Poel] while [Niederleithinger, 2012a] shows that the waves are less smooth, which is probably closer to reality.

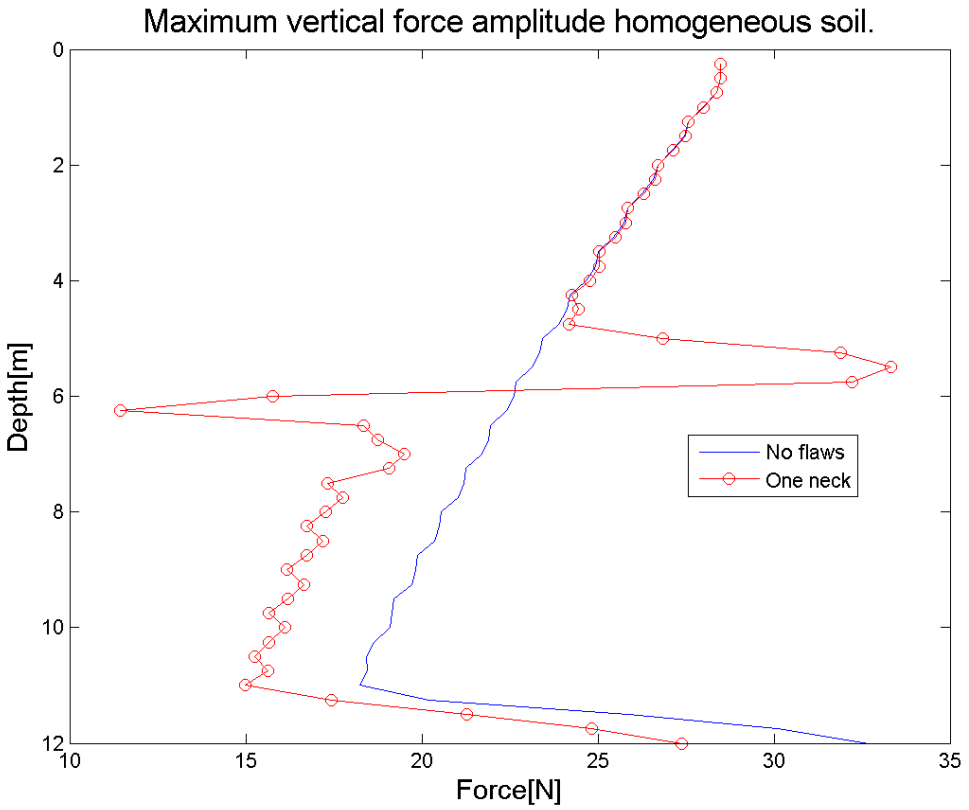

FIGURE 4.8: Maximum vibration force in an intact and necking pile placed in a homogeneous clay layer.

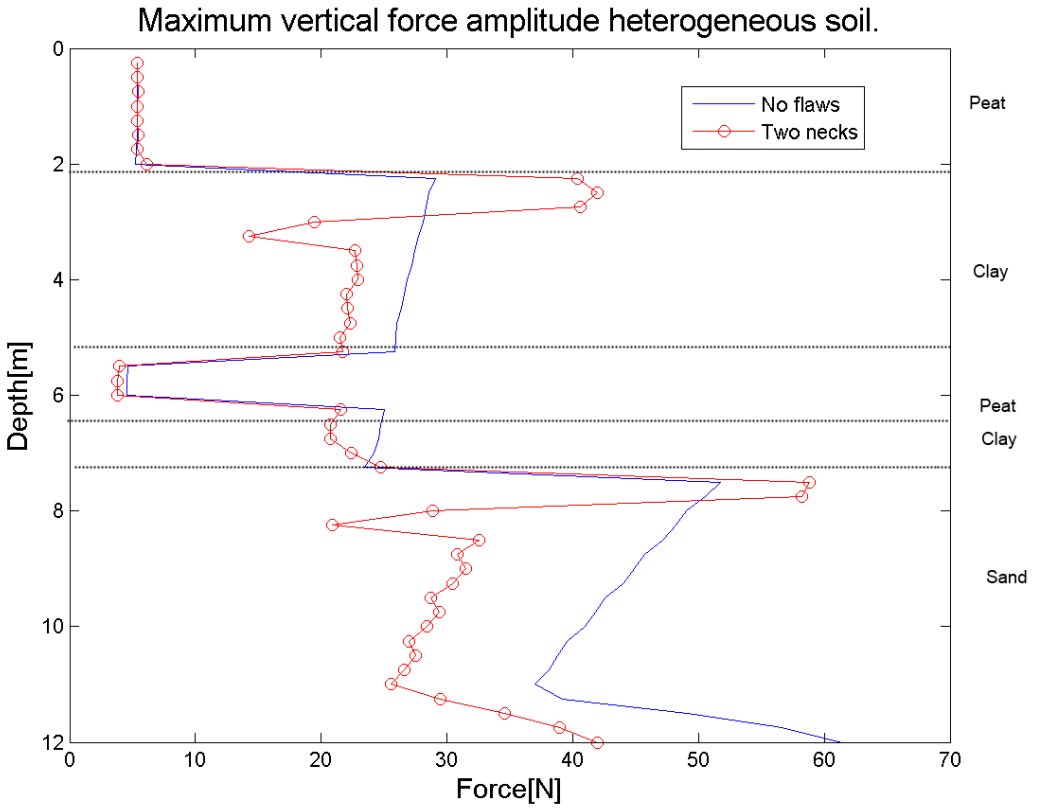

FIGURE 4.9: Maximum vibration force in an intact and necking pile placed in layered soil.

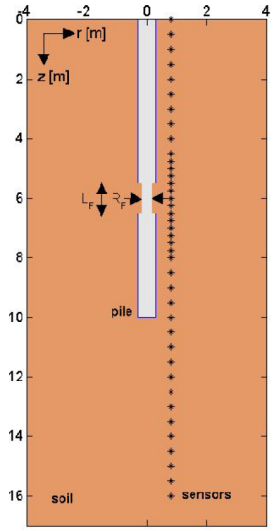

FIGURE 4.10: Test conditions used by Ernst Niederleithinger to simulate the PS with a defect.

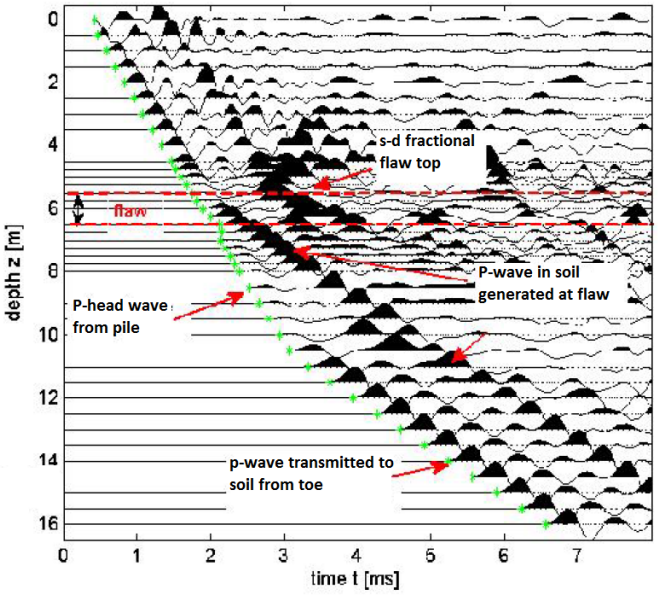

FIGURE 4.11: Results from the simulation done by Ernst Niederleithinger [Niederleithinger, 2012a]. In addition to the arrival of the head waves, this graph shows vibrations arriving in a less ordered fashion which can be interpreted as reflections caused by the flaw and pile toe.

Pile Conditions		**Unit**
Pile Length	10	m
Average Diameter	0.6	m
Sensor Distance	0.5	m
Flaw		
Type	Neck	
Width	0.15	m
Height	0.5	m
Soil Conditions	**Depth**	
Sand	0 to 20	m
Young's Modulus[3]	155	Mpa
Density	1800	kg/m^3
Impulse Conditions		
Duration	0.001	s

TABLE 4.4: Test conditions used in simulations done before [Niederleithinger, 2012a].

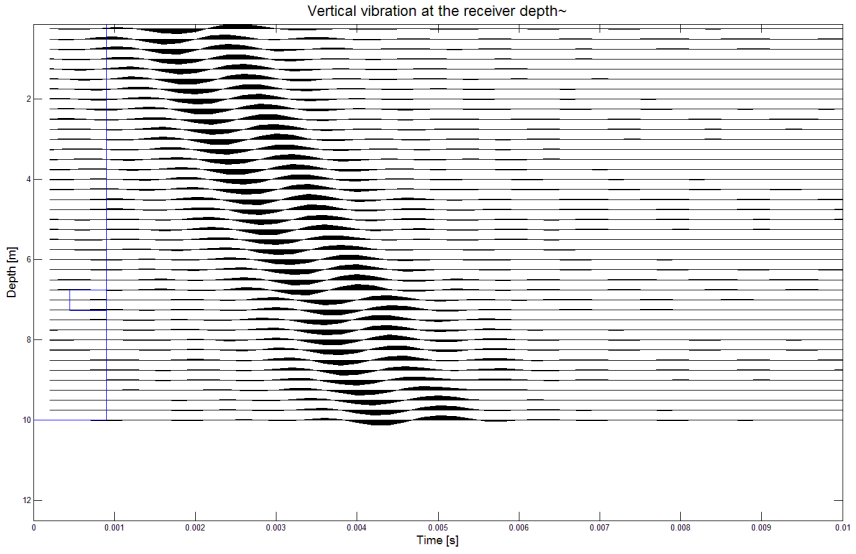

FIGURE 4.12: The seismograph result from the model running the parameters given in table 4.4.

4.4 Scenario study

To find out in which situation the PS could be useful or how the PS should be done for a particular scenario, a scenario study is done. First a homogeneous soil condition is taken and the vibrations for both a flawless pile and a pile with defects are calculated. This is followed by a similar study with layered soil.

4.4.1 Homogeneous soil

The first scenarios are a pile in homogeneous soil. Three pile conditions are studied in different soil types.

Intact pile in a clay layer

To start, an intact pile is simulated in a clay layer. The pile's length is $12m$, diameter is $0.6m$, the receivers are $2m$ away from the pile, and there are no flaws. An impulse of $1ms$ is introduced on the pile's head and vibrations are calculated.

Figure 4.13 shows the resulting seismograph and figure 4.14 shows the force transmitted to the soil. The a.t at varying depths slowly increases. The velocity of the shear wave in clay is $66.2m/s$ and in the concrete is $3802m/s$. So theoretically, the wave half-way the pile should arrive in about $32ms$ $(6/3802 + 2/66.2)$. The arrival of the first wave according to the model at $6m$ is $27.2ms$.

The force that the pile exerts on the soil is illustrated in figure 4.14. It shows that the waves in the pile are reflected at the pile toe and at the top.

Furthermore the prominent frequency of vibrations at the receivers is between 120 and $200Hz$, shown in figure A.2 in appendix A.

Finally, the maximum amplitude of the vibrations is shown in figure A.3 in appendix A. As expected the amplitude slowly decreases and at the bottom the vertical vibrations increase.

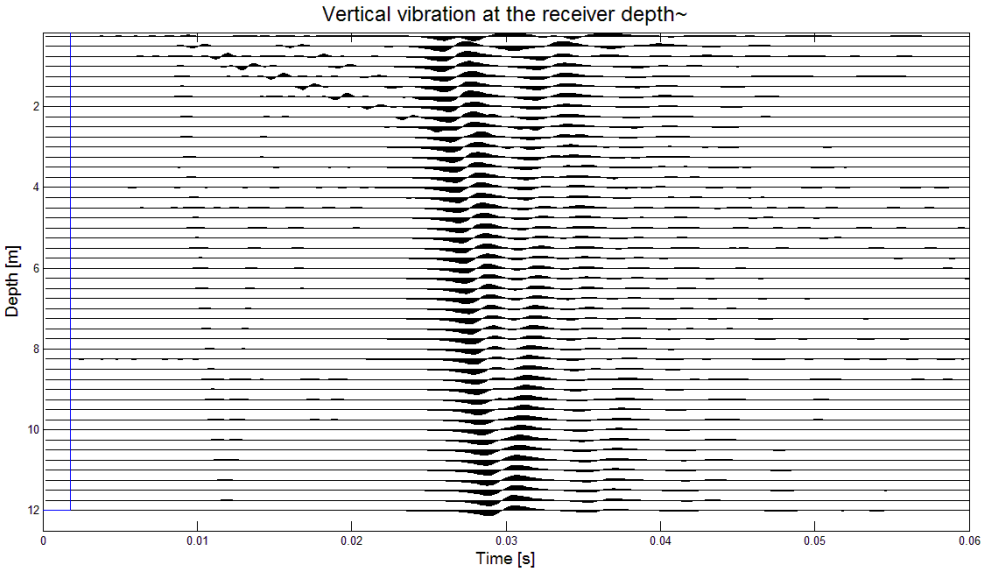

FIGURE 4.13: The seismograph calculated for an intact pile in homogeneous clay layer. The arrival of head waves is between $25ms$ and $30ms$. The second waves are caused by reflections in the pile that radiate out again.

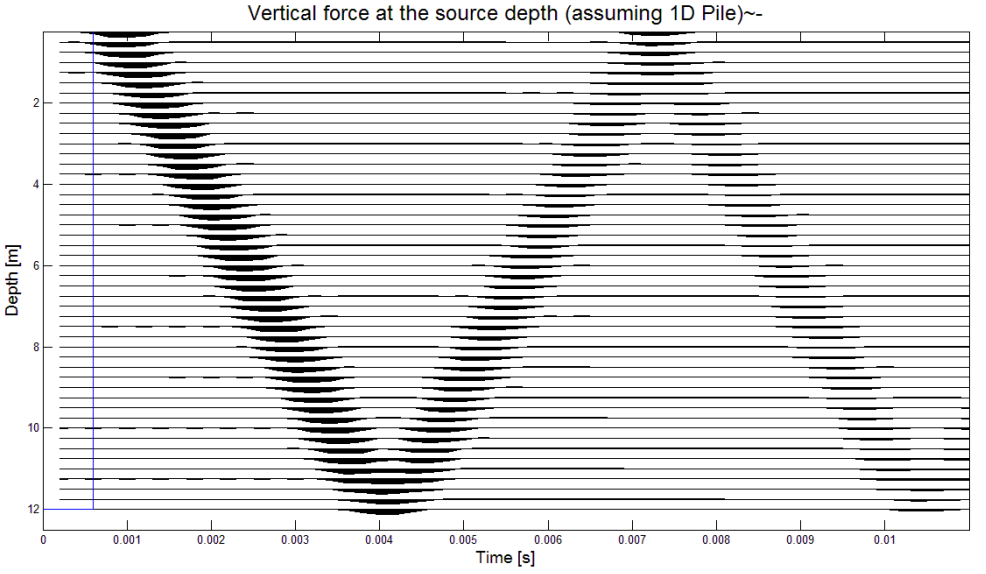

FIGURE 4.14: The force per source calculated for an intact pile in a homogeneous clay layer, showing reflections of vibrations within the pile. The amplitude of the waves are corrected for depth so damping in the pile cannot be seen in this figure.

Intact pile in a sand layer and in a peat layer

Using the same pile dimensions, a similar simulation was run in sand and peat conditions, with the material properties given in table 4.2. The resulting seismographs and force are shown in appendix A, figures A.4 and A.8.

The a.t in sand at $6m$ is $16.0ms$. In peat this value is $98.0ms$. Using V_s values of $129.1m/s$ and

$17.6m/s$ for the sand and peat, the approximate a.t should be $17.0ms$ in sand and $115.2ms$ in peat.

So for all three soil types, the simulated waves arrive earlier than calculated using simple shear wave velocities. Compared to each other the results make sense, peat has the latest arrival and sand has the earliest.

In appendix A the vibrations in the frequency domain are shown in figures A.6 and A.10. These results show that prominent frequencies in sand are around 600 Hz for all depths while for peat the prominent frequency peaks at $150Hz$. Therefore, it can be concluded that the simulation suggests that in stiffer soils, lower frequency vibrations are damped more.

Finally figures A.7 and A.11 show the maximum amplitudes. The magnitudes are all in the same range. Even though softer soils often have an amplification effect for vibrations, the transmission of the vibrations from the pile to soil has a higher amplitude in stiffer soils according to equation 4.1. The vibrations within the pile damp quicker if the surrounding soil is stiffer which can be deduced from the reflections seen in figure A.5 and A.9 in appendix A.

Pile with necking cross-section

Following the study of an intact pile, the same simulations are done with a pile that contains a neck. At $6m$ depth an axisymmetric flaw is introduced. Its width is $0.15m$ and height is $0.5m$.

In homogeneous soils, the flaw should simply be detectable based on wave a.t's. Since the wave is expected to travel through soil for a longer distance at the depth of the flaw, a delayed a.t is expected. Table 4.5 shows the a.t's of shear waves at the receiver at $6m$ depth.

Wave speeds in sand resemble most closely to speeds in concrete so one would expect the smallest difference in travel time. This is indeed observed. Furthermore, due to the neck, reflections are present in the pile. This is translated to multiple waves in the seismograph shown in figure 4.15 which shows the simulation of the neck in clay.

Another interesting result is the amplitudes of vibrations. Since the source force is dependent on the local pile diameter, its magnitude changes in the presence of the neck. Figure 4.16 shows that there is a significant decrease in amplitude at the depth of the neck. Peat and sand show similar results, shown in appendix A.

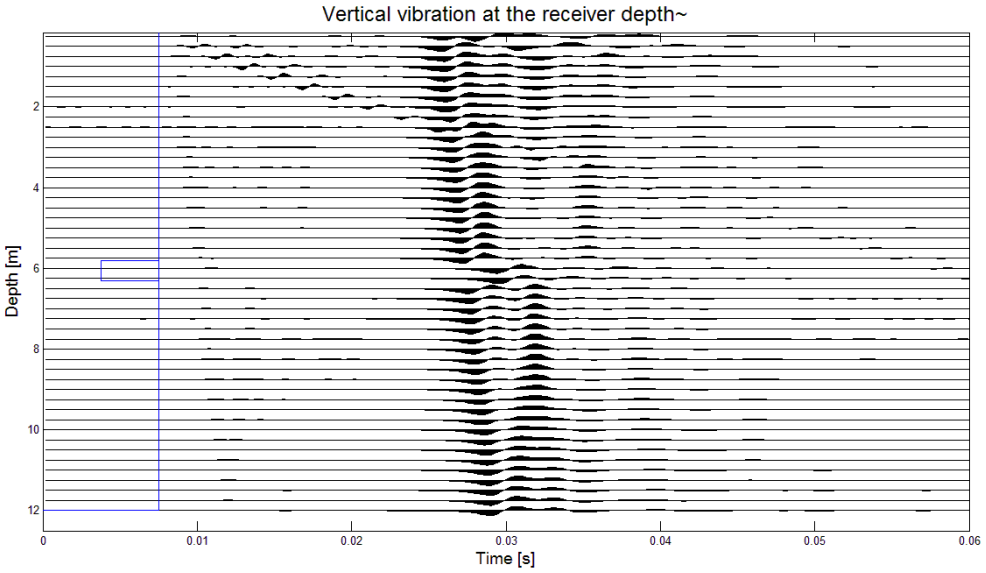

FIGURE 4.15: The seismograph calculated for a pile in homogeneous clay layer with a neck at $6m$.

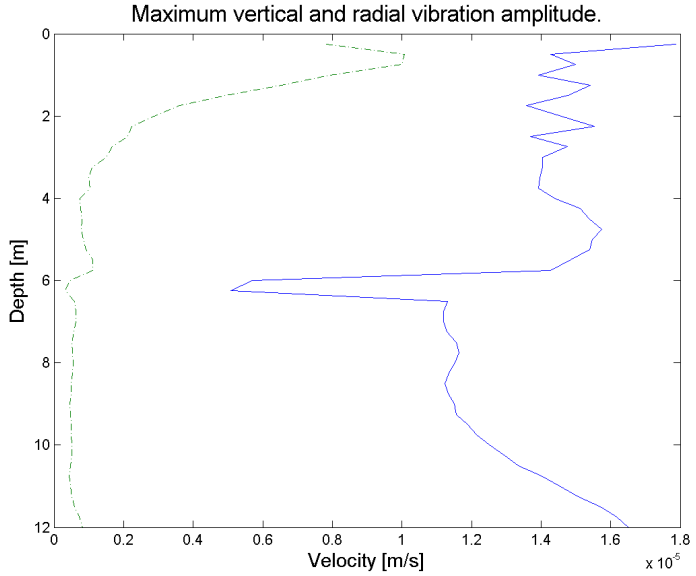

FIGURE 4.16: The maximum amplitude of vibrations in the soil calculated for a pile in homogeneous clay layer with a neck at $6m$.

	Peat	**Clay**	**Sand**
No flaw	$98.0ms$	$27.2ms$	$16.0ms$
Neck	$106.2ms$	$29.4ms$	$17.0ms$

TABLE 4.5: A.t's of shear waves at the depth of the neck where there is a neck flaw and where there is no flaw.

Pile with bulging cross-section

Similarly to the simulation with a necking cross-section, a bulging cross-section is tested. At $6m$ depth an axisymetric bulge is introduced. Its width is also $0.15m$ and height is $0.5m$. Table 4.6 shows the a.t's of shear waves at the receiver at $6m$ depth. Again in sand the difference in a.t is the shortest.

Also the amplitude of vibrations in the soil increase in the proximity of the bulge. Figures A.19 to A.27 in appendix A show the result for each soil type.

	Peat	**Clay**	**Sand**
No flaw	$98.0ms$	$27.2ms$	$16.0ms$
Bulge	$89.6ms$	$25.0ms$	$14.0ms$

TABLE 4.6: A.t's of shear waves at the depth of the bulge when there is a bulge flaw and where there is no flaw.

4.4.2 Heterogeneous soil

The focus of this research is to determine if the PS will show flaws in heterogeneous soils. As mentioned in chapter 2 heterogeneous soils complicate the situation. To model this problem, the same three piles are simulated as in the homogeneous scenario.

The soil used is similar to the soil found at the test site in Delft based on CPT tests. Table 4.7 shows the layering of the soil used in this simulation which is based on the CPT data in appendix B. The properties of the soil layers are given in table 4.2.

Soil layer	**Depth lower boundary[m]**
Peat	4.45
Clay	7.8
Peat	8.63
Clay	9.66
Sand	14.98

TABLE 4.7: Subsurface used to simulate heterogeneous soil. Depths are given with respect to the *Normaal Amsterdamse Peil (N.A.P)*

Intact pile

Figure 4.17 shows the seismograph of a flawless pile simulated in heterogeneous soil. The a.t's clearly vary a lot as may be expected.

The jumps may be mistaken for flaws if the local soil properties are not known. This highlights the importance of knowing the soil properties when detecting flaws.

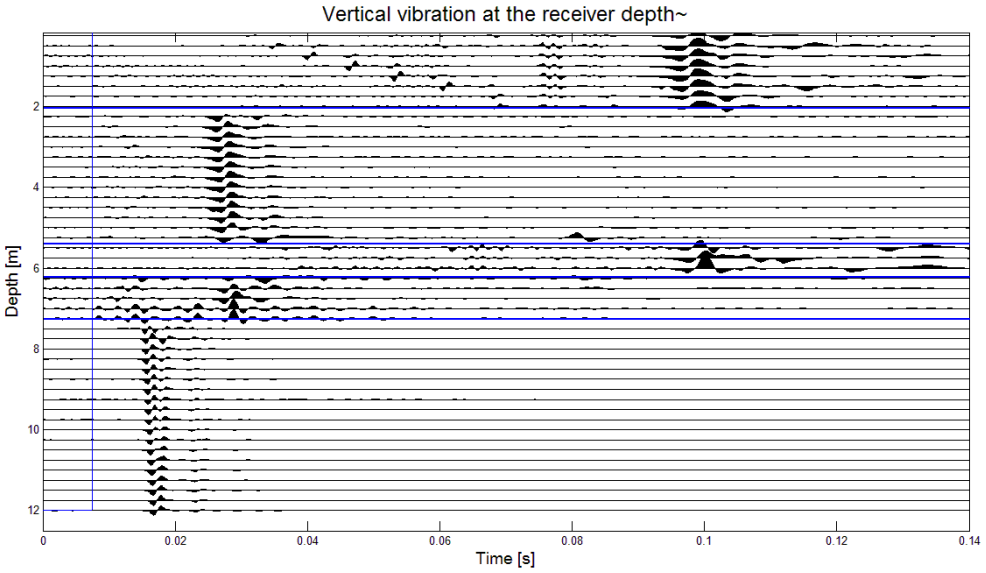

FIGURE 4.17: Seismograph of a flawless pile in heterogeneous soil. The depth is from ground surface, which at the test sight is -2.3m below N.A.P. Each soil boundary is given by the thick horizontal line.

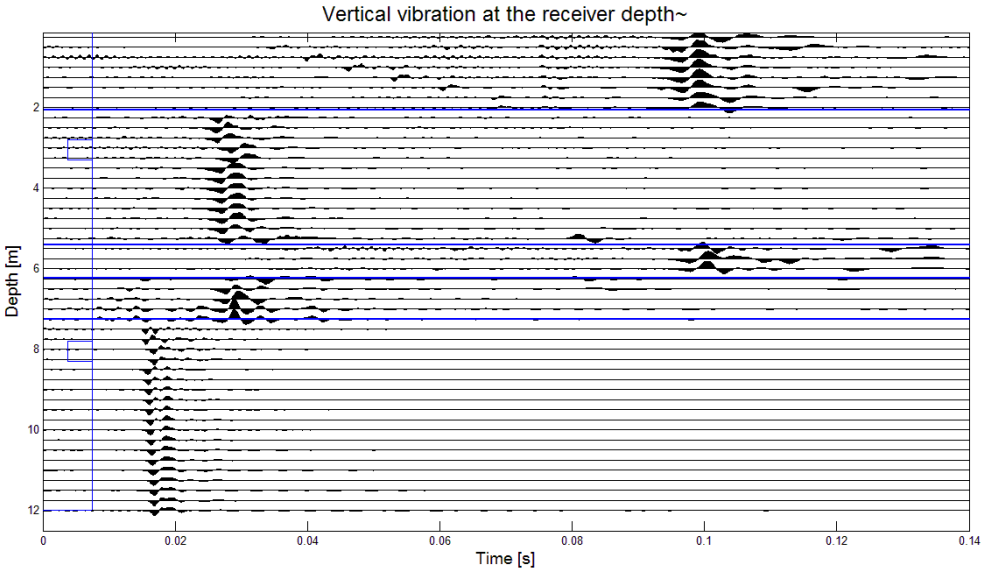

FIGURE 4.18: Seismograph of a pile with two necks in heterogeneous soil. Notice the small increase in a.t at the depths of the necks.

Pile with necking cross-section

The soil is layered therefore the effect a flaw will have on the seismograph depends on the location of the flaw. Therefore, in this simulation two flaws are introduced, one at 4m and one at 7m each reducing the local diameter to 0.3m. Figure 4.18 shows the resulting seismograph and the a.t's of head waves.

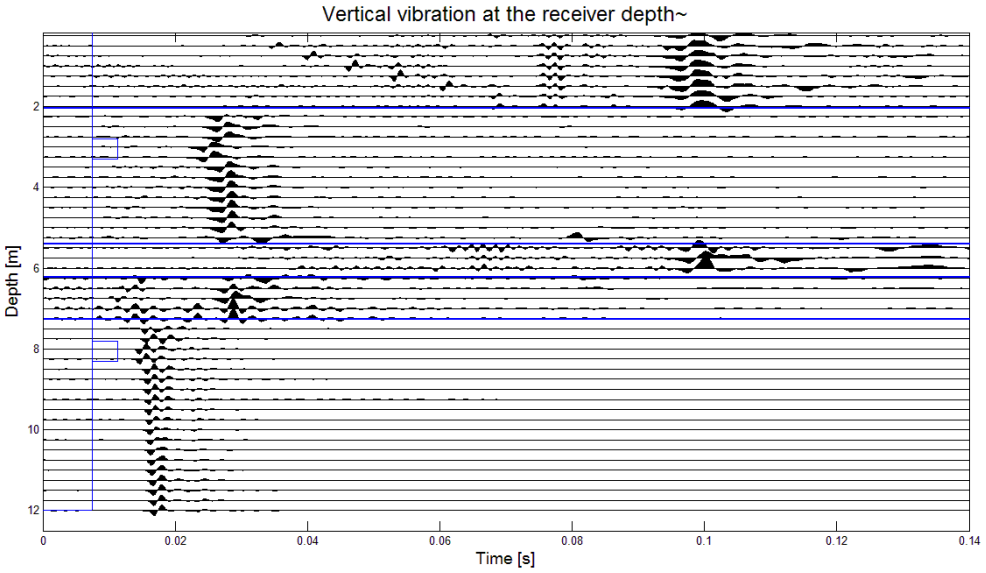

FIGURE 4.19: Seismograph of a pile with two bulges in heterogeneous soil. Notice the small decrease in a.t at the depths of the bulges.

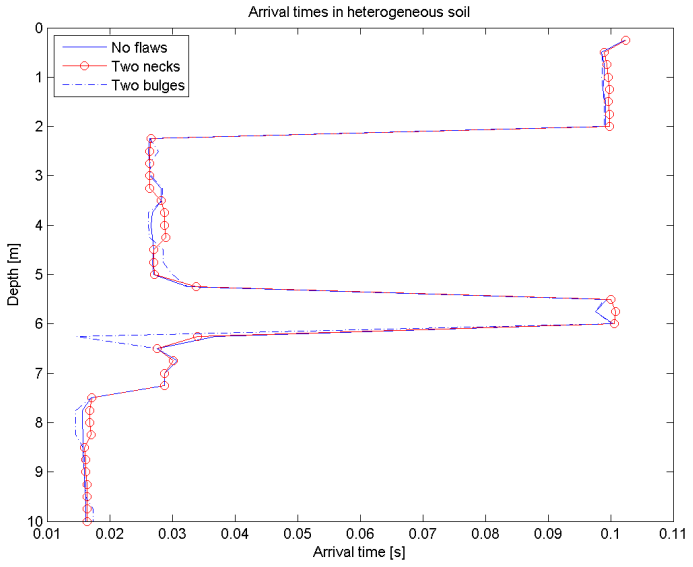

FIGURE 4.20: A.t's of a pile in heterogeneous soil. Each line represents a different pile.

Pile with bulging cross-section

Figure 4.19 shows the resulting seismograph when simulating the same pile with two bulges instead of necks. An interesting observation is the comparisons between a.t's for the three piles, shown in figure 4.20. Only small deviations can be observed where the flaws are located. This would lead to small errors in determining the location of the flaw. The presence of the flaws are however observable, it is simply harder to find if the flaw is in layered soil.

4.5 Discussion

To be able to predict the response in the subsoil when performing the PS, a model was built. This model combines two programs, ScatMat and D.A.C.

Verification of the simulation shows that a few assumptions made to simplify the problem are acceptable. This however also simplifies the results which might cause difference from the true PS results. The results are expected to show multiple vibrations, including noise which might need to be filtered.

The scenario tests show that changing soil conditions have a very big effect on the results. Flaws have a much smaller effect. The changes due to soil properties however are very sudden which is not exactly representative of the subsoil. In truth soil properties change gradually and so will the results of the PS. In addition, the results also show that the amplitude of vibrations is in the range of 1E-5 m/s which is very low but possible to measure.

The model may need to be extended to improve the simulation of the PS. An important issue is the definition of the soil. In this model the soil is assumed linearly elastic. However, the Young's modulus (E) for example depends on the magnitude of stress because soil is not linearly elastic. As stress increases, E decreases which will cause wave speed to reduce. E changes with depth and distance from the impulse hence wave speeds and vibration amplitudes may change. ScatMat has a limited works with discrete layers with constant properties. So gradual changes in for example E are not possible.

The model gives an idea of how vibrations might be measured in a PS. Differences are expected though, and validation of the model using data from the field test may help improve the model.

Chapter 5

Results from the First Field Test

5.1 Introduction

To gain an understanding of using the PS test in the field, a first field test is done. In appendix C the procedure for this test is described. This includes the construction of a pile field, introduction of flaws, and the procedure of the PS itself.

The main objective of the first test it to see how well the PS can be carried out. Design choices like pile-to-receiver distance and measurement plans are explored. Following this field test, the results help make the right design choices. Furthermore, by coupling the results back to the simulation in chapter 4, the model is validated. This is done in chapter 7

In this chapter the preliminary design choices are mentioned. This is followed by data processing to create readable figures that can be used for interpretation. Then the processing of the s-wave and p-wave velocity tests is shown. Some preliminary detections are made for pile 3. Finally the lessons from the field test are discussed.

5.2 Preliminary design choices

For the first field test the choice is made to increase the resolution[1] of measurements near the expected flaw depths. This is done to decrease the total number of measurements and save time while collecting a lot of data at depths of designed flaws. Little is known beforehand of what may be expected, so gathering data at a high resolution will improve the results. After processing the results, it may be realized that a lower resolution may be used.

The main weakness of the choice to focus measurements at expected flaw depths is that the locations of potential flaws is given. This means that the pile tests are not completely blind which will reduce the integrity of the detection. However increases in resolution do not always correspond to flaw locations since these are also done at locations without flaws to see if this

[1]The resolution is the density of measurements in depth.

may be detected as well. Therefore, this field test is only partially blind.

In addition, the depths at which the resolution is increased is based on the *surface* level. The depth of designed flaws are based on the height of the *re-enforcement*. The difference was only measured after the field test. The results are corrected for the difference but the original increase in resolution do not coincide exactly with flaw depths. The depths at which resolution is increased are not always at the depths of the flaws. This could lead to errors in detection.

A **pile-to-receiver** distance of $2m$ is chosen. Around the piles there is a ditch that hinders the CPT from being done any closer. However, this should be sufficiently close to the pile to measure vibrations [Finno et al., 1997].

5.3 Data processing

From the raw data collected in the field test, data processing is done. First the quality of the data is evaluated and, if possible, improved. Then the data is plotted in useful graphs. Vibration in x- and y- directions are measured, these are vibrations in horizontal direction.

5.3.1 Data cleaning

The first step in data processing is to order and *clean* the raw data. Using Matlab the data is imported so that plots can be presented in the time domain. Figure 5.1 shows the vibrations at $9.88m$ when pile 3 is hit. Although the wave is quite clear, clarity can be improved. Filtering out the noise is an option.

By transferring the signal to the frequency domain using a fast Fourier transform (FFT) function, the prominent frequencies can be seen. Comparing this to the frequencies observed in the background noise, it is possible to find which frequencies might be damped. This is done using a low-pass and high-pass frequency filter[2].

Low-pass filter: The aim of a low-pass filter is to filter out **high** frequencies while allowing vibrations below a certain frequency to remain. First the mean average may be removed to compensate for any systematic error in the measurement apparatus[3]. Then, an elliptical filter is used where beyond a certain frequency the amplitude is gradually scaled down.[Matlab, 2014] The low-pass cutoff frequency is $200Hz$.

High-pass filter: This filter works in the same way as the low-pass except that it filters out vibrations that have a frequency **lower** than a desired cut-off frequency. Based on the

[2] A Matlab code written by a colleague at Deltares, Bruno Coelho, is used in this thesis. The code uses an inbuilt Matlab funciton, *ellip*

[3] Removing the mean average is important if integration is desired to find displacements. This is not necessarily relevant for this thesis.

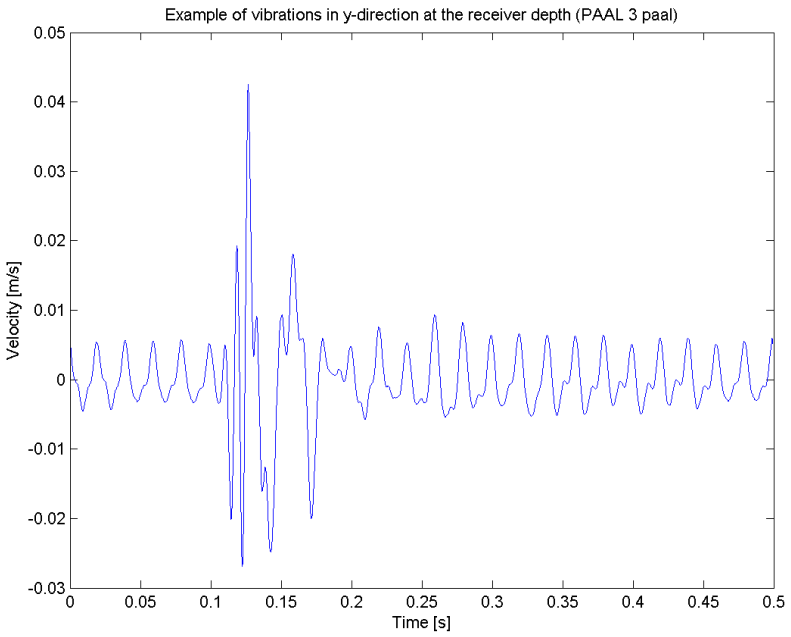

FIGURE 5.1: Horizontal vibrations in y-direction at 9.88[m] depth while testing pile 3.

frequency of the signals and the noise, the high-pass cutoff frequency is $60Hz$.

Figure 5.2 shows the signal from figure 5.1 in the frequency domain. One plot is only the data before the impulse of the hammer and the other is the total signal. This shows the prominent frequencies in the noise, which are highest around $50Hz$. Similarly when looking at the frequency plot of the entire signal, the frequencies between 60 and $150Hz$ are increased suggesting that this is the range of frequencies in which the vibrations caused by the hammer can be found.

When the signal is transferred back to the time domain using an inverse FFT it can be seen that the signal of the passing wavelet remains while the background noise is damped. This makes it easier to discern the wavelet from the noise. Figure 5.3 shows how the signal changes after using filtering.

5.3.2 Seismographs

By plotting the signals in the time and space domain, seismographs are created. The aim of these plots is to compare the vibrations in time of individual depths. This will help find patterns in the signals that could possibly point towards significant changes in soil types, pile toes, or even pile defects.

Figure 5.5 shows an example of a seismograph. Both the p-wave and the s-wave can be seen although p-waves are very small.

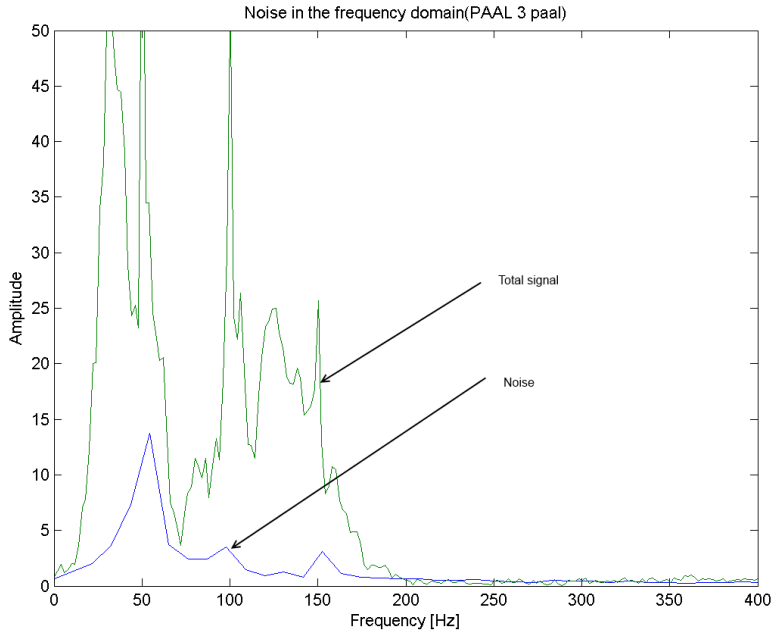

FIGURE 5.2: This figure shows the dominant frequencies in the noise and the total signal. The noise is the lower line that spikes at 50 and $100Hz$.

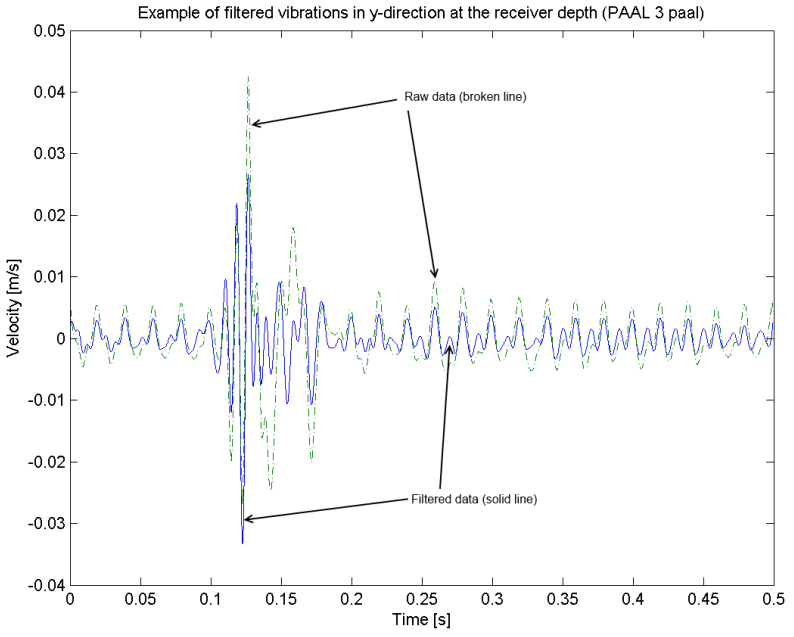

FIGURE 5.3: This figure shows the same signal, both raw (dotted/green) and filtered (full/blue) frequencies. Although the total processed signal has a smaller amplitude, the difference between the noise and the desired data is clearer.

Seismographs can be compared to each other to determine if particular patterns can be associated with the tested pile or with the ground. Appendix D shows the seismographs for all pile tests.

5.3.3 Arrival time

As mentioned in preceding chapters, the first and foremost challenge is to find flaws based on the a.t of p- and s- waves. This can be done by looking closely at the seismographs. However, if there were for example a bulge of $10cm$, this would reduce the a.t by roughly $0.02ms$. This seems hard to spot in the seismograph, see figure 5.5. Therefore a more extensive method should be used.

The wave is assumed to start if the vibration in the signal exceeds twice the standard deviation of the total signal vibrations. This is assumed to be the arrival of the p-wave. Also the arrival of the following s-wave is registered as the point in time when vibrations amplitude exceeds 65% of the maximum amplitude. The a.t's for each PS test are shown in appendix D.

This method does not exclusively give the p- and s-wave since the orientation of the cone and sensors will effect the amplitude ratio between the p- and s-wave. Therefore solely looking at the a.t could lead to misinterpretations of the data.

5.3.4 Amplitude

The amplitude will help determine changes in soil types so that possible changes in a.t's or reflections can be traced back to soil layering. Jumps in amplitude are also seen in the simulations in chapter 4 at flaws. Appendix D shows the maximum amplitude of vibrations at each depth per pile test.

Since the source of the signal is a human induces hammer impulse the amplitude may very slightly per signal. Therefore it is important to compare multiple measurement runs and avoid using extra "loud" or "soft" signals.

5.4 Wave speed measurements

Besides testing the piles, measurements were done to determine the s- and p-wave speeds in the soil. The corresponding seismographs are shown in appendix D.

Mostly the first wave is interpreted as a p-wave while the second is the s-wave. Figure 5.4 shows the seismograph of the s-wave test done near pile 3. Also the maximum amplitude plots are given in appendix D. From these a clear drop in amplitude can be seen around $3m$ depth. For the rest the amplitude reduces with depth which is what is expected due to spatial dispersion and material damping.

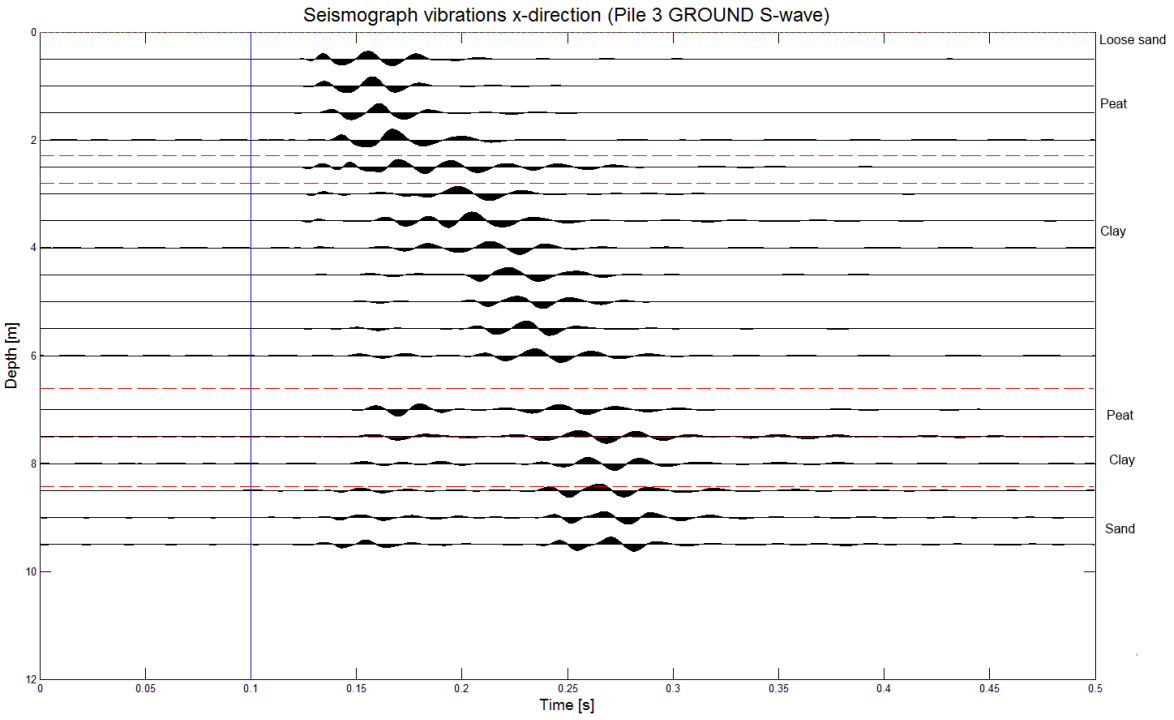

FIGURE 5.4: Seismograph of x vibrations from the s-wave speed test near pile 3.

The interpretation of the wave speed tests is based on finding the a.t of each wave at each depth. This is done by pin pointing similar points along the wave signal with the human eye. The error that may develop using this method is quite significant. Therefore using this test to accurately profile the subsoil is not possible. The test is however useful in providing a more qualitative description of wave propagation in the soil.

Seismographs with amplified p-waves

Besides the format used for the seismographs, it is possible to amplify the p-waves. This is done for the p-wave test since this wave is often smaller and may be lost in the seismographs.

Using the a.t of the p-wave a starting point is found. From this point the amplitude of the data is reduced according to equation 5.1. The result is that all following vibrations are relatively damped, making the first waves more visible in the seismograph.

$$p'(t) = \begin{cases} 0 & \text{if } t < a.t_{p-wave} \\ \frac{p(t)}{10t^3} & \text{if } t \geq a.t_{p-wave} \end{cases} \tag{5.1}$$

5.5 Results per PS test

Based on the graphs shown in appendix D and the wave speed profile an attempt is made to detect flaws in the piles. Per pile the following questions are answered, concluding with a location and type of flaw(s).

1. What is already known? - any notes taken during testing phase.
2. What can be seen in the seismograph on pile specific patterns, reflections, etc.?
3. What can be said from the maximum wave amplitude?
4. What can be said from the a.t of the p- and s-waves?
5. What can be said from the comparison of all pile tests to determine overall patterns specific to the site or testing procedure?
6. Which defects are detected?

The process taken per pile is described in appendix D. In the next section pile 3 is taken as an example.

5.6 Results pile 3 from the first field test

Based on the increased resolution at $3m$ and $6m$, a defect is possibly found at these depths. This is already known.

In the seismograph figures 5.5 and 5.6 there is a small hint of a reflection at $7.7m$. This could be caused by a defect but also by the sand layer below. The amplitude shown in figure 5.9 dips around $6m$ deep and peaks around $4m$ and $8m$.

Figure 5.7 shows a delay for the first wave at $4.48m$. This is however not seen as a defect. At this level p-waves pretty much vanish and only s-waves are present which will cause delays since the first arrival is an s-wave and not a p-wave. At $6.98m$ there is an early arrival, which is a p-wave. This all means that there is possibly a bulge at $7m$ below the pile head. There is no conclusive proof of a defect at $3m$.

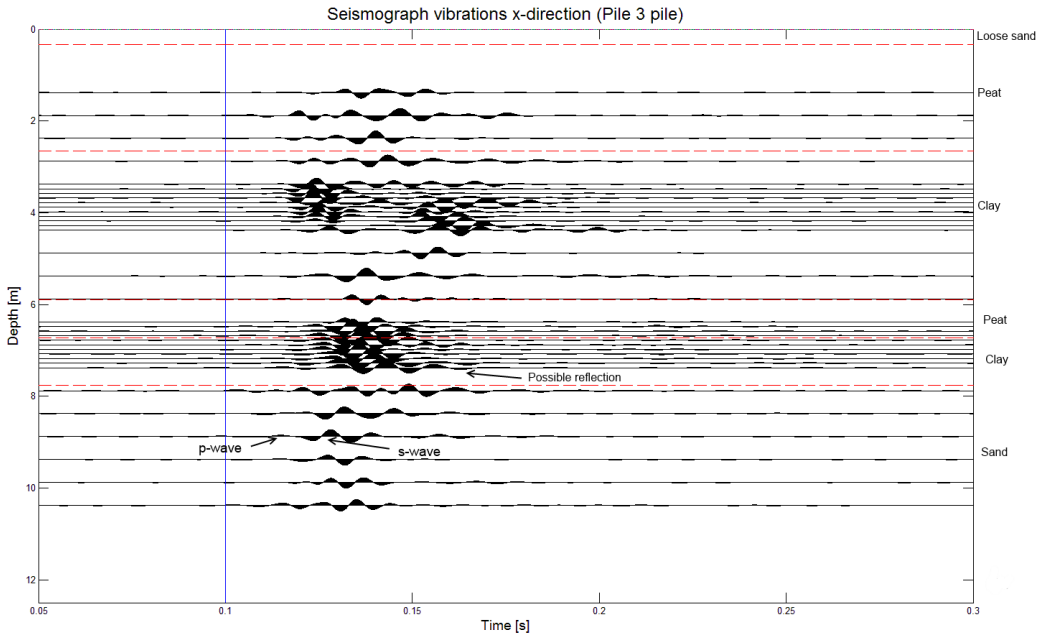

FIGURE 5.5: Seismograph for PS test on pile 3, vibration in x-direction. The vertical line at 0.1[s] signifies the time of hammer impact.

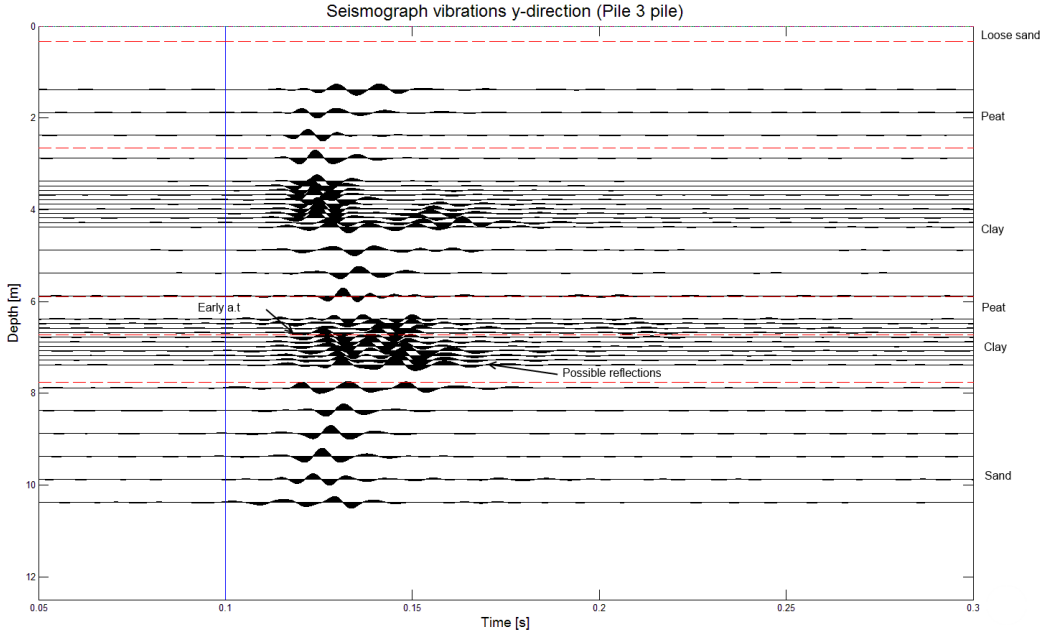

FIGURE 5.6: Seismograph for PS test on pile 3, vibration in y-direction. The vertical line at 0.1[s] signifies the time of hammer impact.

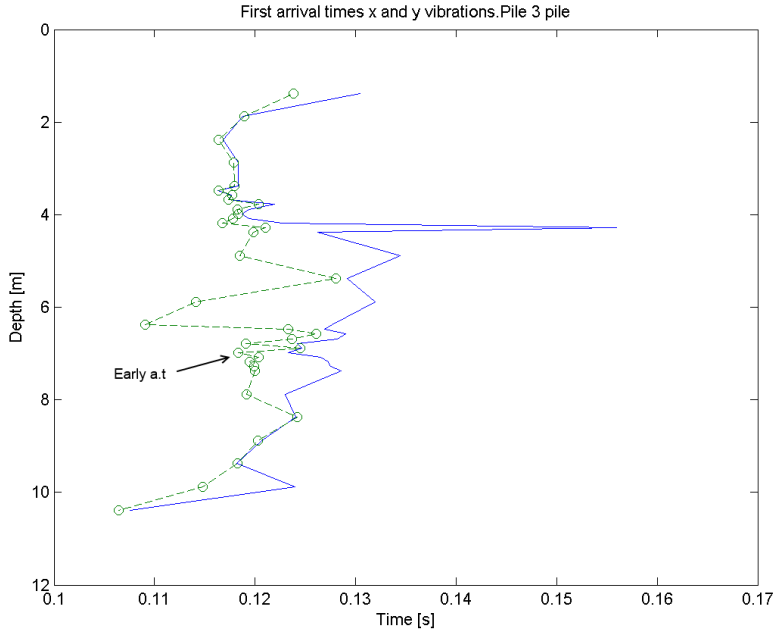

FIGURE 5.7: First a.t's vibration is x- and y-direction for PS test on pile 3. x- is the blue full line and y- is the green broken line.

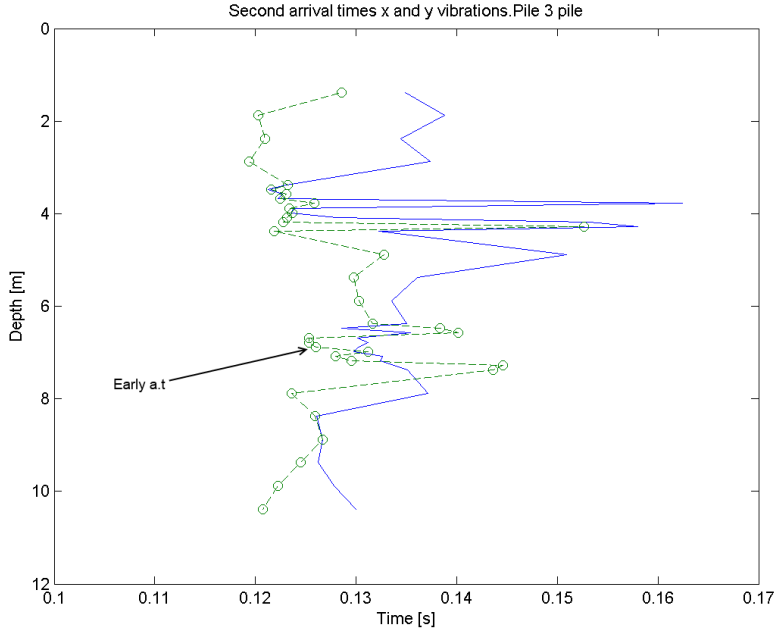

-

FIGURE 5.8: Second a.t's for PS test on pile 3. x- is the blue full line and y- is the green broken line. In both lines a small decrease is a.t can be seen around $7m$.

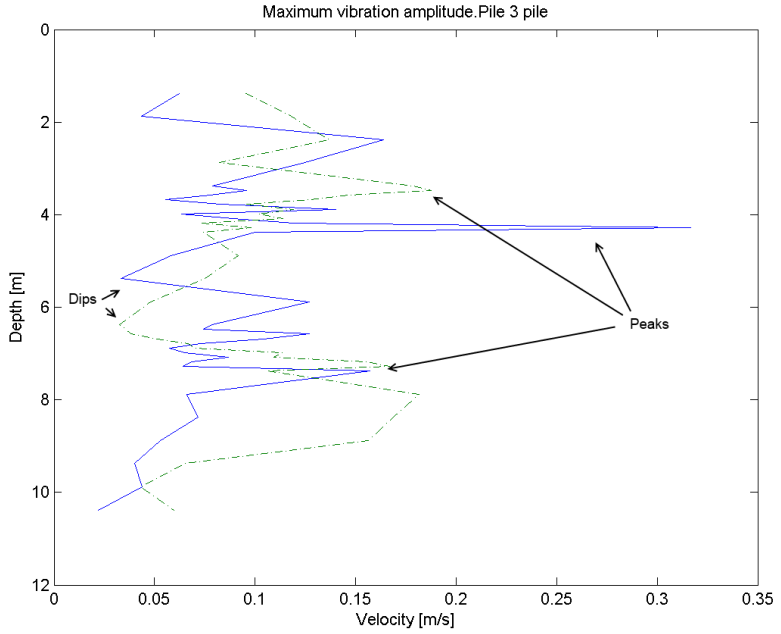

FIGURE 5.9: Maximum vibration amplitude for PS test on pile 3. x- is the blue full line and y- is the green broken line. As mentioned before in chapter 4, peaks and dips arise both at soil boundaries and at flaws.

5.7 Evaluation of the results

The aim of the first field test was to get an idea of how successful the PS test can be when detecting defects in heterogeneous soil conditions and how it could possibly be improved. The predictions made are shown in the middle column of table 5.1 and the designed flaws are in the right column. In appendix D the difference between detection and design per pile is analyses. From these differences lessons learned from this field test can be formulated.

The first main conclusion that can be taken from the results is the importance of the underlying patterns. The main processing tool is to find outstanding wave behavior that cannot be traced back to soil conditions or testing procedures. This is done by comparing each test to the underlying patterns. Therefore doing p-wave and s-wave tests are very useful. Also testing piles that are known to be flawless helps.

Another lesson is that using delays in a.t is only useful if there is sufficient data above and below the flaw for comparison. It might also help to keep a constant distance between the pile and the sensors for all tests, although this is not always possible. To measure the distance to the cone and try to analytical calculate the a.t is not a good option because measuring the wave velocity in the soil is very inaccurate, which will lead to relatively huge errors.

Finally using $50cm$ intervals is too big while $10cm$ intervals takes a lot of time which limits the range of data that can be collected.

From the results discussed in this chapter it can be concluded that the PS test has enough room for improvement. For the next field tests the total length of the pile will be measured at $25cm$ intervals to ensure enough data for comparison of a.t's. Also some piles will be measured beyond the pile toe to see if the PS can find the toe and how this might help find flaws. Finally, the results above are all based on vibrations in horizontal directions. In theory the vertical vibrations are the largest so these should also be included in the measurements.

Pile number	**Predicted flaw**	**Depth [m]**	**Designed Flaw**	**Depth [m]**
3	Bulge	7.88	Bulge	3
			Neck	6
7	Neck	7.98	Bulge	8
8	None		None	
13	Bulge	8.83	Neck	8
14	None		None	
17	Neck	3.17	Crack	3
			Neck	8

TABLE 5.1: The detected flaws compared to the designed flaws in the tested piles.

Chapter 6

Results from the Second Field Test

6.1 Introduction

Equipped with the lessons from the first field test, a second test is performed. This is done to determine if the PS is improved and to test more piles. The procedure is similar to the first test except for the changes mentioned at the end of chapter 5. The main changes are to:

1. Measure at $25cm$ intervals.
2. Include a test designed to find the the pile toe.
3. Include a test with an impulse on top of the pile.
4. Include measurements of vibrations in the z- direction.

In this chapter the results of the second test are presented. Section 6.2 shows how the data is organized and processed to make sense of the data and an evaluation of the changes mentioned above. This is followed by the process for detecting flaws and an elaborated example evaluation of pile 1. Finally the results of the detection are discussed followed by the lessons that can be taken from this field test.

6.2 Processing the results

Using the raw data received from the SCPT for each pile, the vibrations are plotted in seismographs. Furthermore a.t figures are made to see when the waves arrive at the receivers and the maximum amplitude is plotted per receiver as well. For this data the incoming waves are very clear, so no filtering is needed.

6.2.1 Graphing the results

The seismograph

Figure 6.1 shows the seismograph for the test done on Pile 8, vibrations in the x-direction. All results for pile 8 are shown in appendix E. Pile 8 is designed without any flaw.

From 0-3.6m the plot shows the arrival of the direct waves that are radiated from the pile shaft, through the soil and to the the cone. Between 3.6m and 6m waves start to arrive earlier as depth increases. Between 6m and 8m the wave arrivals delay but after 8m they start reducing again. Finally after 10.5m the arrival time increases again.

Multiple scenario's might explain decreasing a.t's with increasing depth. One possibility is that soil becomes stiffer with depth and wave velocity increases. Although the waves travel a larger distance in the pile, the part traveled through the soil is quicker and results in a shorter travel time. Another possibility is that the path through the soil shortens while the path through the pile increases, like in a bulge. A third explanation is that the measured vibrations originate from one particular point along the pile and travel both upwards and downwards.

The red sloping lines on figure 6.1 show the arrival of the s-waves. The lines form two inflection points at 6m and at 10.5m. The two inflection points created by the lines on figure 6.1 show vibrations measured originate from the pile at 6m and at 10.5m.

The slope of the arrival of s-waves below 10.5m corresponds to the speed of waves propagating from the pile toe through the soil. The slope of the arriving waves above 10.5m is the same as below. Therefore the origin of the waves is at 10.5m and the velocity in the soil does not change much from 8m to 14m.

Using the same reasoning, the waves measured between 4m and 8m originate from the a point at 6m. This could theoretically be a sudden flaw. Pile 8 however should not contain any flaws so this is caused by a local change in soil conditions that experiences larger excitations between the pile and the soil. The same can be seen in results from other piles.

The modified seismograph

For the p-wave speed tests in chapter 5, the p-waves were amplified in modified seismographs. This is done for all pile tests as shown in figure 6.2.

Since later arriving waves are damped, earlier waves become clearer. These could be the waves that are radiated of the pile at the depth of the receiver since these follow the shortest path in the soil. According to the theory from chapter 3, these waves should show the changes in a.t due to local defects.

The waves could also be the p-waves radiating from other points along the pile. These waves show similar behavior as can be seen in the original seismographs (figure 6.1) as the lines of a.t in figure 6.2 show. The slopes are steeper since p-waves travel quicker than s-waves.

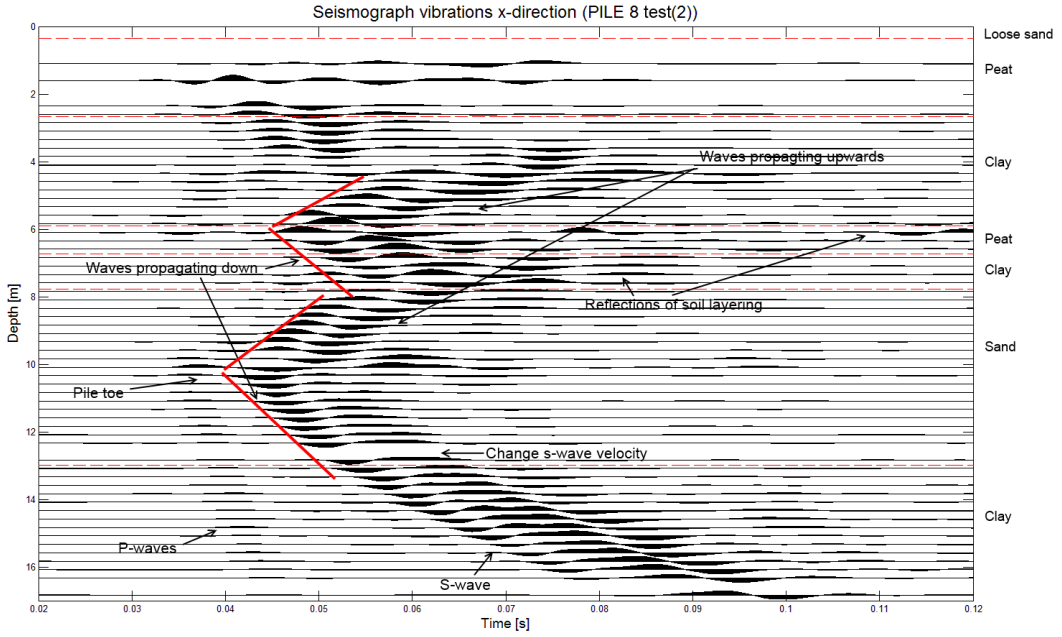

FIGURE 6.1: Seismograph for PS test on pile 8, vibration in x-direction. The time axis starts at the point of hammer impact and depth starts at the level of the reinforcement. Note the variations in vibrations caused by the local soil conditions.

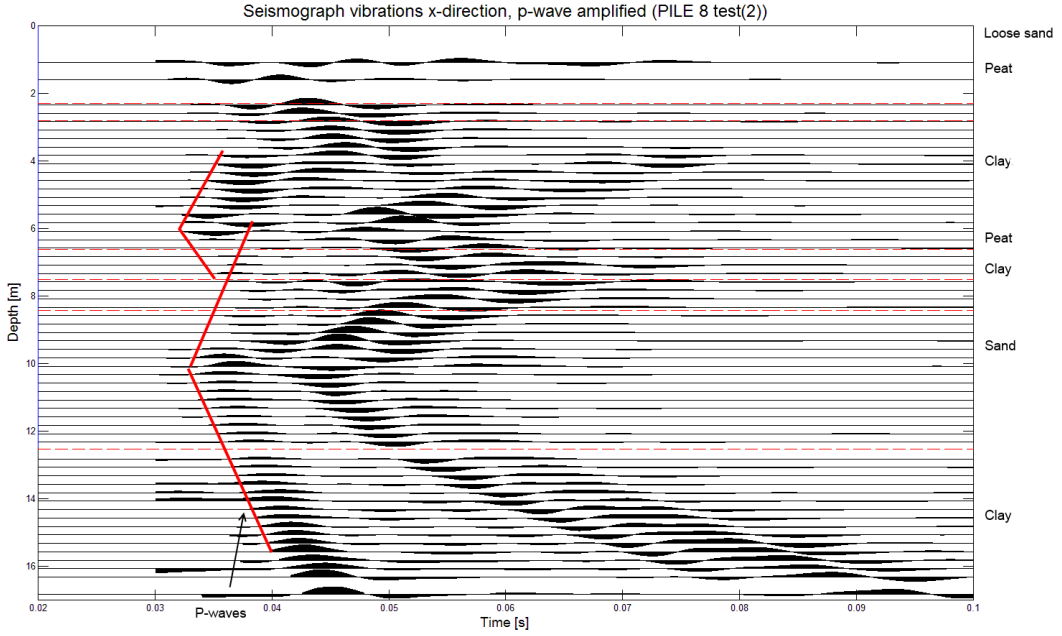

FIGURE 6.2: Modified seismograph for PS test on pile 8, vibration in x-direction. The time axis starts at the point of hammer impact and depth starts at the level of the reinforcement.

The arrival time plots

Figures 6.3 and 6.4 show the arrival times of the wave. Figure 6.3 shows the arrival of the first vibrations, defined as the point at which the amplitude exceeds the stander deviation of the

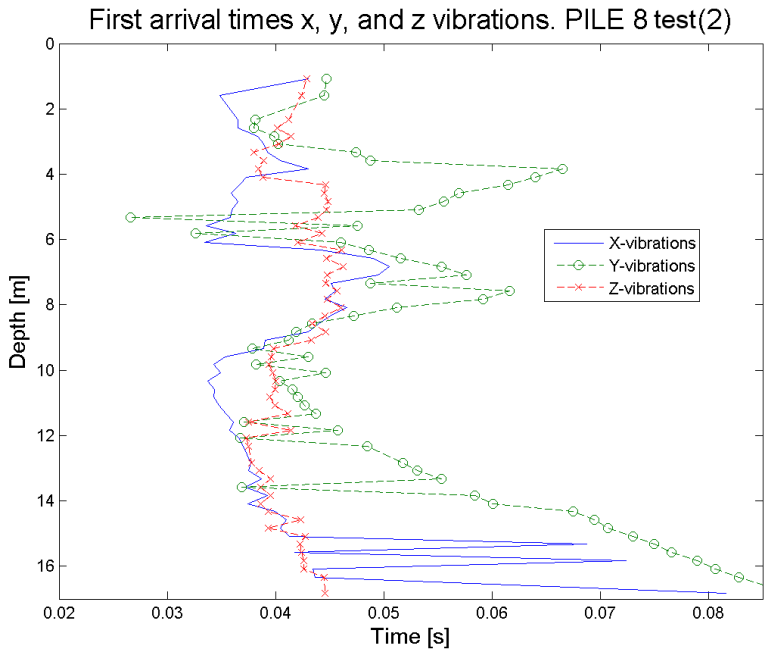

FIGURE 6.3: First a.t's for PS test on pile 8. x- is the blue full line, y- is the green broken and circled line, and z- is the red dashed and crossed line.

total signal. Figure 6.4 shows the times at which the vibrations exceed 65% of the maximum amplitude, which is a bit later.

The two figures show again that the arrival of s-waves point to two prominent sources, at $6m$ and $10.5m$. The arrival of shaft waves can be seen in the first arrivals (figure 6.3) of waves above $6m$ while the arrival of toe waves can be seen above $10.5m$.

The amplitude plot

Figure 6.5 shows the amplitude plot. The changes in amplitude correspond to changes in soil conditions. Peaks can be seen at $3.5m$ and $8m$ where soil boundaries are present.

Directly below $10.5m$ the amplitude increases as well. This is due to vibrations of the pile toe, which can also be seen in the results of the model in chapter 4.

6.2.2 Finding the pile toe

For pile 8 and 13, measurements are done up to $16m$ below the surface to see if the PS can show the pile toe. In this thesis this is done using the seismographs by finding the point at which a.t's start to increase. The toe can also be seen due to the waves dispersed upwards as mentioned before.

Figure 6.1 clearly shows an increase in a.t below $10.5m$ from the top of the reinforcement. In addition the results show reflections above this point that originate from the toe tip. The

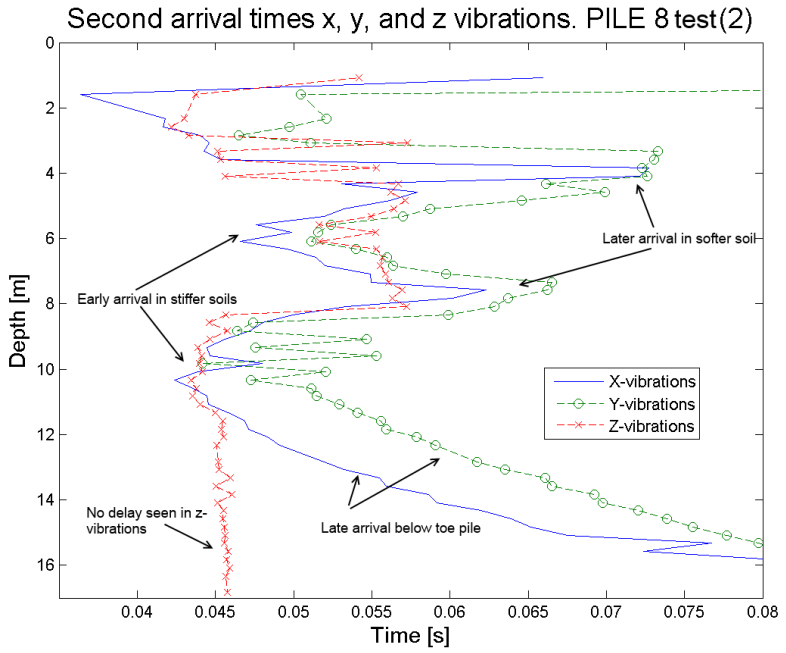

FIGURE 6.4: Second a.t's for PS test on pile 8. x- is the blue full line, y- is the green broken and circled line, and z- is the red dashed and crossed line.

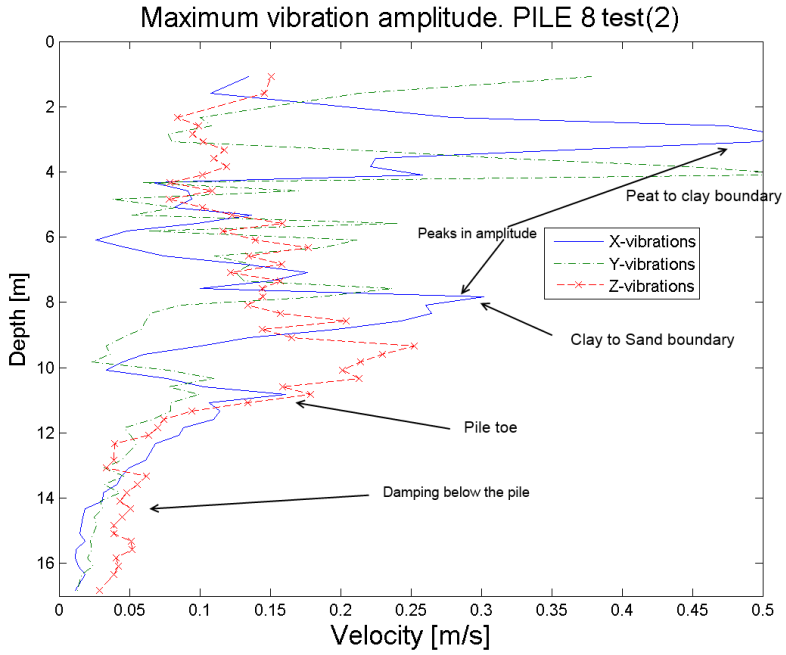

FIGURE 6.5: Maximum vibration amplitude for PS test on pile 8. x- is the blue full line, y- is the green broken and circled line, and z- is the red dashed and crossed line. Peaks in amplitude correspond to the soil layering. In the deeper soil layers the vibrations reduce due to damping.

top of the reinforcement is $0.48m$ above surface level, hence the pile to is $10.52m$ deep.

Using the same method for pile 13 and the figures E.66 and E.65 in appendix E the toe can be found. This is at $11m$ from the top, and $10.35m$ from surface level.

6.2.3 Introducing shear waves

Another variation on the PS test is to introduce s-waves in the pile instead of p-waves. This is done on pile 3, which was also already tested in the first round. The results are shown in appendix E.

The steel block, on which the hammer is hit, is mounted on top of the pile. The block is then hit sideways which creates a shear wave that propagates downwards into the pile.

Theoretically, s-waves travel slower. However the transfer from the pile to the soil will create p-waves that travel to the cone. In addition this should increase the amplitude of horizontal vibrations (x- and y-) and reduce the vertical vibrations (z-).

The results show that the vibrations from the pile toe are not as high. Contrary to the other tests, the amplitude of vibrations does not peak at the pile toe. Therefore, the seismographs show waves radiated directly from the pile shaft more clearly. This should theoretically improve the chances of detecting flaws along the pile shaft.

In practice the difference in results is small. The amplitude of horizontal vibrations is increased by about 20%. The known flaws at $3m$ and $6m$ do not become clearer with this method.

This alternate form of the PS remains an option for further research. Orientating the hammer hit towards the cone might improve the results, and increase the measurements of shaft vibrations. However, mounting the block on top of the pile is less convenient when testing piles that are already carrying structures on top.

6.2.4 Including z- vibrations

Figure 6.6 shows the vibrations measured by the SCPT in the vertical (z) direction. Theoretically these vibrations should have the highest amplitude because this is the same direction as the impulse of the hammer. Hence this data should improve detectability. In truth the situation is not that simple.

The first clear observation that can be made is the constant arrival time of waves at the cone. Below the toe of the pile the a.t is expected to increase since waves travel more through soil, yet this cannot be observed. Second, the variations of a.t seen in the x- and y- vibrations is not seen in the z- vibrations. The z- vibrations seem unchanged by soil layering.

Both observations prove that the vibrations measured in the cone travel through the bar rather than through the soil. Vibrations from the pile cause the bar to vibrate as a whole, which is what the geophones measure.

Since the bar itself is made of steel, vibrations have a very high propagation speed. Hence the a.t's will hardly reduce with depth. This also explains why the a.t is less affected by the changing soil conditions. This means that the data in the cone will not reflect the properties of the pile at the depth of the measurements but rather that of the bar itself.

At $8m$ below the surface, the results shows some interesting changes. The waves seem to arrive earlier, and become a single wavelet rather than multiple vibrations. Figure 6.5 also shows a jump in amplitude at this depth. This change in wave properties corresponds to the transition from a clay layer to the stiffer sand layer.

When the cone tip is in the stiffer sand layer, vibrations in the bar are damped quicker since the bar becomes effectively stiffer. Also the vibrations form at the tip of the pile rather than along the pile shaft or at the the top. The waves then travel through the sand which has a much higher wave velocity, resulting in early arrivals.

The observation that the amplitude of z-vibrations increases a lot beyond the $8m$ mark and decreases again after about $11m$ can also be traced back to the sand layer. It proves that vibrations at the toe are radiated upwards and stopped by the clay-sand boundary. These vibrations are much "louder" than vibrations from other parts of the pile, resulting in a spike in amplitude when the receiver enters the sand layer. Further away from the pile toe the amplitude reduces again due to damping in the bar.

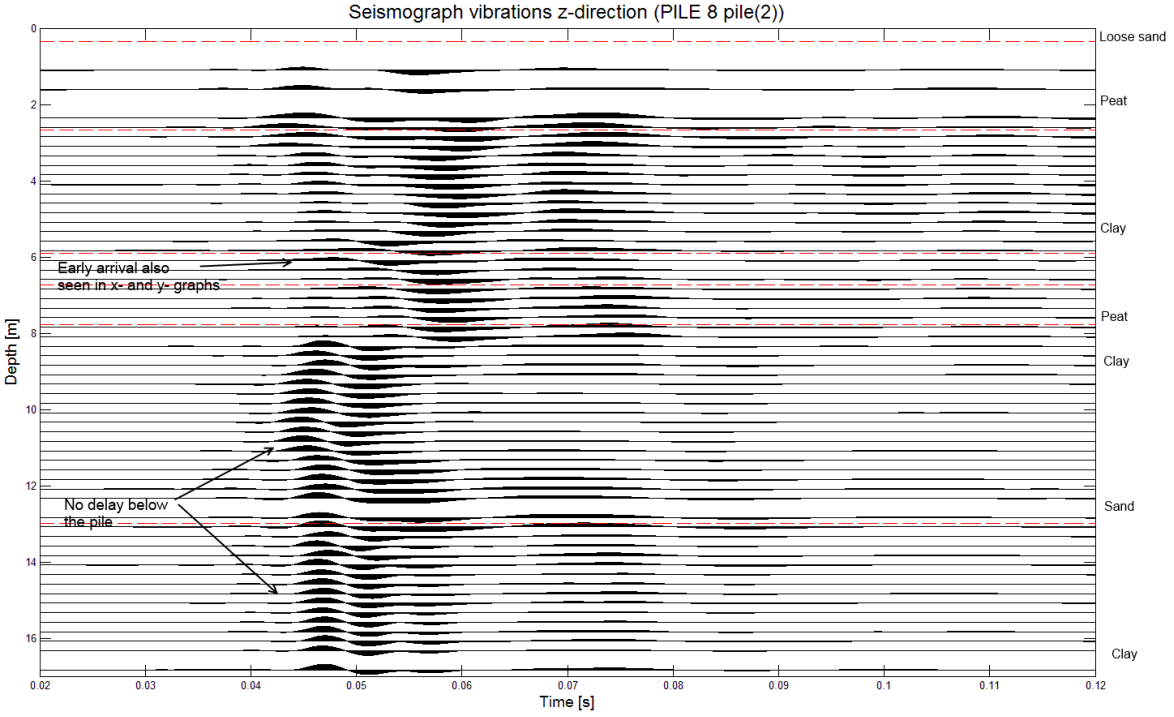

FIGURE 6.6: Seismograph for PS test on pile 8, vibration in z-direction. The time axis starts at the point of hammer impact and depth starts at the level of the reinforcement. The chosen time scale is the same as the other seismographs for comparison.

6.3 Detecting defects

The main objective of the test is to detect flaws in the pile. For each pile the seismographs, a.t figures, and amplitude figures are made. Using these, an attempt is made to find anomalies in the results that are evidence of flaws. In appendix E this is done for piles 2, 4, 9, 10, 11, 12, and 18. Piles 3, 8, and 13 are repeated to see how the PS is improved in comparison to the first tests and if there are further improvements possible. Here the detection of flaws in pile 1 is shown as an example of the process.

6.3.1 Example pile 1

The first pile to process is pile 1. Measurements are done every $25cm$ and the hammer impulse is placed on a steel block attached to the side of the pile. This will introduce compressional (p-) waves.

In pile 1 flaws $3m$ and $8m$ are detected. At $3m$ signs of a crack can be seen while at $8m$ the type of flaw might be a neck. Finally the pile toe can be seen between 10.5 and $11m$ from the top.

The seismographs show reflections around the $3m$ mark. From the lessons learned while looking at pile 17 in the first test, the presence of reflections might be caused by a crack. Furthermore at this depth, arrival times of the maximum amplitude vary a lot locally.

The seismographs also shows that waves arrive earlier from $4m$ to $7m$. This could be wave propagating upwards from a defect at $8m$. Another option is shaft vibrations measured by the cone while the cone is deviating towards the pile. The change in a.t is about $0.05s$ which corresponds to a deviation of about 6^o which is rather high but possible.

The seismographs and a.t figures show late arrivals around $8m$ deep, similar to the pattern seen in pile 3 (figure E.65). This could be caused by a neck at this depth which should also be present in pile 3.

After the $10.5m$ mark, arrival times start to increase. Also above this mark reflections can be seen in the seismographs. This means that the pile toe is probably at this depth.

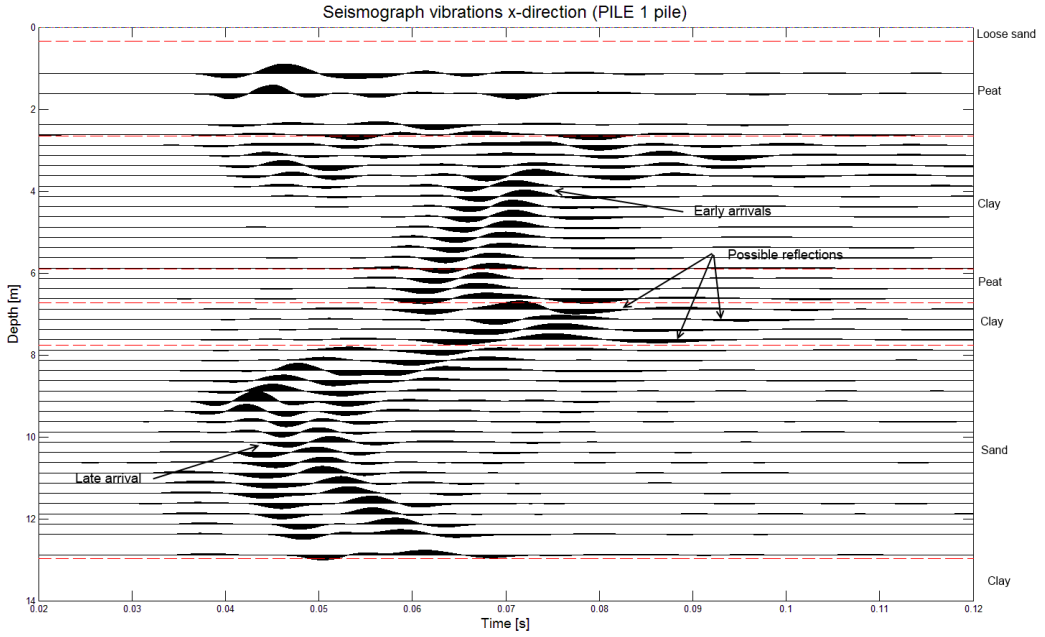

FIGURE 6.7: Seismograph for PS test on pile 1, vibration in x-direction. The time axis starts at the point of hammer impact and depth starts at the level of the reinforcement.

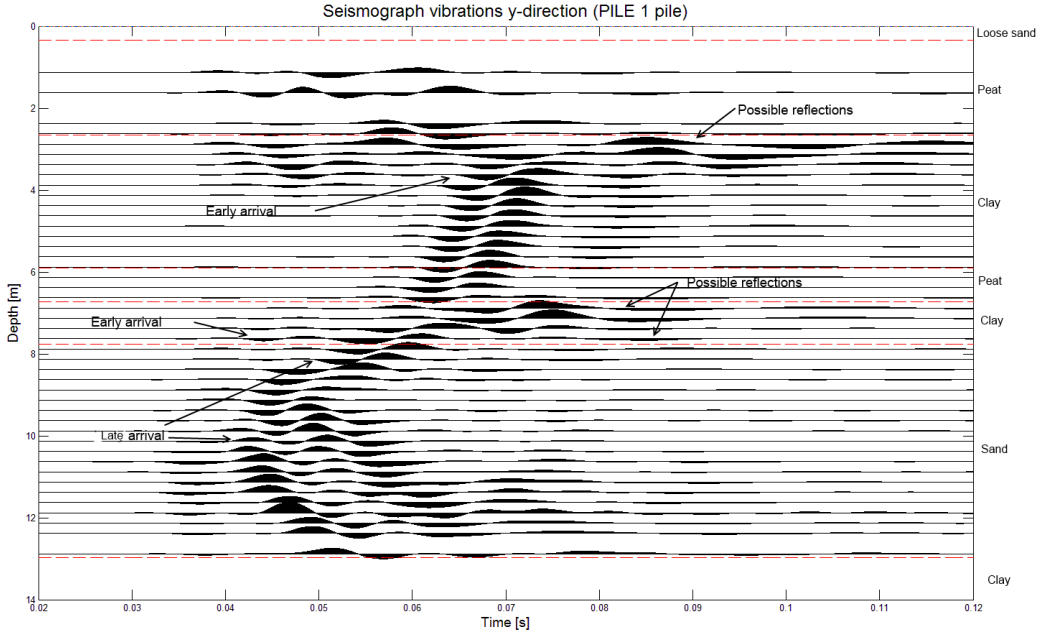

FIGURE 6.8: Seismograph for PS test on pile 1, vibration in y-direction. The time axis starts at the point of hammer impact and depth starts at the level of the reinforcement.

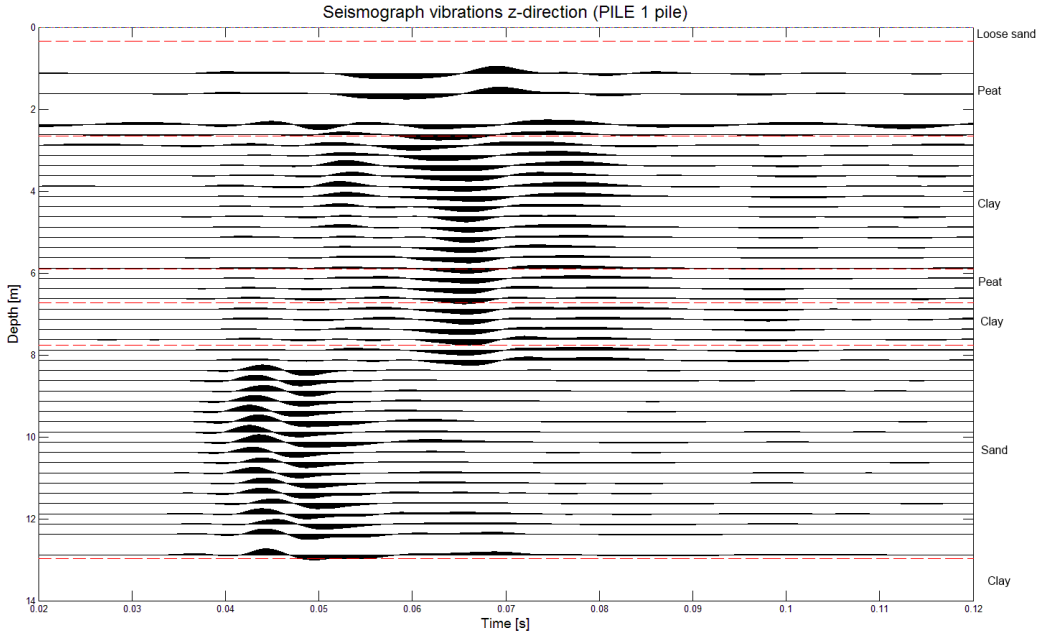

FIGURE 6.9: Seismograph for PS test on pile 1, vibration in z-direction. The time axis starts at the point of hammer impact and depth starts at the level of the reinforcement.

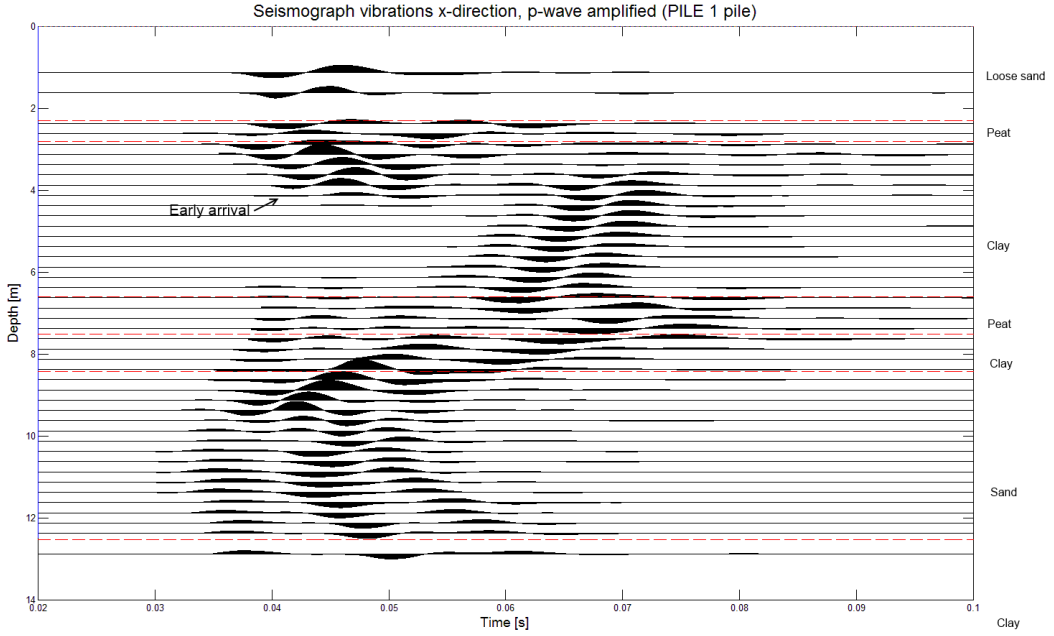

FIGURE 6.10: Modified seismograph for PS test on pile 1, vibration in x-direction. The time axis starts at the point of hammer impact and depth starts at the level of the reinforcement.

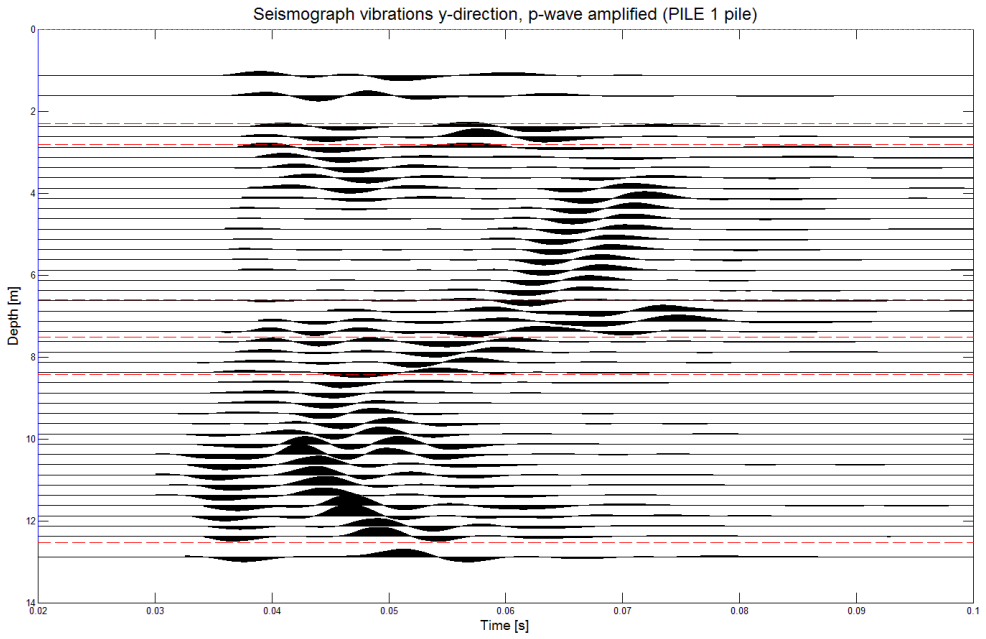

FIGURE 6.11: Modified seismograph for PS test on pile 1, vibration in y-direction. The time axis starts at the point of hammer impact and depth starts at the level of the reinforcement.

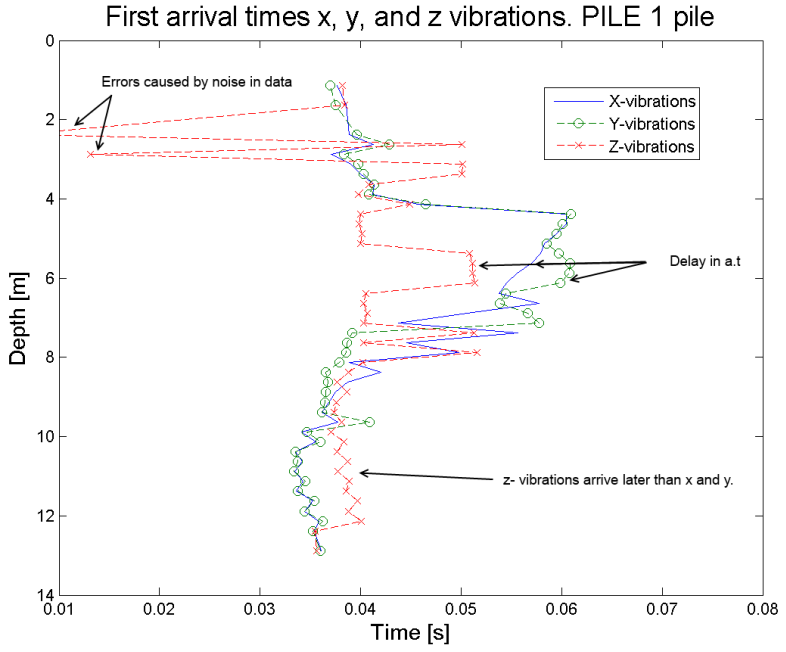

FIGURE 6.12: First a.t's for PS test on pile 1. x- is the blue full line, y- is the green broken and circled line, and z- is the red dashed and crossed line.

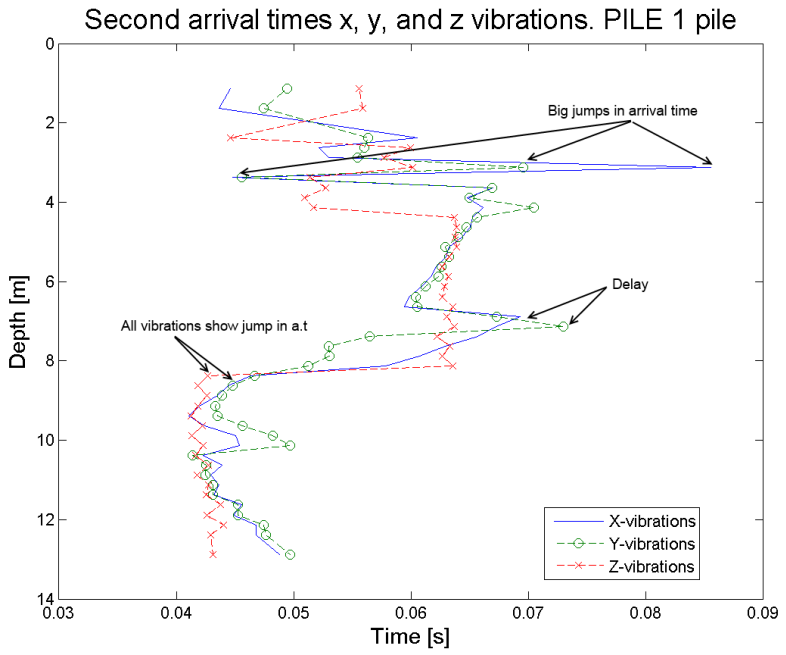

FIGURE 6.13: Second a.t's for PS test on pile 1. x- is the blue full line, y- is the green broken and circled line, and z- is the red dashed and crossed line.

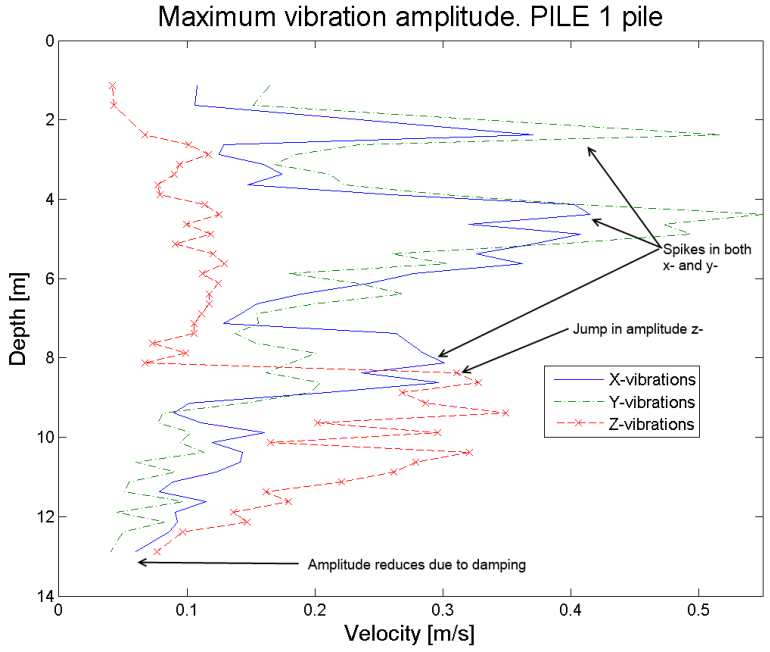

FIGURE 6.14: Maximum vibration amplitude for PS test on pile 1. x- is the blue full line, y- is the green broken and circled line, and z- is the red dashed and crossed line.

6.4 Results detections

Table 6.1[1] shows the results of the detection. The predictions are compared to the designed flaws in the right-hand column. By comparing the detected flaws to the designed flaws it is

[1]NS in the table stands for non-symmetric.

possible to asses how well the PS performed. A few improvements were realized in the second field test while still many weaknesses remained. The following observations can be made.

Pile number	**Predicted flaw**	**Depth [m]**	**Designed Flaw**	**Depth [m]**
1	Crack	3	Bulge	3
	Neck	8	Bulge	6
2	Bulge	6	Crack	3
			Bulge	6
4	Bulge	3	Crack	3
			Neck	6
9	Bulge	3	Bulge(NS)	8
	Crack	8		
10	Neck	4	Bulge	3
	Bulge	8	Neck	8
11	Bulge	4	Crack	3
	Bulge	8	Bulge(NS)	6
12	Crack	3	None	
	Bulge	6		
18	Neck	8	Bulge	3
			Bulge(NS)	8

TABLE 6.1: Detected flaws versus designed flaws.

- Using $25cm$ measurement increments allows for better interpretation of the results. The resolution is high enough to see the patterns created by the soil layering and small variations caused by the changes in the pile. In practice it takes about 90 minutes to set up and measure one pile. This is roughly 10 minutes longer than if $50cm$ increments are used. So the time loss is small while the gain in data is high.

- Finding the pile toe is done successfully. The pile toe can be seen in all the tests since it was shallower than expected and all measurements exceeded the toe.

  According to design, the piles are placed $12m$ below NAP which is about $10.4m$ below surface level. The toe of pile 8 was measured at $10.5m$ and of pile 13 at $10.35m$ below the surface. All the other pile toes are in a similar range, suggesting that the PS is indeed successful in locating the pile toe with less than 1.0% error.

- Using vertical vibrations is not successful in this field test. Even locating the pile toe is impossible. This resulted in untrustworthy data that is not used to detect flaws.

- Reflections are both present at flaws and soil layers. Reflections caused by the soil are seen in the results of all the PS tests while the reflections of flaws deviate between tests. Reflections do not help identify the shape of the flaw and have been measured in piles with cracks and bulges. In general if there are many more reflections with high amplitudes, there are flaws present.

- Although the simulations in chapter 4 suggest that using a.t as an indicator of flaws is difficult in heterogeneous soils, it still proved relatively useful. When waves arrive unusually early or late there is often a flaw.

  These variations do need to be very clear, small variations are often mistaken for flaws. Also the type of flaw remains unknown since the a.t is relative. In this field test, the variation of a.t is too small for flaws at $3m$ but clearer at $6m$ and $8m$ flaws.

- The amplitude variations are correlated to soil conditions which helps characterize the subsurface. Variations in amplitude however do not correlate with flaws. It often changes when there is no flaw. One exception is the bulge in pile 2 which is detected with the help of a jump in amplitude and a.t.

- For this site the soil conditions around 6-7m make the detection of flaws nearly impossible. There are small clay and peat layers followed by a stiff sand layer. This causes many variations in a.t and amplitude. Also many reflections of the sand layer disguise traces of flaws.

  At $3m$ reflections of flaws are often clear. The flaw is very close to the hammer impulse so the amplitudes are higher, including that of reflections. The heterogeneity is still however a big problem and often disguises flaws and their shape.

  All flaws at $8m$ are found. Only the definition of the flaw is wrong. At this depth the soil is much more homogeneous. Hence the effects of the flaws on the vibrations are much clearer than at shallower depths. For the field test the piles are only $10m$ deep. Although the soil heterogeneity is a smaller problem at this depth, the toe vibrations mask the shaft vibrations and still need to be taken apart.

Chapter 7

Validation of the Model

7.1 Introduction

Following the field tests, it is possible to use the results to validate the model from chapter 4. First the p-wave and s-wave test results can be used to see how well ScatMat simulates the field test. Secondly the total PS test results can be compared to the program.

7.2 Simulating the p- and s-wave tests

A large part of the program is the use of ScatMat that analytically simulates the propagation of elastic waves through layered soil. Part of the program discussed in chapter 4 is run according to the steps shown in figure 7.1.

7.2.1 Validating the p-wave test

The first simulation is to run a p-wave test. The main input for this simulation is the soil. The soil layering is defined according to table 4.7 shown in chapter 4. In this case a layer of loose sand fill ($0.48m$ thick) is added to the top since this is also present at the pile field. The properties of these soils are given in table 4.2. Furthermore the impulse hammer hit is simulated as a vertical impulse.

Figure 7.2 shows the resulting seismograph for vibrations in the radial (horizontal) direction. It is clear that the results are very different than from the field test. At $2.5m$ a clay layer is present that changes the wave completely. The results below this point do not compare to the results for the field test shown in figures D.10 or D.11. In addition the top layer also experiences

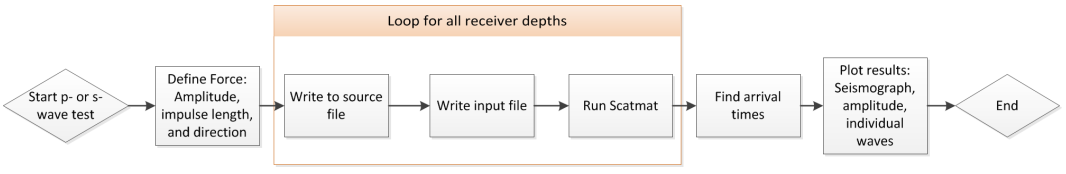

FIGURE 7.1: Simulation of the p- and s-wave tests.

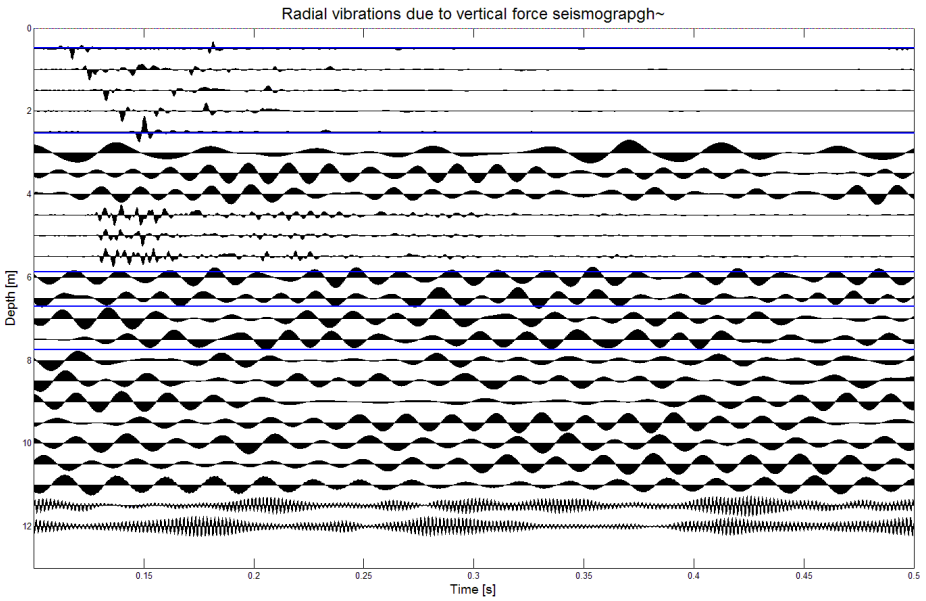

FIGURE 7.2: Simulation of the p- wave test in layered soil. The result shows that ScatMat has trouble calculating the vibrations in the layered soil.

reflections coming of the clay layer which are not seen in the field data.

It is clear the ScatMat program does not calculate the wave propagation correctly. The large changes in soil properties lead to strange results. The input for the program is based on a few highly varying soil types which complicates calculations and does not reflect the true properties of the subsurface. In reality the changes in soil properties are much more gradual which explains why there are fewer reflections seen in the top layer in the field test.

If the ScatMat program is run in a homogeneous clay layer, the results are much more realistic. Figures 7.3 and 7.4 show the simulated p-wave test. Also the amplitude follows a similar pattern to the field data, shown in figure D.12. The magnitude however is much smaller in the model. Amplitudes measured in the field test are two orders of magnitude larger.

7.2.2 Validating the s-wave test

The second simulation is the s-wave test. Again the same two simulations are run: layered soil and homogeneous clay. Only now the impulse is a horizontal forcing.

Figure 7.5 shows the resulting seismograph for layered soil and again proves that the simulation does not yield acceptable results. Figure 7.6 shows the resulting seismograph for homogeneous soil. This figure is very similar to figure D.4 and D.5 so again homogeneous simulations relate more to reality. Also the amplitude in figure 7.7 shows a similar pattern to the field test results.

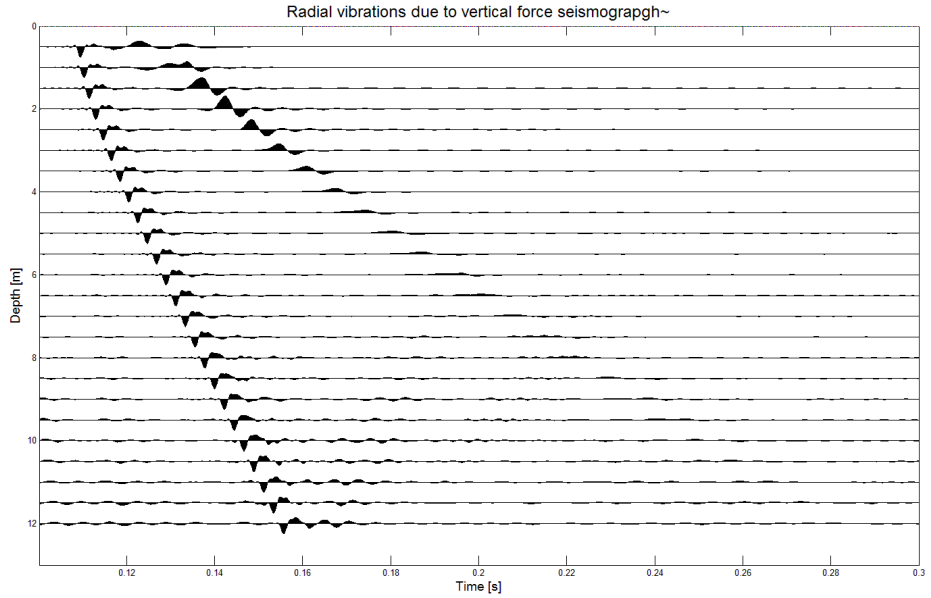

FIGURE 7.3: Simulation of the p- wave test in homogeneous clay.

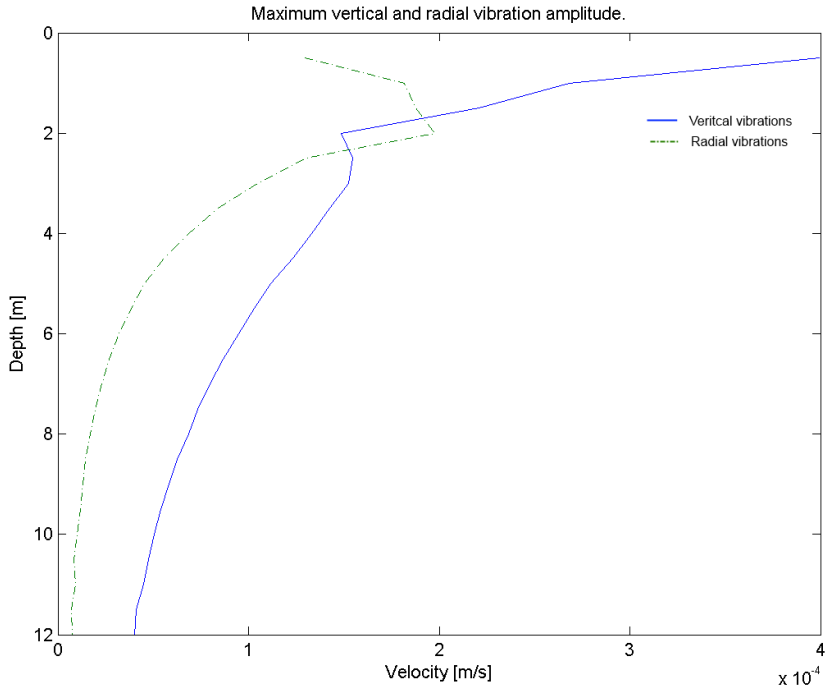

FIGURE 7.4: Amplitude of maximum vibrations of the simulated p- wave test in homogeneous clay.

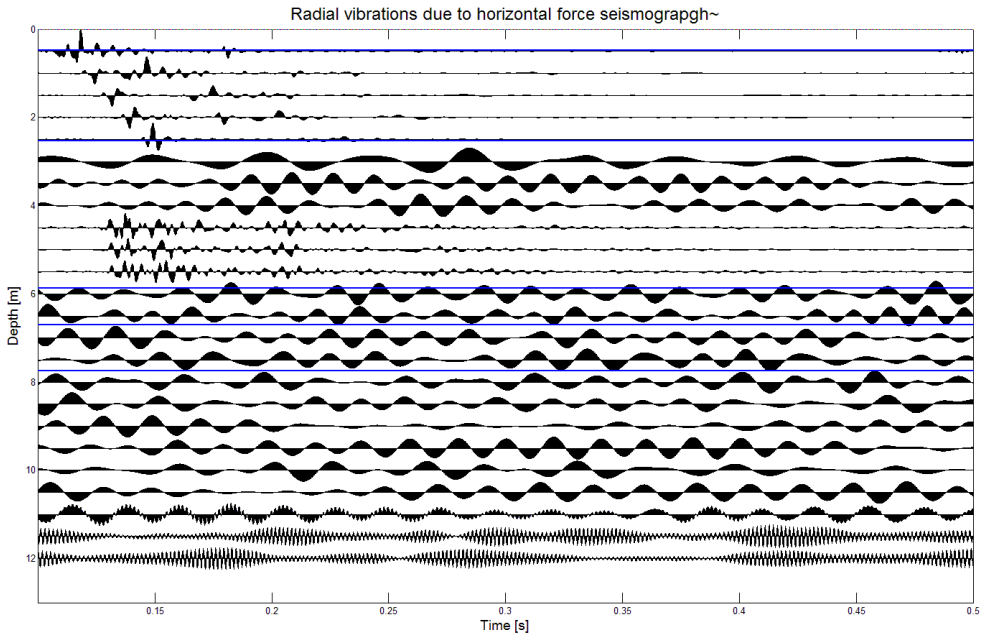

FIGURE 7.5: Simulation of the s- wave test in layered soil.

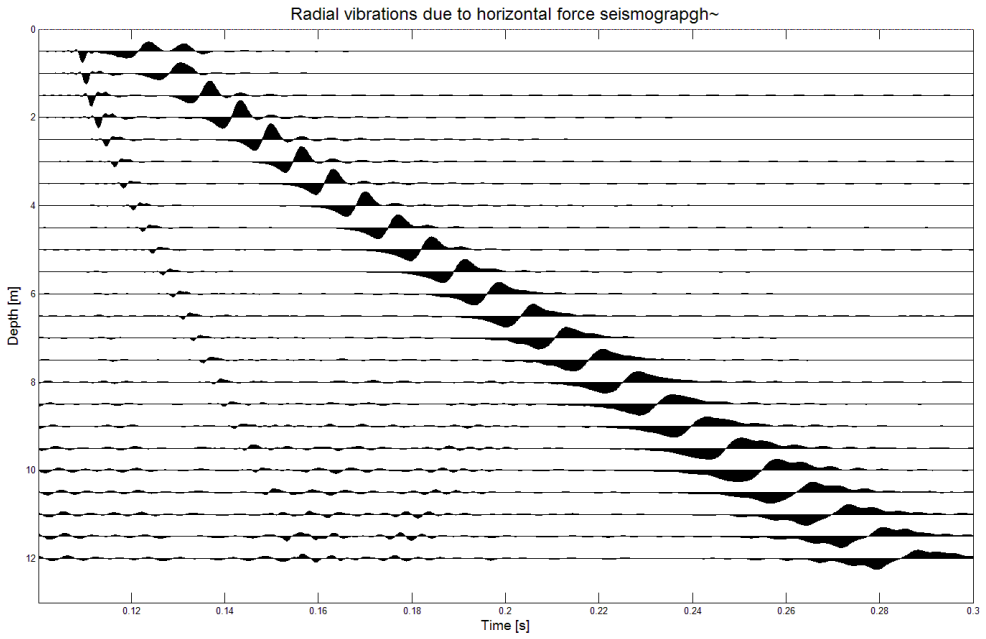

FIGURE 7.6: Simulation of the s- wave test in homogeneous clay.

The field test does however show more variations. Therefore modeling as homogeneous soils is not correct but does remain the better option.

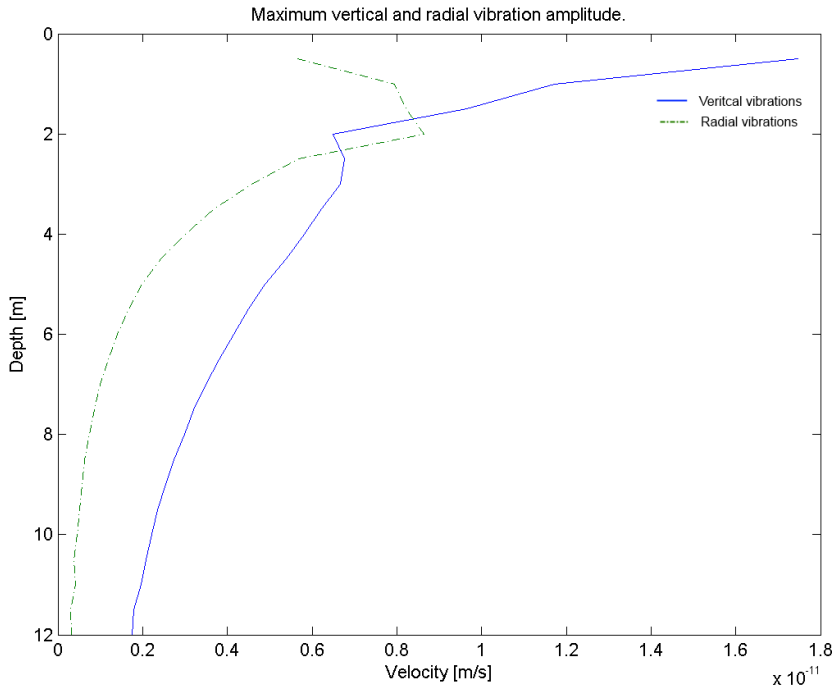

FIGURE 7.7: Amplitude of maximum vibrations of the simulated s- wave test in homogeneous clay.

7.3 Simulating the PS tests

Comparing the results of the field test can also help validate the full program from chapter 4. The results discussed in chapter 4 focus on the vibrations in the z-axis. In the field test this direction of vibration is either not measured or are disturbed by the bar that brings the receivers at depth. Therefore to correctly compare the model to the field test, the simulation of radial vibrations is discussed. Also, one of the assumptions mentioned in chapter 4 is that the pile is fully embedded in the ground. The piles used in the test are not fully embedded, this is taken into account when comparing results.

Figure 7.8 shows the radial vibrations calculated using the model for the scenario discussed in chapter 4. The soil layering and properties are given in tables 4.7 and 4.2. It is clear that these vibrations do not completely reflect reality. Waves arrive much earlier in the lower sand layer and differences across soil boundaries are very big. On the other hand both sets of results show reflections at similar depths, caused by the soil layers and pile toe.

Figure 7.9 shows the amplitude of vibrations. The amplitude of radial vibrations are about $1E-4m/s$. Amplitudes measured in the field test are much higher. The relative changes however are quite similar. There are peaks at soil boundaries and flaws.

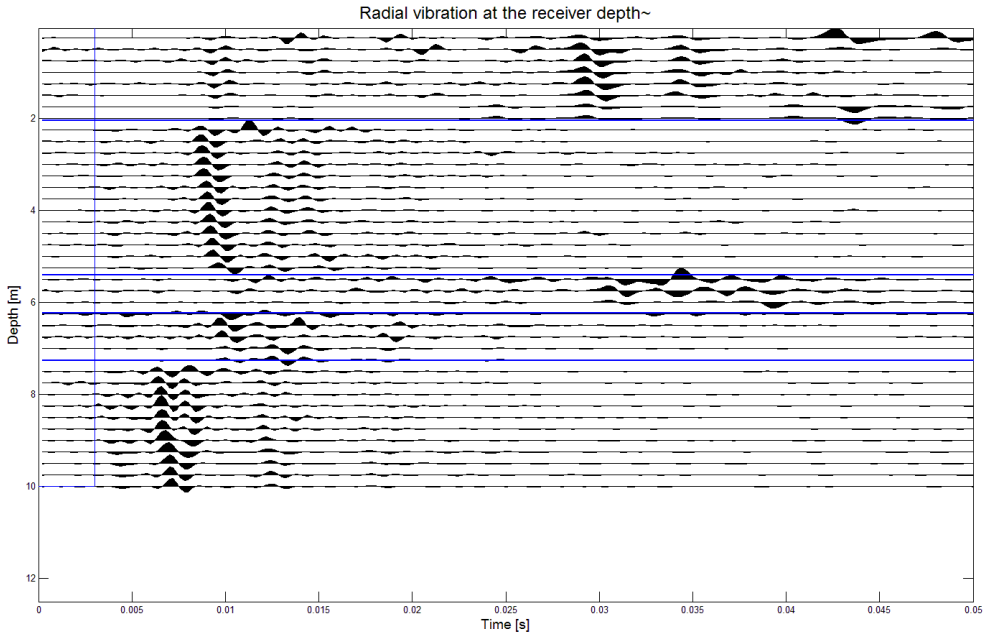

FIGURE 7.8: Simulation of the PS test in layered soil with according original soil properties taken from CPTs. This pile has no flaws.

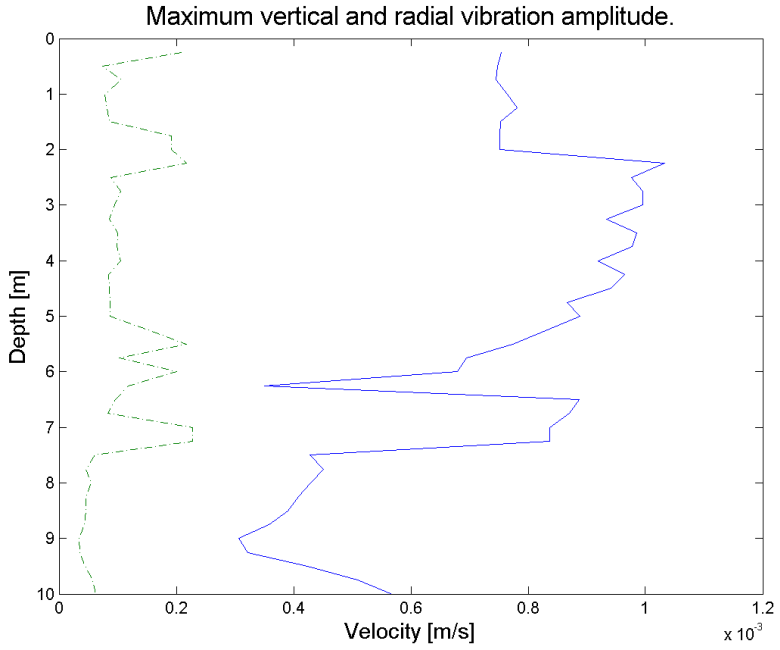

FIGURE 7.9: Amplitude of maximum vibrations of the simulated PS test with ground according to the original soil properties taken from CPTs. The dotted green line corresponds to radial(horizontal) vibrations which are measured in the first field test.

Changing soil properties and impulse magnitude

From the simulated s- and p- wave tests, it is clear that the simulations done for layered ground are exaggerated. This is reiterated in the results of the field tests and the simulation of the PS. Therefore, the first option to improve the model is to change the soil properties used. Also the input impulse magnitude is increased from $400N$ to $4000N$ which is more representative of the actual impulse.

Extending the domain and summing up vibrations from all depths

The results of the field test show that it is interesting to see how vibrations develop below the pile as well. It is possible to extend the model beyond the pile with a few changes in the code. This is done by adding receivers without including more sources.

It is clear that in the original model, that only calculates the vibrations originating from the pile at the same depth, that receivers below the pile toe will not show any vibrations. Therefore this simplification of the problem needs to be taken out, and the vibrations at the receivers need to be calculated for **all** sources. This will improve the reproduction of vibrations caused by the pile toe that propagate far above and below as shown in the results of the field test.

To sum up vibrations from all sources for each receiver should improve the results of the model. The downside is already mentioned in chapter 4. This will increase the calculation time, from about $10min$ per pile in a homogeneous soil to about $3hr$. Also, from the p- and s-wave tests it can be seen that this will also disturb the results in a layered soil.

7.3.1 Results of proposed changes

The model is re-run with the proposed changes. Due to the difficulties they bring when modeling heterogeneous soils, since ScatMat has trouble with this function, only homogeneous soil is used. In all simulations clay from table 7.1 is used.

The changed model is used to simulate three scenarios. The first is a flawless, $10m$ pile. The second and third are piles with either a bulge or a neck, at different depths.

Figures 7.10, 7.11, and 7.12 show the seismographs from radial vibrations. The results look a lot more similar to the results of the field test. A p-wave is measured around $0.02s$ with a very small amplitude. The s-waves have higher amplitudes, just like the results of the field test show. Furthermore, the pile toe is very clear. There is a reduction in a.t below the pile, and clearly there are many vibrations propagating from the toe, both upwards and down. The seismographs also shows many small vibrations at times where none are expected. This probably arises when ScatMat transforms the calculated vibrations from the frequency domain to the space-time domain.

The seismographs also show how hard it could theoretically be to find the flaws using radial vibrations. These models only account for homogeneous soils. The bulge shows an early arrival of the s-waves while the p-waves are too small to observe.

The maximum amplitude of simulated radial vibrations remains much lower than measured. The patterns however do follow that of the field test. The amplitude peaks at the pile toe, increasing already before the toe and reducing again after the toe. Also the amplitudes are again affected by the flaws. $1m$ above and $2m$ below the flaws show deviations. The amplitude plots may be found in appendix F.

Figures 7.13, 7.14, and 7.14 show the simulated vertical vibrations. Theoretically if the vertical vibrations were to be successfully measured, the results would look like the data in these seismographs. Here the flaws are very clear to see. Still this simulation is done in homogeneous soils, therefore the true results will not be as clear. These figures show the importance of being able to measure vertical vibrations without the disturbance from the cone or any other tools.

Soile Type	**G**$[Mpa]$	$\gamma[kg/m^3]$	**K**$[Mpa]$	**Damping**	**Depth** (m)
Peat	1	1100	12.6	2.1	0
Peat-Clay	2	1300	20.6	2	2.4
Clay	3.5	1600	34	1.9	2.9
Clay-Sand	6	1700	54	1.8	7.4
Sand	8	1800	75	1.8	7.9

TABLE 7.1: The soil profile at the field test site during the PS test.

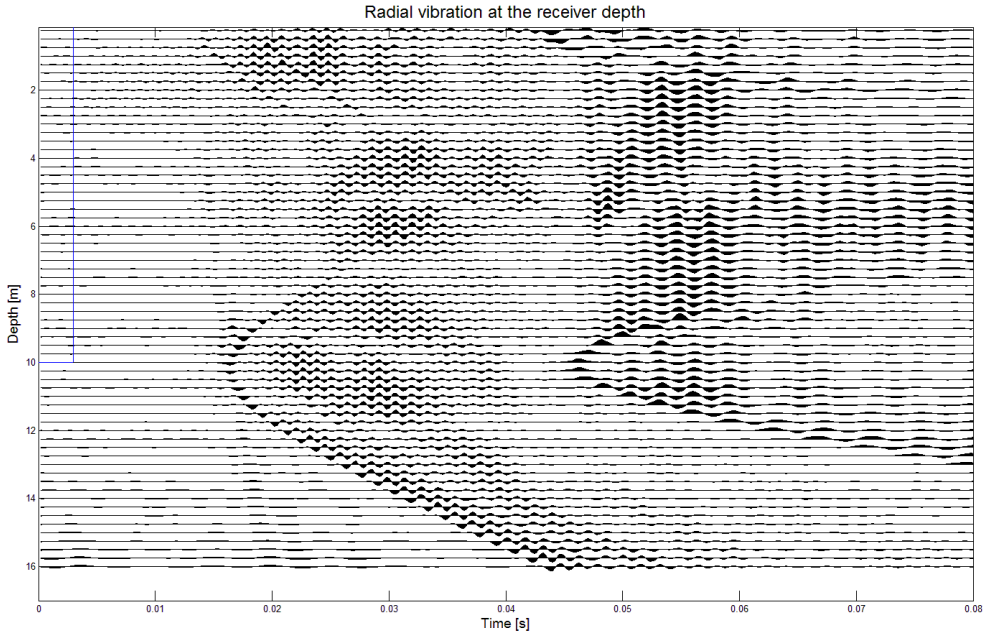

FIGURE 7.10: Simulation of the PS test in homogeneous soil, adding up vibrations from all sources per receiver. This pile has no flaws.

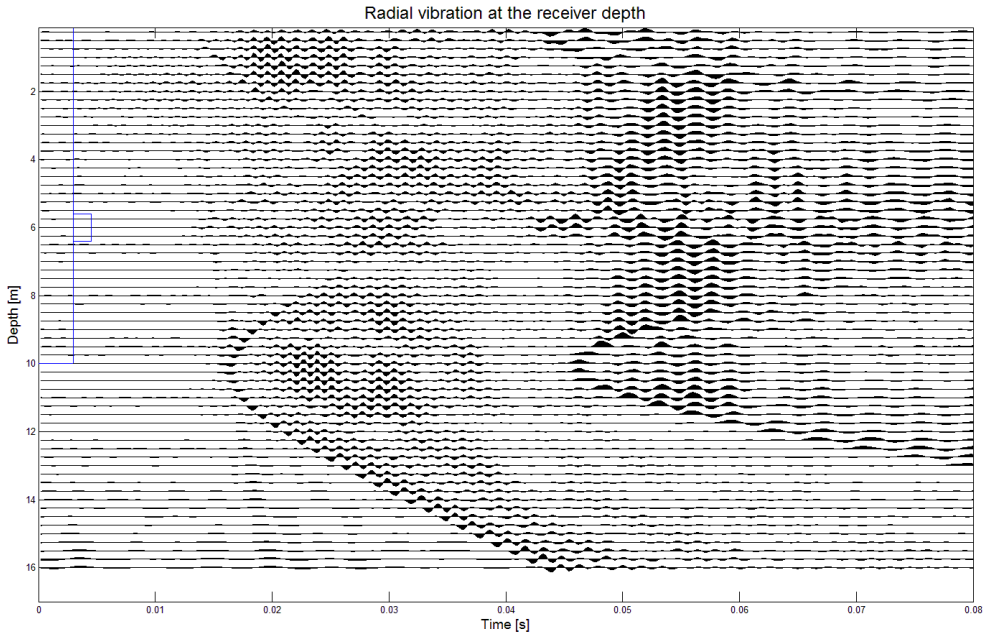

FIGURE 7.11: Simulation of the PS test in homogeneous soil, adding up vibrations from all sources per receiver. This pile has a bulge at $6m$ depth.

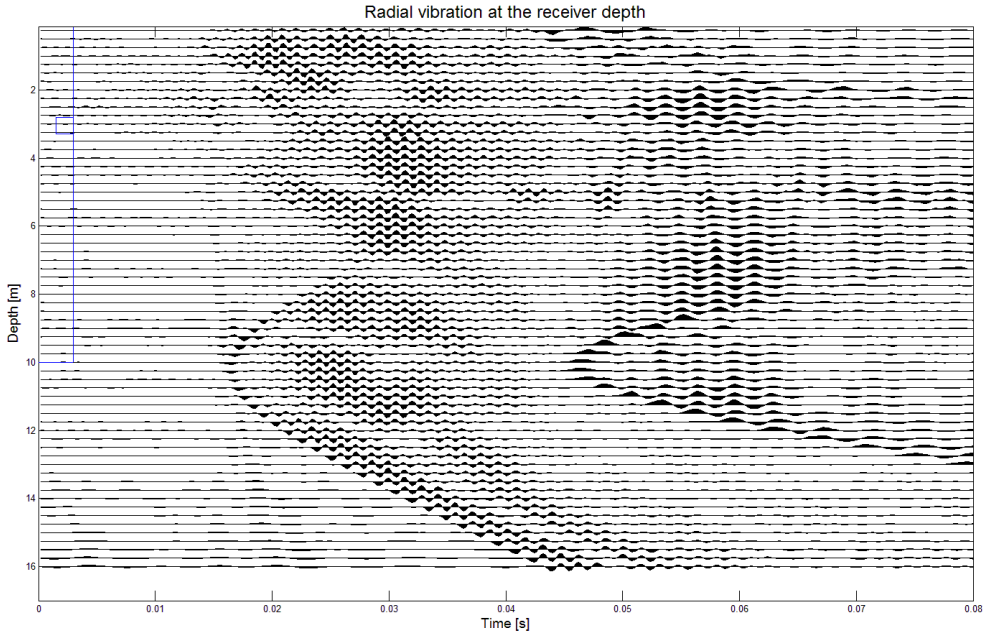

FIGURE 7.12: Simulation of the PS test in homogeneous soil, adding up vibrations from all sources per receiver. This pile has a neck at $3m$ depth.

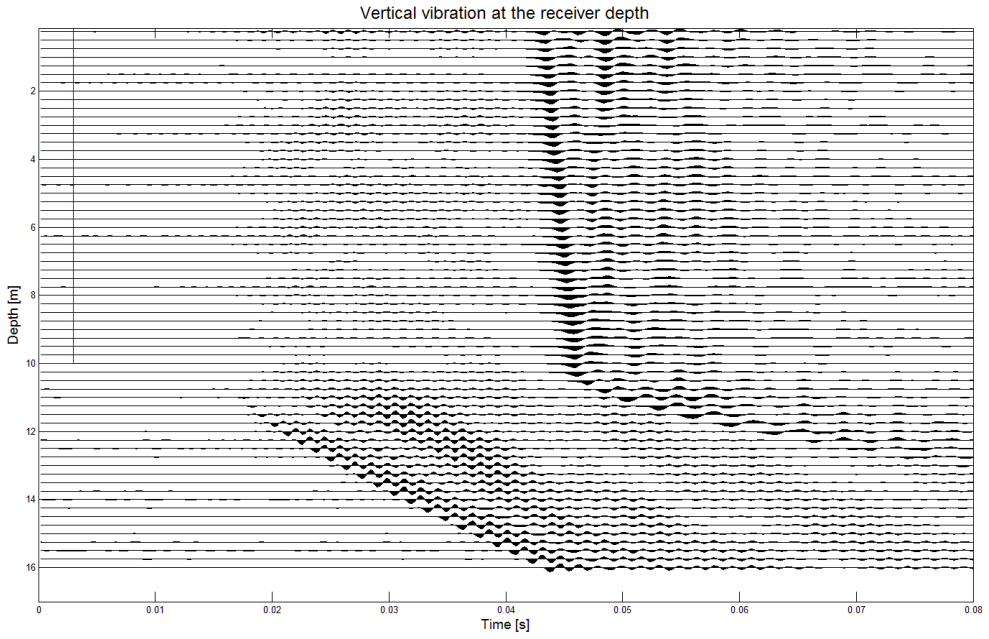

FIGURE 7.13: Seismograph of validated model of the PS test in homogeneous soil showing vertical vibrations, adding up vibrations from all sources per receiver. This pile has no flaws.

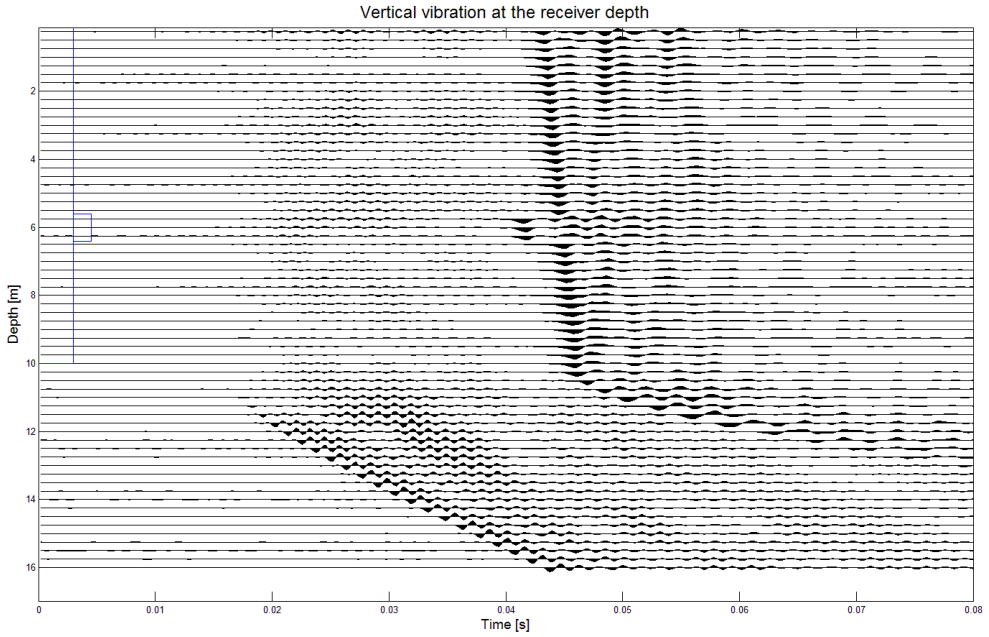

FIGURE 7.14: Seismograph of validated model of the PS test in homogeneous soil showing vertical vibrations, adding up vibrations from all sources per receiver. This pile has a bulge at $6m$ depth.

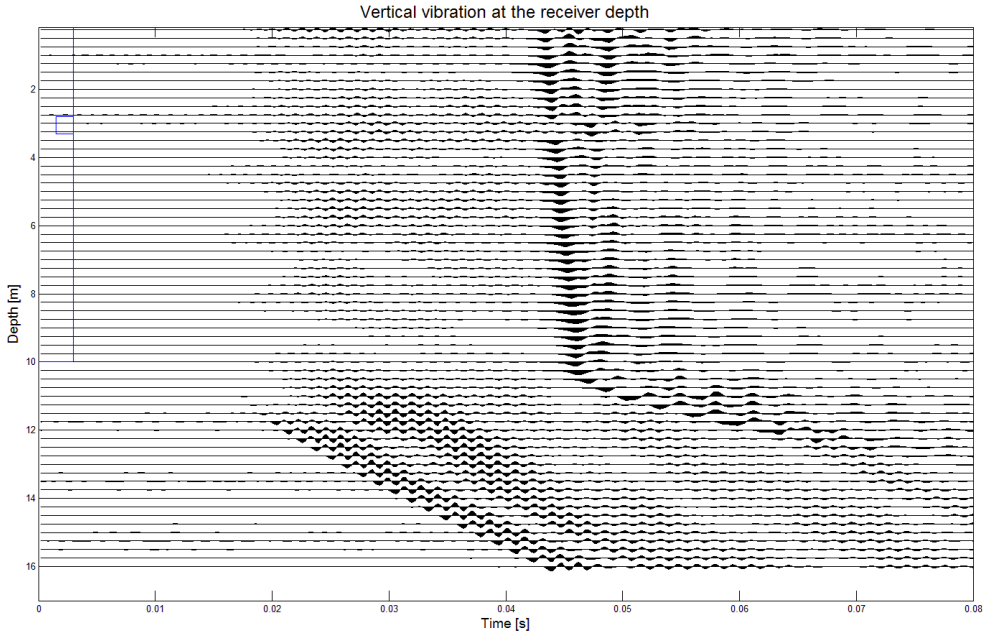

FIGURE 7.15: Seismograph of validated model showing vertical vibrations, adding up vibrations from all sources per receiver. This pile has a neck at $3m$ depth.

Chapter 8

Conclusions and Recommendations

8.1 Introduction

In this chapter the findings from the previous chapters are discussed. First the developed understanding of wave propagation in the soil is summarized. Following, the research questions stated in chapter 1 are restated and a small explanation of how these questions are answered is given. Subsequently, the main research question is answered. Finally possible improvements are suggested that may make the Parallel Seismic(PS) more successful and recommendations for further research are presented.

8.2 Wave propagation during the PS

To be able to use the PS to detect flaws it was important to develop a thorough understanding of the dynamics within the pile and soil domain. Figure 8.1 shows a simple schematic of the main vibrations that develop during the PS. The waves may be subdivided into three categories: surface waves, body waves from the pile shaft, and body waves from the pile toe. There are many other waves such as noise vibrations and reflections due to soil layering. These are often smaller in amplitude and may be filtered out if possible.

Surface waves: According to literature and the model, in the uppermost measurement depths, vibrations due to surface waves develop. This is also seen in the results from the field test, showing large amplitude vibrations propagating at relatively slow velocity.

Shaft body waves: The second category is body waves generated by the movement of the pile shaft. Theoretically, these vibrations may be used to determine the state of the pile. If a vertical compression impulse is placed on the pile head, the shaft will mostly radiate vertically oriented shear vibrations. If a horizontal impulse is used, shear waves travel down through the pile, thus radiating horizontally oriented p- and s-waves.

If there is a defect along the pile shaft, this should affect the shaft vibrations. Locally, the

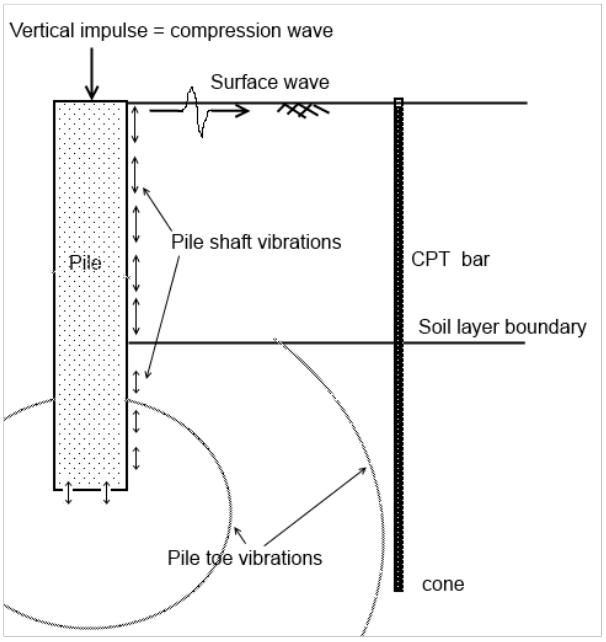

FIGURE 8.1: The figure shows the waves generated during the PS test due to a vertically induced impulse.

path of the waves change, thus changing arrival times. Furthermore the changing pile shape causes changes in amplitudes of vibrations and causes reflections. According to the model these changes are very small, and in practice they are very hard to see.

Toe body waves: The final category is body waves originating from the pile toe. The toe acts as a point source and radiates large amplitude vibrations in all directions. These waves include p-waves, horizontal s-waves, and vertical s-waves. This allows for easy detection of the pile toe.

8.3 Conclusions on the research

The main research question was to determine if it possible to use the PS method for detecting flaws in in-situ constructed foundation piles as an alternative to existing testing methods. To help answer this question, a few subquestions were formulated and answered in this thesis.

What is the current state of research on the use of PS?

From a literature study, the most recent developments of the PS were studied. Using the PS to find the pile toe is a common area of research. Using the PS to find flaws in constructions is however not very common.

A handful of researches have attempted to model the PS, either in computer programs or in small scale experiments. [Niederleithinger, 2012a],[Liao et al., 2005] These authors mostly

concluded that finding the pile toe can be done successfully while finding flaws is much harder. Even in homogeneous soils, small flaws may be missed. However being able to detect flaws is not completely ruled out.

What are the physics of sonic wave propagation in concrete piles and heterogeneous soils?

Research was done to understand the way vibrations theoretically propagate through piles and soil. This included wave behavior in different mediums, specifically concrete and soil, and at medium boundaries. Also, a study was done on the effects of damping.

The theory on vibrations in soils and piles was used for the following phases of the research. First the PS was simulated on the computer using the phenomena explained by the theory. Then the PS test was designed and the results were interpreted, making links between the measured vibrations and the theory.

What vibrations are measured if the PS is modeled on the computer?

In chapter 4 a model is explained that was made to simulate the PS and later validated and improved in chapter 7. An analytical approach was used to simulate an impulse on a flawed pile. The resulting vibrations radiated into the soil were calculated at receivers placed at multiple depths.

The results of the simulations show that vertical and radial (horizontal) vibrations can be measured at the location of the receivers. The amplitude of vertical vibrations is much higher than that of radial vibrations. In addition, near the toe, radial vibrations from the shaft are masked by vibrations originating from the shaft. This is less present in the vertical vibrations.

The simulation shows that using the PS in homogeneous soils to find defects is possible from the vertical vibrations. Small changes in arrival times and amplitudes of vibrations show the location and type of flaws.

If the soil is layered, detection of flaws was much harder. Both amplitude and wave speed is affected by soil properties, therefore heterogeneity can mask the presence of flaws.

To be able to find the flaws in heterogeneous soils, the model highlights the importance of knowing the ground conditions. This makes it possible to discern changes in results caused by soil layering or by flaws.

What vibrations are measured if the PS is performed in a field test?

A field of piles with designed flaws was installed and the PS was done on a few piles. In total 14 piles were tested in two rounds, measuring vibrations in three directions.

Vibrations could be measured in the horizontal and vertical directions. Horizontal vibrations propagated through the soil from the pile. Vertical vibrations propagated mostly through the bar of the CPT[1] which made these vibrations useless for detecting defects.

Vibrations radiating from the toe could be clearly measured in the field test. Both p- and s- waves propagate above and below the toe. As shown in figure 8.1 the results shows that the waves propagating upwards from the pile toe do not pass the clay-sand boundary at $8m$.

Other vibrations that could be measured were reflections from soil layering and very subtle shaft vibrations. Surface waves could be seen at measurements done near the surface.

Is it possible to find the designed flaws from a field test?

From the field tests and model became clear that a combination of amplitudes, arrival times, and reflections seen in the results need to be used to detect defects. Due to the variations in soil properties the measured vibrations change a lot with depth. These variations form a pattern seen in the results of all the pile test. To find any defects, the deviation from this pattern in measurements should be identified by comparing results from all the piles to eachother. Knowledge of the local soil profile is necessary as well.

Detecting flaws was not fully successful. Only one pile was completely correctly accessed and only one flaw was correctly found and characterized.

The main reasons why the flaws were not detected were already seen in the model. Changes in ground conditions have more affect on the measurements than flaws. This masks changes caused by the flaws. Also shaft vibrations were hardly measured. Most vibrations measured originated from the pile toe or ground surface.

In which conditions is the PS useful and what are its weaknesses?

The results of the detection with the PS vary per scenario. It depends on the soil conditions around the flaw, the characteristics of the flaw, and the location of the flaw in the pile.

In general flaws at $8m$ depth were easier to detect than shallower flaws. Therefore the PS is probably a good option for inspecting piles that are founded at depths exceeding $8m$ which is very common in the Netherlands if it is possible to discern toe vibrations from shaft vibrations.

[1] A Cone Penetration Test apparatus was used to bring the geo phones down.

Cracks created large reflections that could be seen in seismographs while necks hardly caused the expected delays in arrival times. A flaw is also much harder to detect if it is smaller or if the flaw is non-symmetric.

For the second field test an extra test was done to see how well the PS may detect the pile toe. This was done very well, with only about 1% error[2].

8.3.1 Answering the main research question

From the results of the field test it was not possible to detect flaws in the foundation piles using the PS. The procedure did not sufficiently measure the vibrations radiated from the pile shaft while avoiding interference from other vibration sources or soil heterogeneity.

As mentioned above, the vibrations originating from the pile toe and the ground surface have a relatively large amplitude. Also they may be measured along the shaft of the pile. These vibrations may then mask the vibrations radiated from the shaft and any present flaws. This problem is seen in both the model and field test results.

The model also shows that if all other vibrations are ignored, and only shaft vibrations are considered, detection is still difficult. If for example a defect is too small, vibrations are simply received from around the defect, masking the presence of the defect. Another example is the effect of the heterogeneity, which causes similar results as a defect would.

The model suggests that the best way to measure the shaft body waves is to measure vertical vibrations if a vertical compression impulse is used as acoustic source. In the field test this is attempted but failed due to the apparatus chosen. The bar that is used to bring the receivers at depth acts as a medium for the vertically vibrating waves, resulting in a misrepresentation of the vibrations in the soil.

Alternative non destructive testing methods are not more successful, so developing the PS is still a promising initiative. The model has proven that changes to the procedures of the PS might provide better results. These changes should reduce the vibrations from the pile toe, making shaft vibrations clearer. Some options are presented in the next section.

8.4 Recommendations to improve the PS

An objective of Geoimpuls, the initiator of this research is to develop techniques to successfully detect flaws in foundations. Although detection of flaws with the PS was not yet successful,

[2]The error is equal to $\frac{true\ pile\ length - measured\ pile\ length}{true\ pile\ length} \times 100$

there are a few options available to improve the procedure and possibly increase the success of detection:

- The PS test should include useful measurements of vertical vibrations. According to the theory, vertical vibrations from the shaft should be the easiest to see. However, in this research, the PS was done with a penetration bar that interfered with the vertical vibrations.

  To be able to use vertical vibrations, it is necessary to bring the receivers at depth without the use of a connected cone. This could be a bore-hole filled with water or bentonite or lined by a tube, in which receivers are lowered down.

  An alternative is to use an unconnected cone. If the cone is only connected to the rest of the bar via wires to transmit data, the bar will not interfere. This might be possible if the cone is first pushed down to the largest depth and then pulled up step by step for each measurement. The receiver is then pulled up by wires and a small space is left between the receiver and the bar.

  A downside to the alternative method is that the connection between the soil and the cone might not be rigid, reducing the effectiveness of the geophones. If this is the case, the cone needs to increase in diameter before returning up to ensure a good connection between soil and cone.

- The PS test should include knowledge of the exact location of the receiver. Measuring the inclination of the cone/bore-hole to compensate for the changing distance of the receiver to the pile will improve interpretation of the results. Part of detection is based on the arrival time, which is directly affected by the distance of the receiver and the pile.

- The PS test results should include the orientation of the x-,y-, and z- vibrations w.r.t the pile location. If the orientation of the receiver is known, interpretation of the wave type will be improved.

  By overlaying the three signals and comaparing the amplitudes it is possible to deduce the direction of vibrations and direction of propagation w.r.t to the x-y-z orientation. This will separate upwards propagating toe vibrations from horizontally propagating shaft vibrations.

- The PS test should present the most likely pile conditions. This could be done with the help of probabilistic methods to give the probability of certain flaws, and ultimately the reliability of the pile.

8.5 Recommendations for further research

Following the research done in this thesis, many issues can be raised for further research. Some of these issues are useful to improve the PS method for detection of flaws. Others are interesting to improve the understanding of vibrations in foundations and soils.

8.5.1 Research towards the development of the PS

The following research could be useful to improve the detection of flaws with the PS.

- A numerical model as opposed to the analytical one in this thesis could be developed. This will help increase the understanding of the PS since more complicated problems with heterogeneous soil conditions could be solved. The results of the field test show that the vibrations in the soil are very complicated with many sources and wave paths.

- Finding the arrival times of waves automatically could speed up data processing. Therefore it is recommended to develop computer aided methods to locate wave arrivals.

- Another good development is a computer aided method for quick comparison of results. In this thesis each pile was individually observed and compared to other piles by eye. This will be faster if it is done using computer algorithms that compare signals for each depth and each pile.

- Further research could be done into different impulse frequencies. The impulse frequency affects the propagation properties of the vibrations. For example, a low frequency impulse will travel further while a high frequency impulse will be more precise.

- An opportunity to increase the understanding of the PS results is to know the exact orientation of the vibration sensors.

- The conclusions drawn in the thesis are based on the assumption that the piles are installed according to design. This includes the designed flaws and pile toe. To complete the study, at least a few piles need to be pulled out to compare the pile design to the true pile properties.

- The reinforcement in piles is not always as long as the concrete. It could be interesting to test the PS on piles with changes in material properties. This will help determine if the vibrations measured travel through the steel reinforcement or through the concrete.

- Lab testing of scale piles in layered soil could be done as further research. If the PS could be done in a more controlled environment, the following questions could be answered:

    1. Is it possible to cancel out the vibrations from the pile toe?
    2. How big does a defect need to be to be seen?
    3. Where in the seismograph can the reflections of pile defects be found?

8.5.2 Research towards the understanding of vibrations in foundations and soils

The following topics could be of interest to improve the understanding of sonic waves in foundations and heterogeneous soils.

- Research on the prorogation of sonic waves is dependent on the soil type will help understand where vibrations originate and how they should be interpreted.

- In the PS, the local wave velocities are used to justify changes in arrival time. It became clear that the correlations between CPT tests and sonic wave speeds are unclear and site specific. The soil wave velocity tests are relatively easy to perform, and developing improved interpretation techniques will increase the accuracy of measured shear wave velocities.

- From the field test, the propagation of vibrations in the bar was seen. For other non destructive tests or soil wave velocity tests, it could be interesting to research how waves propagate through a steel bar in the ground that encounters changes in surrounding soil properties.

- Seismic data often includes a lot of noise, masking the desired data. Filtering is often done based on the frequency of the signal, with the assumption that the desired vibrations have another frequency than the noise. In this thesis, the signal and noise frequencies were very similar (around $55Hz$). Understanding the noise sources and the affect of soil type on the frequency of vibrations will improve filtering techniques.

Appendix A

Appendix: Simulation of the Parallel Seismic Test

A.1 Introduction

In this appendix, figures regarding the model from chapter 4 are presented. First a flow chart is shown that shows the connection between the main model and the program written by Paul Holscher to simulate vibrations in a flawed pile. Then results from the scenario study done in chapter 4 are shown.

A.2 Structure of the simulation

Figure A.1 shows the steps taken to implement the *Deep acoustic check* model in the main program. Using pile dimensions and soil properties, the script is run and the output is the vibration of the pile at each source depth. This is translated to forcing on the surrounding soil using the spring and dash pot system explained in chapter 4.

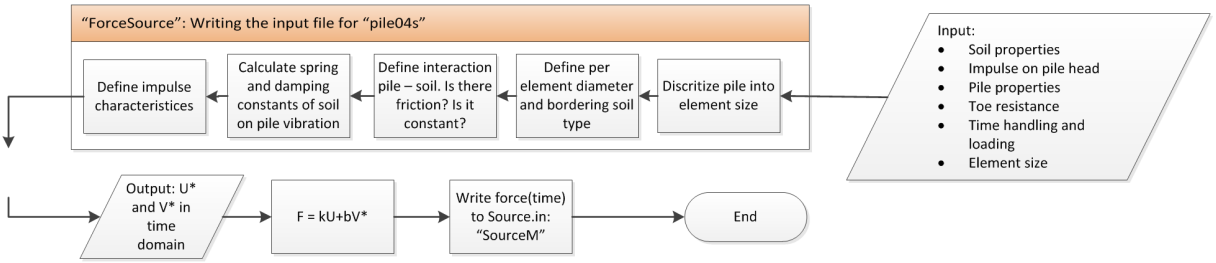

FIGURE A.1: Structure of the altered script written by Paul Holscher for deep acoustic checks of piles. $*U$ and V are the local displacement and velocity of the pile. F is the force on the neighboring soil which depends on k, the spring constant, and c, the dash-pot constant.

A.3 Scenario study

In this section the results of the scenario study mentioned in chapter 4 are presented. First the results of a flawless pile in homogeneous soils are presented. This is followed by the results of a

pile with a flaw in homgeneous soils.

A.3.1 Homogeneous soil and no flaw in the pile

The following figures are results of simulating a flawless pile in homogeneous soil conditions.

Simulation of a flawless pile in a homogeneous clay layer

Figure A.2 shows the prominent frequencies of vibrations at the receiver between $3.25m$ and $4.00m$ deep. Figure A.3 shows the maximum amplitude of vibrations at the each receiver depth.

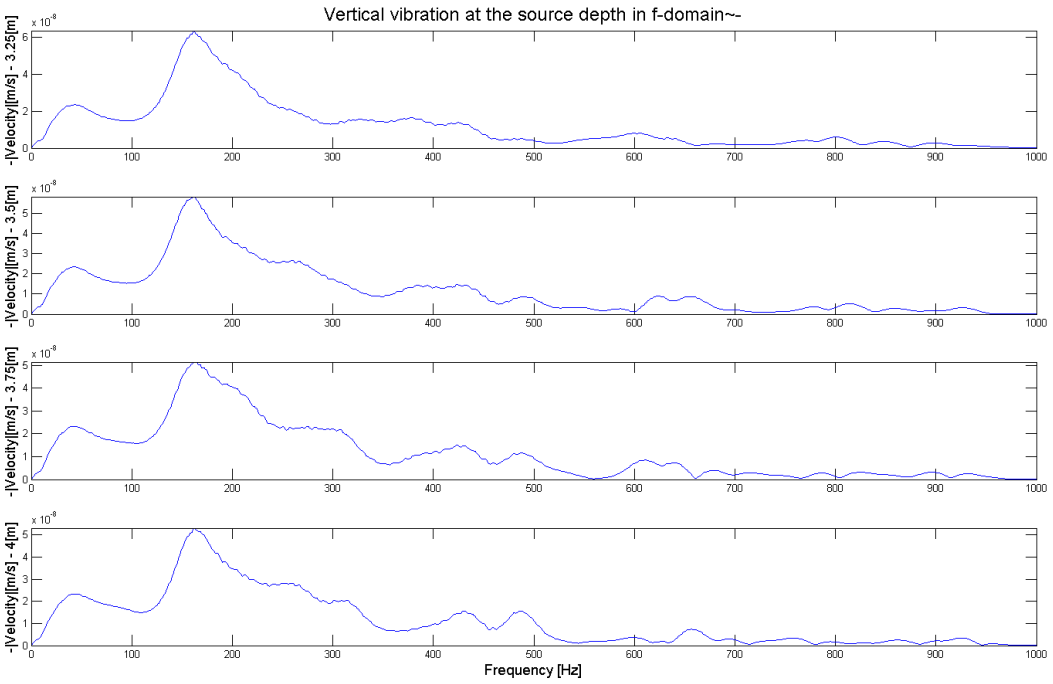

FIGURE A.2: Vibrations in receiver depths $3.25m$ to $4m$ in homogeneous clay layer. The prominent frequency range is around $150Hz$.

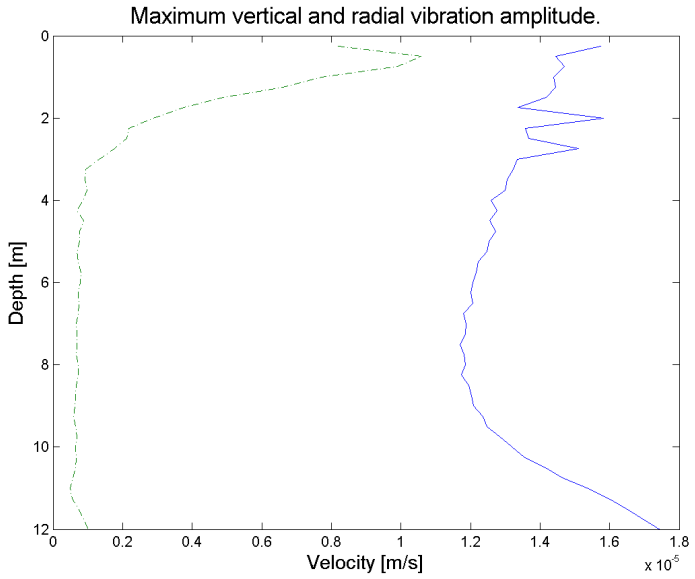

FIGURE A.3: Maximum vibration amplitude. The maximum velocity at $5m$ is around $1.2 \times 10^{-5} m/s$.

Simulation of a flawless pile in a homogeneous sand layer

Figure A.4 is the seismograph resulting from the simulation of an intact pile in sand. Figure A.5 is the forcing in the time domain simulated on the soil. Figure A.6 shows the prominent frequencies of vibrations at the receiver between $3.25m$ and $4.00m$ deep. Figure A.7 shows the maximum amplitude of vibrations.

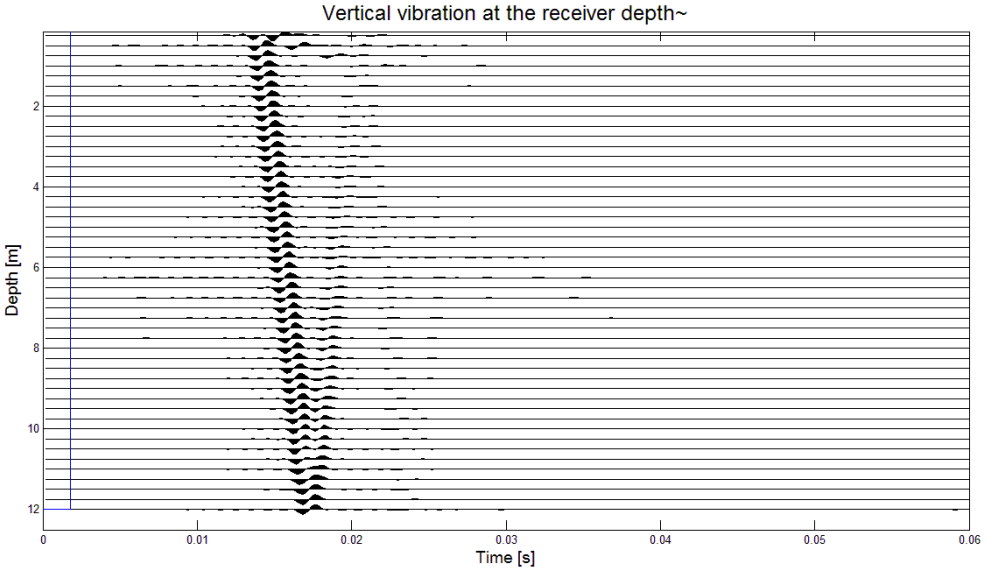

FIGURE A.4: The seismograph calculated for an intact pile in homogeneous sand layer.

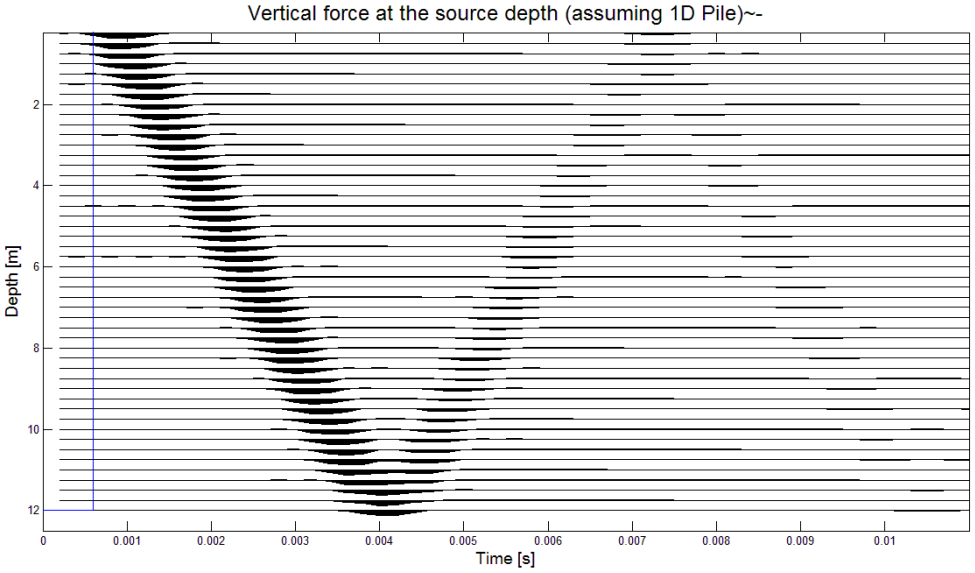

FIGURE A.5: The force per source calculated for an intact pile in homogeneous sand layer, showing reflection of vibrations within the pile. The amplitude of the waves are corrected for depth so damping in the pile cannot be seen in this figure.

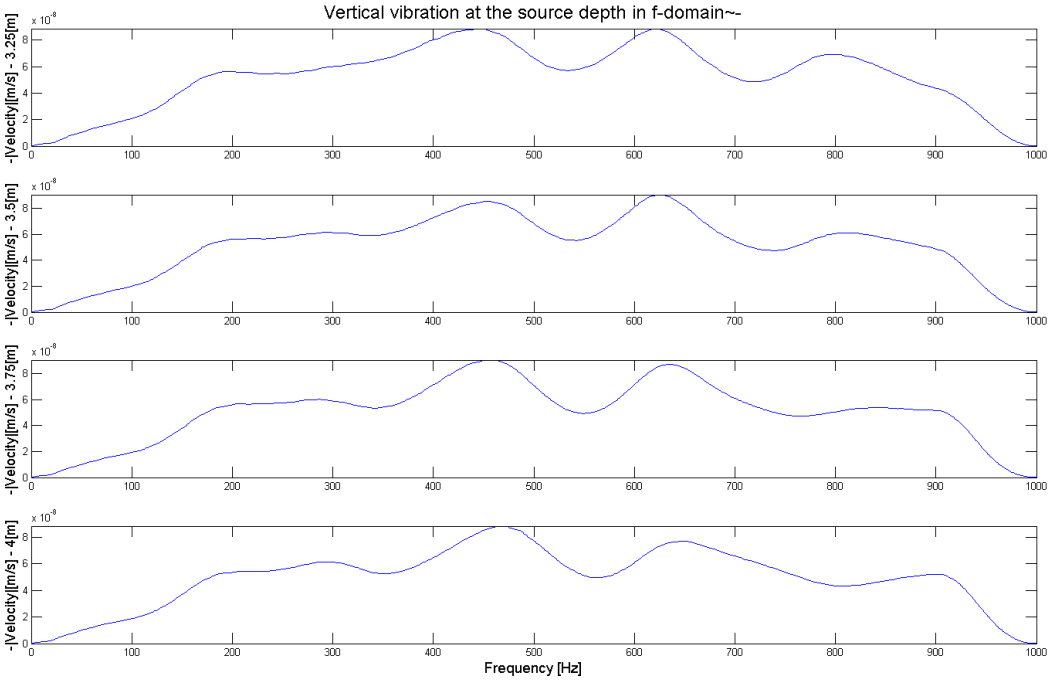

FIGURE A.6: Vibrations in receiver depths $3.25m$ to $4m$ in homogeneous sand layer. The prominent frequency range is around $450Hz$.

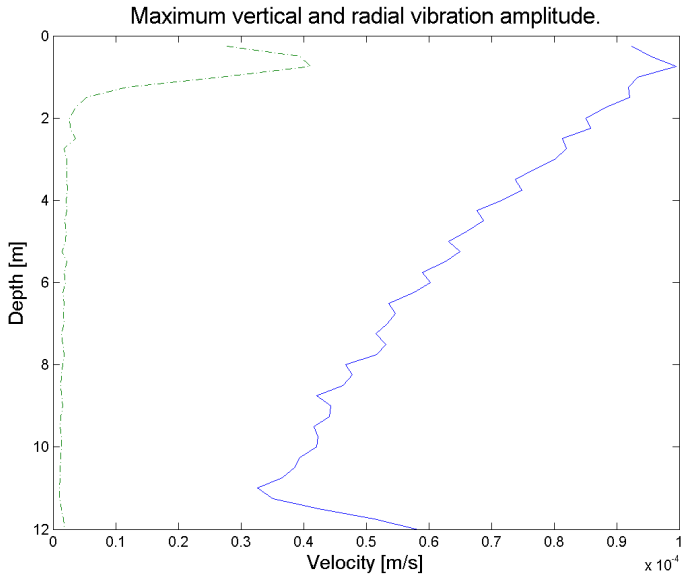

FIGURE A.7: Maximum vibration amplitude. The maximum velocity at $5m$ is around $6 \times 10^{-5} m/s$.

Simulation of a flawless pile in a homogeneous peat layer

Figure A.8 is the seismograph resulting from the simulation of an intact pile in sand. Figure A.9 is the forcing in the time domain simulated on the soil. Figure A.10 shows the prominent frequencies of vibrations at the receiver between $3.25m$ and $4.00m$ deep. Figure A.11 shows the maximum amplitude of vibrations.

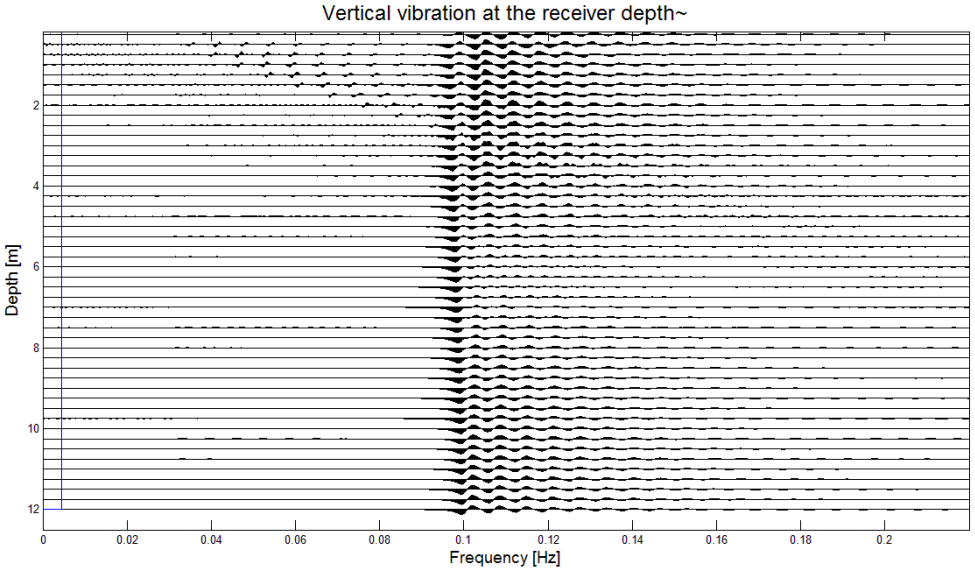

FIGURE A.8: The seismograph calculated for an intact pile in homogeneous peat layer.

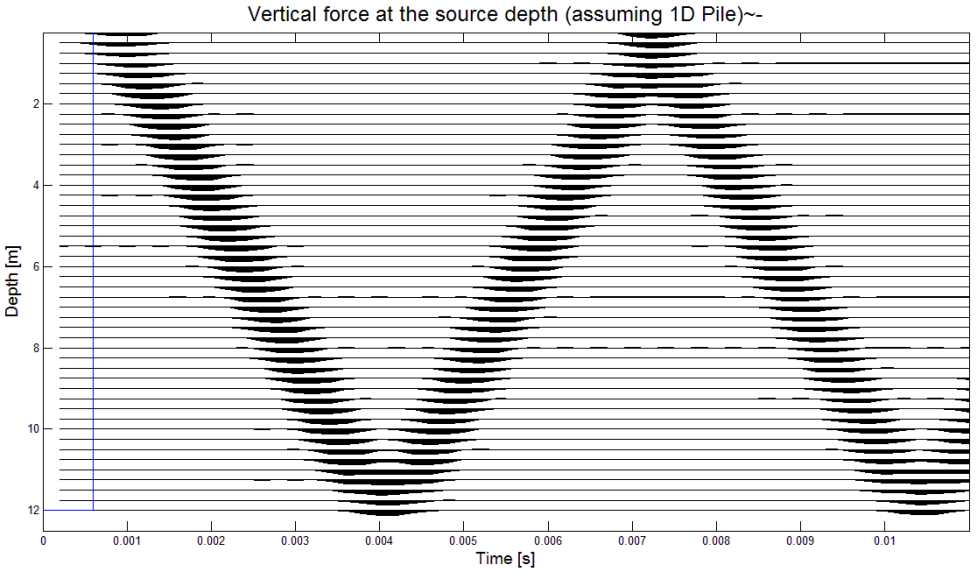

FIGURE A.9: The force per source calculated for an intact pile in homogeneous sand layer, showing reflection of vibrations within the pile. The amplitude of the waves are corrected for depth so damping in the pile cannot be seen in this figure.

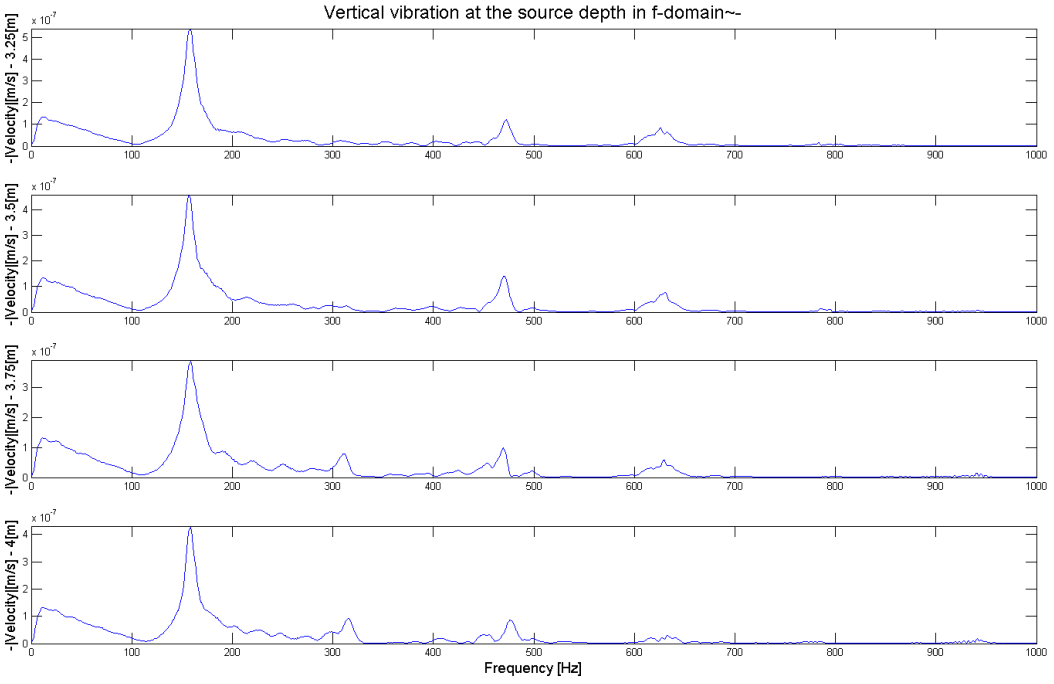

FIGURE A.10: Vibrations in receiver depths $3.25m$ to $4m$ in homogeneous peat layer. The prominent frequency range is around $150Hz$.

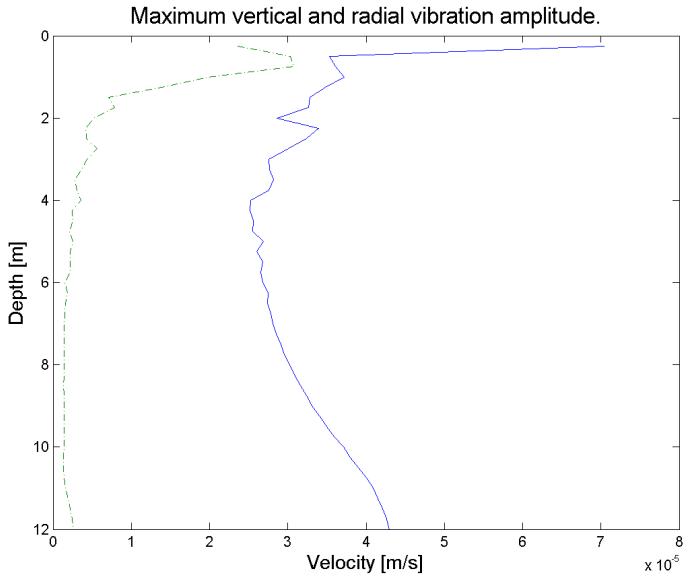

FIGURE A.11: Maximum vibration amplitude. The maximum velocity at $5m$ is around $3 \times 10^{-5} m/s$.

A.3.2 Homogeneous soil and a neck in the pile

The following results are simulations of a pile in homogeneous soil conditions with a neck at $6m$ depth.

Simulation of a pile with a neck in a homogeneous clay layer

Figure A.12 shows the resulting force as a function of time from the PS simulation on a flawed pile in a homogeneous clay layer.

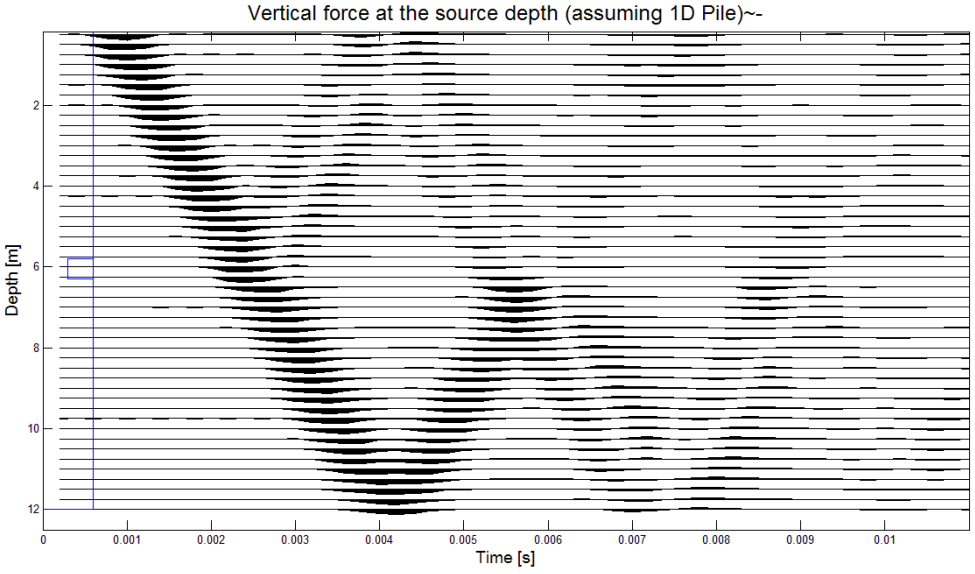

FIGURE A.12: The force per source calculated for a pile in homogeneous clay layer with a neck at $6m$, showing reflections of vibrations within the pile.

Simulation of a pile with a neck in a homogeneous sand layer

In the figure A.13 the seismograph from the PS simulation on a flawed pile in a sand layer is shown. Figure A.14 shows the resulting force as a function of time. The development of amplitude is given in A.15.

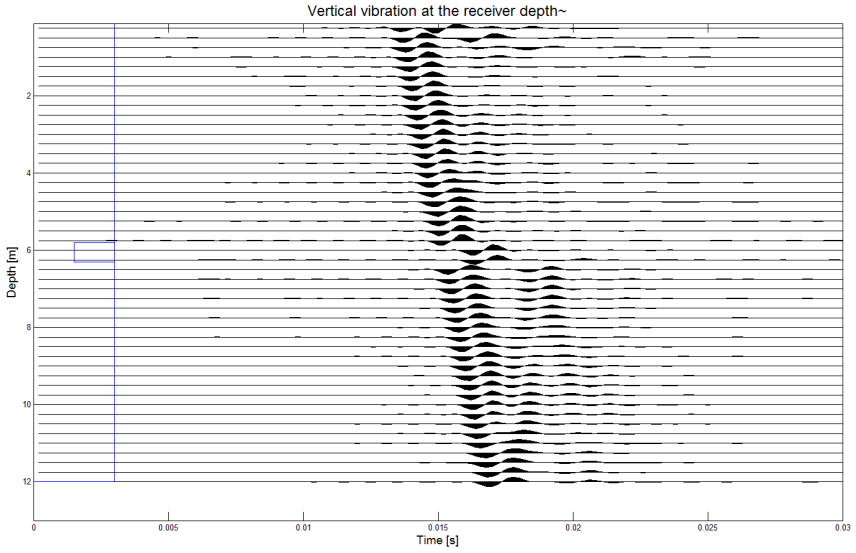

FIGURE A.13: The seismograph calculated for a pile in homogeneous sand layer with a neck at $6m$.

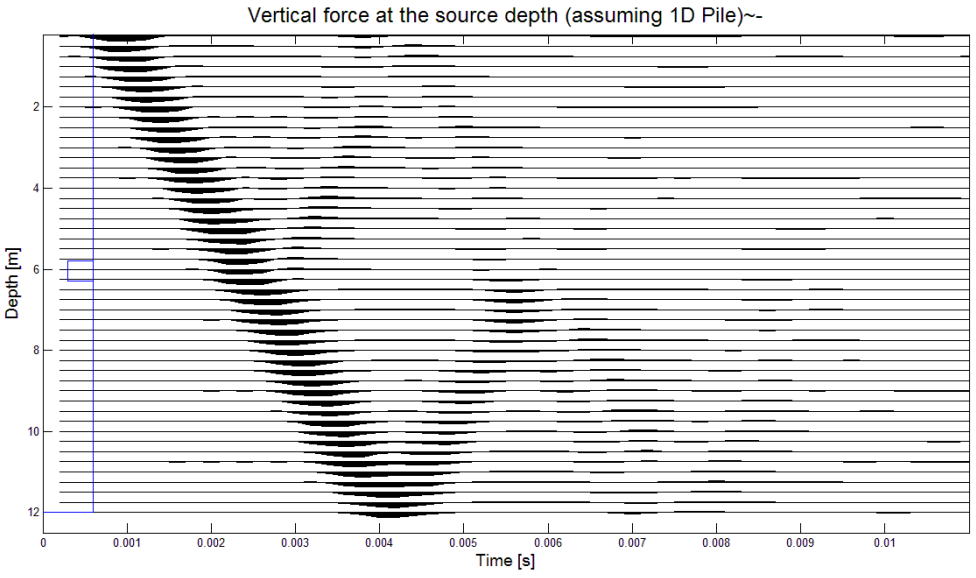

FIGURE A.14: The force per source calculated for a pile in homogeneous sand layer with a neck at $6m$, showing reflections of vibrations within the pile.

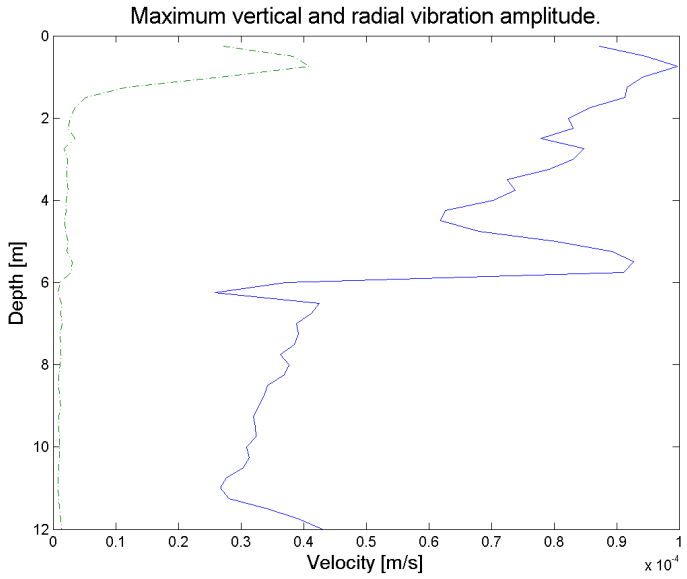

FIGURE A.15: The maximum amplitude of vibrations in the soil calculated for a pile in homogeneous sand layer with a neck at $6m$.

Simulation of a pile with a neck in a homogeneous peat layer

In the figure A.16 the seismograph from the PS simulation on a flawed pile in a peat layer is shown. Figure A.17 shows the resulting force as a function of time. The development of amplitude is given in A.18.

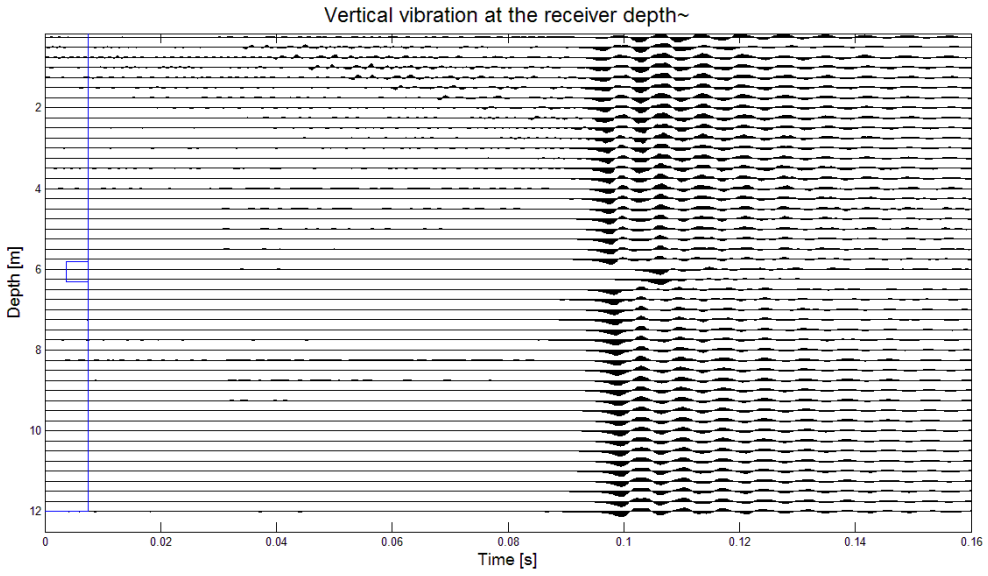

FIGURE A.16: The seismograph calculated for a pile in homogeneous peat layer with a neck at $6m$.

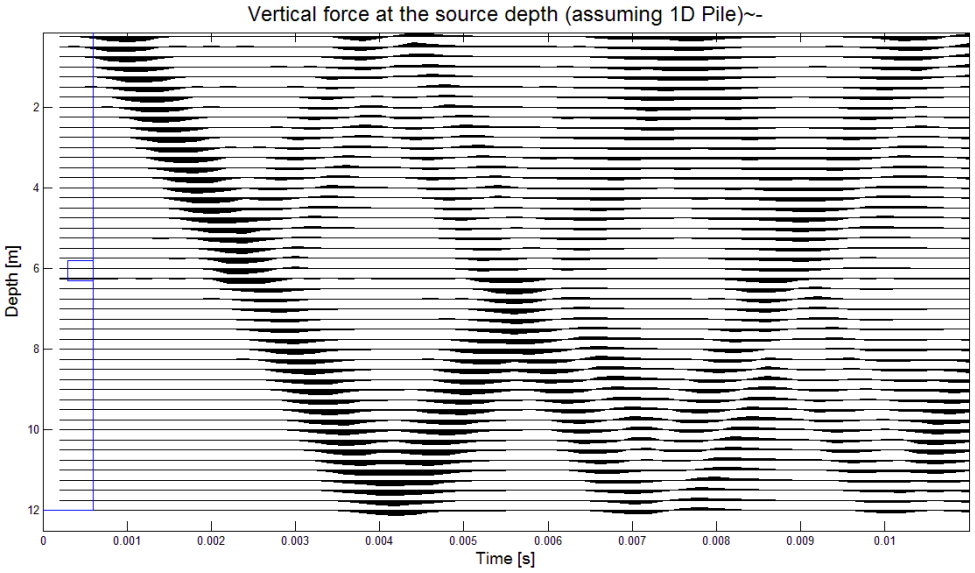

FIGURE A.17: The force per source calculated for a pile in homogeneous peat layer with a neck at $6m$, showing reflections of vibrations within the pile.

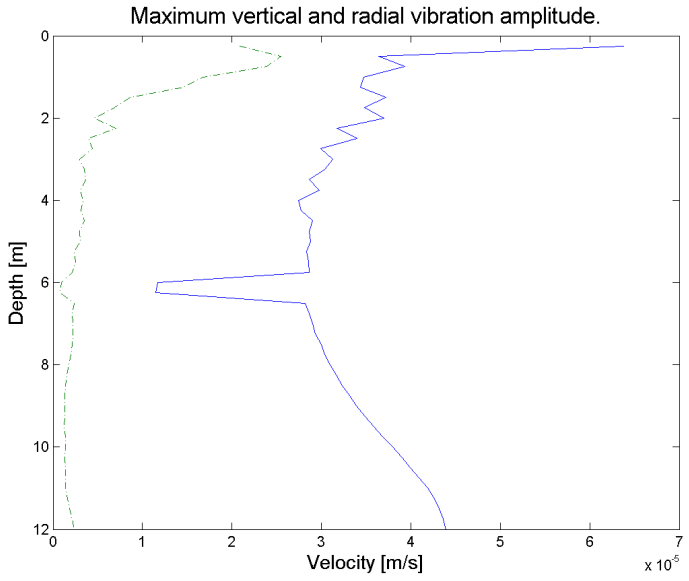

FIGURE A.18: The maximum amplitude of vibrations in the soil calculated for a pile in homogeneous peat layer with a neck at $6m$.

A.3.3 Homogeneous soil and a bulge in the pile

The following results are simulations of a pile in homogeneous soil conditions with a bulge at $6m$ depth.

Simulation of a pile with a bulge in a homogeneous clay layer

In the figure A.19 the seismograph from the PS simulation on a flawed pile in a clay layer is shown. Figure A.20 shows the resulting force per pile element as a function of time. The

amplitude as a function of depth is given in A.21.

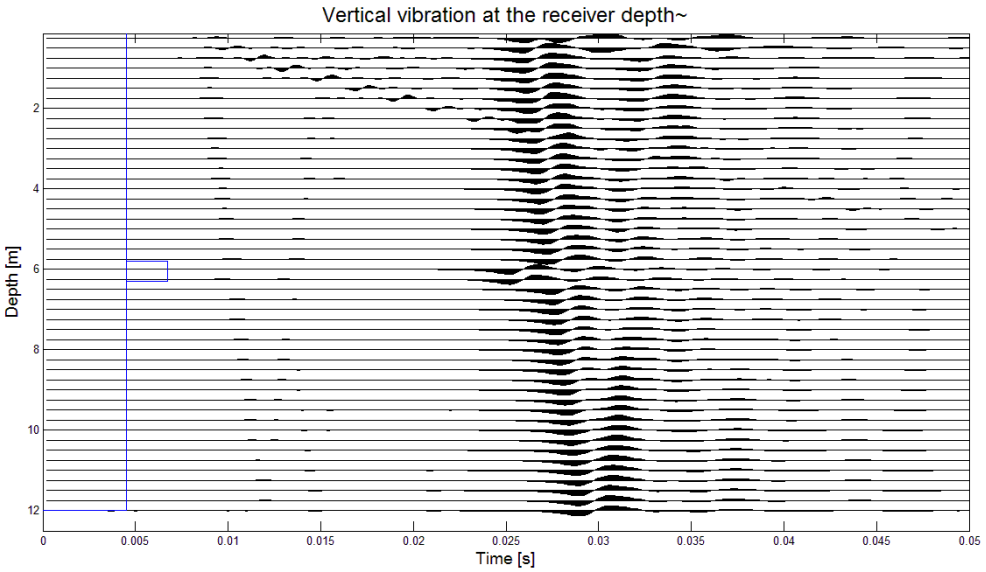

FIGURE A.19: The seismograph calculated for a pile in homogeneous clay layer with a bulge at $6m$.

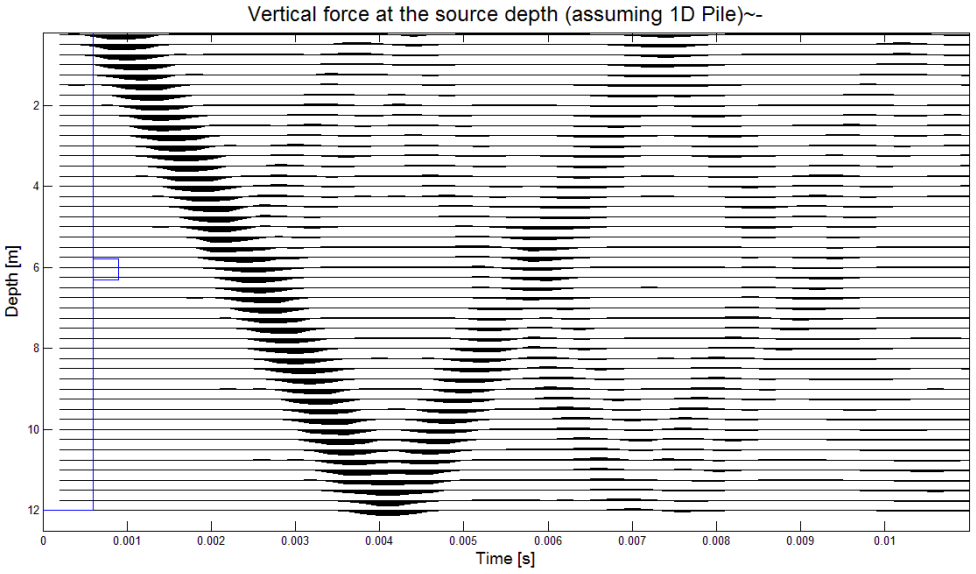

FIGURE A.20: The force per source calculated for a pile in homogeneous clay layer with a bulge at $6m$, showing reflections of vibrations within the pile.

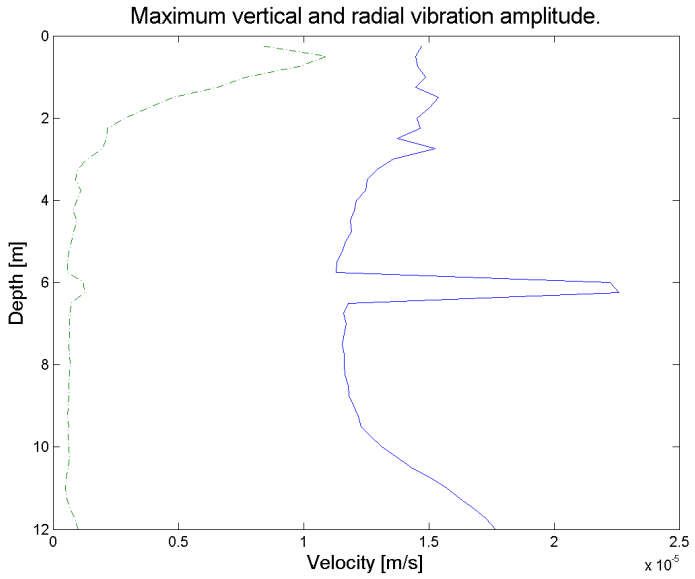

FIGURE A.21: The maximum amplitude of vibrations in the soil calculated for a pile in homogeneous clay layer with a bulge at $6m$.

Simulation of a pile with a bulge in a homogeneous peat layer

In the figure A.22 the seismograph from the PS simulation on a flawed pile in a sand layer is shown. Figure A.23 shows the resulting force per pile element as a function of time. The amplitude as a function of depth is given in A.24.

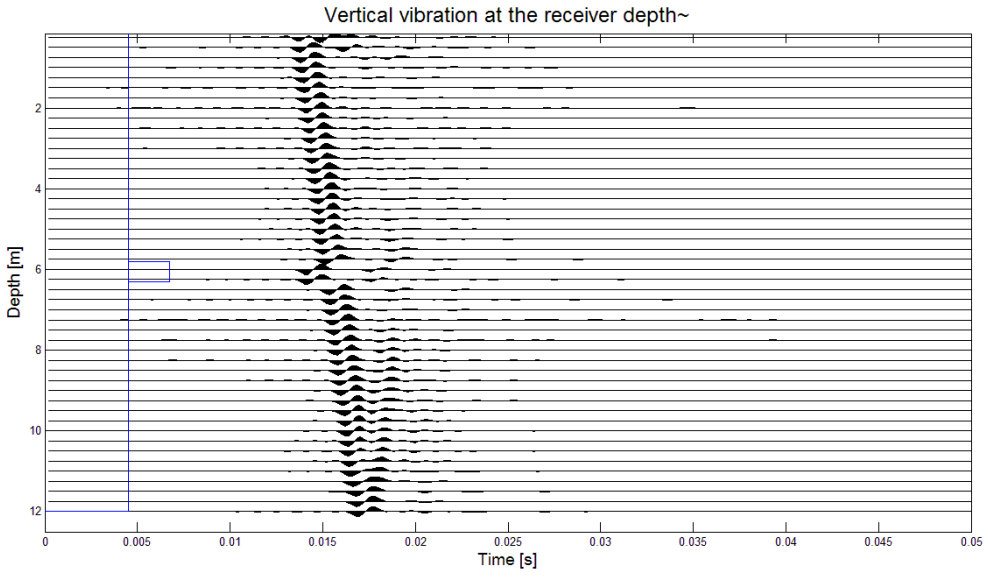

FIGURE A.22: The seismograph calculated for a pile in homogeneous sand layer with a bulge at $6m$.

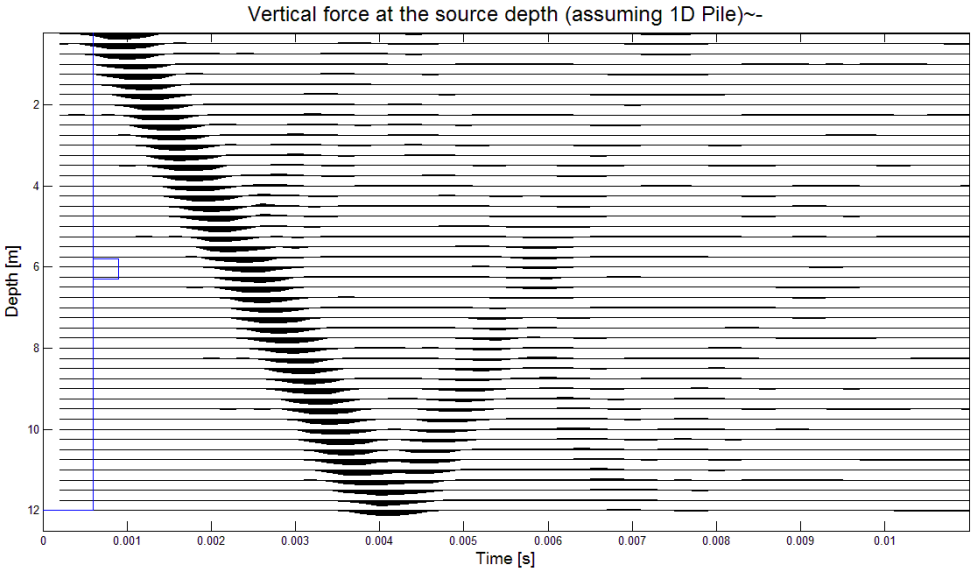

FIGURE A.23: The force per source calculated for a pile in homogeneous sand layer with a bulge at $6m$, showing reflections of vibrations within the pile.

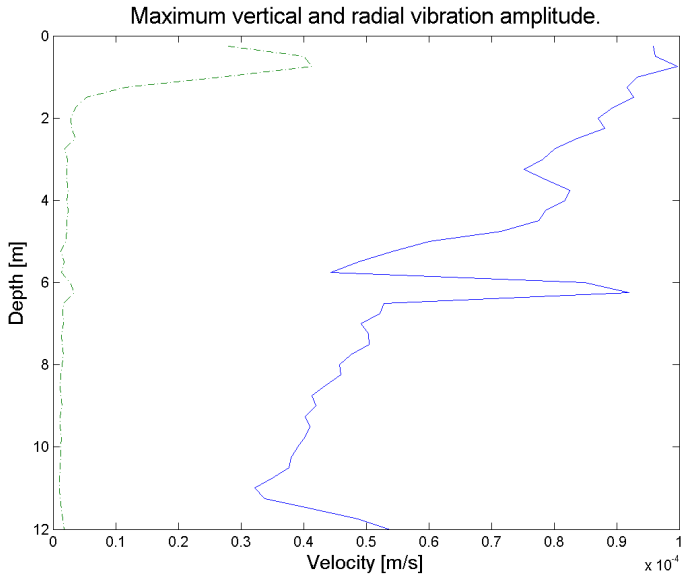

FIGURE A.24: The maximum amplitude of vibrations in the soil calculated for a pile in homogeneous sand layer with a bulge at $6m$.

Simulation of a pile with a bulge in a homogeneous peat layer

In the figure A.25 the seismograph from the PS simulation on a flawed pile in a sand layer is shown. Figure A.26 shows the resulting force per pile element as a function of time. The amplitude as a function of depth is given in A.27.

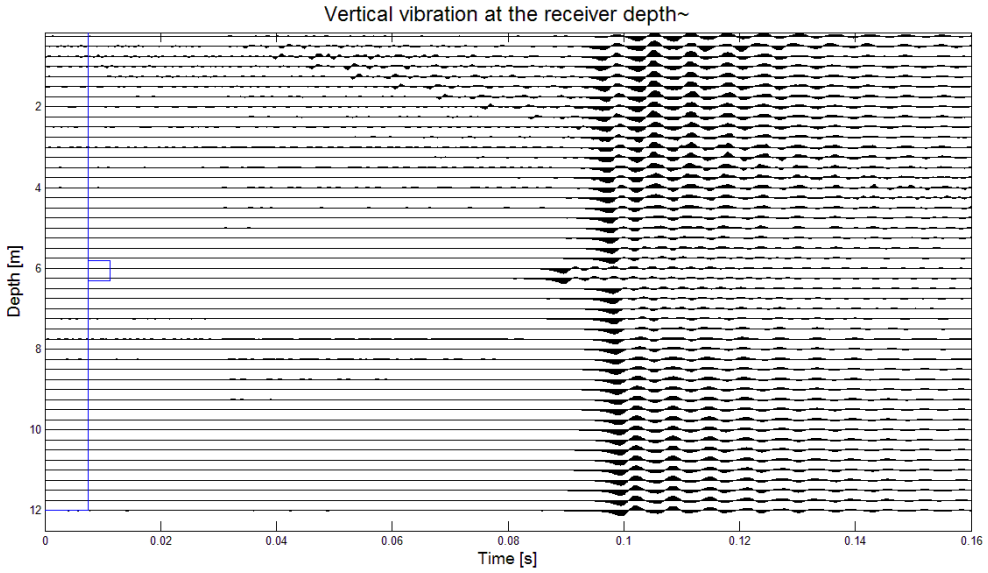

FIGURE A.25: The seismograph calculated for a pile in homogeneous peat layer with a bulge at $6m$.

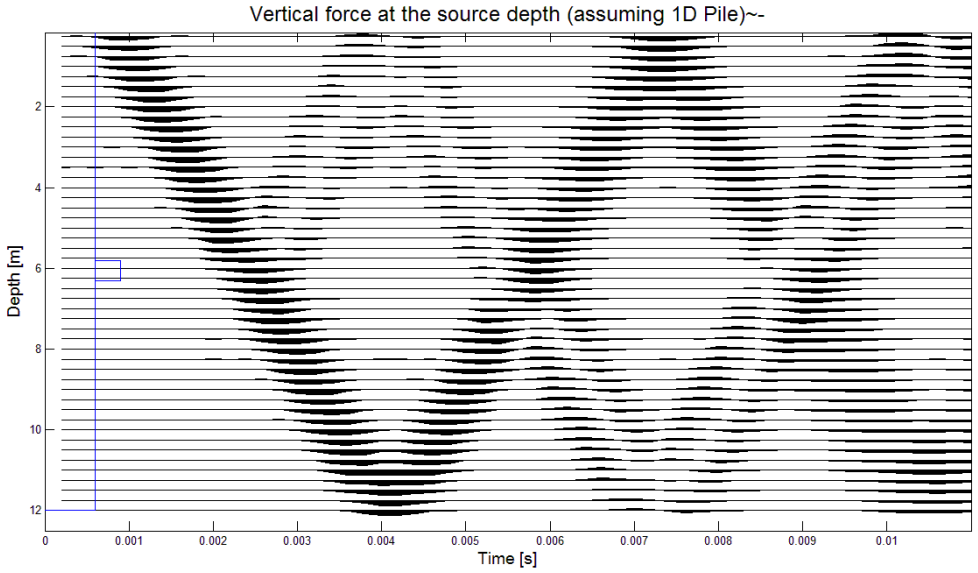

FIGURE A.26: The force per source calculated for a pile in homogeneous peat layer with a bulge at $6m$, showing reflections of vibrations within the pile.

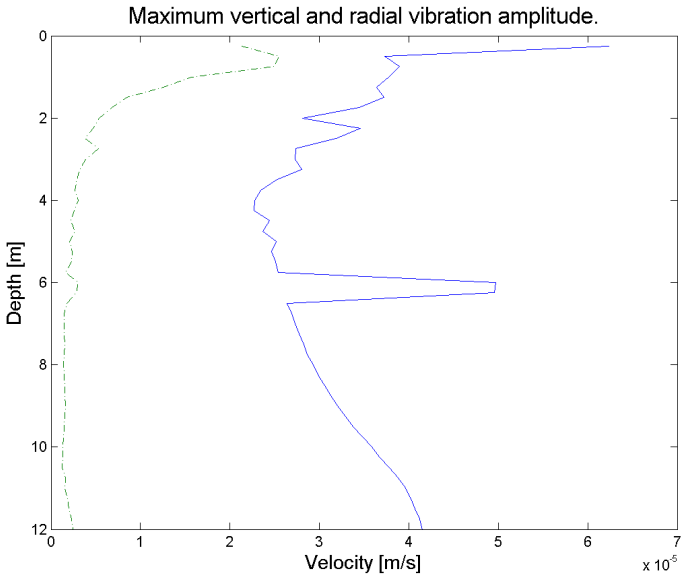

FIGURE A.27: The maximum amplitude of vibrations in the soil calculated for a pile in homogeneous peat layer with a bulge at $6m$.

Appendix B

Appendix: Results of the Preliminary Ground Investigations

B.1 Introduction

The following figures were provided by FUGRO and Deltares. Cone Penetration Tests(CPT) were done prior to any placement of piles or top sand fill. The first figures is a map of the area and the locations of the CPT's. The following figures are CPT profiles used in this report to classify the subsurface.

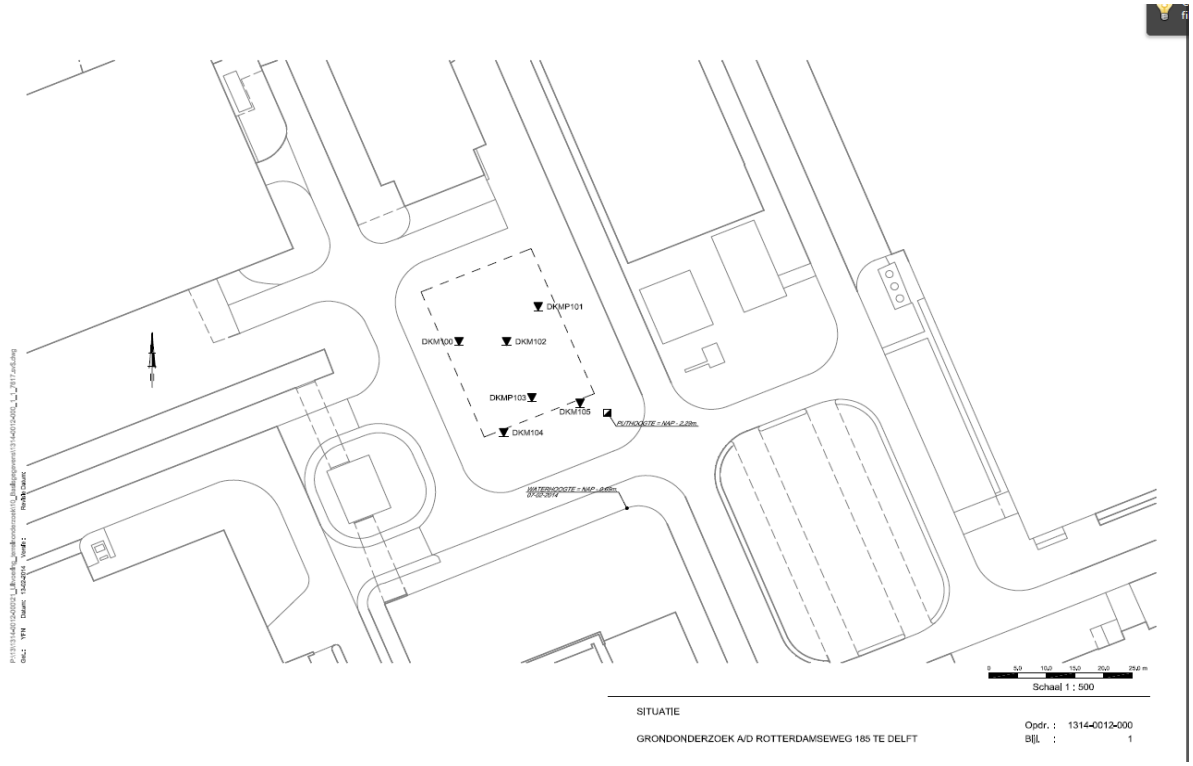

FIGURE B.1: The locations of the CPT are shown above. The planned pile field is marked by the broken outline.

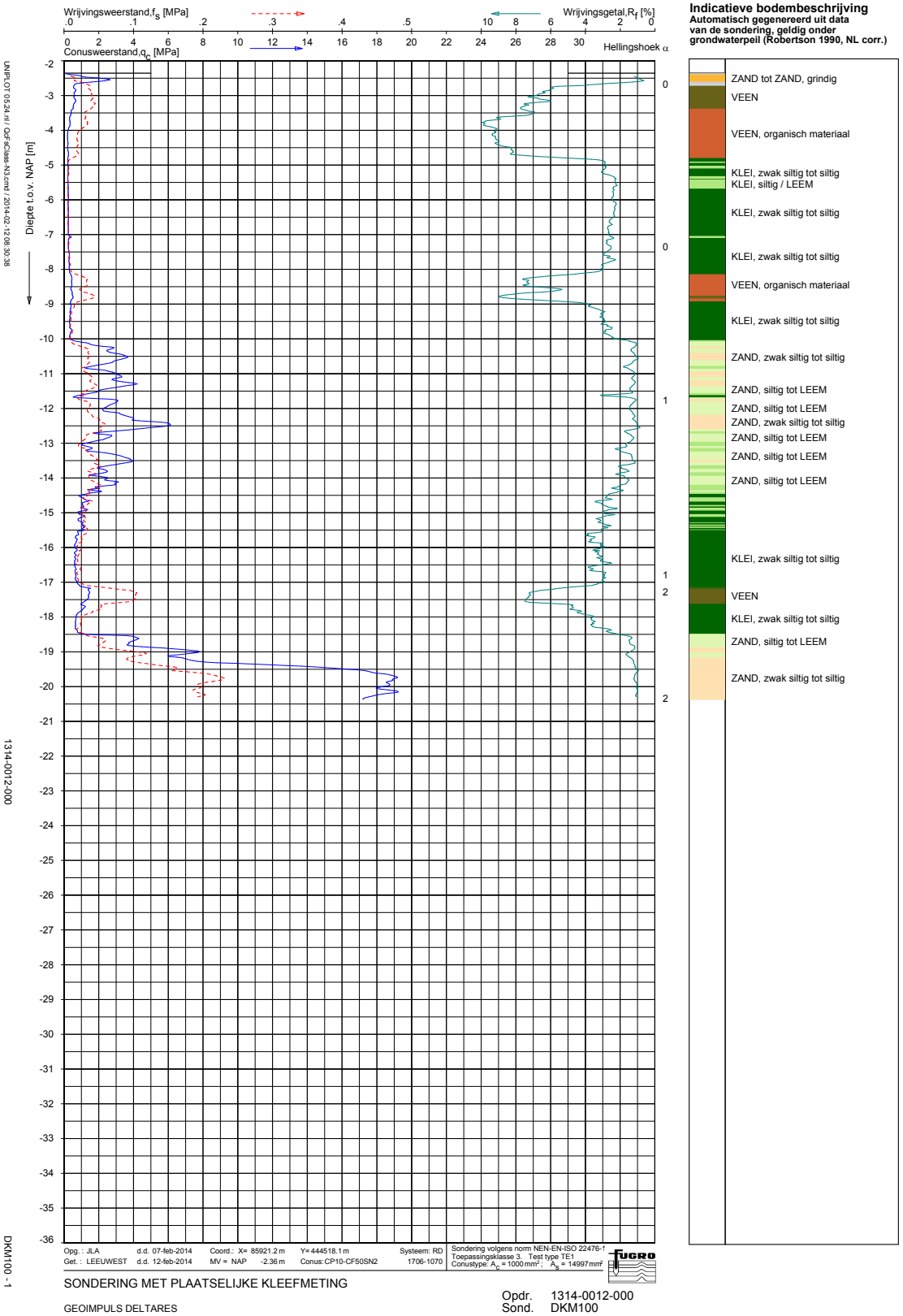
Wrijvingsweerstand,f_s [MPa]
Wrijvingsgetal,R_f [%]
Conusweerstand,q_c [MPa]
Hellingshoek α
Diepte t.o.v. NAP [m]
Indicatieve bodembeschrijving
Automatisch gegenereerd uit data van de sondering, geldig onder grondwaterpeil (Robertson 1990, NL corr.)
ZAND tot ZAND, grindig
VEEN
VEEN, organisch materiaal
KLEI, zwak siltig tot siltig
KLEI, siltig / LEEM
KLEI, zwak siltig tot siltig
KLEI, zwak siltig tot siltig
VEEN, organisch materiaal
KLEI, zwak siltig tot siltig
ZAND, zwak siltig tot siltig
ZAND, siltig tot LEEM
ZAND, siltig tot LEEM
ZAND, zwak siltig tot siltig
ZAND, siltig tot LEEM
ZAND, siltig tot LEEM
ZAND, siltig tot LEEM
KLEI, zwak siltig tot siltig
VEEN
KLEI, zwak siltig tot siltig
ZAND, siltig tot LEEM
ZAND, zwak siltig tot siltig
Opg.: JLA d.d. 07-feb-2014 Coord.: X= 85921.2 m Y= 444518.1 m Systeem: RD
Get.: LEEUWEST d.d. 12-feb-2014 MV = NAP -2.36 m Conus: CP10-CF50SN2 1706-1070
Sondering volgens norm NEN-EN-ISO 22476-1
Toepassingsklasse 3. Test type TE1
Conustype: A_c = 1000 mm²; A_s = 14997 mm²
FUGRO
SONDERING MET PLAATSELIJKE KLEEFMETING
GEOIMPULS DELTARES
Opdr. 1314-0012-000
Sond. DKM100
UNIPLOT 05.24.nl / Opf-sGlaas-N3.cmd / 2014-02-12 08:30:38
1314-0012-000
DKM100 - 1

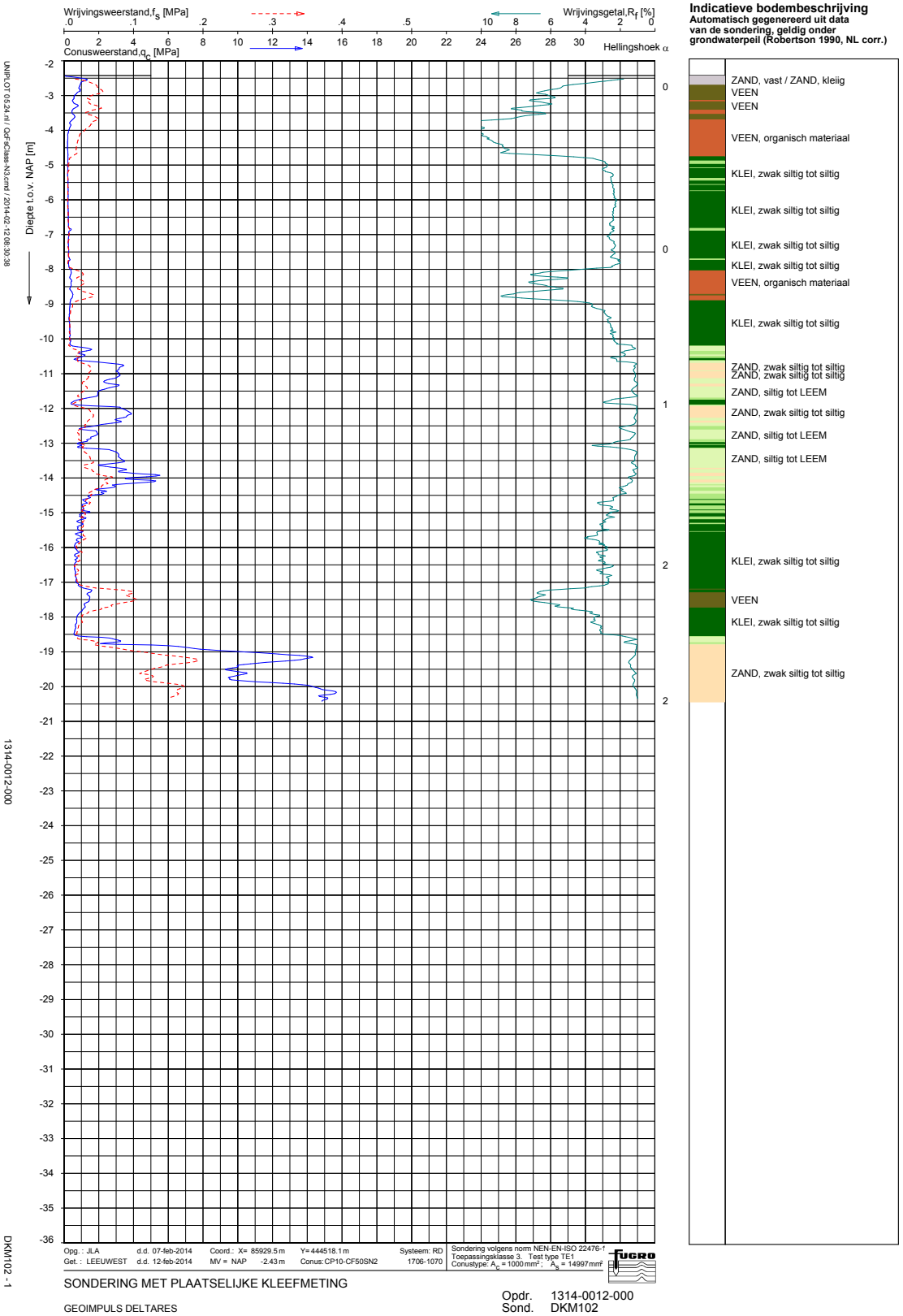
Wrijvingsweerstand,f_s [MPa]
Wrijvingsgetal,R_f [%]
Conusweerstand,q_c [MPa]
Hellingshoek α
Diepte t.o.v. NAP [m]
Indicatieve bodembeschrijving
Automatisch gegenereerd uit data van de sondering, geldig onder grondwaterpeil (Robertson 1990, NL corr.)
ZAND, vast / ZAND, kleiig
VEEN
VEEN
VEEN, organisch materiaal
KLEI, zwak siltig tot siltig
KLEI, zwak siltig tot siltig
KLEI, zwak siltig tot siltig
KLEI, zwak siltig tot siltig
VEEN, organisch materiaal
KLEI, zwak siltig tot siltig
ZAND, zwak siltig tot siltig
ZAND, zwak siltig tot siltig
ZAND, siltig tot LEEM
ZAND, zwak siltig tot siltig
ZAND, siltig tot LEEM
ZAND, siltig tot LEEM
KLEI, zwak siltig tot siltig
VEEN
KLEI, zwak siltig tot siltig
ZAND, zwak siltig tot siltig
Opg.: JLA d.d. 07-feb-2014 Coord.: X= 85929.5 m Y= 444518.1 m Systeem: RD
Get.: LEEUWEST d.d. 12-feb-2014 MV = NAP -2.43 m Conus: CP10-CF50SN2 1706-1070
Sondering volgens norm NEN-EN-ISO 22476-1
Toepassingsklasse 3. Test type TE1
Conustype: A_c = 1000 mm²; A_s = 14997 mm²
FUGRO
SONDERING MET PLAATSELIJKE KLEEFMETING
GEOIMPULS DELTARES
Opdr. 1314-0012-000
Sond. DKM102
UNIPLOT 05.24.nl / Opf-sCase-N3.cmd / 2014-02-12 08:30:38
1314-0012-000
DKM102 - 1

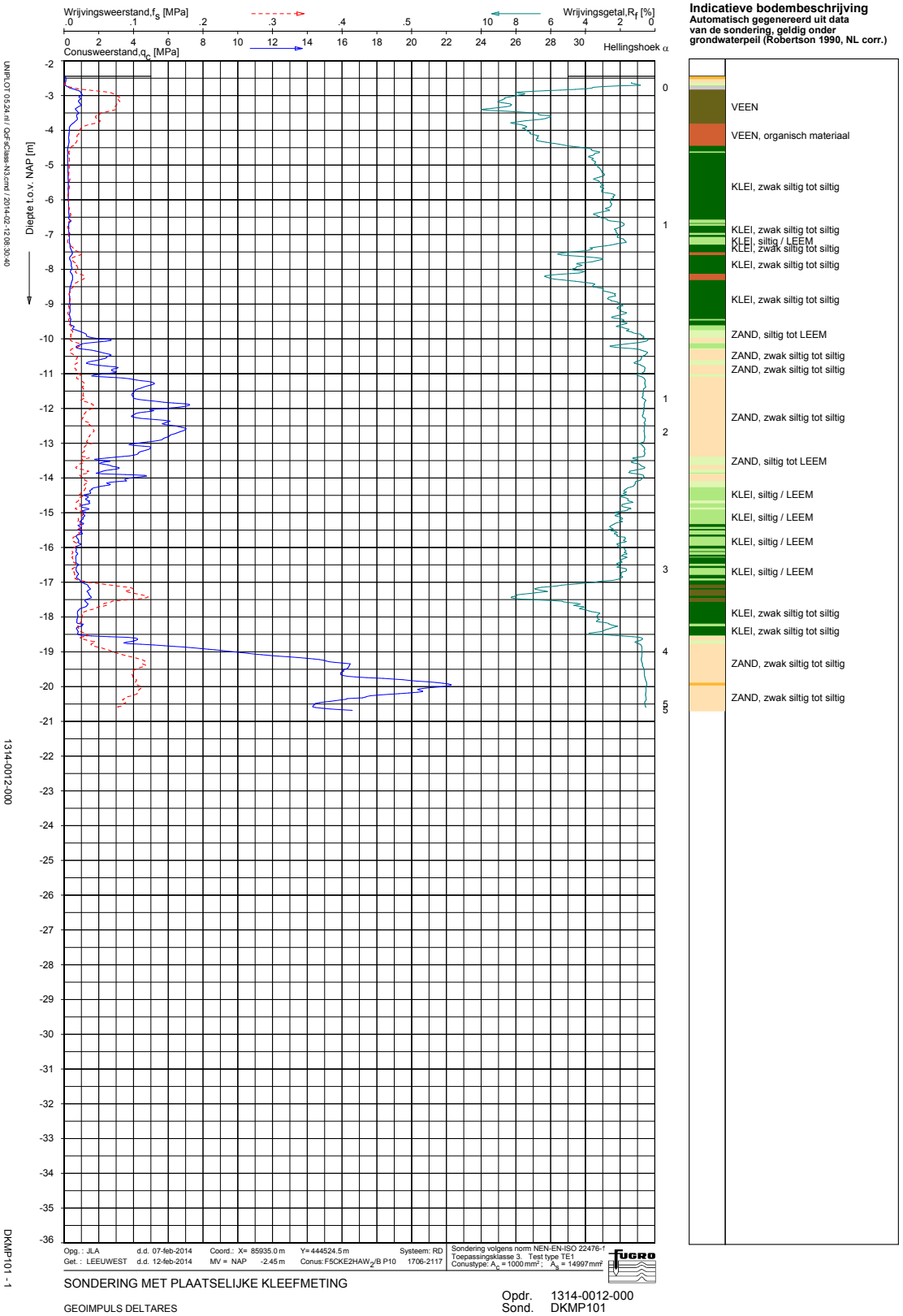
Wrijvingsweerstand,f_s [MPa]
Wrijvingsgetal,R_f [%]
Conusweerstand,q_c [MPa]
Hellingshoek α
Diepte t.o.v. NAP [m]
Indicatieve bodembeschrijving
Automatisch gegenereerd uit data van de sondering, geldig onder grondwaterpeil (Robertson 1990, NL corr.)
VEEN
VEEN, organisch materiaal
KLEI, zwak siltig tot siltig
KLEI, zwak siltig tot siltig
KLEI, siltig / LEEM
KLEI, zwak siltig tot siltig
KLEI, zwak siltig tot siltig
KLEI, zwak siltig tot siltig
ZAND, siltig tot LEEM
ZAND, zwak siltig tot siltig
ZAND, zwak siltig tot siltig
ZAND, zwak siltig tot siltig
ZAND, siltig tot LEEM
KLEI, siltig / LEEM
KLEI, siltig / LEEM
KLEI, siltig / LEEM
KLEI, siltig / LEEM
KLEI, zwak siltig tot siltig
KLEI, zwak siltig tot siltig
ZAND, zwak siltig tot siltig
ZAND, zwak siltig tot siltig
Opg.: JLA d.d. 07-feb-2014 Coord.: X= 85935.0 m Y= 444524.5 m Systeem: RD
Get.: LEEUWEST d.d. 12-feb-2014 MV = NAP -2.45 m Conus: F5CKE2HAW$_2$/B P10 1706-2117
Sondering volgens norm NEN-EN-ISO 22476-1
Toepassingsklasse 3. Test type TE1
Conustype: A_c = 1000 mm²; A_s = 14997 mm²
FUGRO
SONDERING MET PLAATSELIJKE KLEEFMETING
GEOIMPULS DELTARES
Opdr. 1314-0012-000
Sond. DKMP101
UNIPLOT 05.24.nl / Opf-sCase-N3.cmd / 2014-02-12 08:30:40
1314-0012-000
DKMP101 - 1

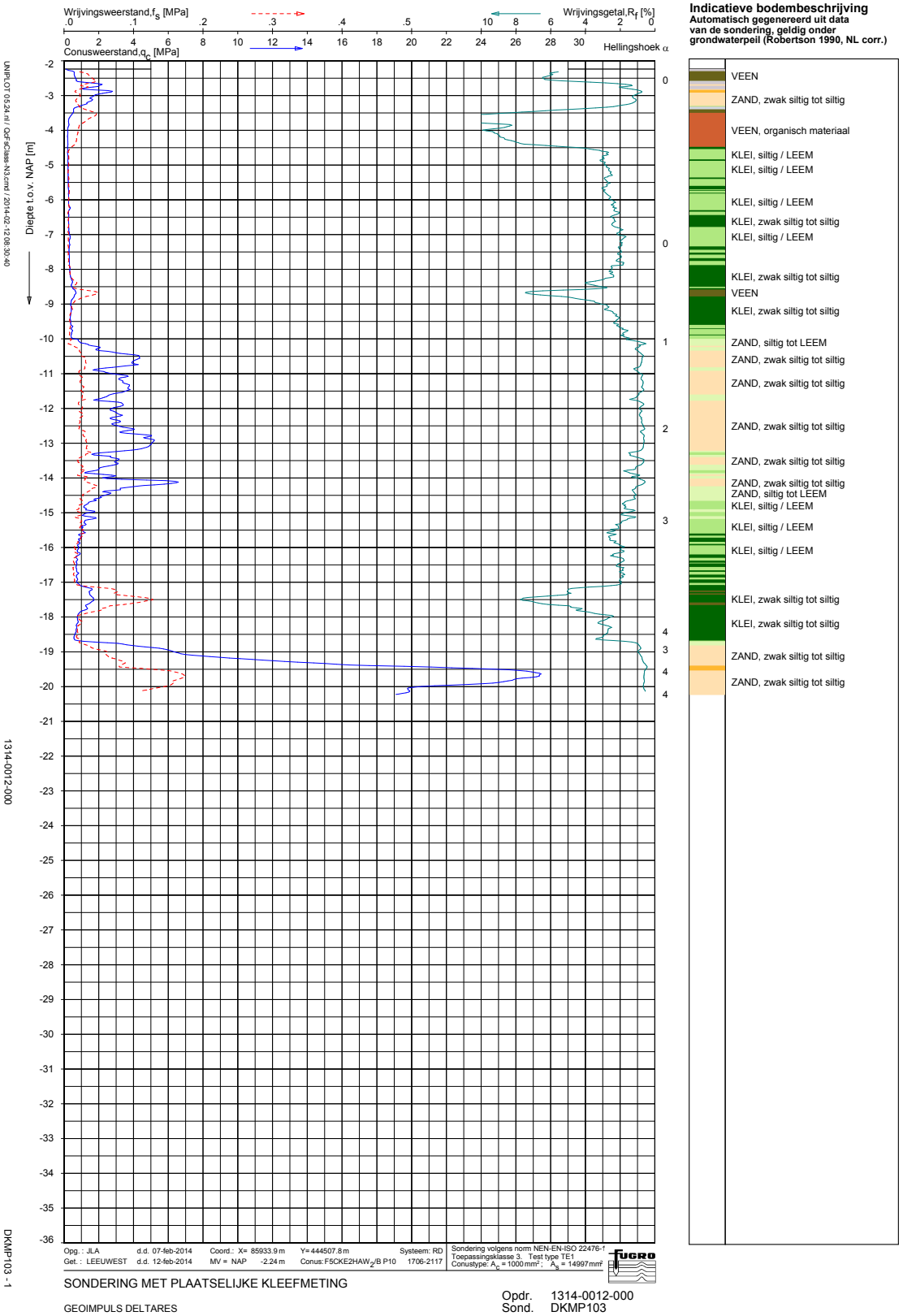
Wrijvingsweerstand,f_s [MPa]
Wrijvingsgetal,R_f [%]
Conusweerstand,q_c [MPa]
Hellingshoek α
Diepte t.o.v. NAP [m]
Indicatieve bodembeschrijving
Automatisch gegenereerd uit data van de sondering, geldig onder grondwaterpeil (Robertson 1990, NL corr.)
VEEN
ZAND, zwak siltig tot siltig
VEEN, organisch materiaal
KLEI, siltig / LEEM
KLEI, siltig / LEEM
KLEI, siltig / LEEM
KLEI, zwak siltig tot siltig
KLEI, siltig / LEEM
KLEI, zwak siltig tot siltig
VEEN
KLEI, zwak siltig tot siltig
ZAND, siltig tot LEEM
ZAND, zwak siltig tot siltig
ZAND, zwak siltig tot siltig
ZAND, zwak siltig tot siltig
ZAND, zwak siltig tot siltig
ZAND, zwak siltig tot siltig
ZAND, siltig tot LEEM
KLEI, siltig / LEEM
KLEI, siltig / LEEM
KLEI, siltig / LEEM
KLEI, zwak siltig tot siltig
KLEI, zwak siltig tot siltig
ZAND, zwak siltig tot siltig
ZAND, zwak siltig tot siltig
Opg.: JLA d.d. 07-feb-2014 Coord.: X= 85933.9 m Y= 444507.8 m Systeem: RD
Get.: LEEUWEST d.d. 12-feb-2014 MV = NAP -2.24 m Conus: F5CKE2HAW2/B P10 1706-2117
Sondering volgens norm NEN-EN-ISO 22476-1
Toepassingsklasse 3. Test type TE1
Conustype: A_c = 1000 mm²; A_s = 14997 mm²
FUGRO
SONDERING MET PLAATSELIJKE KLEEFMETING
GEOIMPULS DELTARES
Opdr. 1314-0012-000
Sond. DKMP103
UNIPLOT 05.24.nl / Opt-Sclass-N3.cmd / 2014-02-12 08:30:40
1314-0012-000
DKMP103 - 1

Appendix C

Appendix: Pile Field Construction and the Parallel Seismic

C.1 Introduction

The PS test was done on a small pile field. This field test was designed to evaluate follow up testing methods to the common pile integrity test. The field test included two main parts, the installations of the piles and defects and performing the PS test. In this chapter, the procedure for construction of the pile field and the procedure of the PS is shown. The results are presented and discussed in chapter 5 and chapter 6.

C.2 Constructing the pile field

The design and installation of the piles was done by *Deltares* in cooperation with *Van t'Hec*. 20 piles were installed at the Deltares office in Delft.

The aim of the pile field is to provide a testing area for multiple NDT's. Therefore in each pile either two, one, or no flaws were introduced. These include necks, bulges, and cracks. Some are axis-symmetric and some are not. These flaws were installed in the reinforcement cage.

C.2.1 Design of the flaws

Figure C.1 shows how a bulge was introduced in a pile. While the concrete cured, grout was injected via a pre-installed tube at the desired depth. To make sure that the grout hardens outwards, a PVC shield was places in the cage. The grout has similar properties as the concrete.

Figure C.2 shows how a neck was made. After depositing the concrete a pre-installed tire was filled with bentonite. During the curing process, this tire was expected to push into the concrete and form a bentonite balloon. The bentonite has similar properties to soil.

Forming the crack was done by taking out a part of the reinforcement as seen in figure C.3.

FIGURE C.1: Procedure for installing a bulge. The picture shows a part of the reinforcement cage where the end of a pipe is placed through which grout can be pumped. *Picture provided by Deltares.*

FIGURE C.2: Procedure for installing a neck. The picture shows the tire that can be inflated with bentonite. *Picture provided by Deltares.*

While the cage was lowered, the missing reinforcement was temporary replaced with steel cables that may be taken out at a later stage. Once the concrete of the pile was hardened a small crack was introduced by driving against the pile. The assumption is that at the location of the weakened reinforcement a crack will form.

C.2.2 Pre-installed testing apparatus

Besides the flaws, there were a number of other extra items installed in the piles:

FIGURE C.3: Procedure for installing a crack. *Picture provided by Deltares.*

- In a few piles, a single PVC tube was installed in the middle of the pile. This was done to allow for single hole logging.
- Some piles have three smaller PVC tubes for cross-hole logging.
- About half of the piles have a pre-installed geosensors placed around the center of the pile. A small cable connects the sensor to the the pile head.
- Remaining sensors that may be found in a few piles are temperature sensors, heating cables, and fiberglass cables.

C.2.3 Mapping the pile field

The results of the PS are found in reference to the surface level and the top of the pile. Therefore, GPS measurements of the surface and concrete to reinforcement cage distance are made. This ensures that the depth of the receivers can be compared to the soil layers and the pile reinforcement.

C.3 Procedure of the PS

The PS test is done with the help of *Fugro*, a company that specializes in geo-sensing and seismics. The aim of the field test is to test the following hypothesis: *The parallel seismic method can be used to detect defects in piles as a follow-up test on impulse response or impact echo.* The following steps are taken for each pile tested:

1. A small CPT caterpillar truck as shown in figure C.4 is driven next to the pile. When necessary the truck is anchored to avoid lifting up when pressing into stiff soil layers. The cone should be about $2m$ from the pile to obtain consistent results.

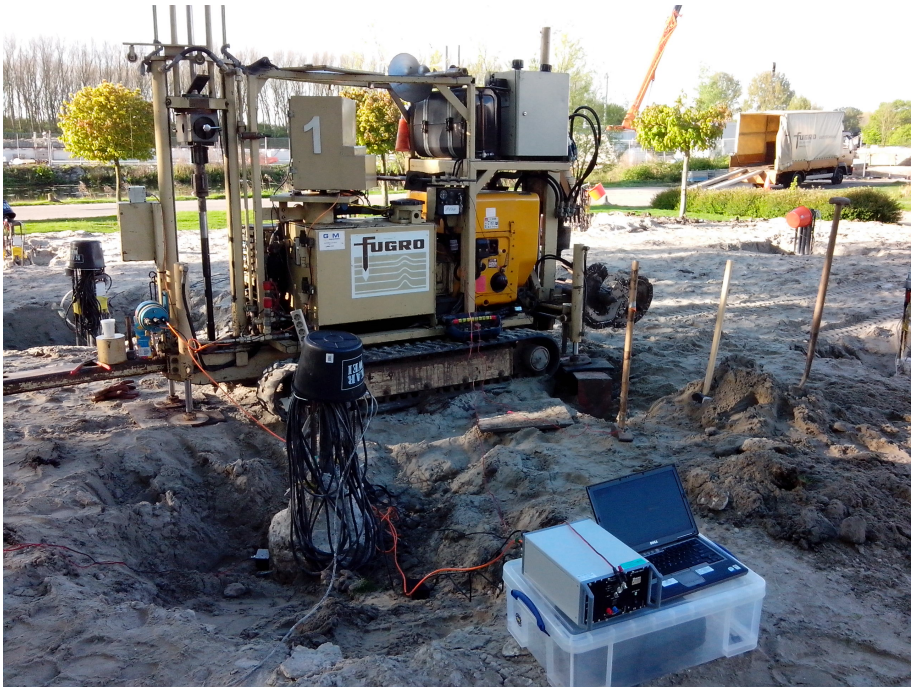

FIGURE C.4: Picture of a CPT truck equipped with a seismic cone tip. In the foreground the laptop with oscilloscope can be seen. The top of the pile is to the left of the center of the foto. *Picture taken during the field test.*

2. A small stud is bored into the side of the pile at the top and a small metal block is fastened against the pile on the stud with a bolt. The metal block is also attached to the end of an electric wire that is connected to an oscilloscope. This can be seen in C.5.

3. A hammer, as shown in figure C.5 is also connected to an electric wire. If it connect to the metal blocks, a circuit is completed, thus signaling the impulse and the start of measurements.

4. A cone tip fitted with two seismic sensors is attached to the truck and pressed into the ground. The sensors are connected to the oscilloscope that transfers vibrations signals to a field laptop.

5. The cone is pressed into the ground to the first predetermined depth. The truck is switched off to reduce vibrations in the ground and the metal block on the pile is struck with the small hammer. This is done multiple times until three acceptable results are saved. This step is repeated for a number of intervals, depending on the desired data resolution and pile length.

6. The cone is removed and the truck is moved to the next pile.

Procedure for P-wave and S-wave test

Besides the PS test, p and s-wave speed profiles of the subsurface are created. Either a steel plate (for the p-wave test) or a steel block (for the s-wave test) is placed $2m$ from the cone.

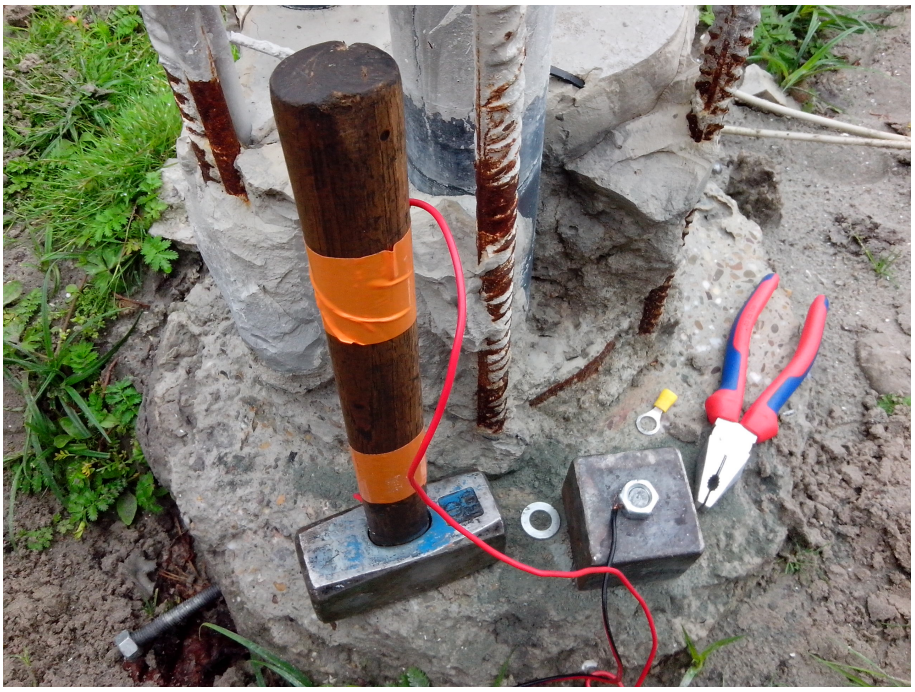

FIGURE C.5: Picture of the impact hammer used to introduce an impulse in the pile. To the left the stud can be seen on which the metal block is attached. *Picture taken during the field test.*

Simultaneously with the PS test the block or plate can be hit as well. This is done with a sledge hammer to ensure large amplitudes that can be detected by the sensors.

Figures C.6 and fig:sWave show how vibrations are made with the sledge hammer for the p-wave test and s-wave test respectively. The plate is hit downwards to create p-waves while the block is hit sideways, creating s-waves. Since the block is anchored in the ground with two flanges, s-waves are passed downwards into the ground. Again the hammer and steel is connected to the oscilloscope with an electric wire so that a circuit is completed on impact. Again this signals the start of measurements.

FIGURE C.6: Forming p-waves by hitting down on the steel plate. *Picture taken during the field test.*

FIGURE C.7: Forming s-waves by hitting sideways on the steel box. *Picture taken during the field test.*

Appendix D

Appendix: Results of the First Field Test

D.1 Introduction

For all the tests done, the results are presented. First the results of the p- and s- wave tests are shown. This is followed by the results of the PS per pile.

For each test, vibrations in the x- and y- direction are plotted in the time and space domain in a seismograph. The broken horizontal lines represent soil layering found in a CPT done prior to the installation of the piles. The first layer is loose sand followed by peat, clay, peat, clay, and stiffer sand.

For the p-wave test, the seismographs are modified. In these graphs the first waves are amplified to make the p-wave clearer.

Finally, the maximum amplitudes of vibrations are plotted versus depth. In addition, the arrival times(a.t) of the first vibration and 0.65% of the maximum amplitudes are plotted as first and second a.t's for all the PS tests.

D.2 Results s-wave test near pile 3

The following figures are the seismographs and amplitude plots made from the s-wave test near pile 3. Changes in wave properties correspond roughly with the soil layering defined by the CPT. It seems that the wave velocity first decreases. After $8m$ the gradient increases, meaning that the wave velocity increases.

The amplitude reduces a lot at $3m$ and then gradually decreases with depth. This may be expected due to damping of the vibrations. The jumps also correspond to the soil layering and may be useful information for the PS.

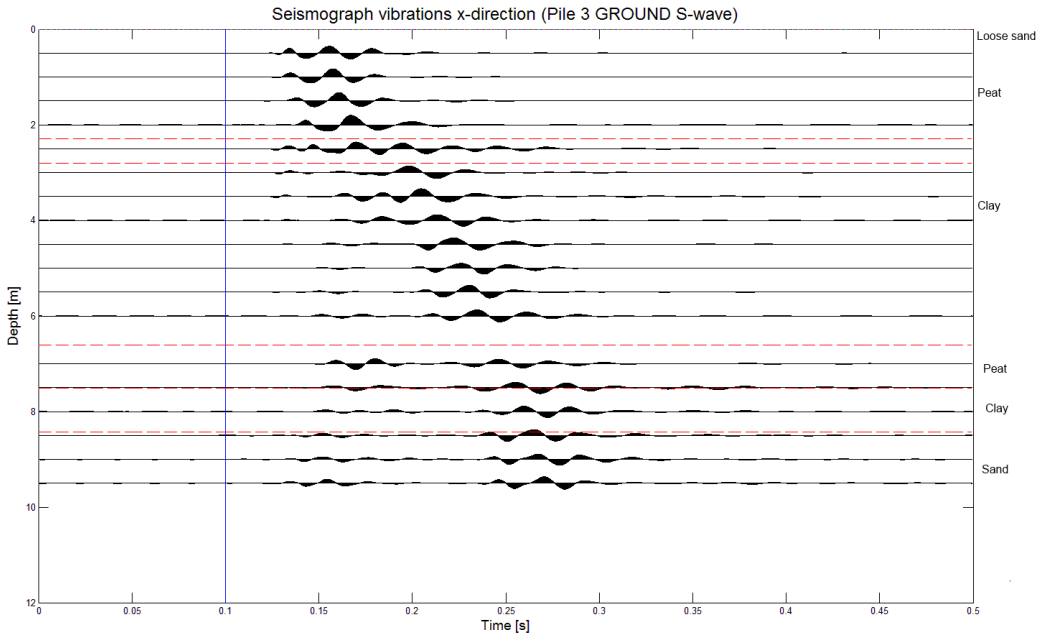

FIGURE D.1: Seismograph for s-wave test, vibration in x-direction. The vertical line at 0.1[s] signifies the time of hammer impact. Earlier small vibrations are p-waves, secondary larger vibrations are s-waves.

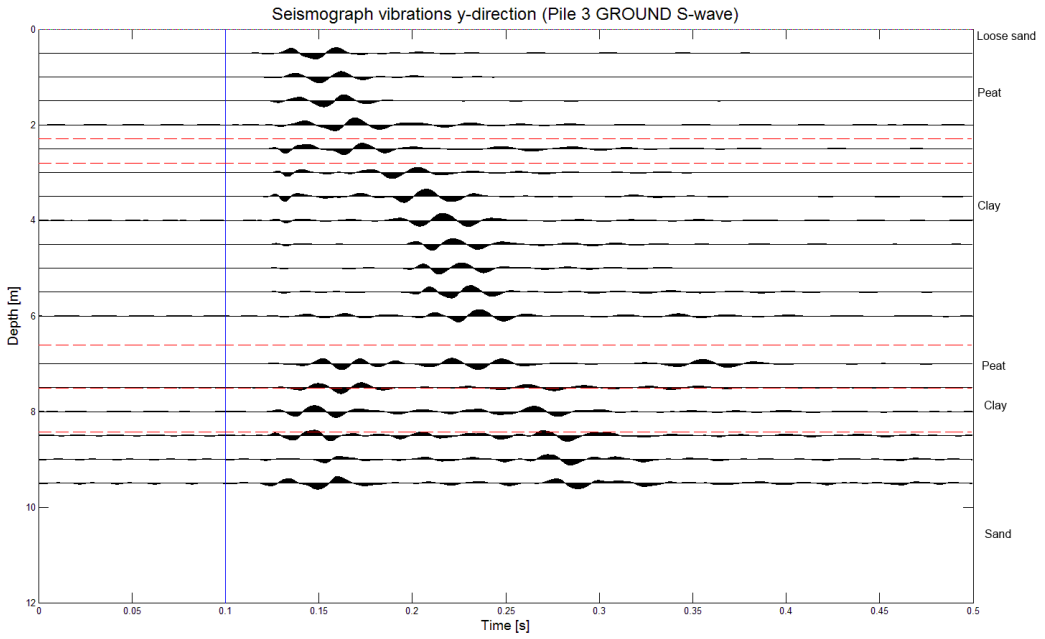

FIGURE D.2: Seismograph for s-wave test, vibration in y-direction. The vertical line at 0.1[s] signifies the time of hammer impact.

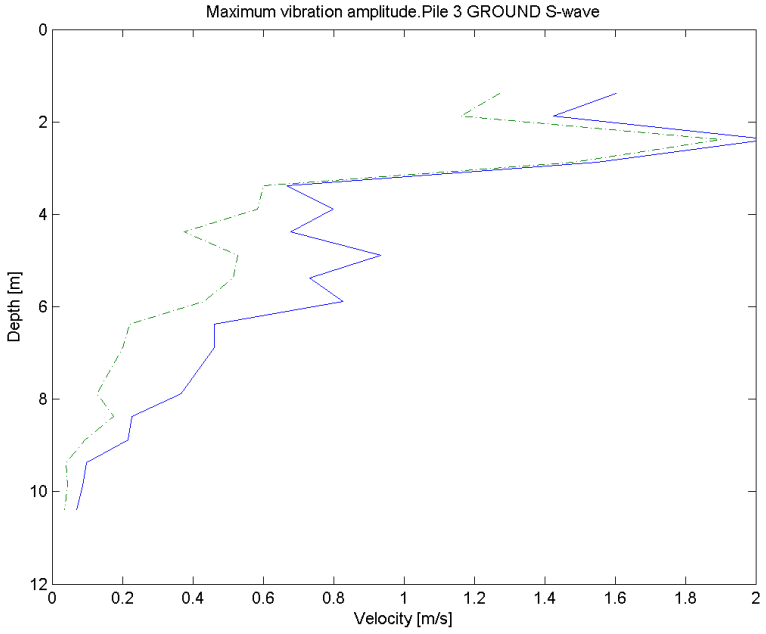

FIGURE D.3: Maximum vibration amplitude for s-wave test. x- is the blue full line and y- is the green broken line.

D.3 Results s-wave test near pile 13

The following figures are the seismographs and amplitude plots made from the s-wave test near pile 13. The patterns seen in figures D.4 and D.5 are very similar to the test near pile 3.

Figure D.6 shows the dip in amplitude at $3m$ as well. In addition, a peak at $7m$ is be observed.

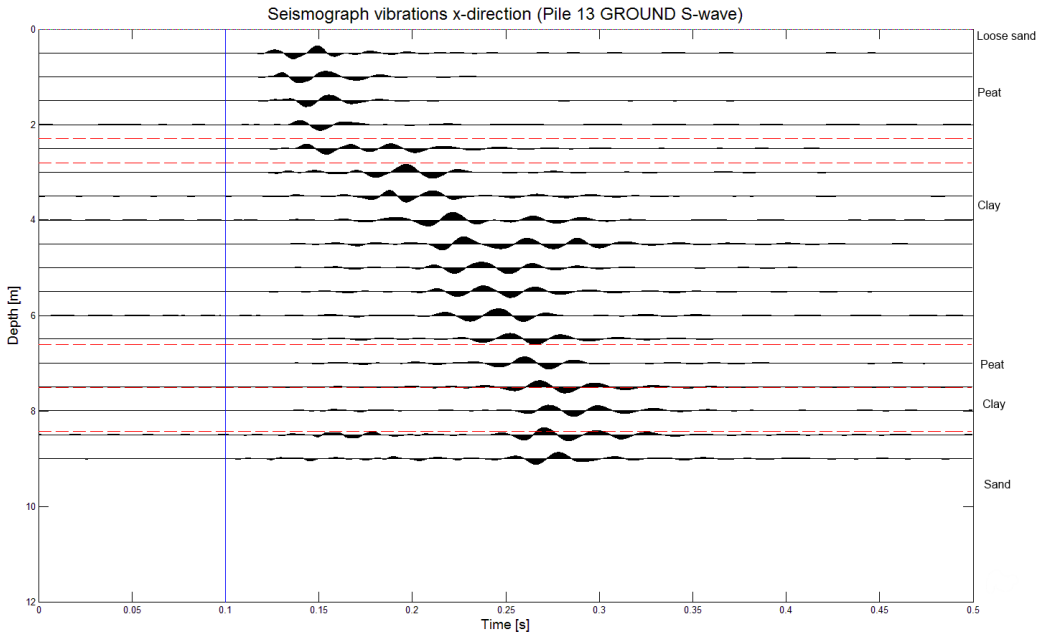

FIGURE D.4: Seismograph for s-wave test, vibration in x-direction. The vertical line at 0.1[s] signifies the time of hammer impact.

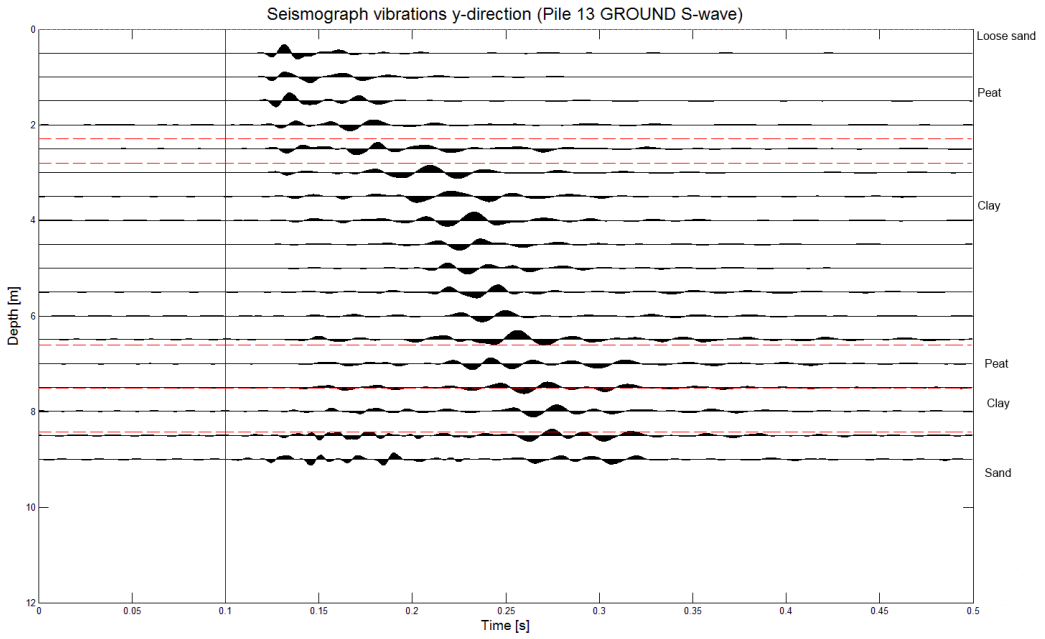

FIGURE D.5: Seismograph for s-wave test, vibration in y-direction. The vertical line at 0.1[s] signifies the time of hammer impact.

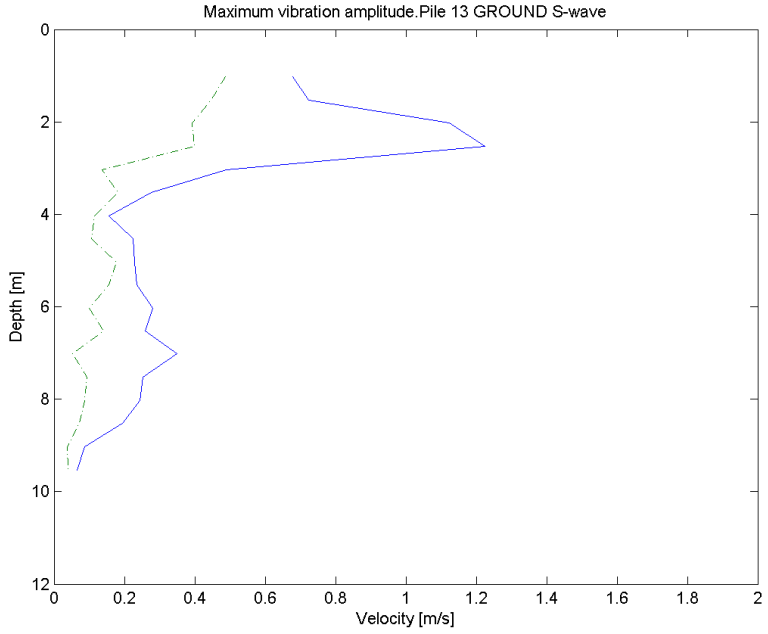

FIGURE D.6: Maximum vibration amplitude for s-wave test. x- is the blue full line and y- is the green broken line.

D.4 Results s-wave test near pile 14

The following figures are the seismographs and amplitude plots made from the s-wave test near pile 14. The s-waves arriving show again the same pattern as the previous two tests. In this test the p-waves are however much more prominent after $7m$ depth.

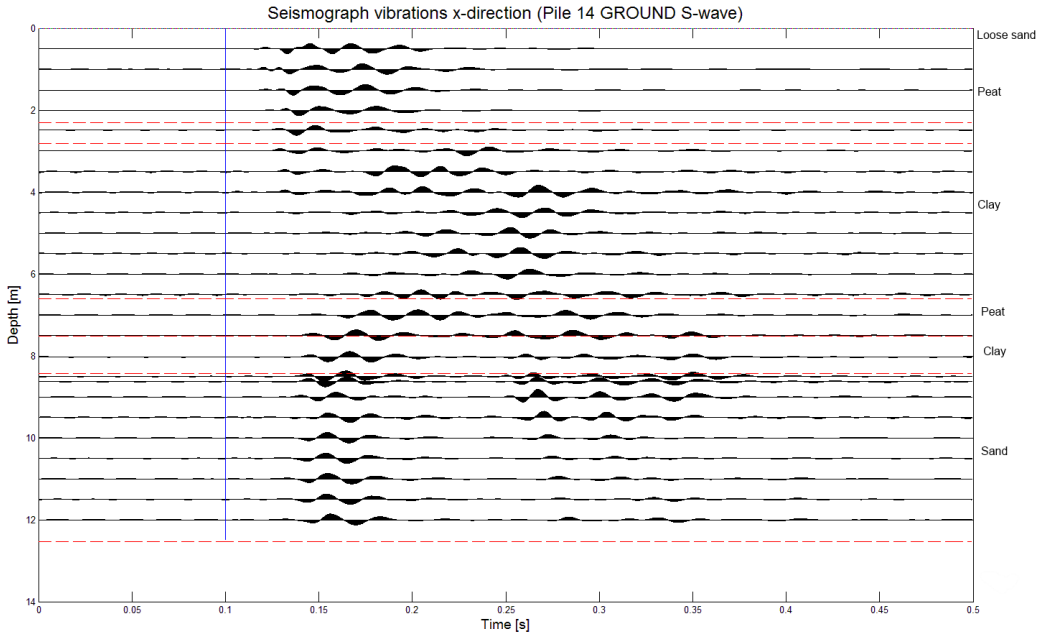

FIGURE D.7: Seismograph for s-wave test, vibration in x-direction. The vertical line at 0.1[s] signifies the time of hammer impact. In the x-direction, the p-waves are realtively large. The orientation of the x- and y- axis of the cone has will cause this.

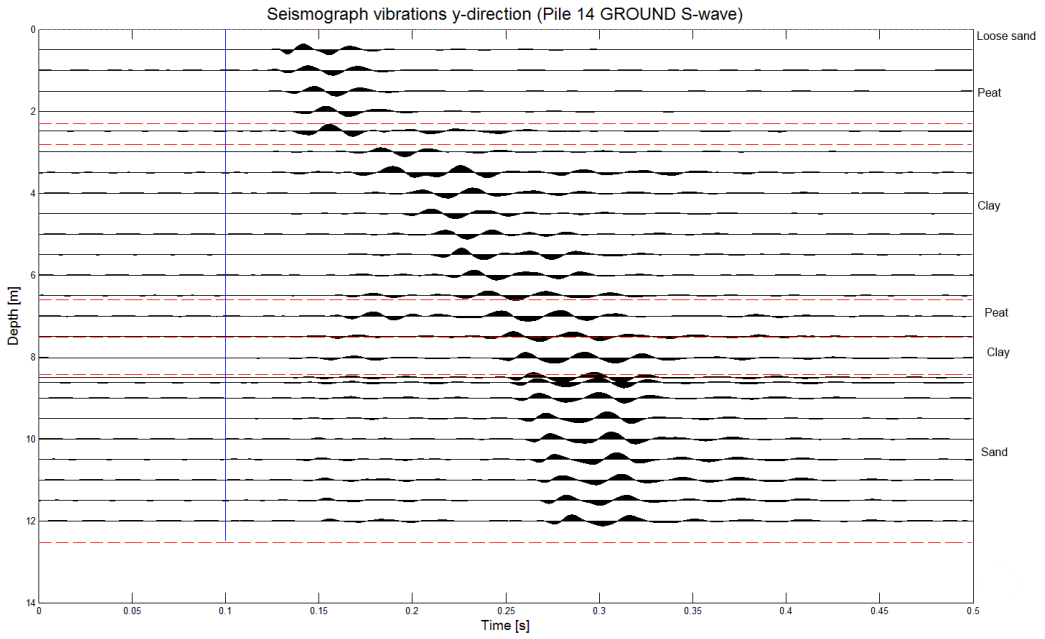

FIGURE D.8: Seismograph for s-wave test, vibration in y-direction. The vertical line at 0.1[s] signifies the time of hammer impact.

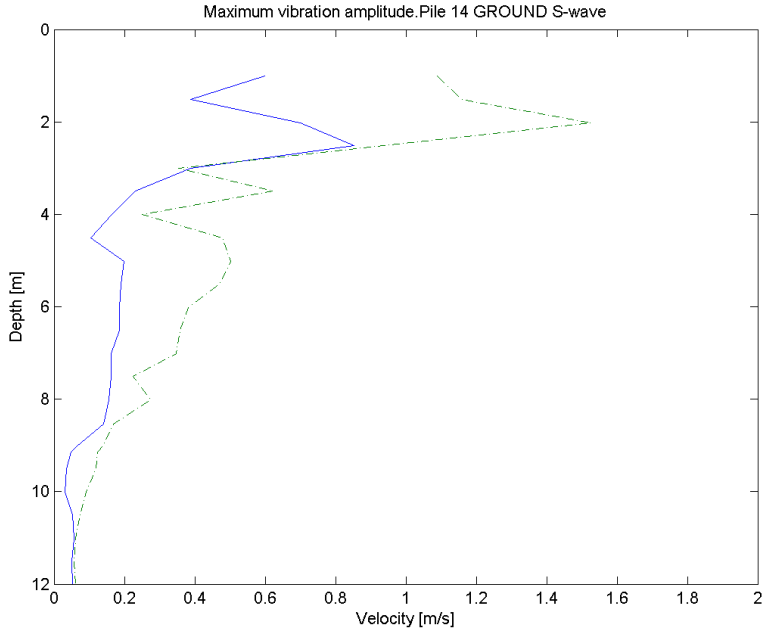

FIGURE D.9: Maximum vibration amplitude for s-wave test. x- is the blue full line and y- is the green broken line.

D.5 Results p-wave test near pile 7

The following figures are the seismographs and amplitude plots made from the s-wave test near pile 7. Figures D.10 and D.11 show that the p-waves are shown more prominent in this test, which is the aim of the test.

Figure D.12 shows that the amplitude dips again at $3m$. The amplitude then again gradually reduces with depth.

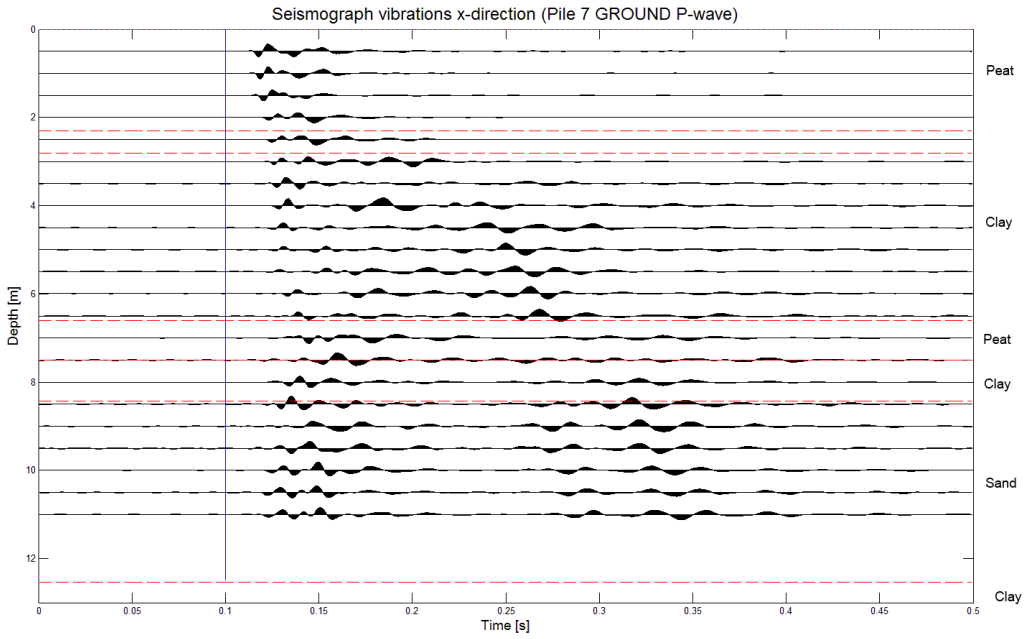

FIGURE D.10: Seismograph for p-wave test, vibration in x-direction. The vertical line at 0.1[s] signifies the time of hammer impact. The p-waves are relatively amplified by damping waves arriving later.

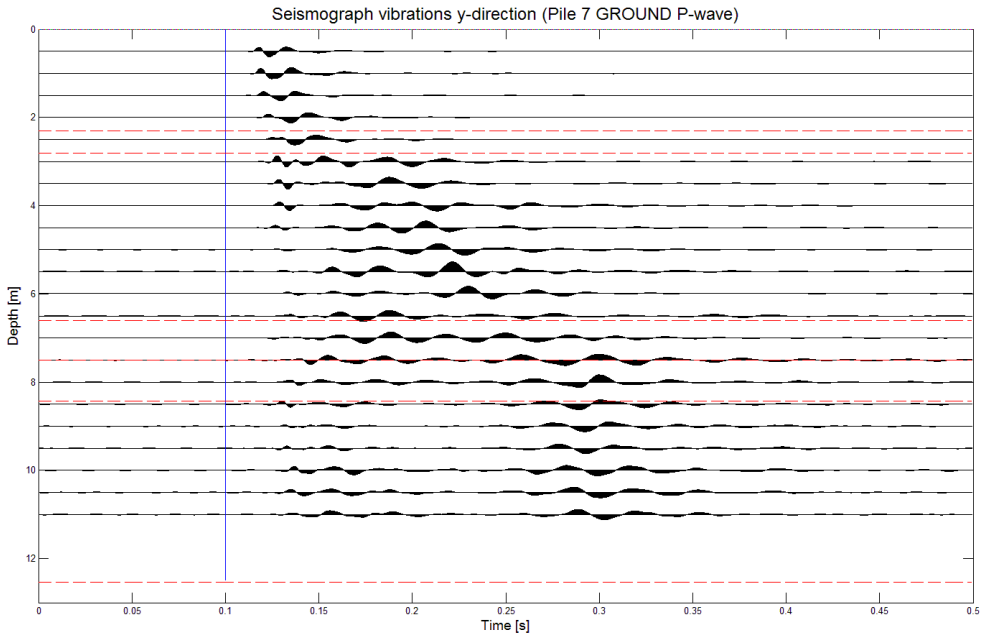

FIGURE D.11: Seismograph for p-wave test, vibration in y-direction. The vertical line at 0.1[s] signifies the time of hammer impact.

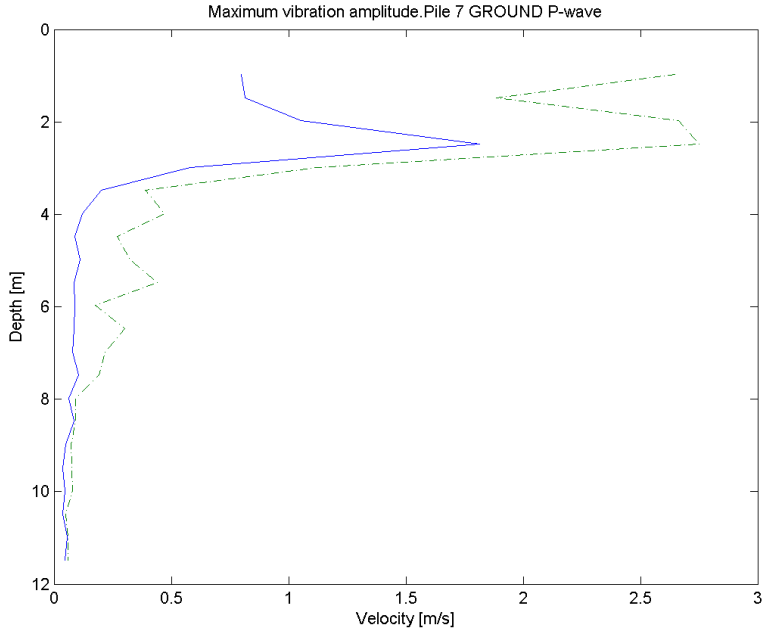

FIGURE D.12: Maximum vibration amplitude for p-wave test. x- is the blue full line and y- is the green broken line.

D.6 Results pile 7 from the first field test

In pile 7 the defect is possibly at $6m$ based on the location of higher resolution measurements.

The seismographs do not show any clear reflections or strange patterns that might suggest defects. The amplitude follows the same pattern as pile 3, this corresponds to soil layering.

From the a.t plots (figures D.15 and D.16) a delay at $8.08m$ and $7.98m$ and an early arrival at $5.48m$ is observed. Furthermore the reducing a.t from 8 - $10m$ is probably due a stiffer soil layer which can be seen back in the gradual increase in v_s and v_p in figure 5.4. In this pile and many others, a.t's increase around 3.5, 7, 8.2, and $8.7m$.

In conclusion the delay at $7.98m$ could be a bulge at this depth.

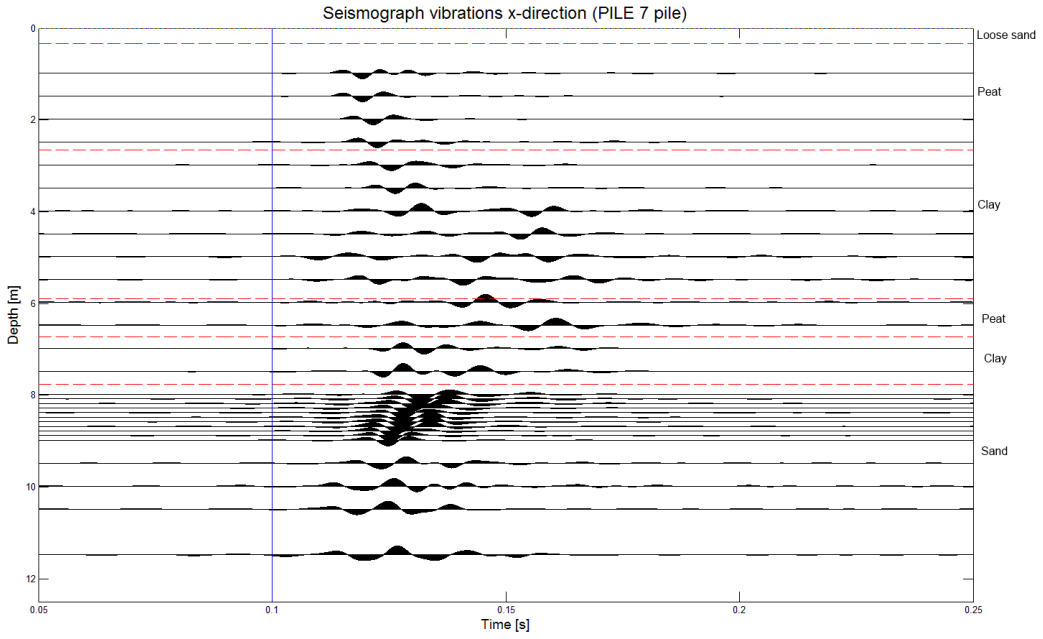

FIGURE D.13: Seismograph for PS test on pile 7, vibration in x-direction. The vertical line at 0.1[s] signifies the time of hammer impact.

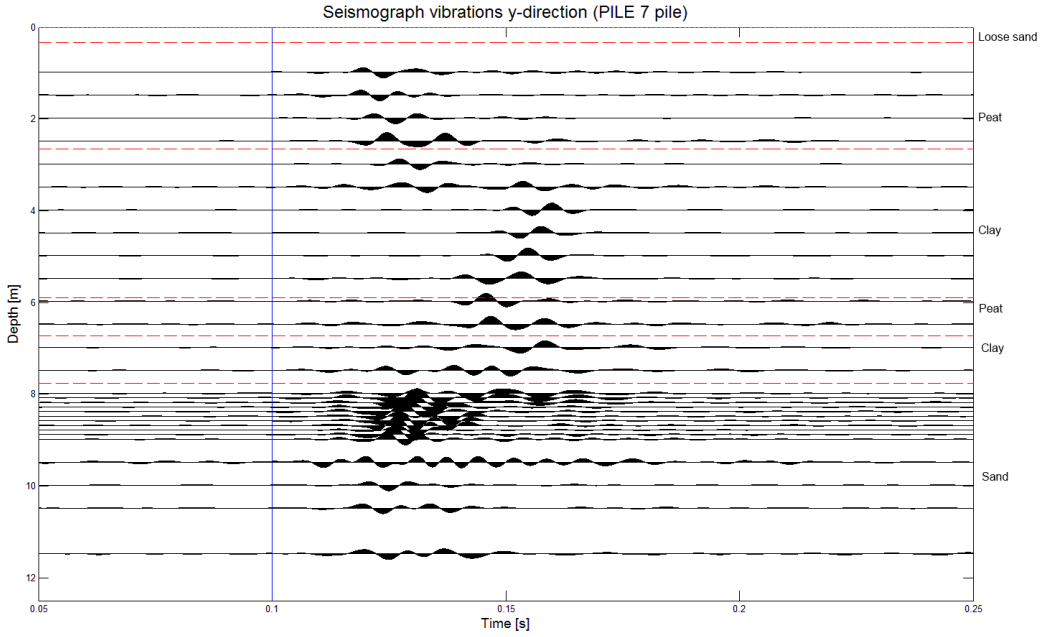

FIGURE D.14: Seismograph for PS test on pile 7, vibration in y-direction. The vertical line at 0.1[s] signifies the time of hammer impact.

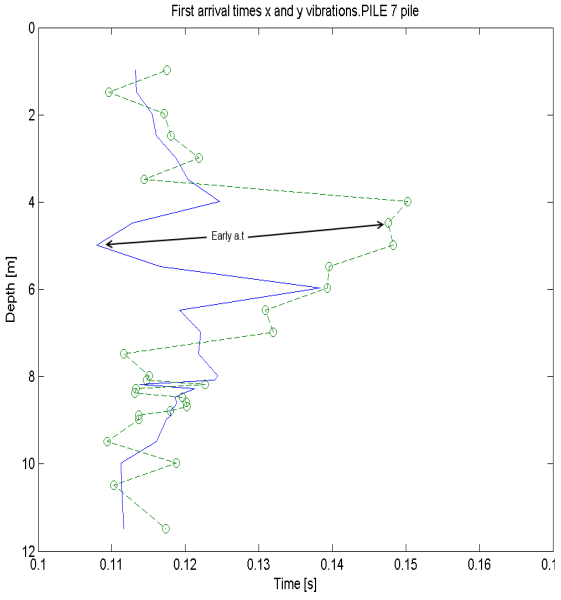

FIGURE D.15: First a.t's for PS test on pile 7. x- is the blue full line and y- is the green broken line.

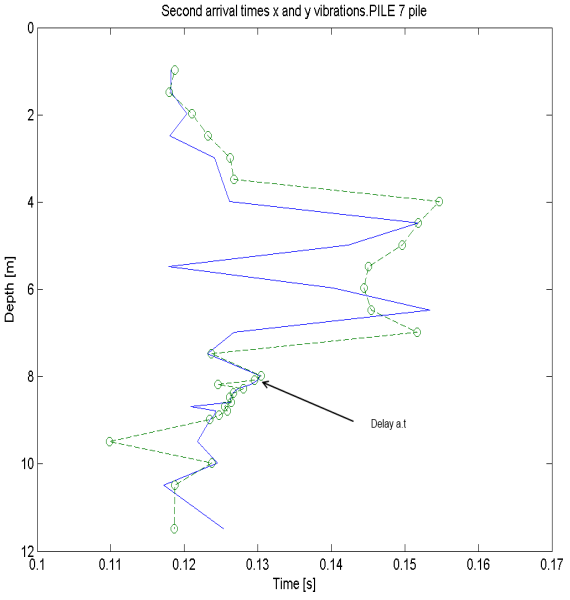

FIGURE D.16: Second a.t's for PS test on pile 7. x- is the blue full line and y- is the green broken line.

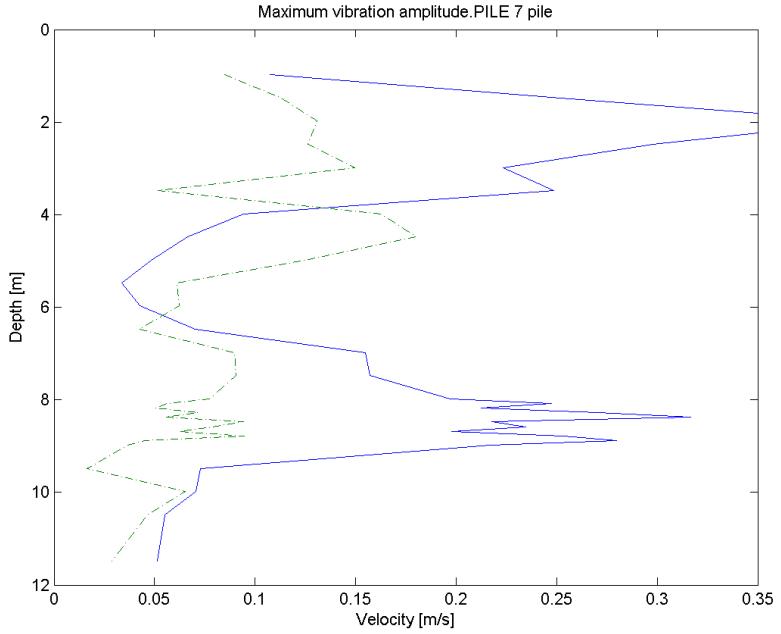

FIGURE D.17: Maximum vibration amplitude for PS test on pile 7. x- is the blue full line and y- is the green broken line.

D.7 Results pile 8 from the first field test

Pile 8 does not have any flaws, this is already known.

Again figure D.22 shows a peak in amplitude at $4m$ and a dip at 6 m which proves that this plot is formed by the soil layering. Also there is a delayed a.t at $4.08m$ and $4.58m$ which suggest that delays at this level are caused by soil layering. This makes it more difficult to find defects if they are present at this depth.

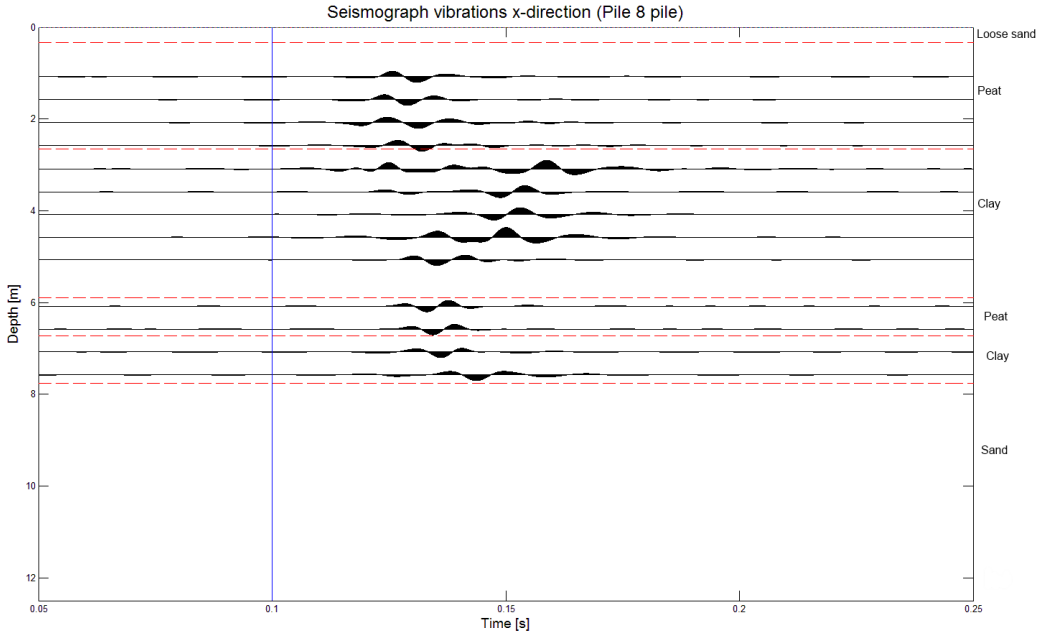

FIGURE D.18: Seismograph for PS test on pile 8, vibration in x-direction. The vertical line at 0.1[s] signifies the time of hammer impact.

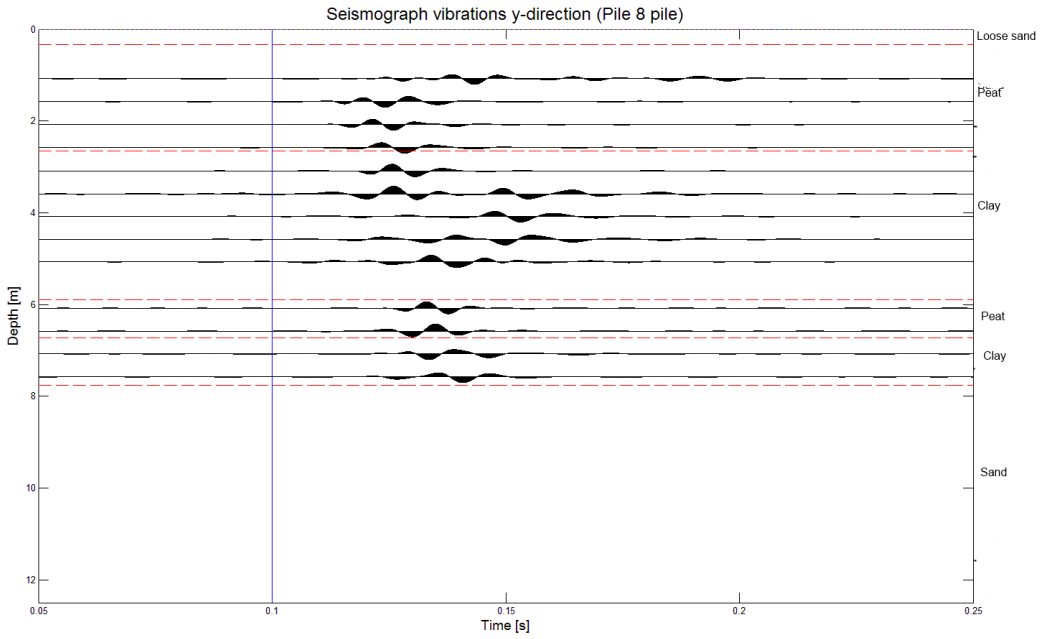

FIGURE D.19: Seismograph for PS test on pile 8, vibration in y-direction. The vertical line at 0.1[s] signifies the time of hammer impact.

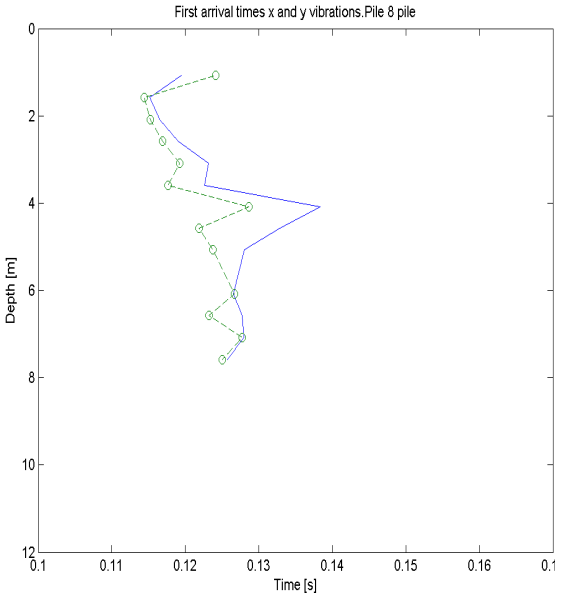

FIGURE D.20: First a.t's for PS test on pile 8. x- is the blue full line and y- is the green broken line.

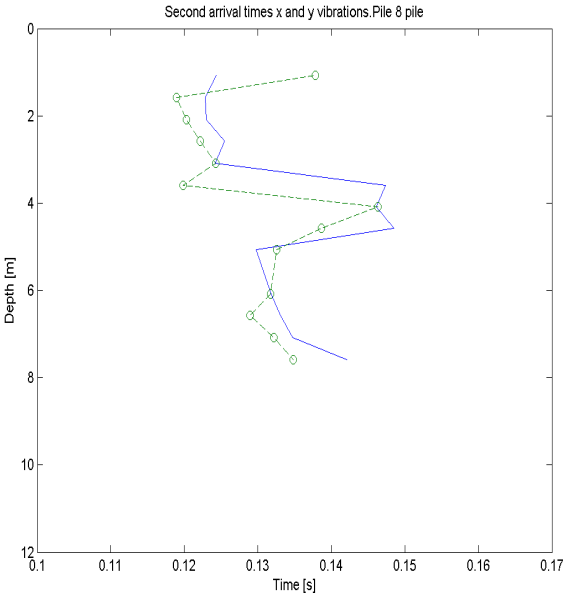

FIGURE D.21: Second a.t's for PS test on pile 8. x- is the blue full line and y- is the green broken line.

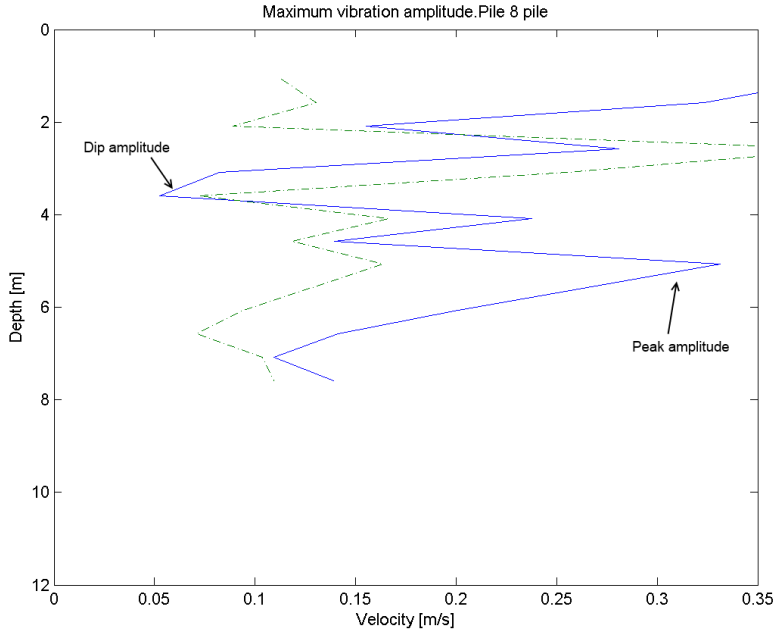

FIGURE D.22: Maximum vibration amplitude for PS test on pile 8. x- is the blue full line and y- is the green broken line.

D.8 Results pile 13 from the first field test

In pile 13 there is possibly a flaw at $8m$ depth.

The seismographs and amplitude figure show a similar pattern as other piles, not showing anything in particular. There is an early arrival of the s-wave between $8.33m$ and $8.63m$ which suggests a bulge at this depth.

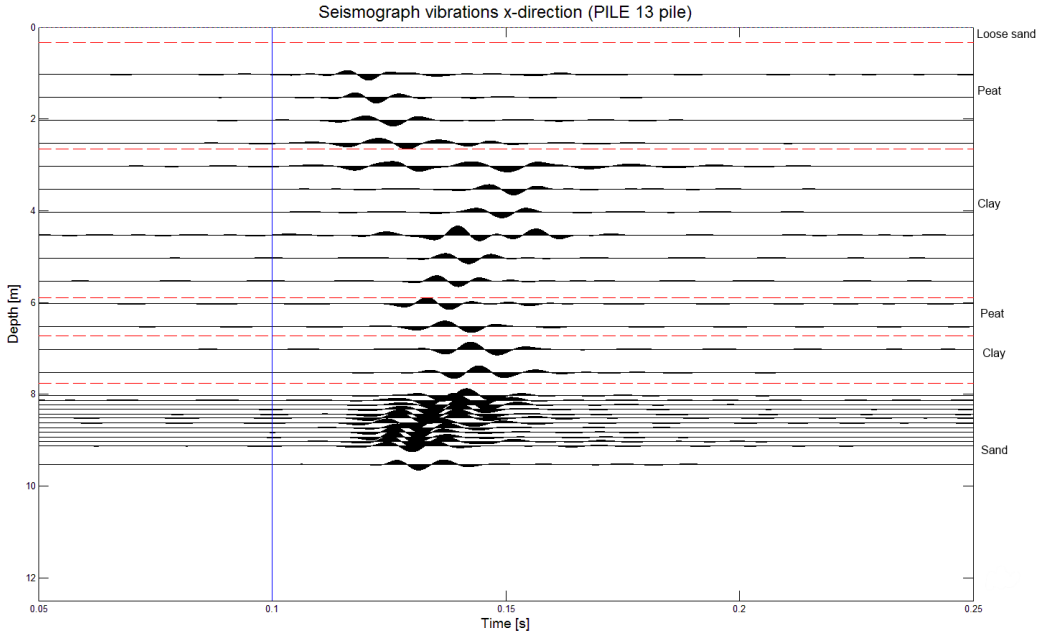

FIGURE D.23: Seismograph for PS test on pile 13, vibration in x-direction. The vertical line at 0.1[s] signifies the time of hammer impact.

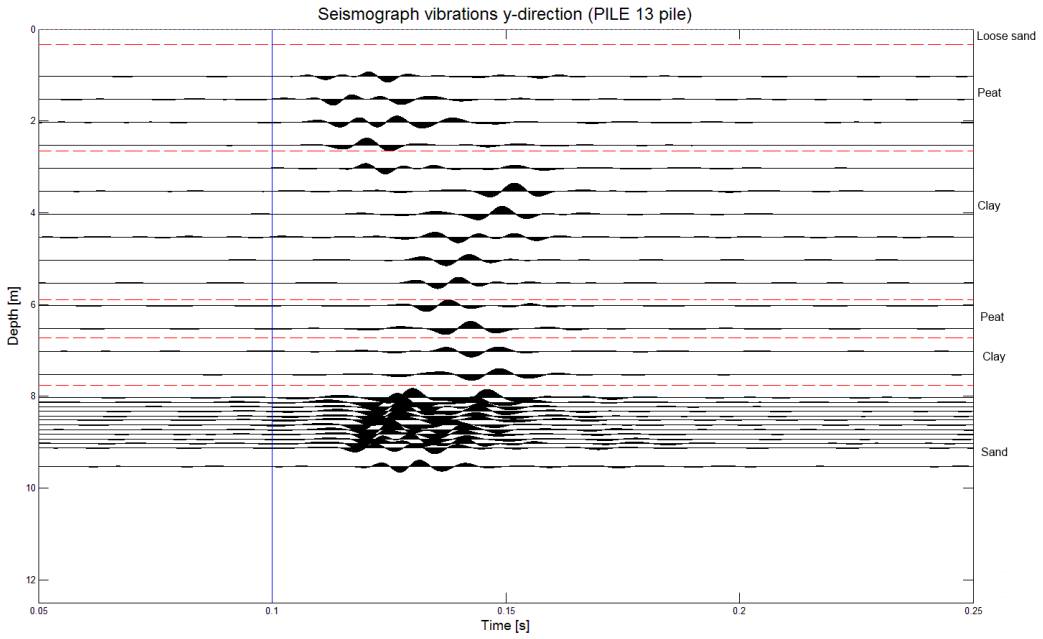

FIGURE D.24: Seismograph for PS test on pile 13, vibration in y-direction. The vertical line at 0.1[s] signifies the time of hammer impact.

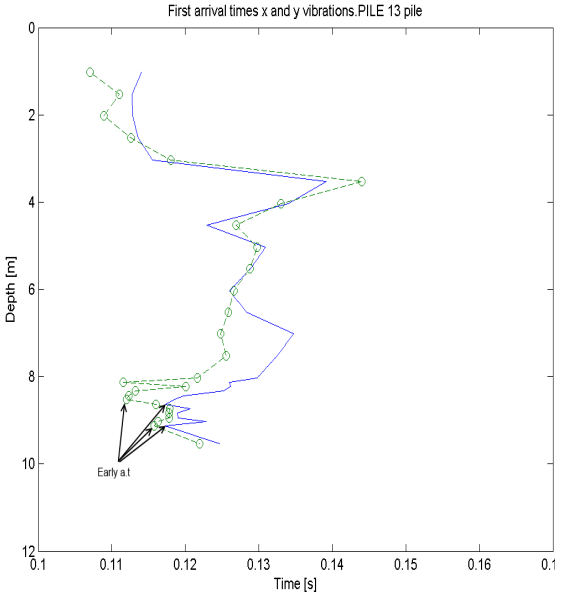

FIGURE D.25: First a.t's for PS test on pile 13. x- is the blue full line and y- is the green broken line.

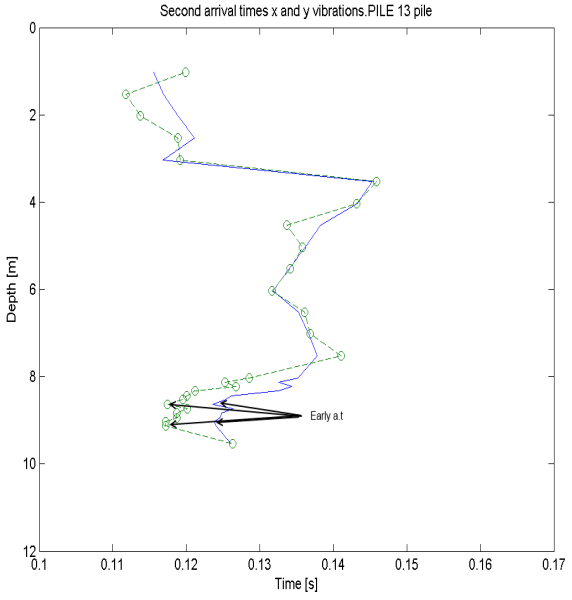

FIGURE D.26: Second a.t's for PS test on pile 13. x- is the blue full line and y- is the green broken line.

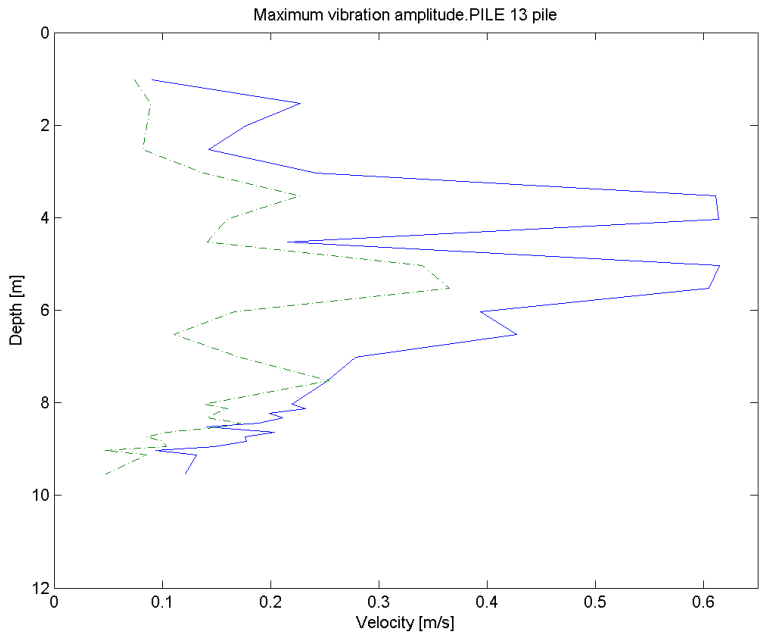

FIGURE D.27: Maximum vibration amplitude for PS test on pile 13. x- is the blue full line and y- is the green broken line.

D.9 Results pile 14 from the first field test

In pile 14 there is possibly a flaw at $8m$.

The seismographs D.28 and D.29 and amplitude plot D.32 are remarkably smooth. Also the a.t plots shows only a few early arrivals which can all be attributed to remaining noise. Compared to patterns found in other piles, this one seems very average suggesting that it actually does not have any significant defects.

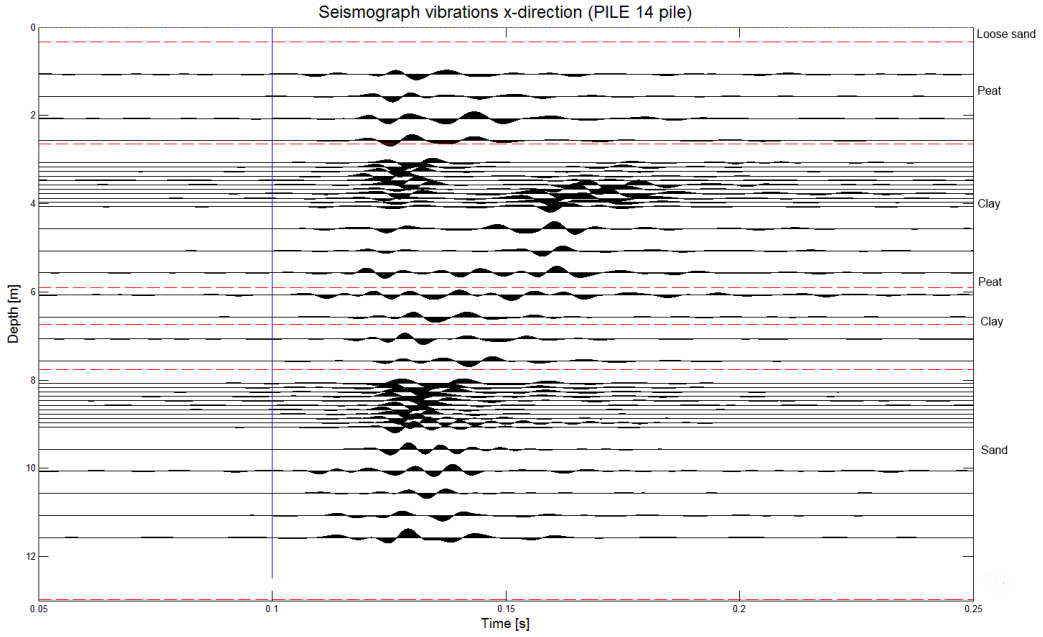

FIGURE D.28: Seismograph for PS test on pile 14, vibration in x-direction. The vertical line at 0.1[s] signifies the time of hammer impact.

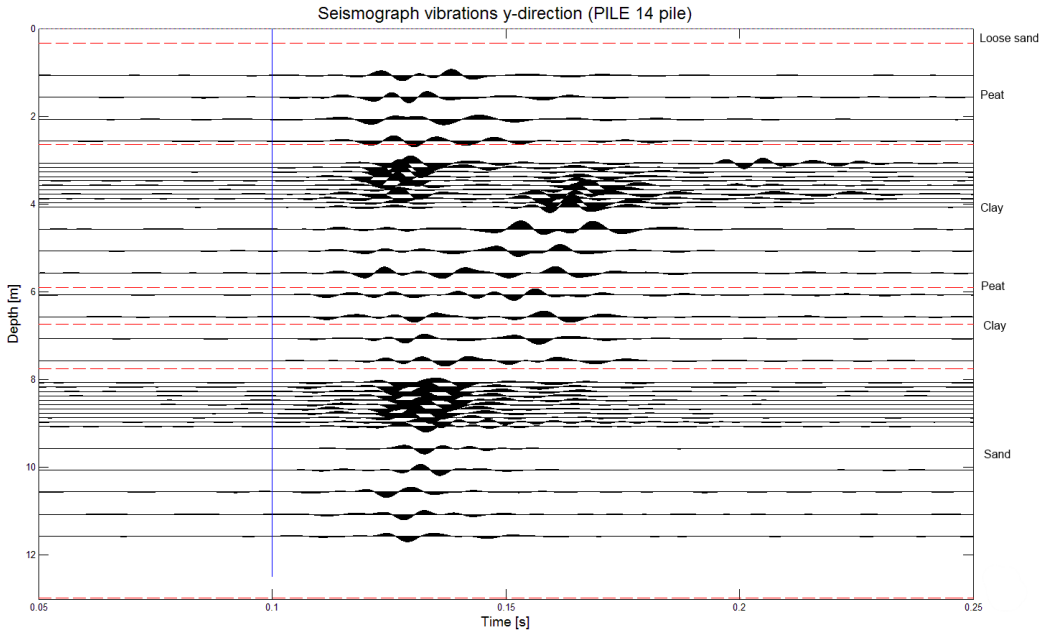

FIGURE D.29: Seismograph for PS test on pile 14, vibration in y-direction. The vertical line at 0.1[s] signifies the time of hammer impact.

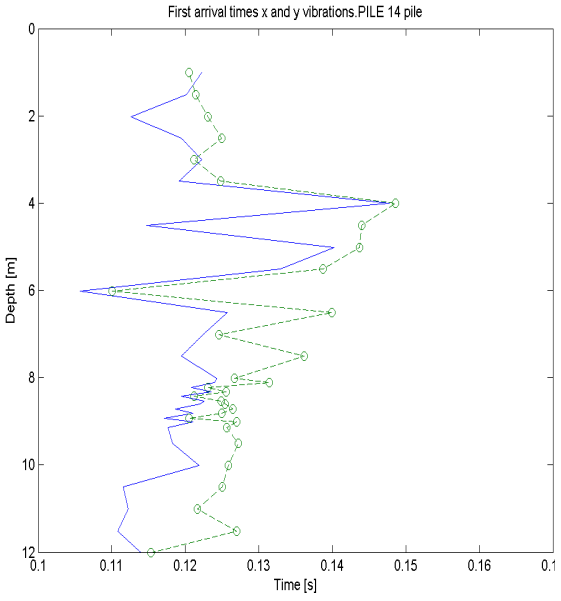

FIGURE D.30: First a.t's for PS test on pile 14. x- is the blue full line and y- is the green broken line.

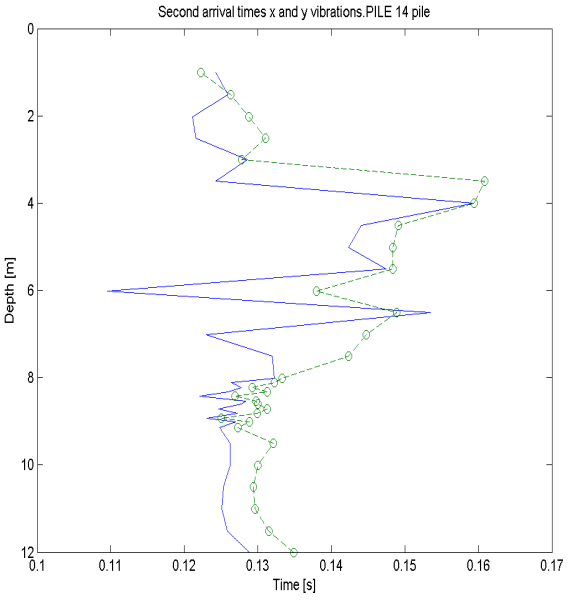

FIGURE D.31: Second a.t's for PS test on pile 14. x- is the blue full line and y- is the green broken line.

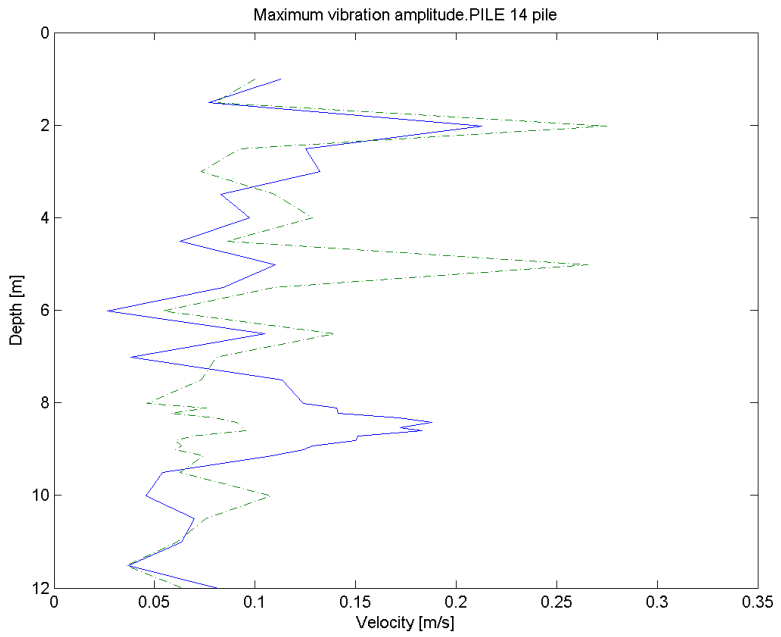

FIGURE D.32: Maximum vibration amplitude for PS test on pile 14. x- is the blue full line and y- is the green broken line.

D.10 Results pile 17 from the first field test

The final pile in the first test round possibly has flaws at $3m$ and $8m$.

The seismograph D.34 shows a reflection at 3.07 and $3.17m$. The reflection is not seen in other tests, but does occur very late ($0.75s$ after the first wavelet). The amplitude behaves like the other tests.

Furthermore there is a small reduction in a.t at $3.17m$ which might be bulge although the reflection might suggest a crack rather than a bulge.

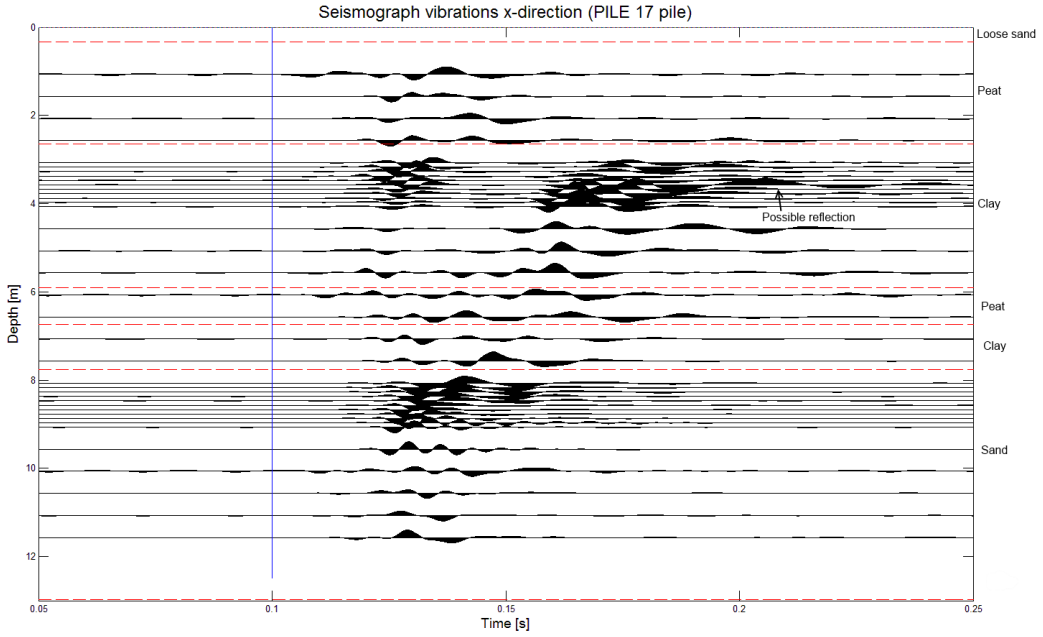

FIGURE D.33: Seismograph for PS test on pile 14, vibration in x-direction. The vertical line at 0.1[s] signifies the time of hammer impact.

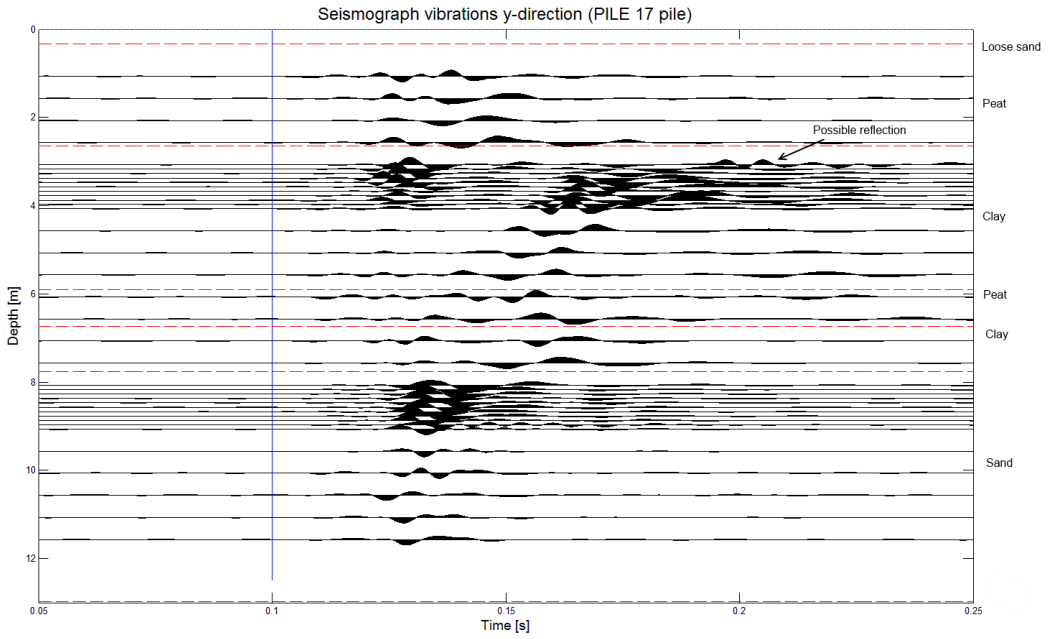

FIGURE D.34: Seismograph for PS test on pile 17, vibration in y-direction. The vertical line at 0.1[s] signifies the time of hammer impact.

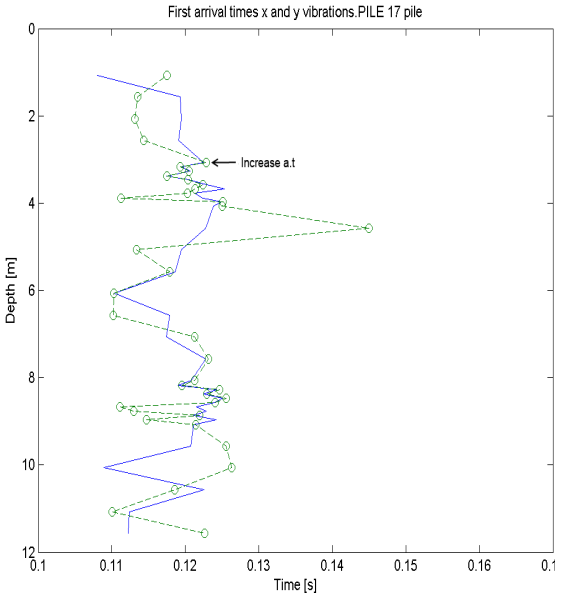

FIGURE D.35: First a.t's for PS test on pile 17. x- is the blue full line and y- is the green broken line.

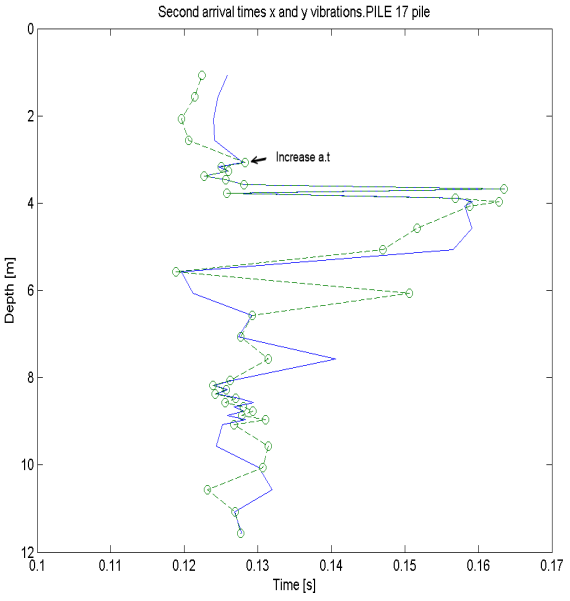

FIGURE D.36: Second a.t's for PS test on pile 17. x- is the blue full line and y- is the green broken line.

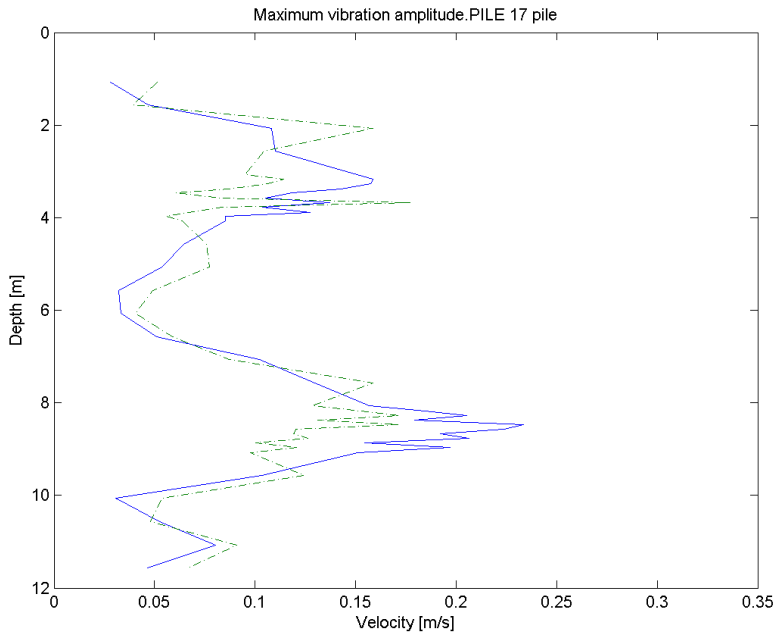

FIGURE D.37: Maximum vibration amplitude for PS test on pile 17. x- is the blue full line and y- is the green broken line.

D.11 Detection of flaws vs. designed flaws

Per pile (except 8, which was already known) the following questions are answered to asses the success of detection from the field test.

1. What is the actual flaw?
2. What was predicted?
3. How can the results be explained?
   (a) Is it caused by soil conditions?
   (b) Is it related to the type of flaw?
   (c) Is it related to the test conditions?
   (d) Could it be seen in hindsight?
4. What can be learned?

Pile 3: In pile 3 the true flaws are a bulge at $3m$ and a neck at $6m$. The detected flaw was a bulge at $7.88m$. Hence the detection went wrong, assuming that the installation of the pile and creation of the flaws went as expected.

The top flaw is a bulge which could cause extra waves passing above and below the flaw. Mainly it is expected to decrease the a.t, which is not detected. The main reason can be deduced from the height of the test. Due to the mistaken flaw depth before-hand the resolution is increased from 3.5 to 4.5 meters, so this would miss the flaw. In hindsight this flaw would still be hard

to find with the collected data.

The second flaw is at $6m$ which is directly between two measurement points ($5.88m$ and $6.38m$). One main reason theses flaws were missed is because of the low resolution around the location of the flaw. Also the effect of the flaw can be seen by comparing two parts of the pile where there are no flaws, therefore the range of data needs to be increased.

The bulge that was identified was based on comparison to vibrations measured around the $6m$. Since this method is relative it will be a common mistake to define a neck at one depth instead a bulge at another depth.

Pile 7: Pile 7 has a bulge at $8m$, which was mistaken for a neck. The depth of the flaw was already known so getting this right does not mean the process went well.

The neck was detected based on a delay in a.t. This mistake could be made due to the local wave velocity. Below $8m$ v_s increases so at these depths the a.t shortens. This would lead to artificial delays at $8m$ when compared to lower depths. Hence changes in v_s can easily confuse results. Also the size of the defect might be too small to show significant changes in measured vibrations.

In hindsight it was too soon to identify the flaw as a neck. With more data above the flaw the bulge might have been identified. The actual presence of a flaw is mainly based on reflected waves seen at $7.48m$. Therefore the seismograph remains useful, although it does not discriminate between flaw types.

Pile 13: Pile 13 should have a neck at $8m$, as opposed to what was detected; a bulge at $8.83m$. The bulge was based on an early a.t which was found in comparison to surrounding measurement depths. As mentioned before it is possible to make this mistake since the evaluation is mostly done based on comparison between waves at varying depths.

In hindsight it would still be hard to see the neck. One way to avoid this mistake is to improve the resolution around the flaw. Only measurements every $50cm$ could miss the flaw if the flaw is smaller than $50cm$ in depth.

Pile 14: In pile 14 there should not be any flaw, which was also the conclusion of the PS results. The results followed the overall trend of all tests which probably meant that the pile had no particular characteristics. This observation could be used to identify piles without flaws.

Pile 17: In pile 17 the only shallow flaw was detected, a neck at $3.17m$. In truth this should be a crack at $3m$ and in addition a neck at $8m$.

The flaw at $3.17m$ was based on a delay in local a.t and reflections at $3.07m$. It seems that the delay was not caused by the flaw, but the reflection could have been. The crack flaw might cause a reflection due to the large change in impedance so the crack might not be completely closed. The reflection arrives 0.075s after the first wave which corresponds to 6.75m with s-wave velocity 90m/s. This is too far, which means that the origin of the reflection remains questionable.

At $8m$ there is no clear proof of the expected delay in a.t. Of course if a neck is too small, waves radiating above and below the neck will be picked up and the neck is simply missed.

Appendix E

Appendix: Results of the Second Field Test

E.1 Introduction

For each test, vibrations in the x- and y- direction are plotted in the time and space domain in a seismograph. Also z-vibrations are plotted, although these proved to less useful. The dashed red horizontal lines represent soil layering found in a CPT done prior to the installation of the piles. The first layer is loose sand followed by peat, clay, peat, clay, stiffer sand, and clay.

For these tests, it is possible to accurately find the time of the first arriving waves. Therefore it is possible to make modified seismographs as mentioned in chapter 5. This will make the earlier waves clearer and increase the information that may be regarded. These plots are made for the vibrations in the x- and y- direction.

In addition the arrival times(a.t) of the first vibration and 0.65% of the maximum amplitudes are plotted as first and second a.t's for all the PS tests. Finally the maximum amplitudes of vibrations are plotted versus depth.

For all tests the time start $0.02s$ before the hammer pulse. In the first field test this was $0.1s$. Furthermore, each graph is plotted on the z-axis which corresponds to the depth of the steel reinforcement. Therefore the zero value is always above surface level.

E.2 Results pile 2 from the second field test

In pile 2 there is a flaw at $6m$, possibly a neck or bulge. The seismographs show many reflections above the $8m$ mark. This is seen more often, and is probably caused by the stiffer sand layer below instead of any flaws in the pile. At $6m$ to $7m$ the a.t varies a lot which could suggest a neck or bulge in that area. Furthermore, figure E.8 shows that the amplitude jumps around $6m$ in a similar pattern as seen in the simulation when a neck or bulge is modeled.

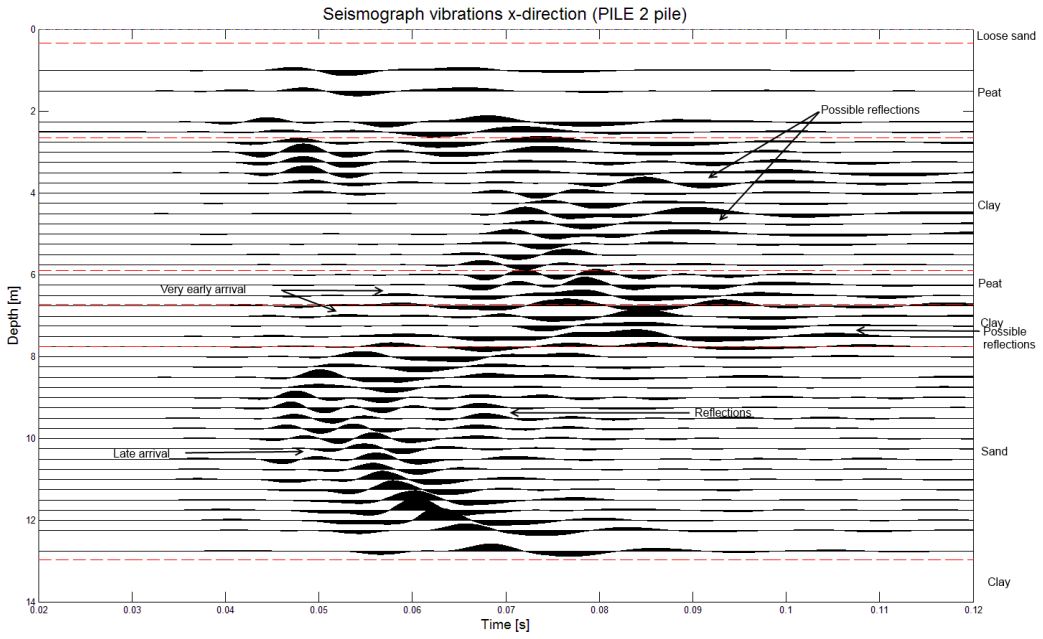

FIGURE E.1: Seismograph for PS test on pile 2, vibration in x-direction. The time axis starts at the point of hammer impact and depth starts at the level of the reinforcement.

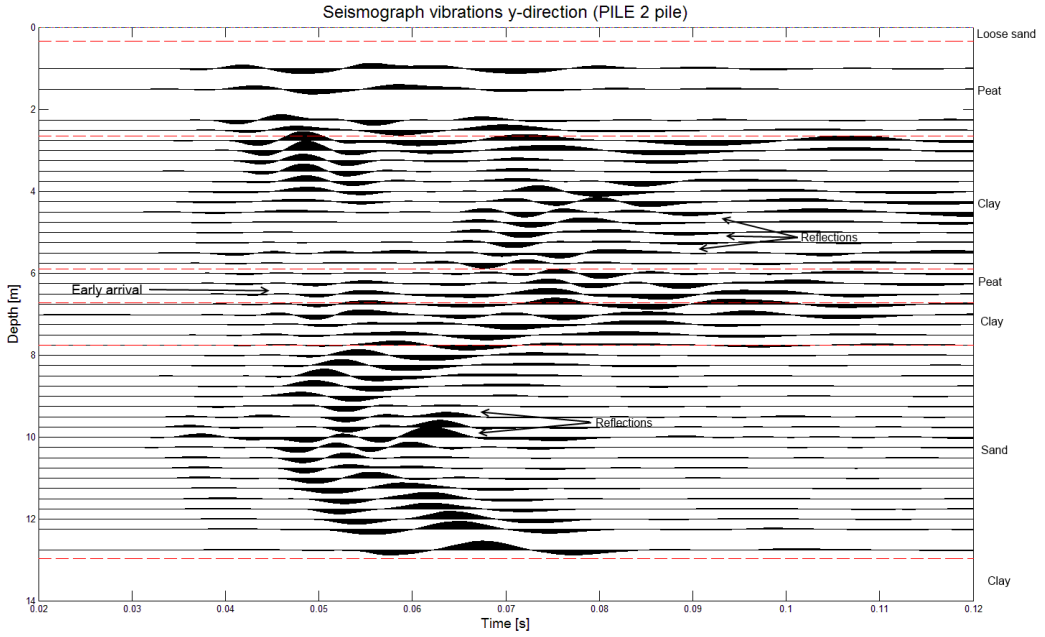

FIGURE E.2: Seismograph for PS test on pile 2, vibration in y-direction. The time axis starts at the point of hammer impact and depth starts at the level of the reinforcement.

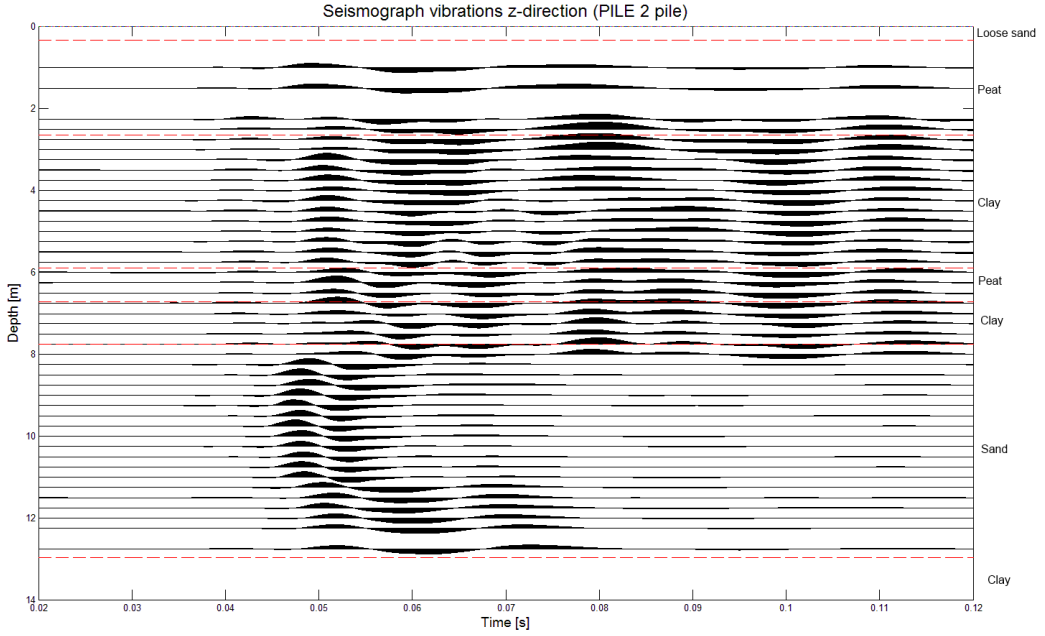

FIGURE E.3: Seismograph for PS test on pile 2, vibration in z-direction. The time axis starts at the point of hammer impact and depth starts at the level of the reinforcement.

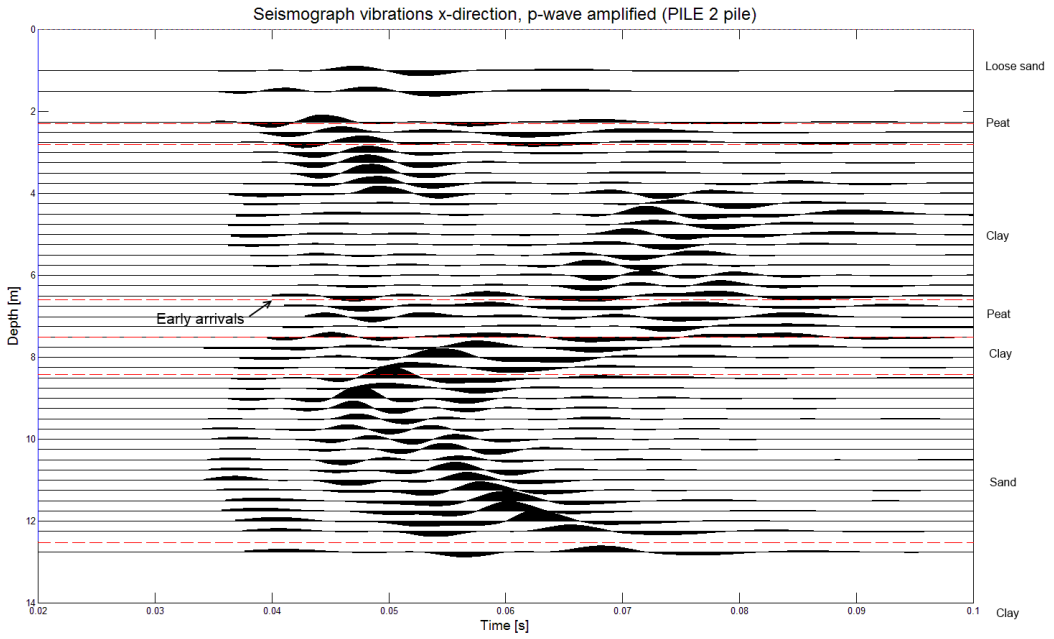

FIGURE E.4: Modified seismograph for PS test on pile 2, vibration in x-direction. The time axis starts at the point of hammer impact and depth starts at the level of the reinforcement.

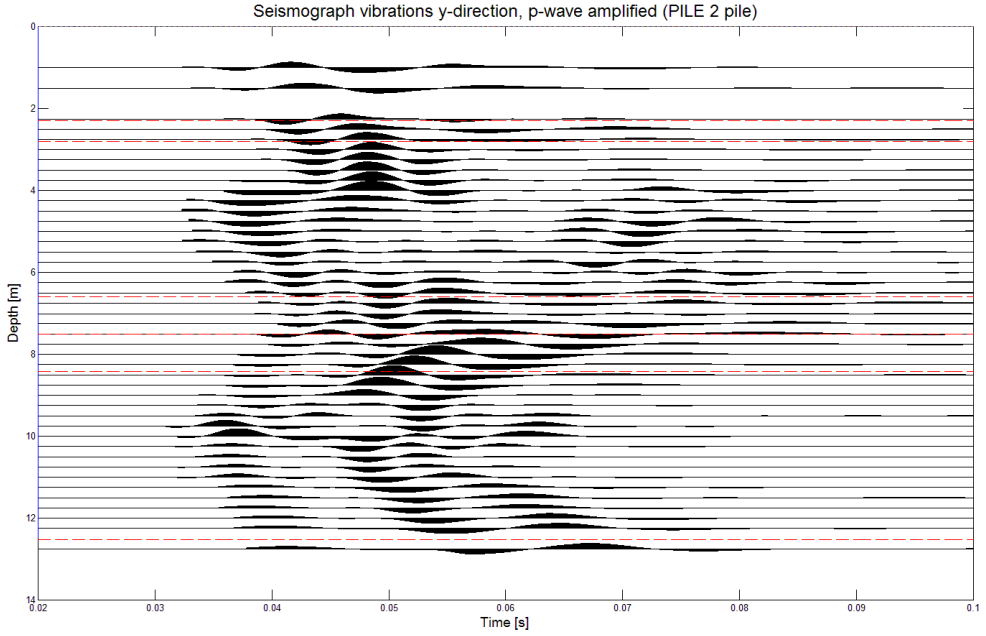

FIGURE E.5: Modified seismograph for PS test on pile 2, vibration in y-direction. The time axis starts at the point of hammer impact and depth starts at the level of the reinforcement.

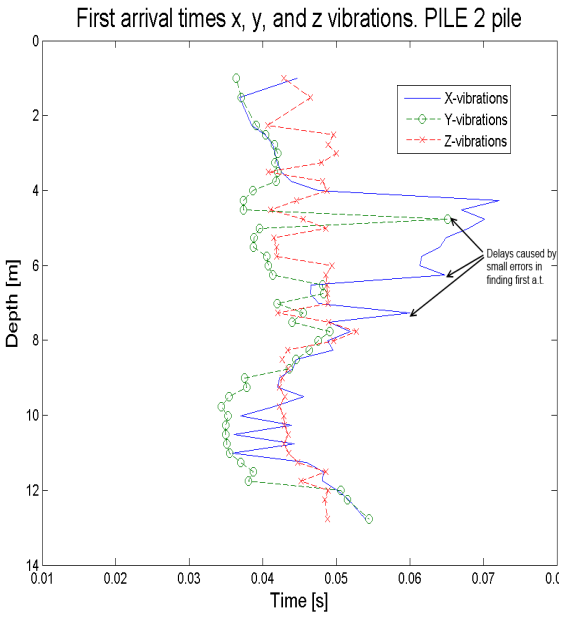

FIGURE E.6: First a.t's for PS test on pile 2. x- is the blue full line, y- is the green broken and circled line, and z- is the red dashed and crossed line.

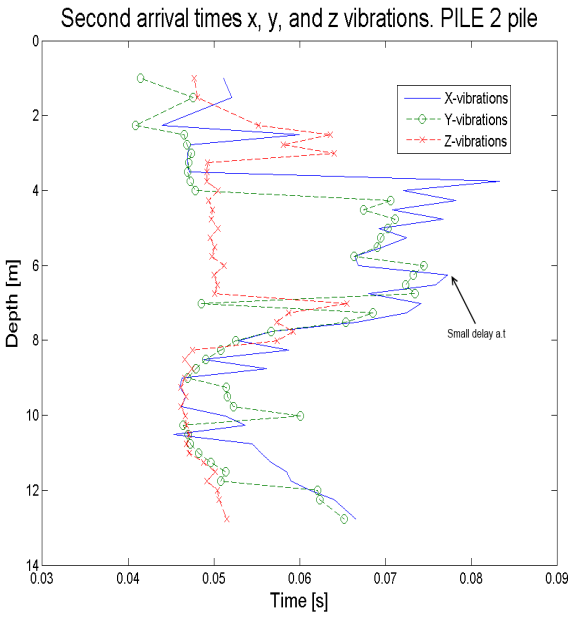

FIGURE E.7: Second a.t's for PS test on pile 2. x- is the blue full line, y- is the green broken and circled line, and z- is the red dashed and crossed line.

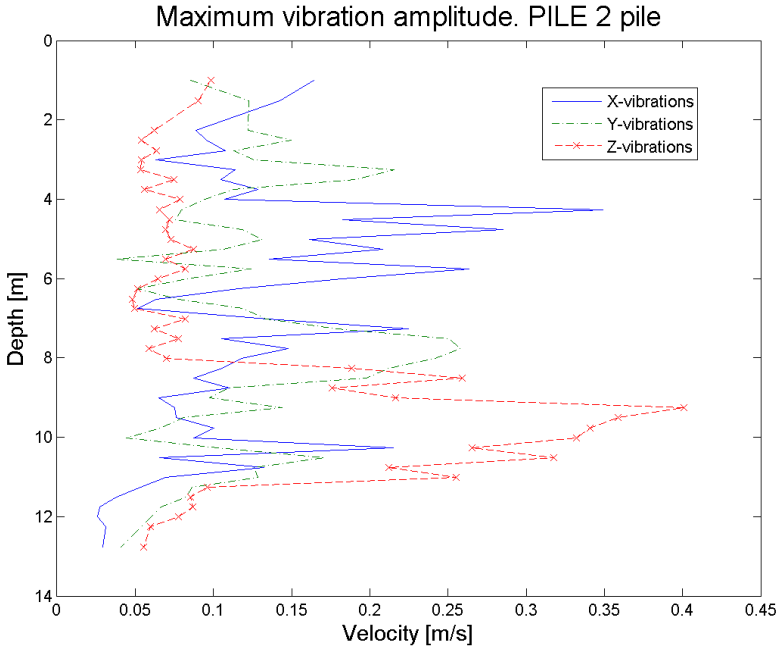

FIGURE E.8: Maximum vibration amplitude for PS test on pile 2. x- is the blue full line, y- is the green broken and circled line, and z- is the red dashed and crossed line.

E.3 Results pile 3 from the second field test

In pile 3 the flaws are already known from the first field test, there should be a bulge at $3m$ and a neck at $6m$. In this test the hitting block was not mounted on the side and hit downwards but rather at the top and hit sideways. This introduced shear waves instead of compression waves. The aim of this test was to see if this would improve results.

The quality of the data is the same in this test as in the others. The amplitude of the measured vibrations is in the same order of magnitude while the noise is too.

Neither seismographs or a.t figures show clear proof of the flaws that should be in the pile. The amplitude at $6m$ is relatively low, which might be a result of the flaw.

Introducing shear waves does not really change the results. It is still possible to find the pile tip but flaws are not really visible.

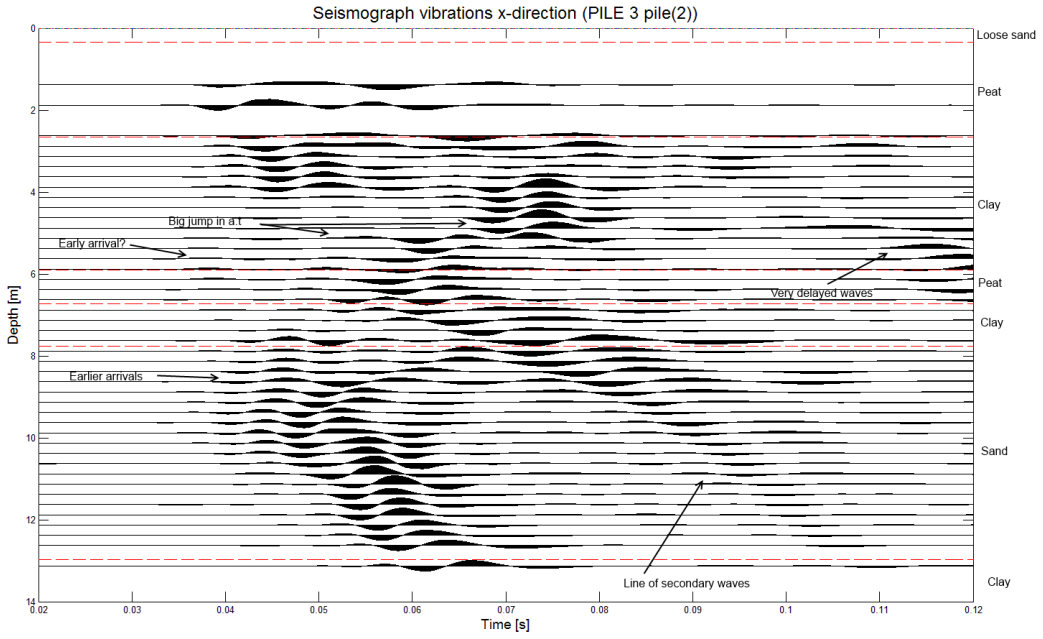

FIGURE E.9: Seismograph for PS test on pile 3, vibration in x-direction. The time axis starts at the point of hammer impact and depth starts at the level of the reinforcement.

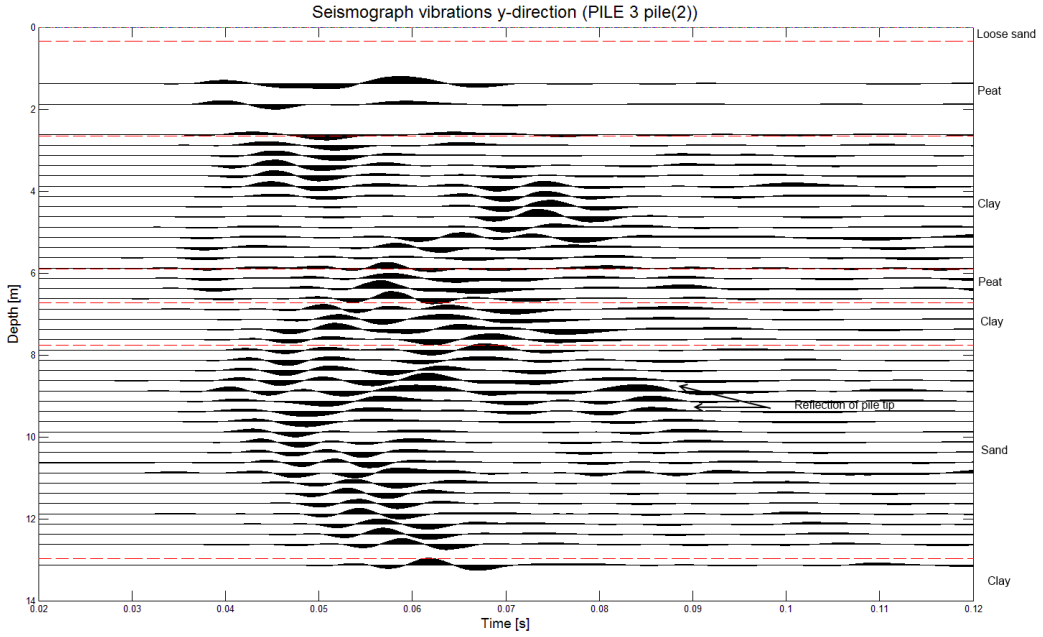

FIGURE E.10: Seismograph for PS test on pile 3, vibration in y-direction. The time axis starts at the point of hammer impact and depth starts at the level of the reinforcement.

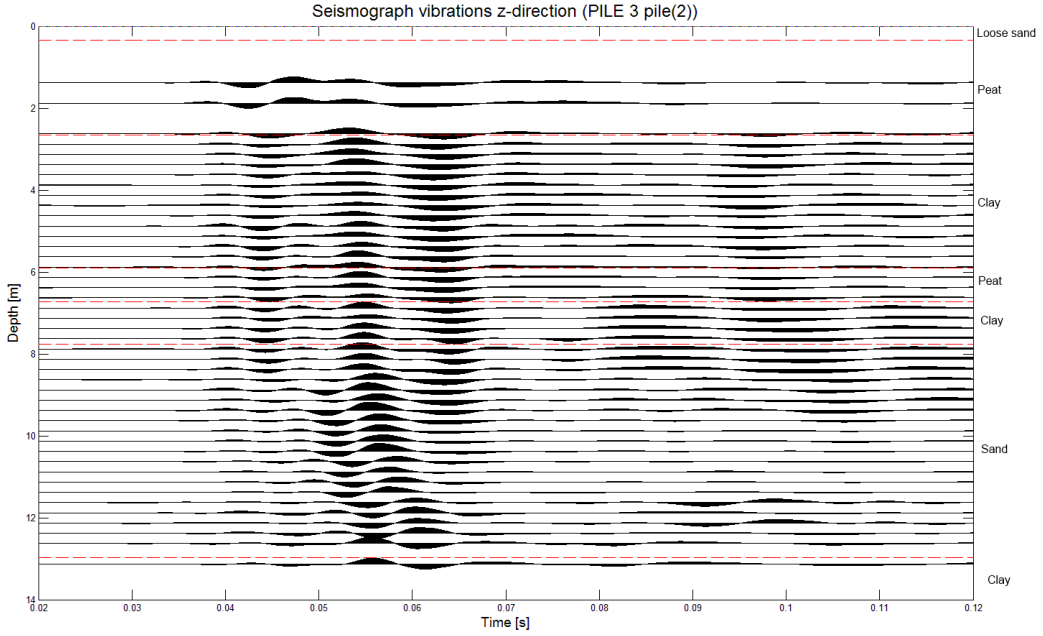

FIGURE E.11: Seismograph for PS test on pile 3, vibration in z-direction. The time axis starts at the point of hammer impact and depth starts at the level of the reinforcement.

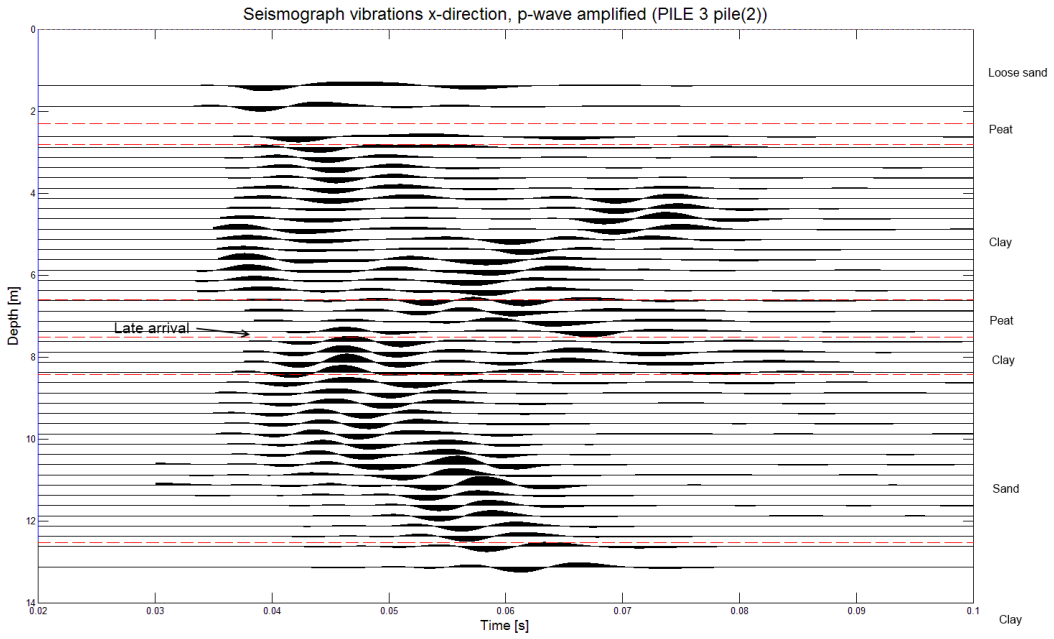

FIGURE E.12: Modified seismograph for PS test on pile 3, vibration in x-direction. The time axis starts at the point of hammer impact and depth starts at the level of the reinforcement.

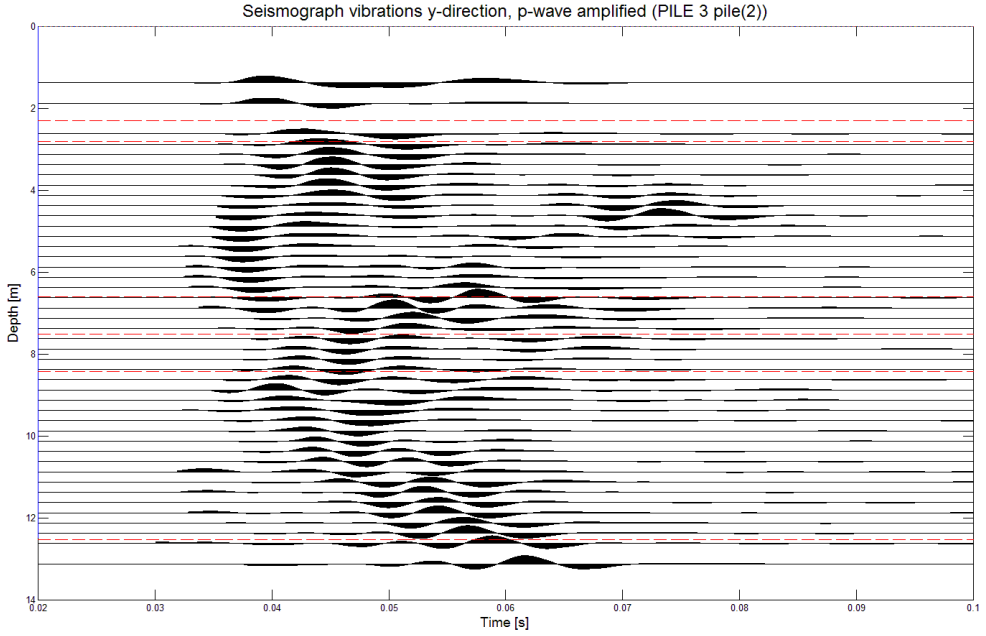

FIGURE E.13: Modified seismograph for PS test on pile 3, vibration in y-direction. The time axis starts at the point of hammer impact and depth starts at the level of the reinforcement.

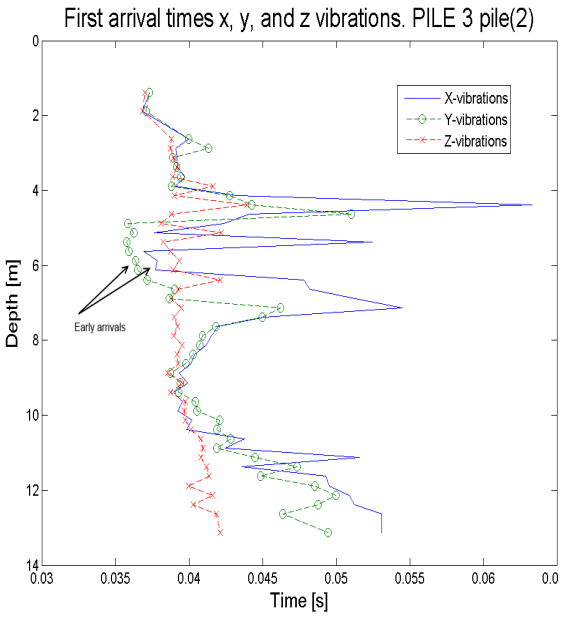

FIGURE E.14: First a.t's for PS test on pile 3. x- is the blue full line, y- is the green broken and circled line, and z- is the red dashed and crossed line.

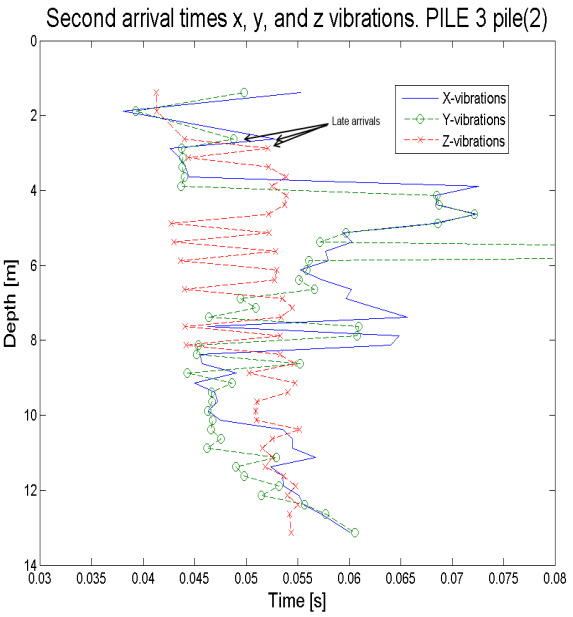

FIGURE E.15: Second a.t's for PS test on pile 3. x- is the blue full line, y- is the green broken and circled line, and z- is the red dashed and crossed line.

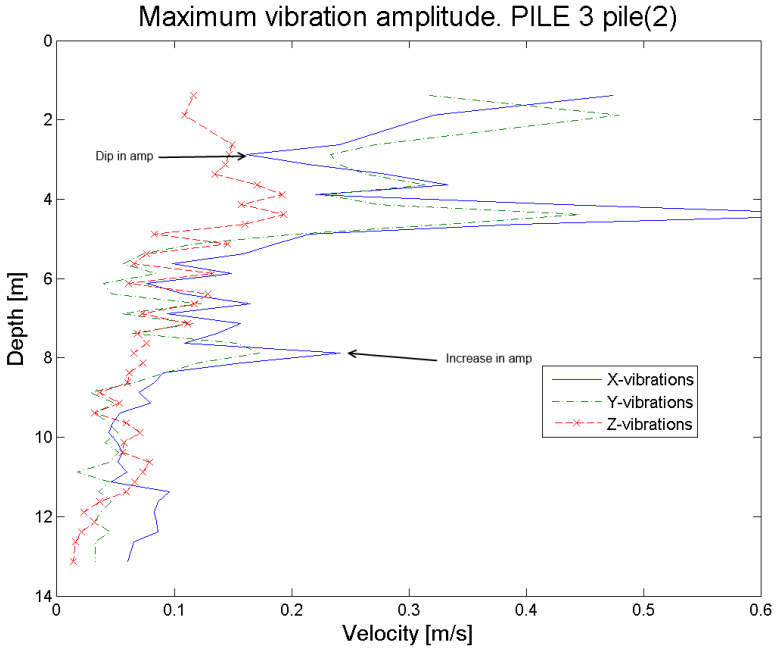

FIGURE E.16: Maximum vibration amplitude for PS test on pile 3. x- is the blue full line, y- is the green broken and circled line, and z- is the red dashed and crossed line.

E.4 Results pile 4 from the second field test

In pile 4, a possible flaw at $3m$ can be detected. There are many changes in a.t and amplitude but these can be seen in many other piles as well and can be attributed to changes in soil properties.

At $3m$ however the seismographs show earlier arrivals around $3m$ and the amplitude also dips which does not occur in pile 8, which is supposedly flawless. The other peaks in amplitude can also be seen in the results of pile 8 in figure E.32.

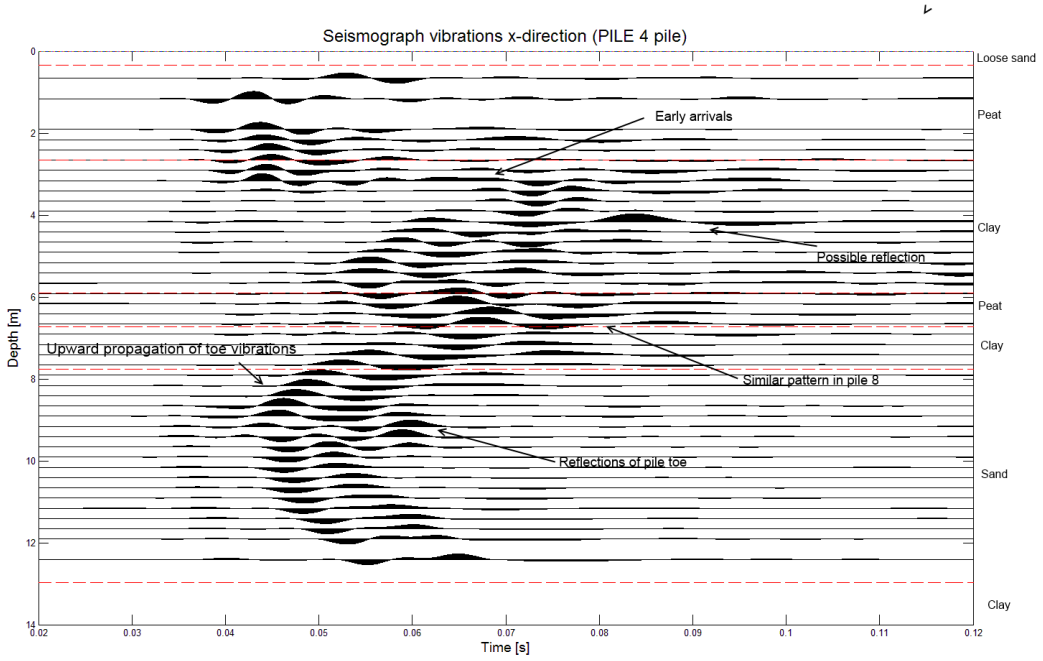

FIGURE E.17: Seismograph for PS test on pile 4, vibration in x-direction. The time axis starts at the point of hammer impact and depth starts at the level of the reinforcement.

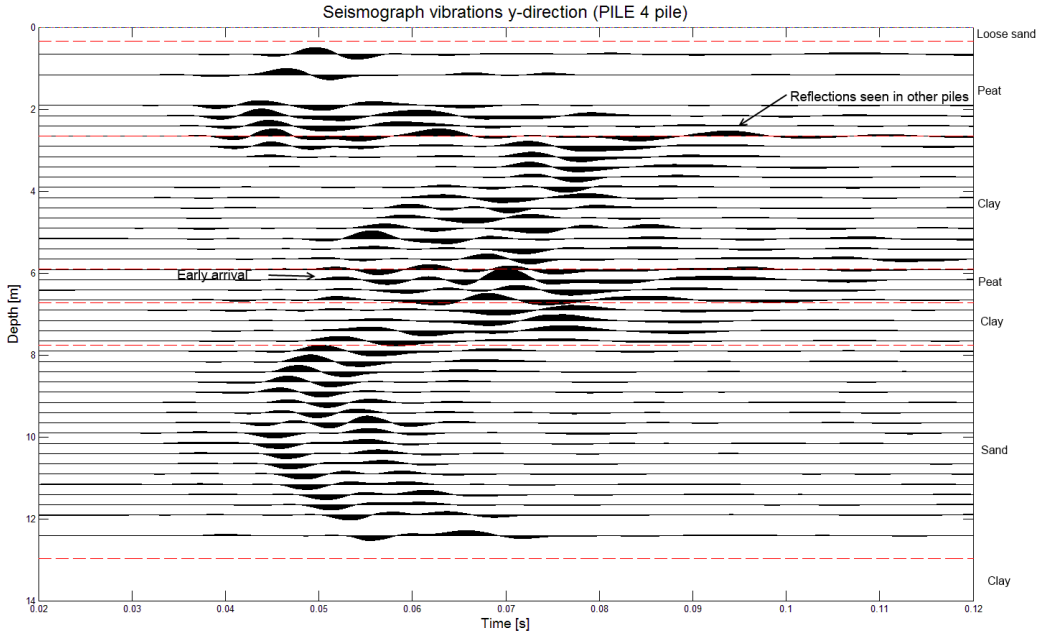

FIGURE E.18: Seismograph for PS test on pile 4, vibration in y-direction. The time axis starts at the point of hammer impact and depth starts at the level of the reinforcement.

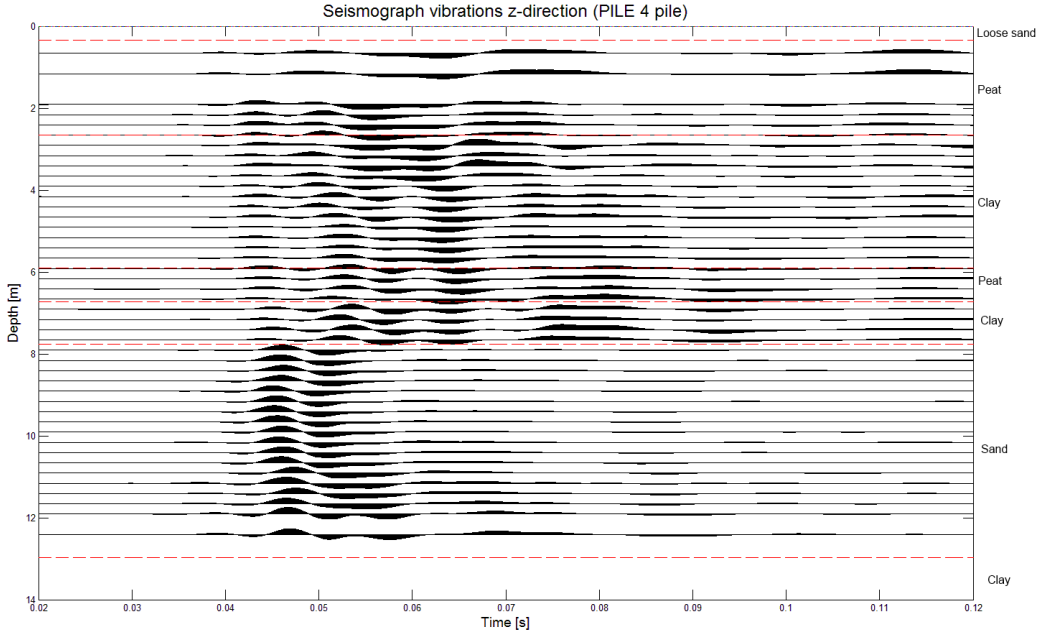

FIGURE E.19: Seismograph for PS test on pile 4, vibration in z-direction. The time axis starts at the point of hammer impact and depth starts at the level of the reinforcement.

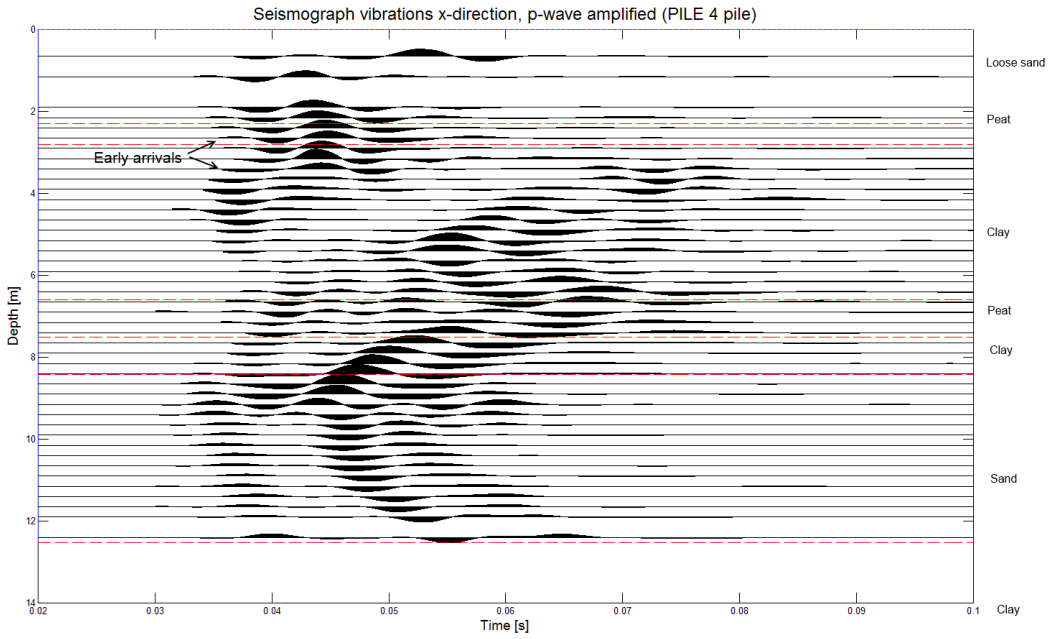

FIGURE E.20: Modified seismograph for PS test on pile 4, vibration in x-direction. The time axis starts at the point of hammer impact and depth starts at the level of the reinforcement.

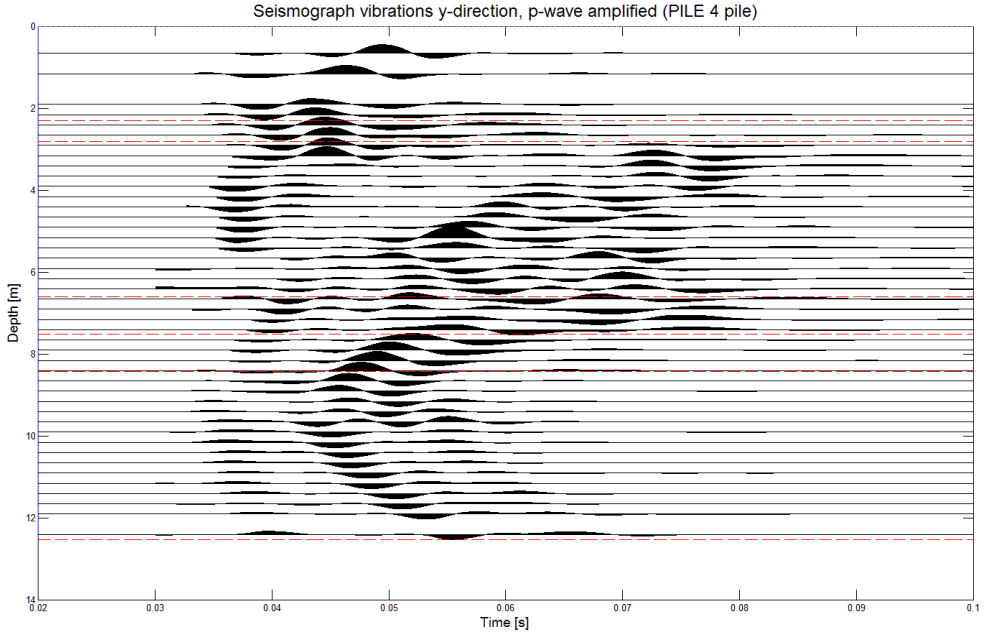

FIGURE E.21: Modified seismograph for PS test on pile 4, vibration in y-direction. The time axis starts at the point of hammer impact and depth starts at the level of the reinforcement.

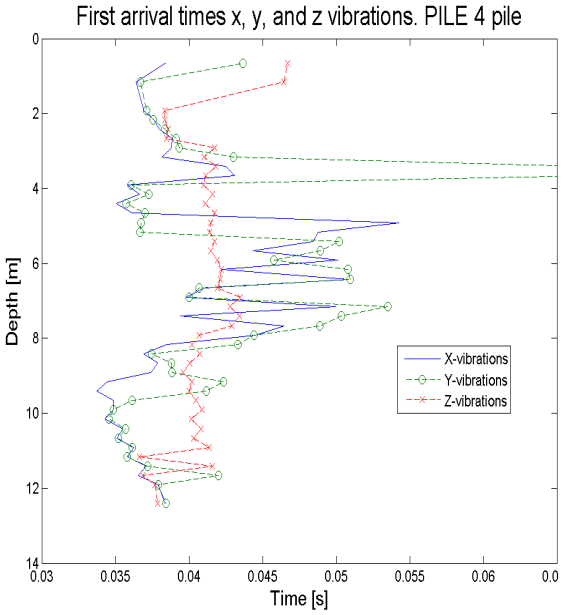

FIGURE E.22: First a.t's for PS test on pile 4. x- is the blue full line, y- is the green broken and circled line, and z- is the red dashed and crossed line.

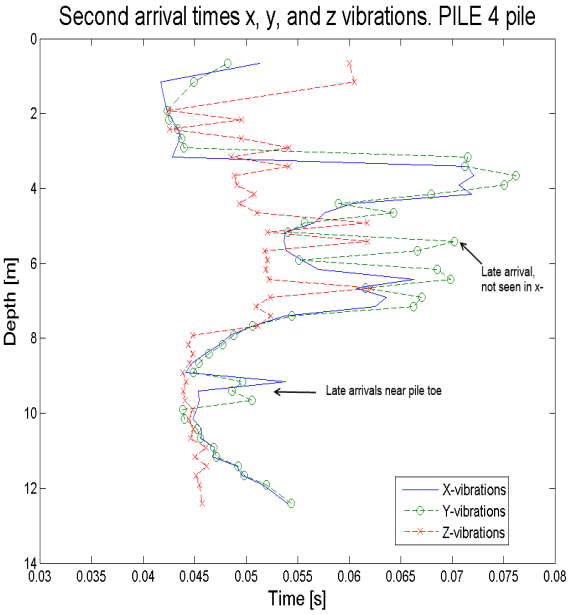

FIGURE E.23: Second a.t's for PS test on pile 4. x- is the blue full line, y- is the green broken and circled line, and z- is the red dashed and crossed line.

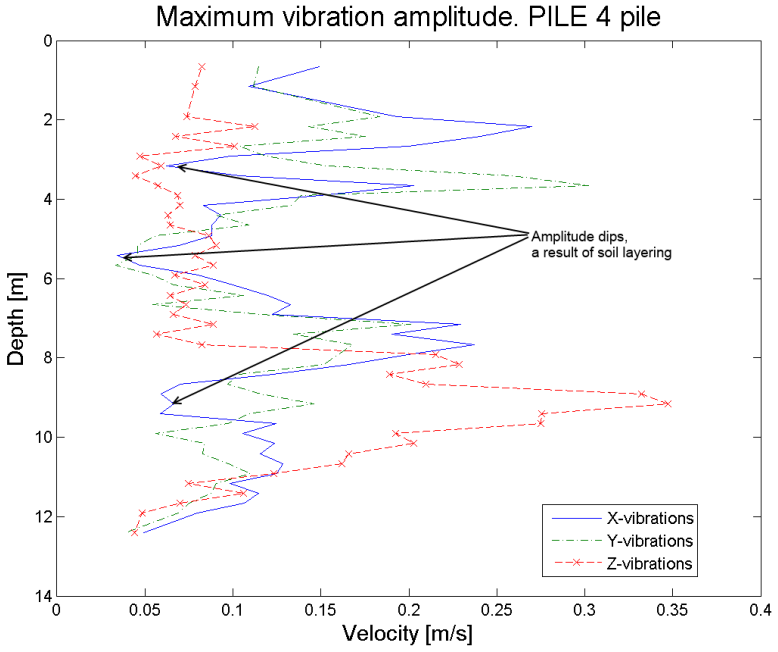

FIGURE E.24: Maximum vibration amplitude for PS test on pile 4. x- is the blue full line, y- is the green broken and circled line, and z- is the red dashed and crossed line.

E.5 Results pile 8 from the second field test

Pile 8 was designed without any flaws. The main objective of this test is to compare the second field test to the first. Also, the measurements are done till $16m$ to clearly show the pile toe.

The seismographs show reflections caused by soil layering at $3m$ and $7m$. Furthermore a.t's increase in softer soils and decrease in stiffer soils. These patterns were also seen in the first field test. In this test the results are much clearer which might be expected with the $25cm$ data increments.

The pile toe is also clearly marked. At around $10.5m$ the a.t starts to increase almost linearly. This suggests that the waves pass through the pile toe into a relatively homogeneous soil before being picked up by the cone.

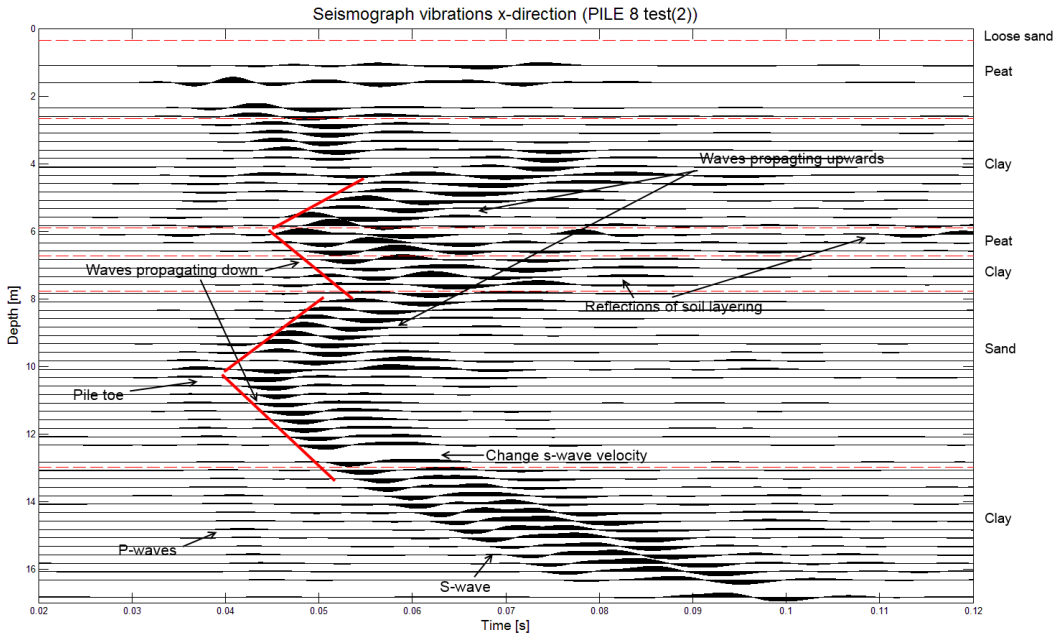

FIGURE E.25: Seismograph for PS test on pile 8, vibration in x-direction. The time axis starts at the point of hammer impact and depth starts at the level of the reinforcement.

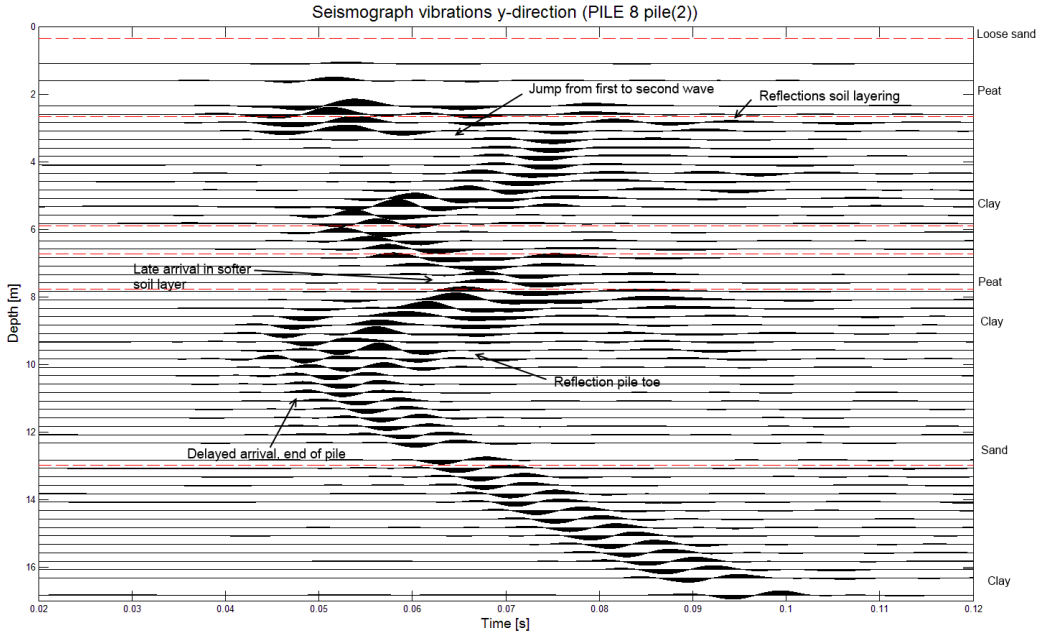

FIGURE E.26: Seismograph for PS test on pile 8, vibration in y-direction. The time axis starts at the point of hammer impact and depth starts at the level of the reinforcement.

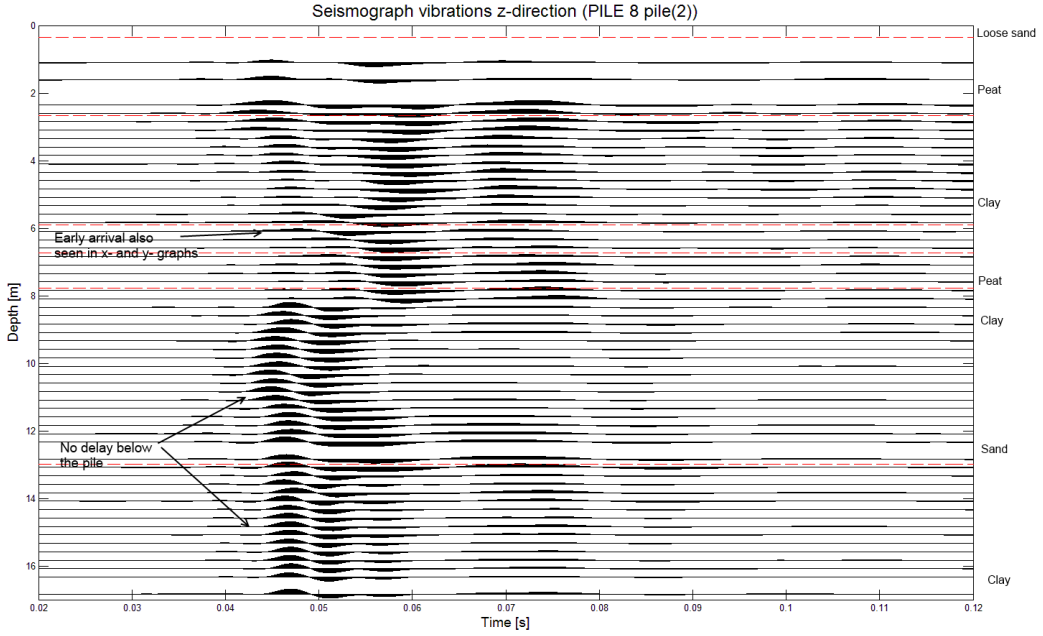

FIGURE E.27: Seismograph for PS test on pile 8, vibration in z-direction. The time axis starts at the point of hammer impact and depth starts at the level of the reinforcement.

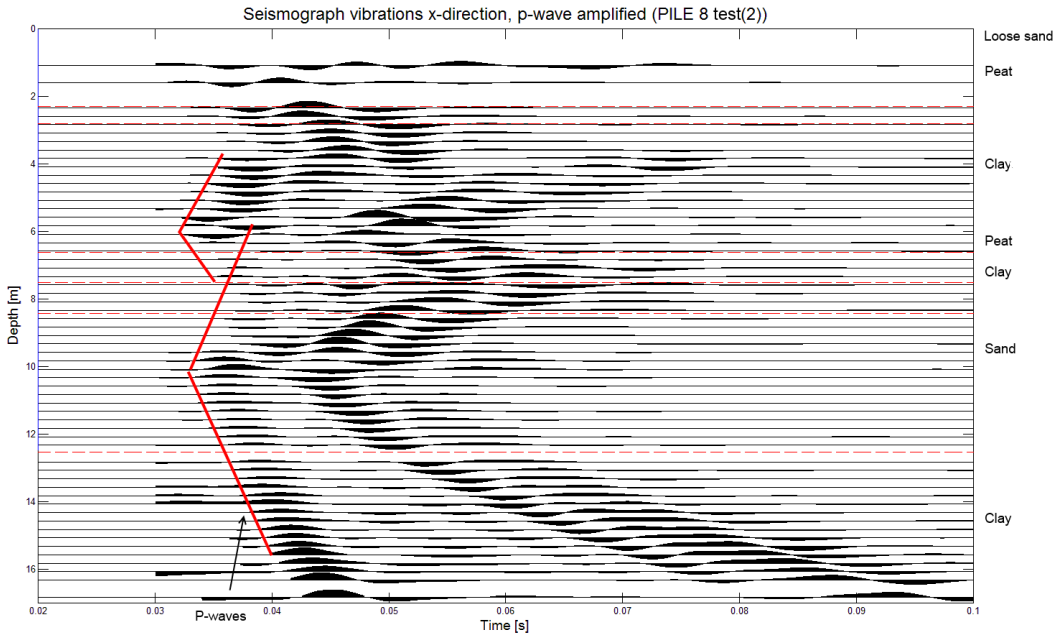

FIGURE E.28: Modified seismograph for PS test on pile 8, vibration in x-direction. The time axis starts at the point of hammer impact and depth starts at the level of the reinforcement.

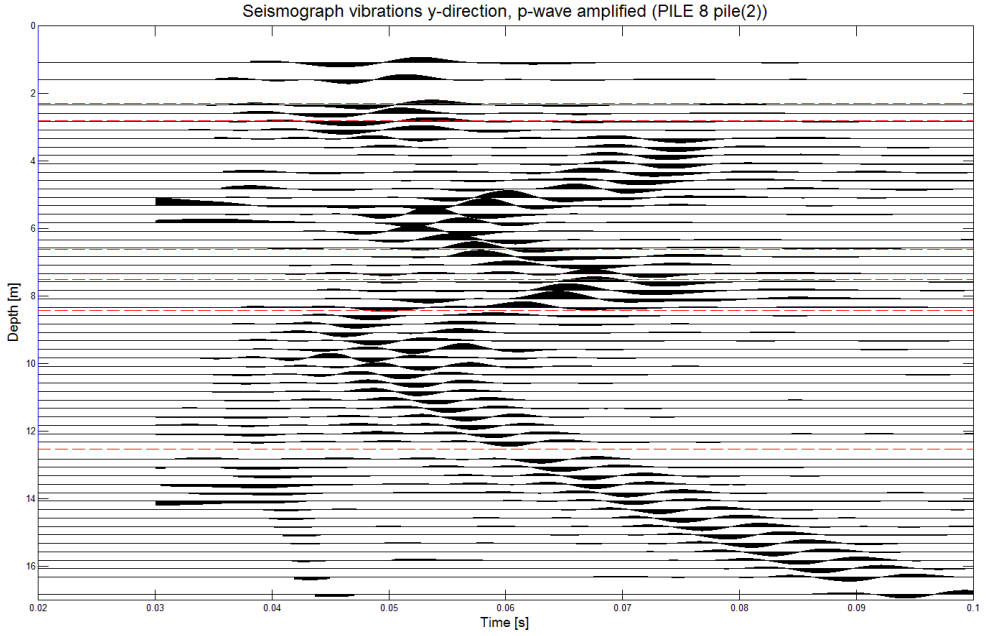

FIGURE E.29: Modified seismograph for PS test on pile 8, vibration in y-direction. The time axis starts at the point of hammer impact and depth starts at the level of the reinforcement.

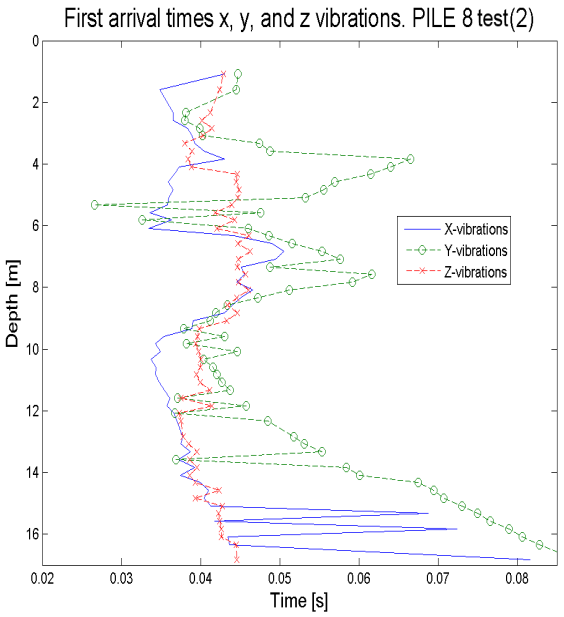

FIGURE E.30: First a.t's for PS test on pile 8. x- is the blue full line, y- is the green broken and circled line, and z- is the red dashed and crossed line.

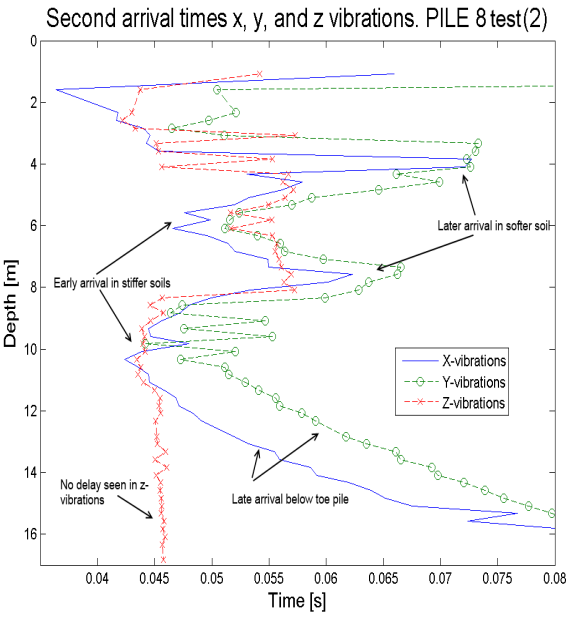

FIGURE E.31: Second a.t's for PS test on pile 8. x- is the blue full line, y- is the green broken and circled line, and z- is the red dashed and crossed line.

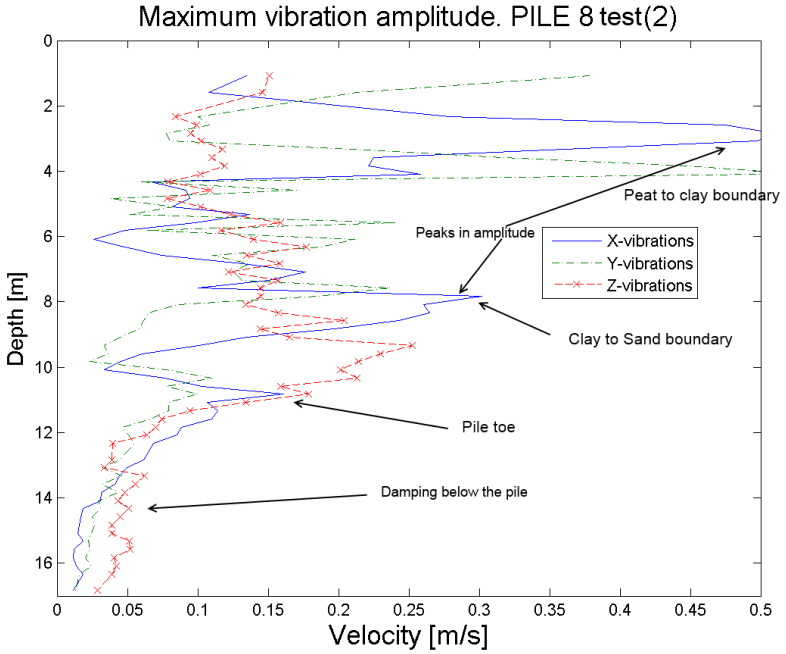

FIGURE E.32: Maximum vibration amplitude for PS test on pile 8. x- is the blue full line, y- is the green broken and circled line, and z- is the red dashed and crossed line.

E.6 Results pile 9 from the second field test

In pile 9 a bulge can be seen at $3m$ and a crack is detected at $8m$.

The bulge is based on an early arrival at $3m$. This can be seen in figures E.33 and E.34.

The crack is based on the more than average number of reflections between $6m$ and $8m$. There are however late arrivals between $7m$ and $8m$ which might mean that the flaw is a neck but this is not very clear. In addition, very early arrivals for vibrations in the x- and y- direction confuse the results even more.

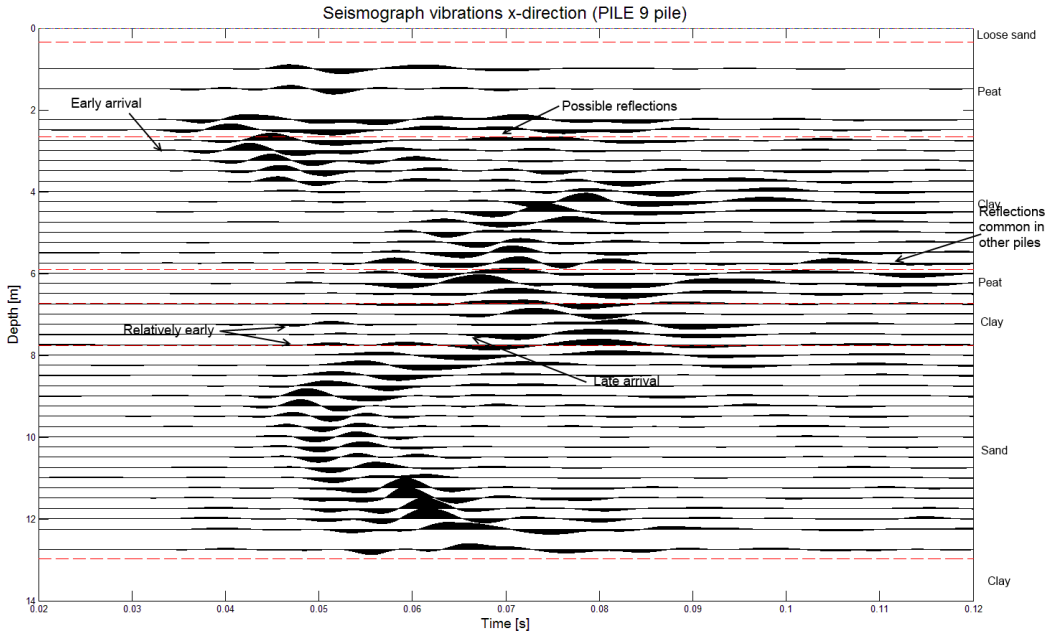

FIGURE E.33: Seismograph for PS test on pile 9, vibration in x-direction. The time axis starts at the point of hammer impact and depth starts at the level of the reinforcement.

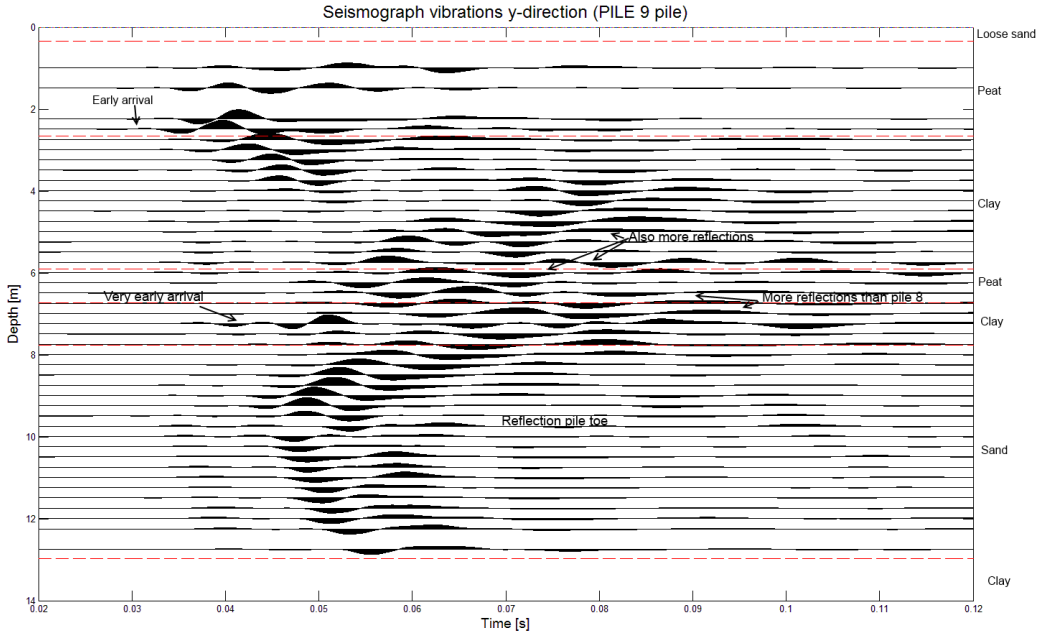

FIGURE E.34: Seismograph for PS test on pile 9, vibration in y-direction. The time axis starts at the point of hammer impact and depth starts at the level of the reinforcement.

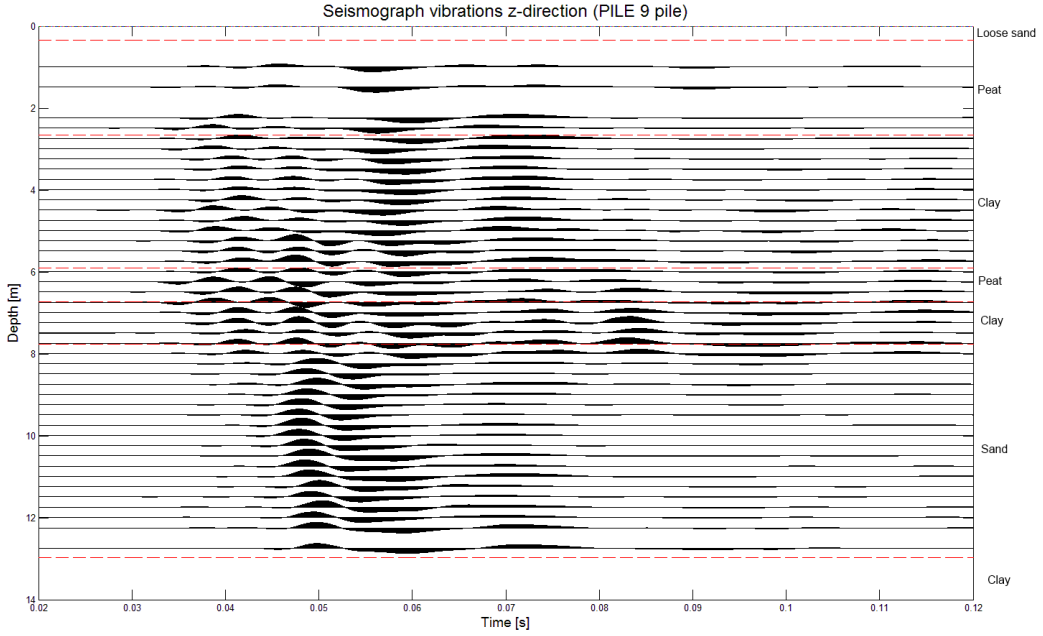

FIGURE E.35: Seismograph for PS test on pile 9, vibration in z-direction. The time axis starts at the point of hammer impact and depth starts at the level of the reinforcement.

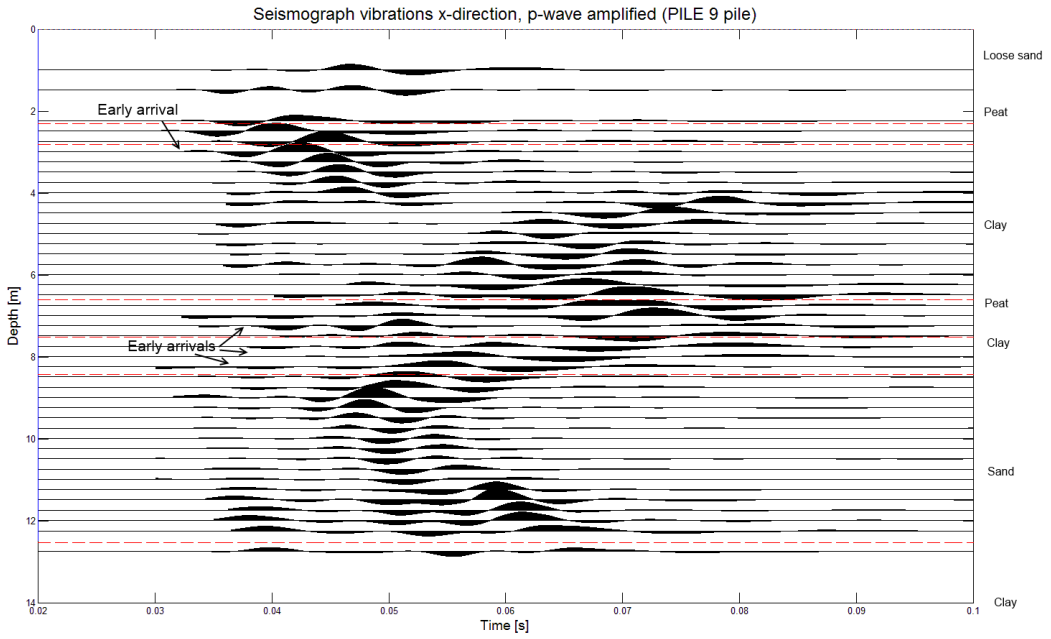

FIGURE E.36: Modified seismograph for PS test on pile 9, vibration in x-direction. The time axis starts at the point of hammer impact and depth starts at the level of the reinforcement.

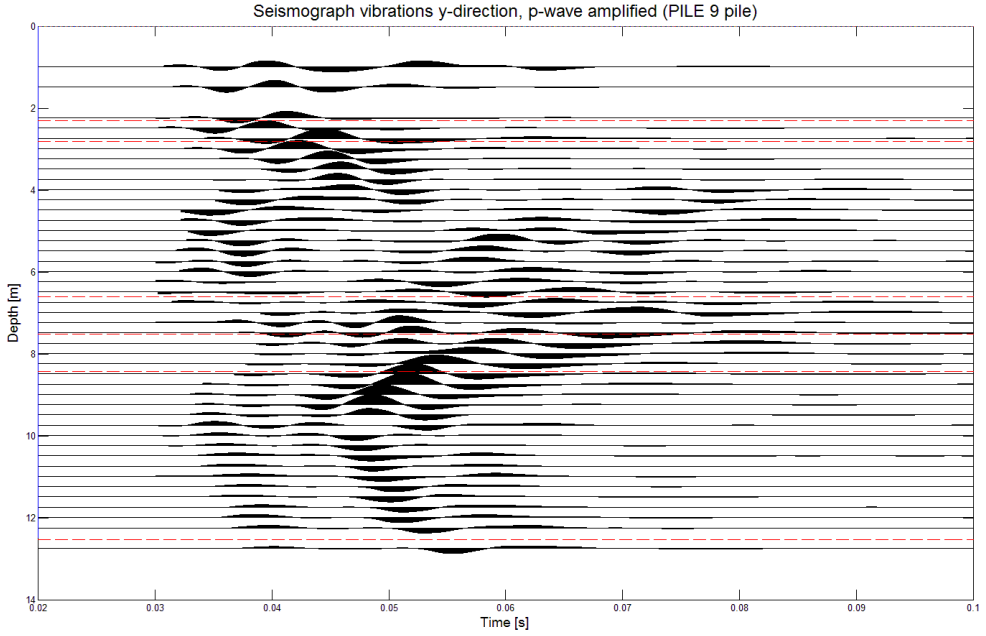

FIGURE E.37: Modified seismograph for PS test on pile 9, vibration in y-direction. The time axis starts at the point of hammer impact and depth starts at the level of the reinforcement.

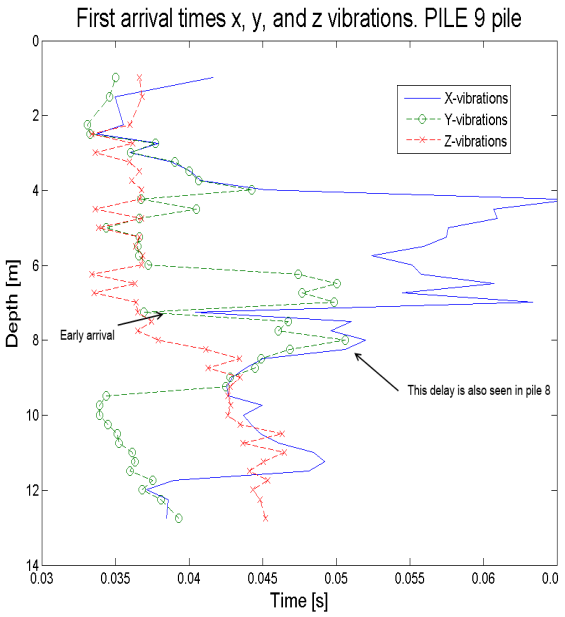

FIGURE E.38: First a.t's for PS test on pile 9. x- is the blue full line, y- is the green broken and circled line, and z- is the red dashed and crossed line.

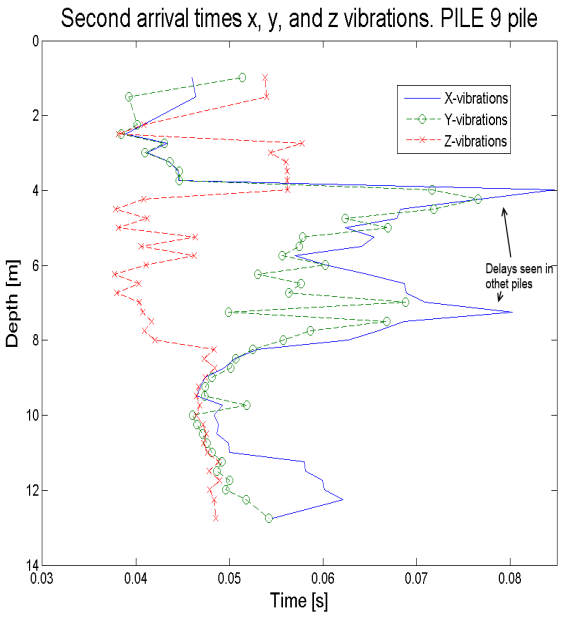

FIGURE E.39: Second a.t's for PS test on pile 9. x- is the blue full line, y- is the green broken and circled line, and z- is the red dashed and crossed line.

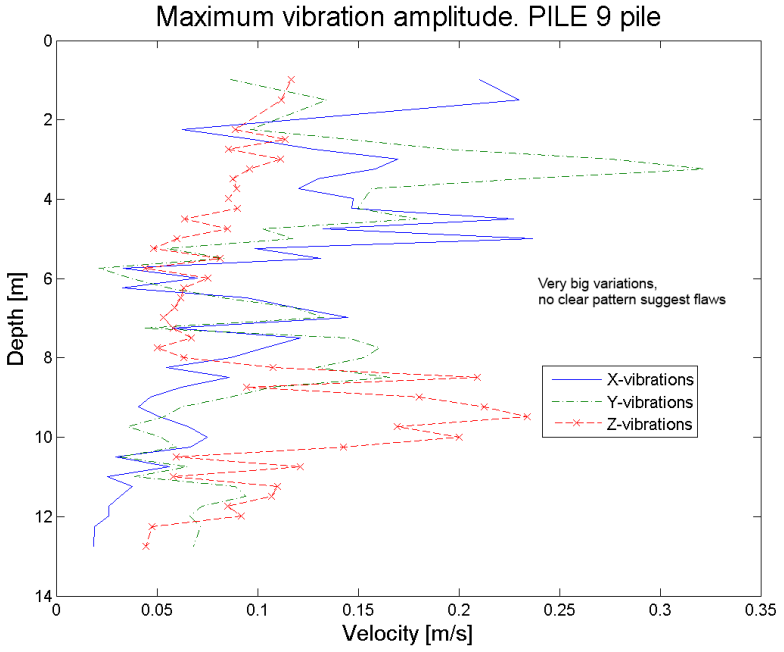

FIGURE E.40: Maximum vibration amplitude for PS test on pile 9. x- is the blue full line, y- is the green broken and circled line, and z- is the red dashed and crossed line.

E.7 Results pile 10 from the second field test

The results for pile 10 shows possible flaws at $4m$ and at $8m$.

At $4m$ the arrivals of the first waves are relatively early, which might suggest a bulge. This could also mean that there is a neck above or below this point which is one of the lessons learned from the first field test. Other proof of the flaw can be seen in the seismographs, where the data at this depth definitely deviates from the pattern seen in other piles.

At $8m$ an early arrival suggests a bulge at this depth. The seismographs and a.t figures shows a small change in the a.t at $8m$.

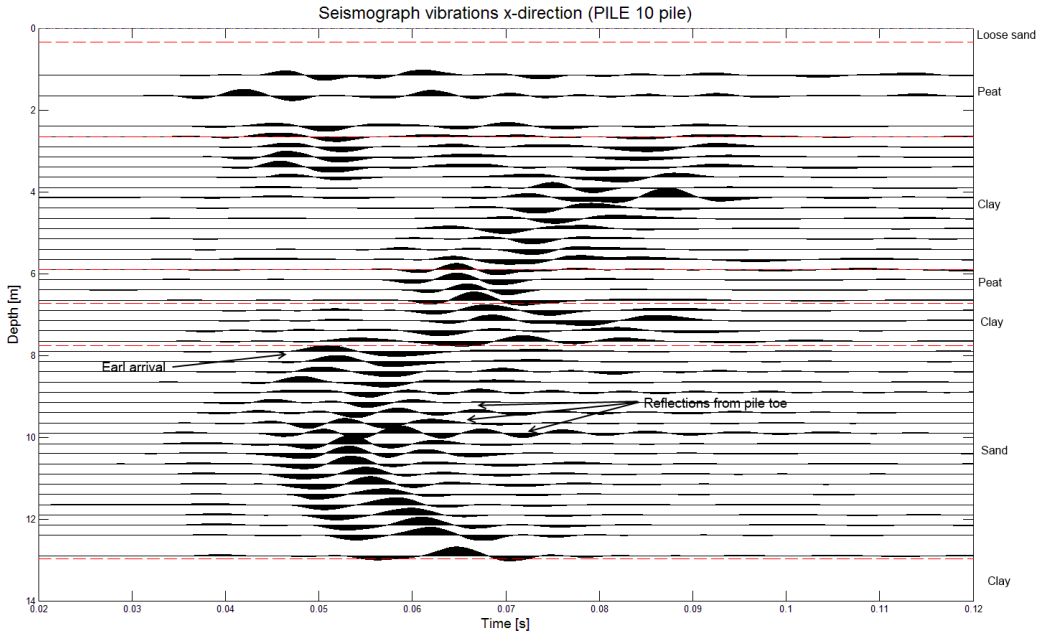

FIGURE E.41: Seismograph for PS test on pile 10, vibration in x-direction. The time axis starts at the point of hammer impact and depth starts at the level of the reinforcement.

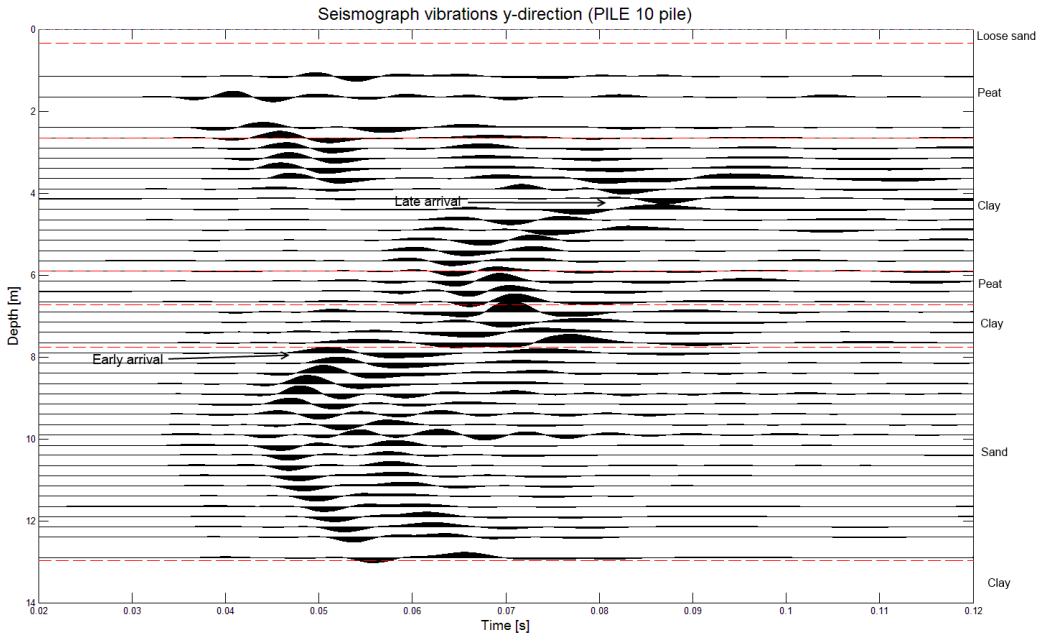

FIGURE E.42: Seismograph for PS test on pile 10, vibration in y-direction. The time axis starts at the point of hammer impact and depth starts at the level of the reinforcement.

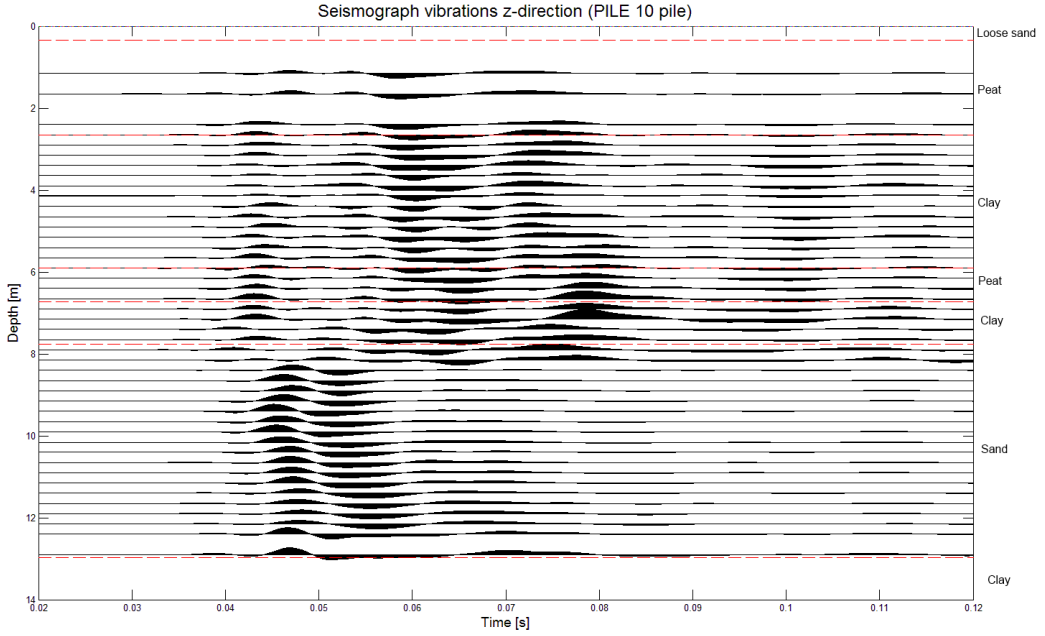

FIGURE E.43: Seismograph for PS test on pile 10, vibration in z-direction. The time axis starts at the point of hammer impact and depth starts at the level of the reinforcement.

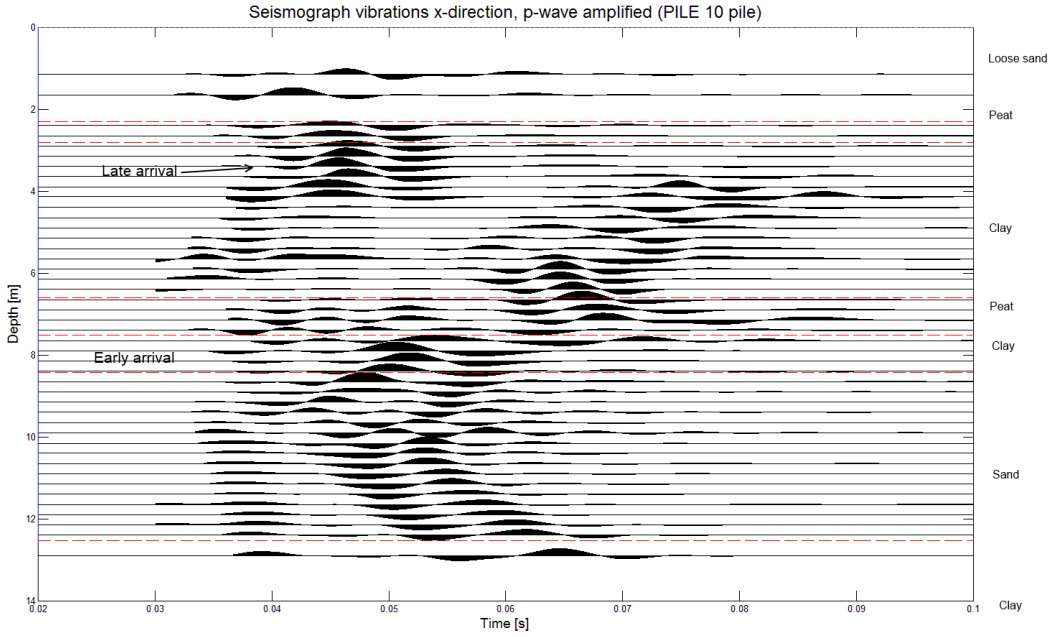

FIGURE E.44: Modified seismograph for PS test on pile 10, vibration in x-direction. The time axis starts at the point of hammer impact and depth starts at the level of the reinforcement.

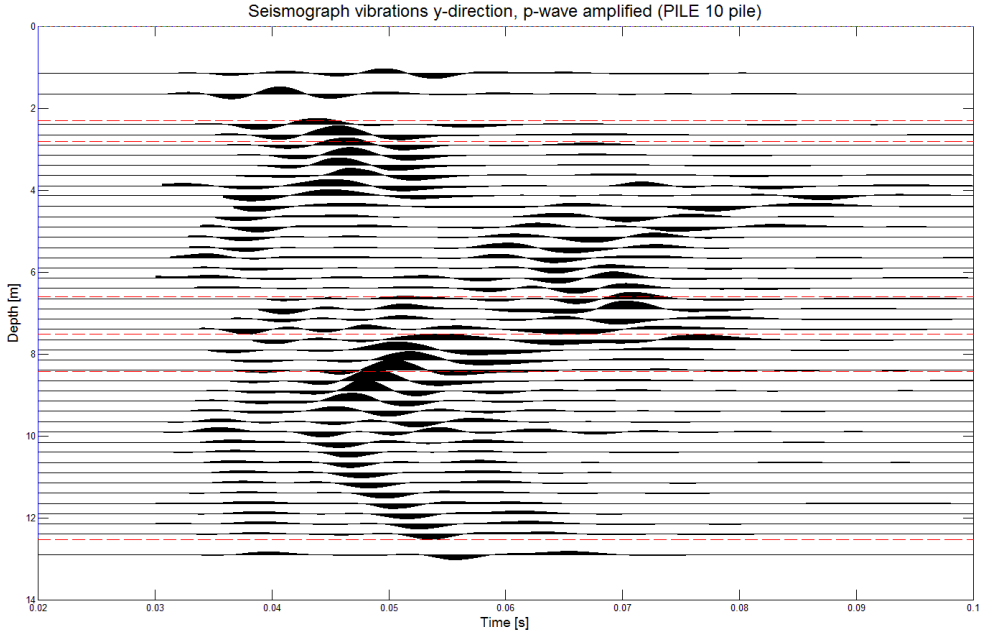

FIGURE E.45: Modified seismograph for PS test on pile 10, vibration in y-direction. The time axis starts at the point of hammer impact and depth starts at the level of the reinforcement.

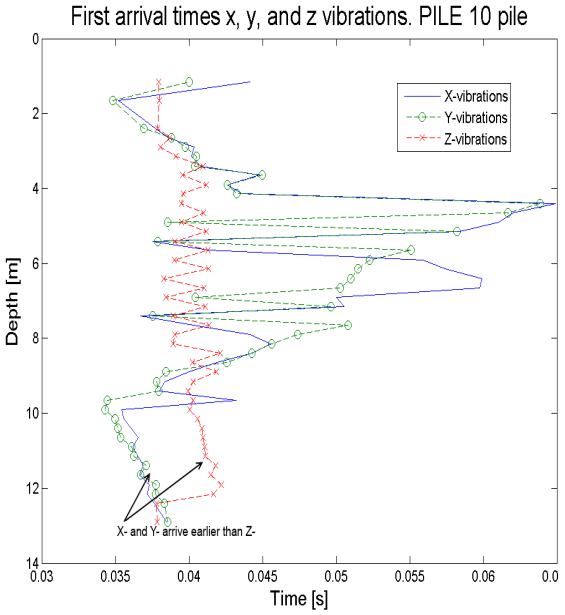

FIGURE E.46: First a.t's for PS test on pile 10. x- is the blue full line, y- is the green broken and circled line, and z- is the red dashed and crossed line.

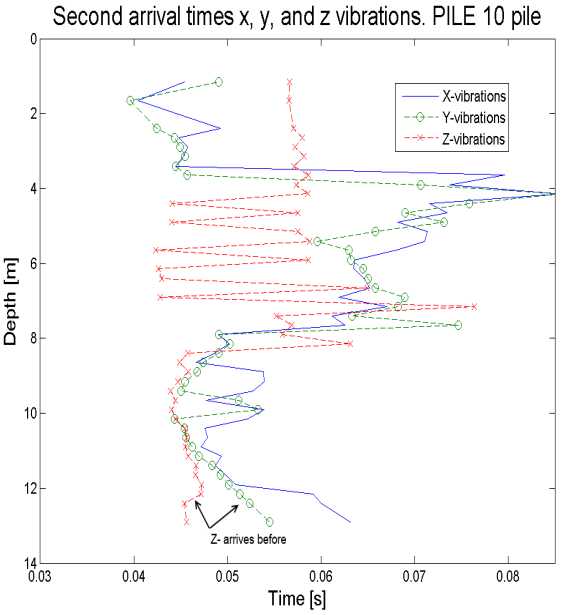

FIGURE E.47: Second a.t's for PS test on pile 10. x- is the blue full line, y- is the green broken and circled line, and z- is the red dashed and crossed line.

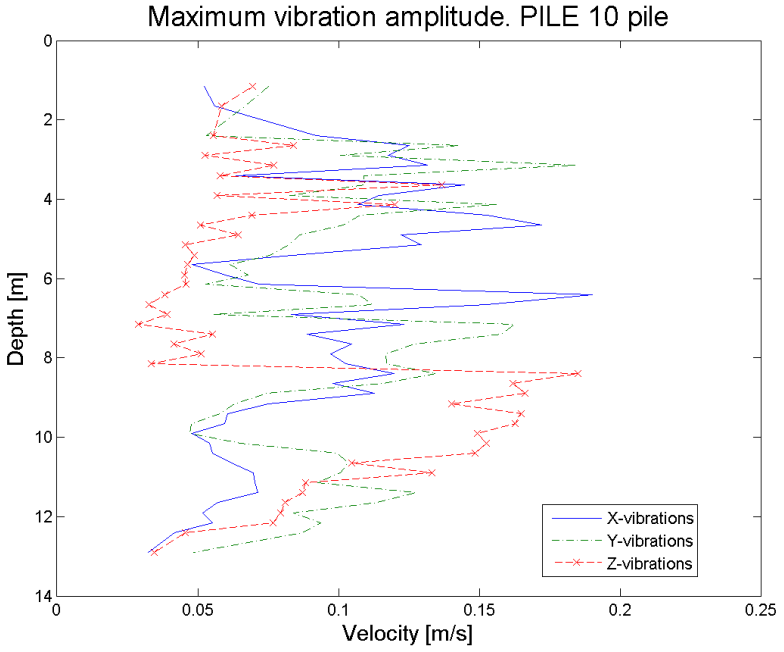

FIGURE E.48: Maximum vibration amplitude for PS test on pile 10. x- is the blue full line, y- is the green broken and circled line, and z- is the red dashed and crossed line.

E.8 Results pile 11 from the second field test

Figures E.49 and E.50 show that the results for pile 11 between $4m$ and $10m$ are very different than other piles. This suggests definite flaws in the second half of the pile.

It is hard to tell whether the vibrations at $5.5m$ to $6.6m$ arrive late or that the surrounding waves arrive extra early. In pile 11, a bulge might be detected at $8m$ and one at $4m$ if the arrivals around $6m$ are assumed *normal*.

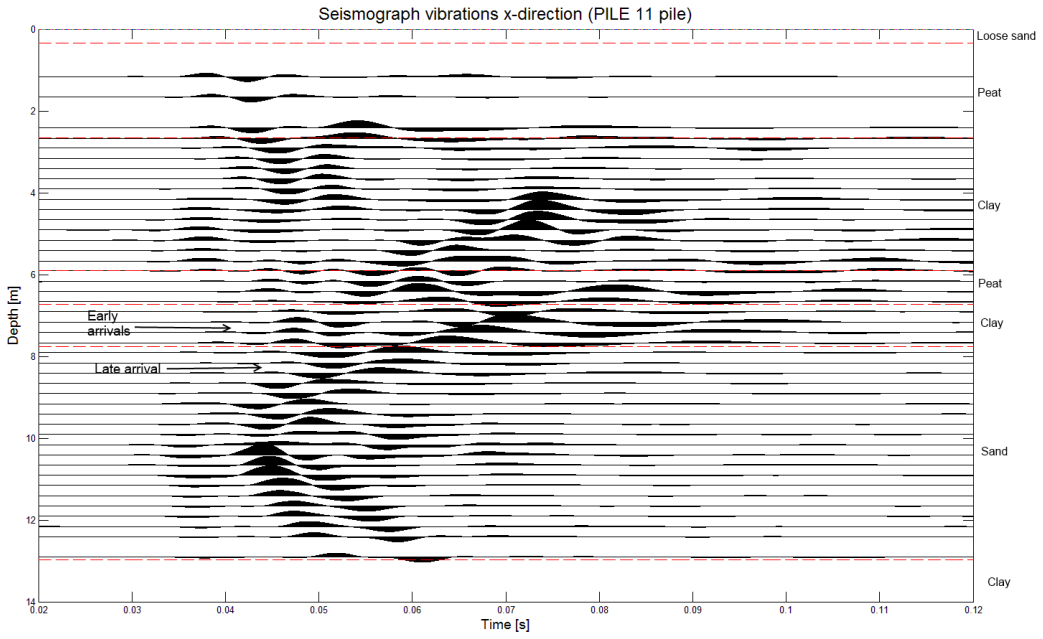

FIGURE E.49: Seismograph for PS test on pile 11, vibration in x-direction. The time axis starts at the point of hammer impact and depth starts at the level of the reinforcement.

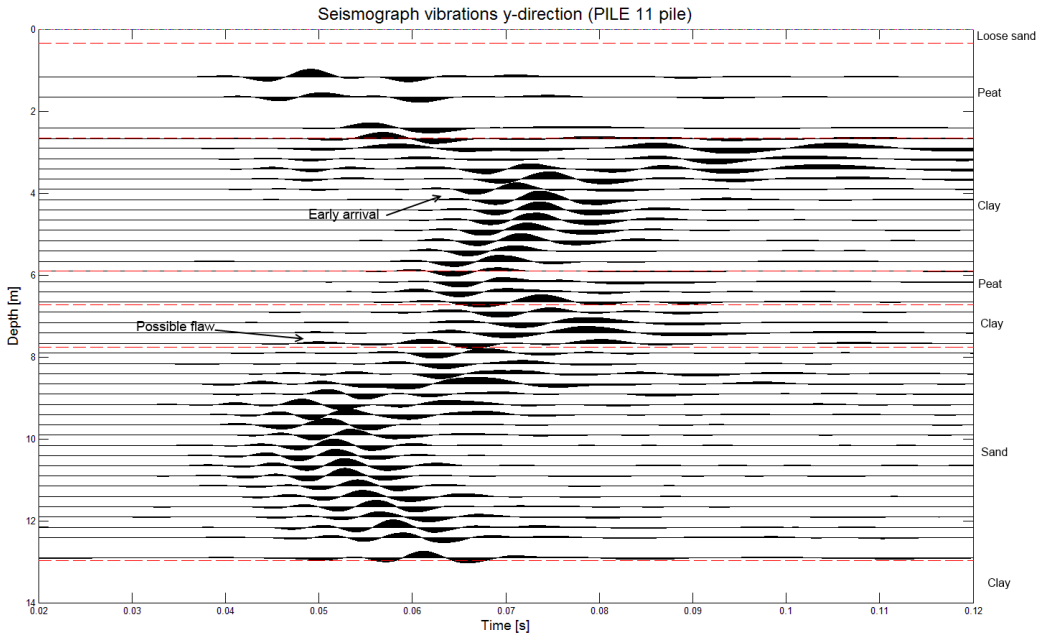

FIGURE E.50: Seismograph for PS test on pile 11, vibration in y-direction. The time axis starts at the point of hammer impact and depth starts at the level of the reinforcement.

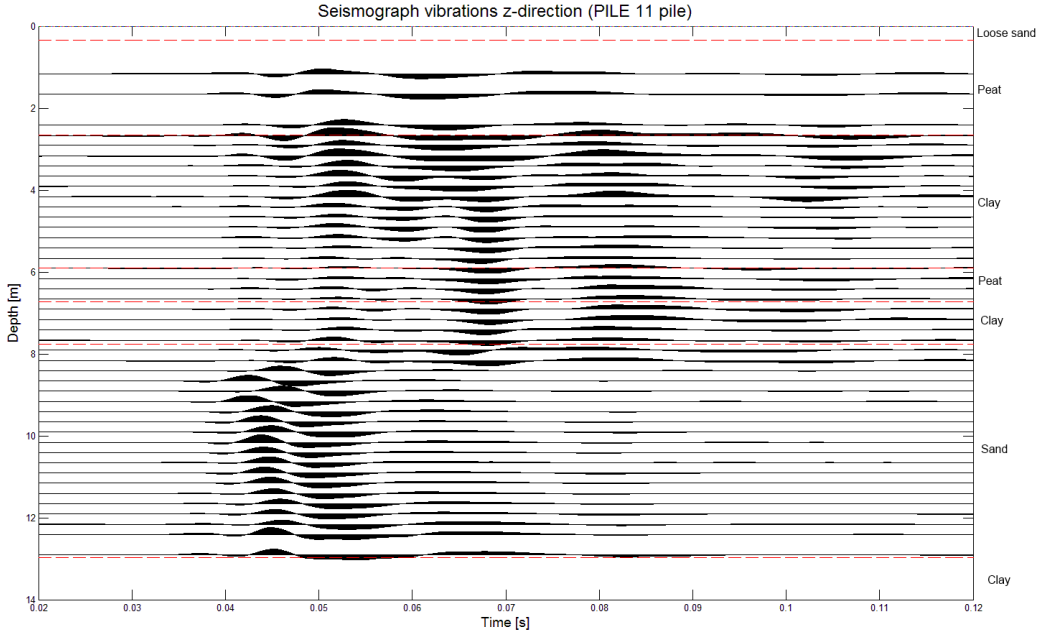

FIGURE E.51: Seismograph for PS test on pile 11, vibration in z-direction. The time axis starts at the point of hammer impact and depth starts at the level of the reinforcement.

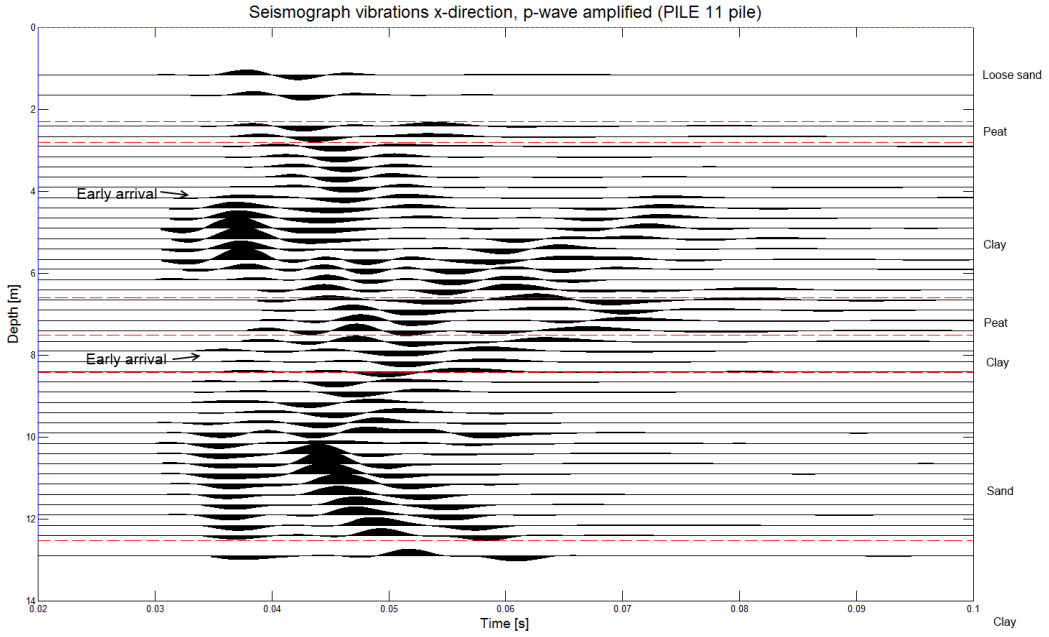

FIGURE E.52: Modified seismograph for PS test on pile 11, vibration in x-direction. The time axis starts at the point of hammer impact and depth starts at the level of the reinforcement.

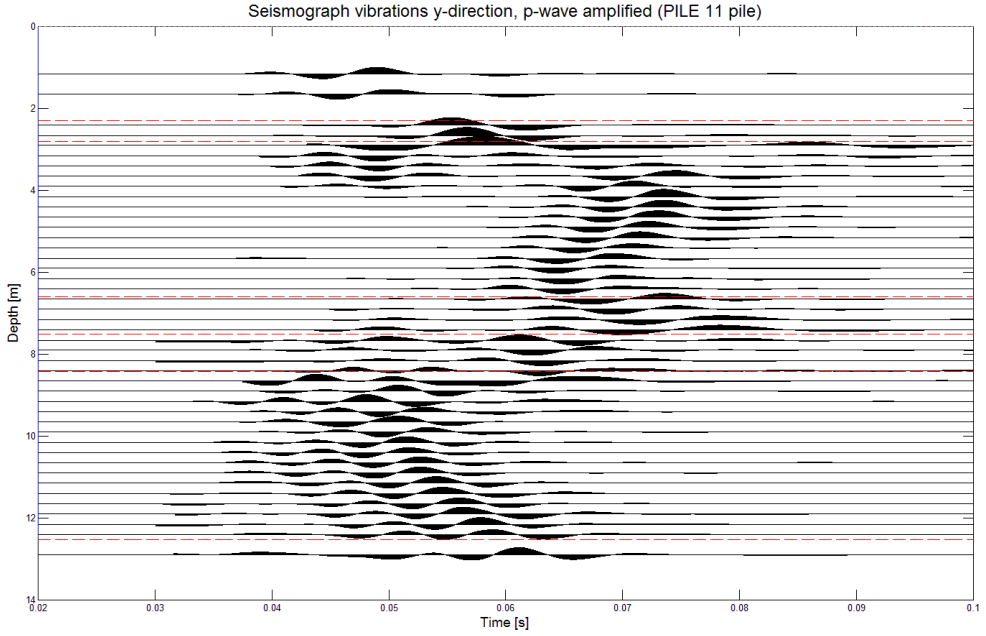

FIGURE E.53: Modified seismograph for PS test on pile 11, vibration in y-direction. The time axis starts at the point of hammer impact and depth starts at the level of the reinforcement.

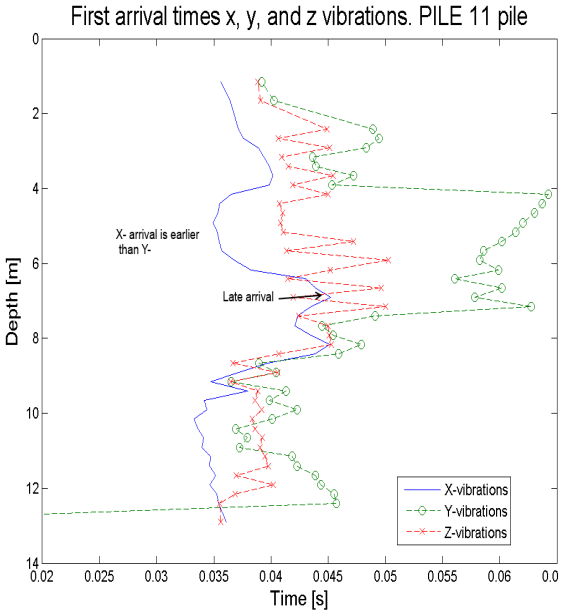

FIGURE E.54: First a.t's for PS test on pile 11. x- is the blue full line, y- is the green broken and circled line, and z- is the red dashed and crossed line.

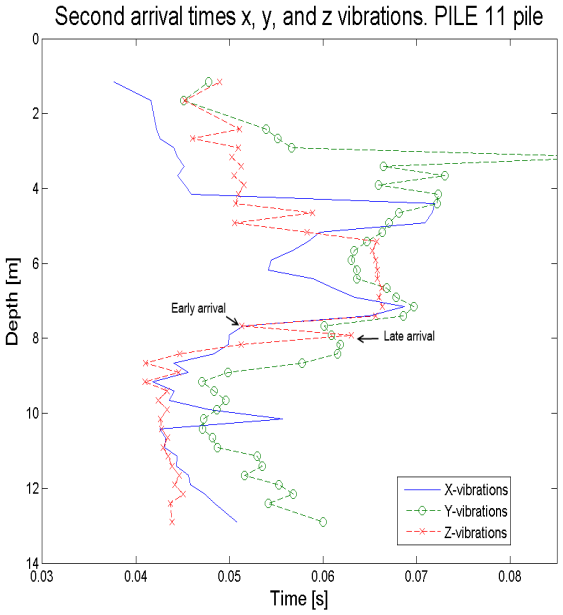

FIGURE E.55: Second a.t's for PS test on pile 11. x- is the blue full line, y- is the green broken and circled line, and z- is the red dashed and crossed line.

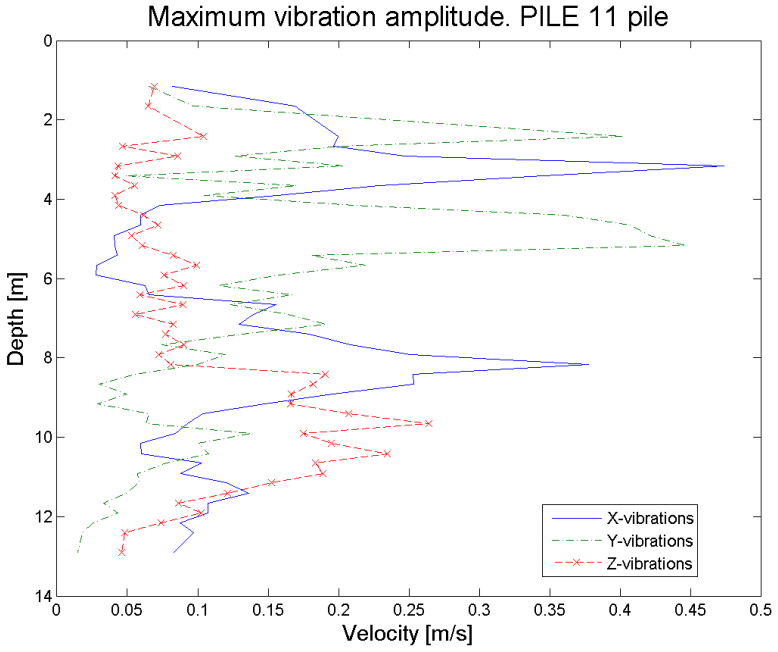

FIGURE E.56: Maximum vibration amplitude for PS test on pile 11. x- is the blue full line, y- is the green broken and circled line, and z- is the red dashed and crossed line.

E.9 Results pile 12 from the second field test

As in pile 11, results from pile 12 deviate from the pattern seen in other piles. Hints of flaws at $3m$ and at $6m$ can be detected.

At $3m$ figure E.57 shows reflections and a clear deviation from the pattern seen in the results of pile 8. There is no clear change in a.t so this flaw is possibly a crack.

Below $6m$ the a.t's normally gradually increase, which does not happen here. Also the a.t at $6m$ is short. Hence a bulge might be present at this depth. This would also explain the drop in x- vibration amplitude directly below which can be seen in figure E.64. This however is not seen in the y-vibrations which casts doubt on this conclusion.

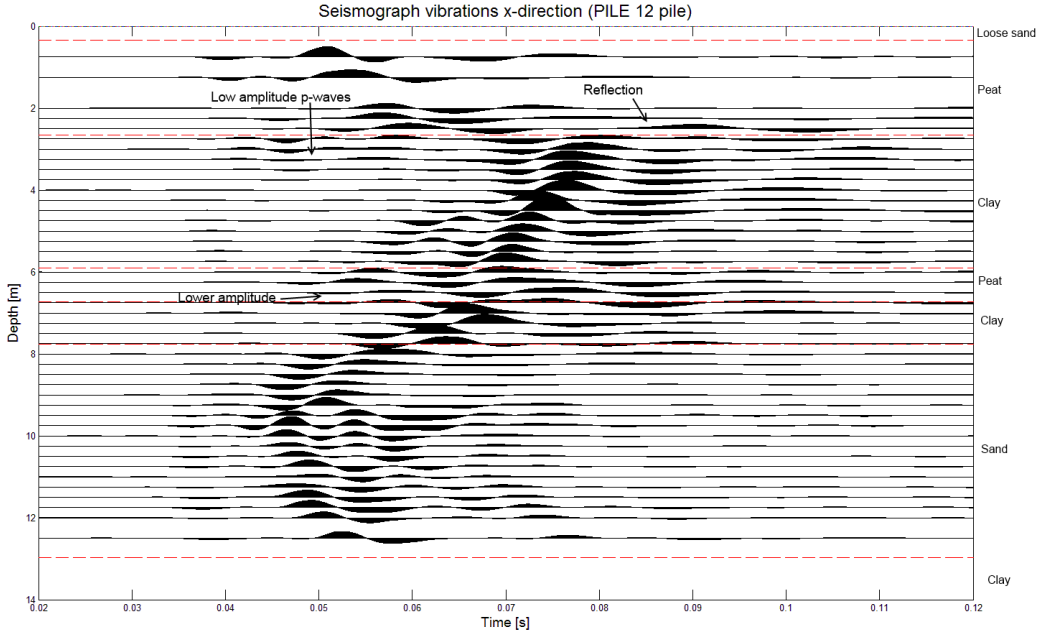

FIGURE E.57: Seismograph for PS test on pile 12, vibration in x-direction. The time axis starts at the point of hammer impact and depth starts at the level of the reinforcement.

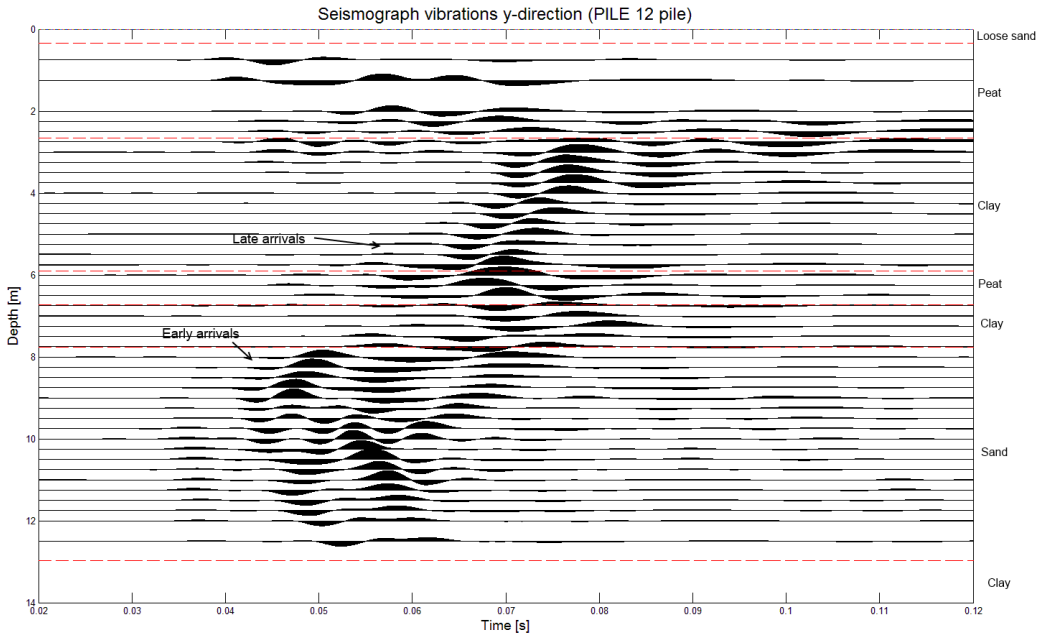

FIGURE E.58: Seismograph for PS test on pile 12, vibration in y-direction. The time axis starts at the point of hammer impact and depth starts at the level of the reinforcement.

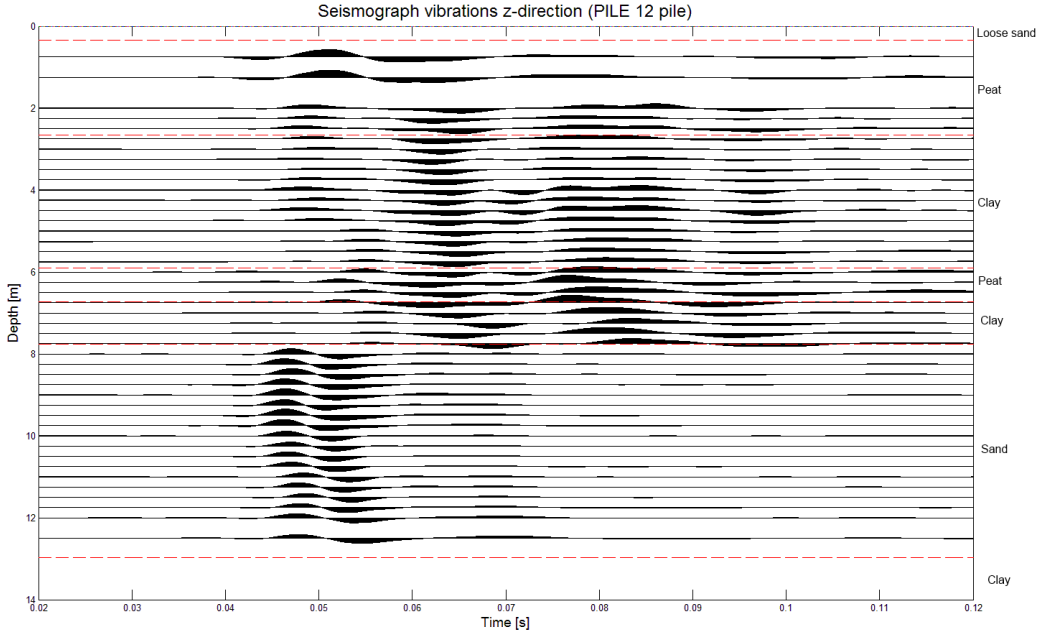

FIGURE E.59: Seismograph for PS test on pile 12, vibration in z-direction. The time axis starts at the point of hammer impact and depth starts at the level of the reinforcement.

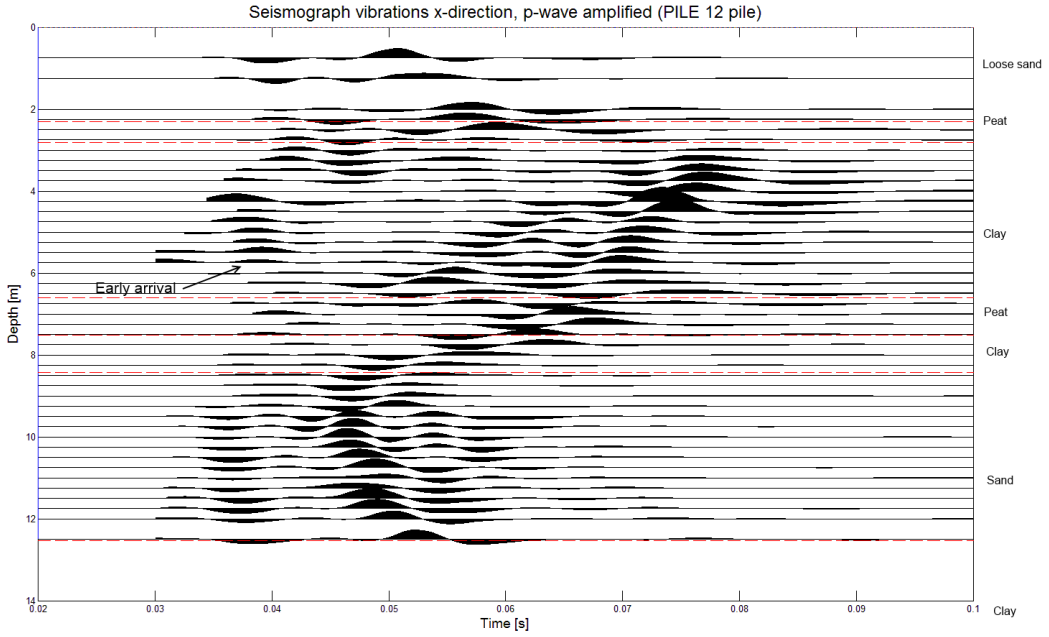

FIGURE E.60: Modified seismograph for PS test on pile 12, vibration in x-direction. The time axis starts at the point of hammer impact and depth starts at the level of the reinforcement.

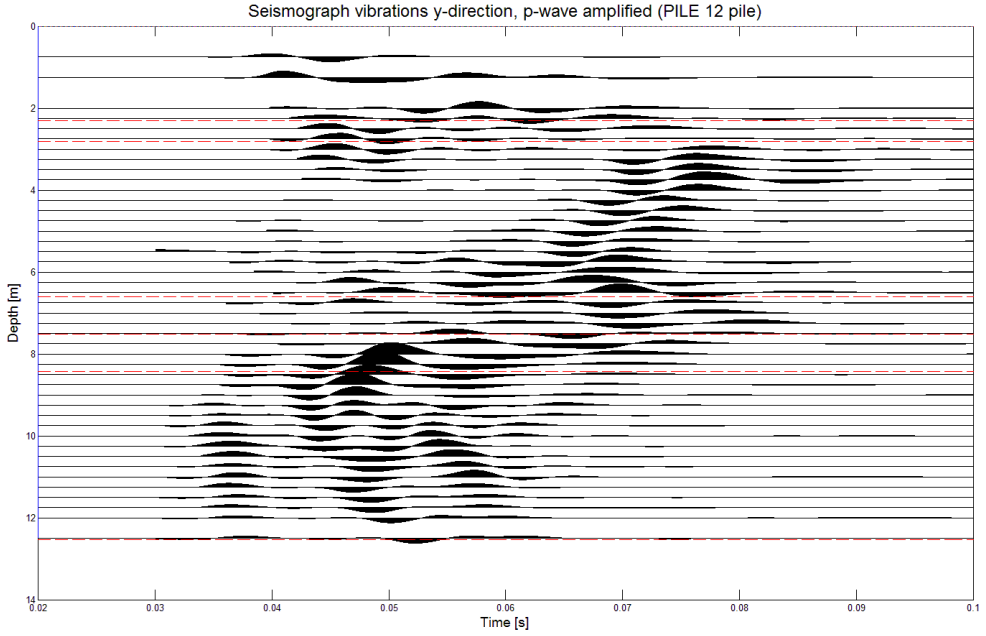

FIGURE E.61: Modified seismograph for PS test on pile 12, vibration in y-direction. The time axis starts at the point of hammer impact and depth starts at the level of the reinforcement.

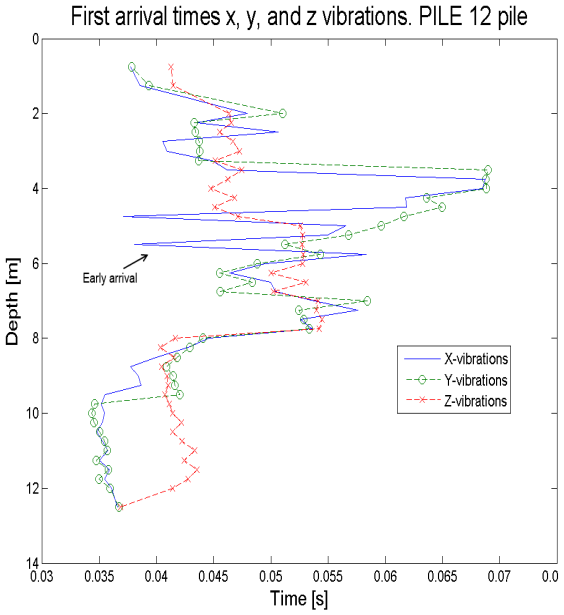

FIGURE E.62: First a.t's for PS test on pile 12. x- is the blue full line, y- is the green broken and circled line, and z- is the red dashed and crossed line.

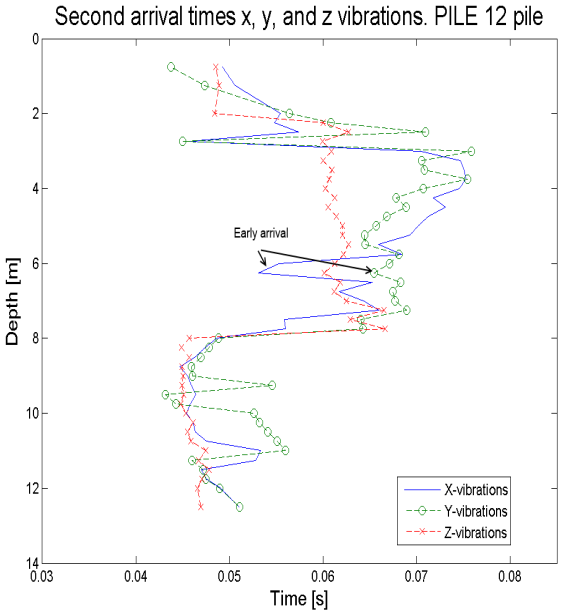

FIGURE E.63: Second a.t's for PS test on pile 12. x- is the blue full line, y- is the green broken and circled line, and z- is the red dashed and crossed line.

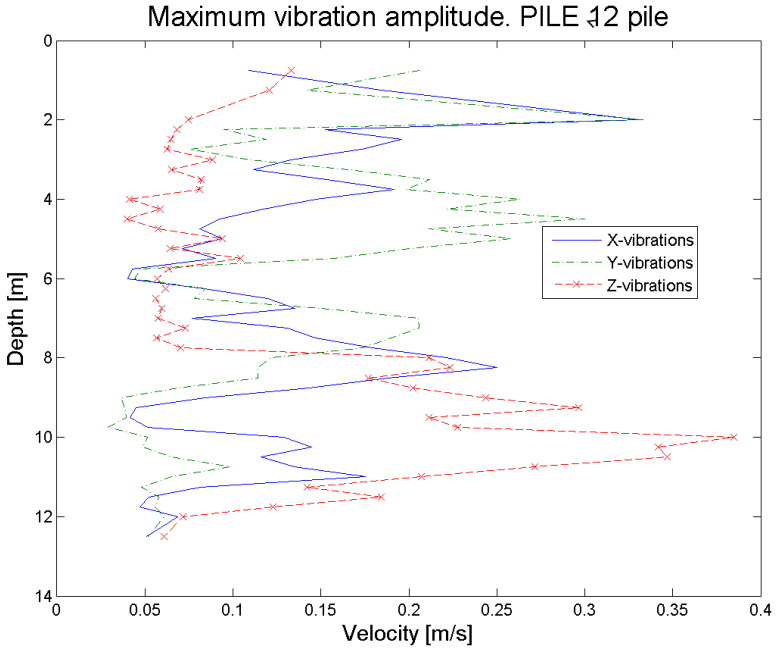

FIGURE E.64: Maximum vibration amplitude for PS test on pile 12. x- is the blue full line, y- is the green broken and circled line, and z- is the red dashed and crossed line.

E.10 Results pile 13 from the second field test

Pile 13 was already tested during the first field test. In this test again the results are compared to the first test and an attempt is made to locate the pile toe.

Pile 13 should have a neck at $8m$, the first field test yielded a bulge at $8m$ instead. After re-testing, small hints of the neck can be defined. In figure E.65 a jump in a.t can be seen at $8.5m$, which suggest late arrivals around $8m$. In pile 8, these vibrations arrive relatively early while in pile 13 they arrive later. So if the location and shape of the flaw is known, it is possible to interpret the signs that it leaves in the results. The amplitude in figure E.72 also shows a large drop at $8m$, which corresponds to the results of the simulations in chapter 4.

The seismographs again clearly show a change in a.t's and reflections around $11m$. This is probably the depth of the pile toe.

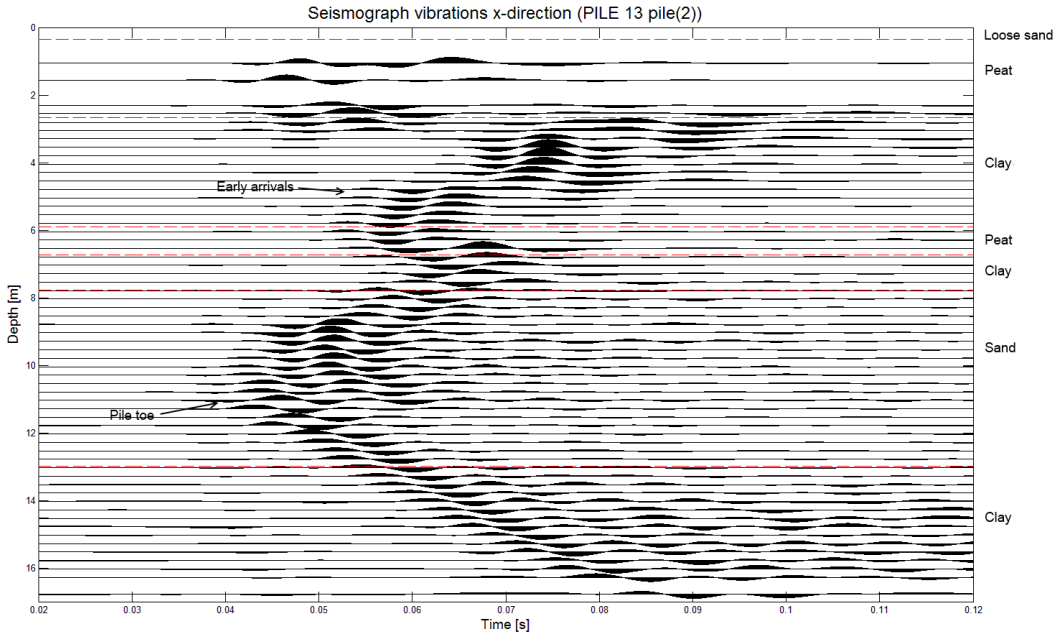

FIGURE E.65: Seismograph for PS test on pile 13, vibration in x-direction. The time axis starts at the point of hammer impact and depth starts at the level of the reinforcement.

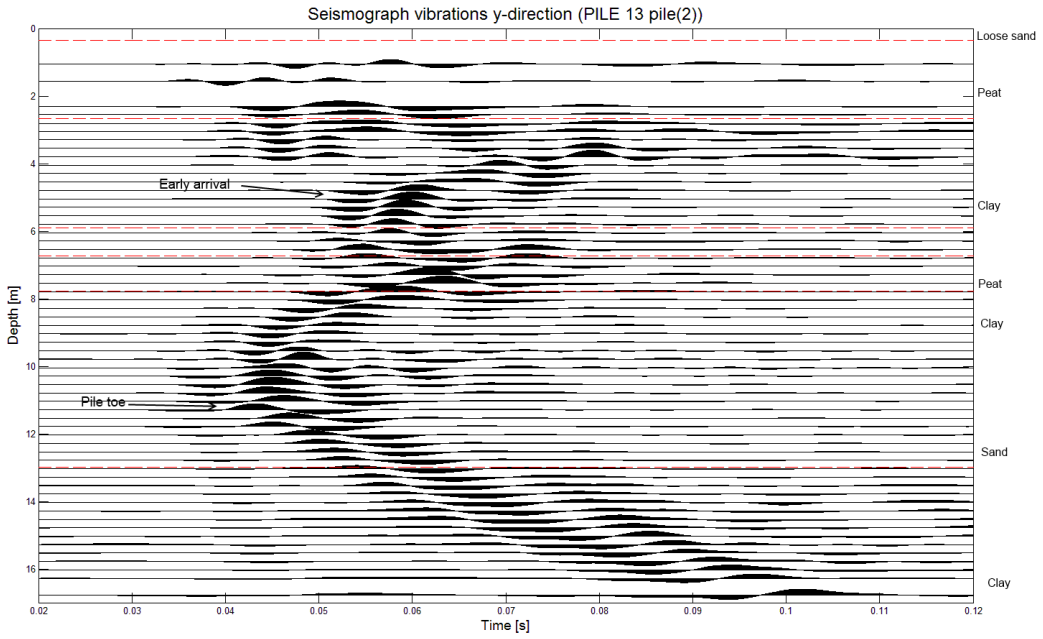

FIGURE E.66: Seismograph for PS test on pile 13, vibration in y-direction. The time axis starts at the point of hammer impact and depth starts at the level of the reinforcement.

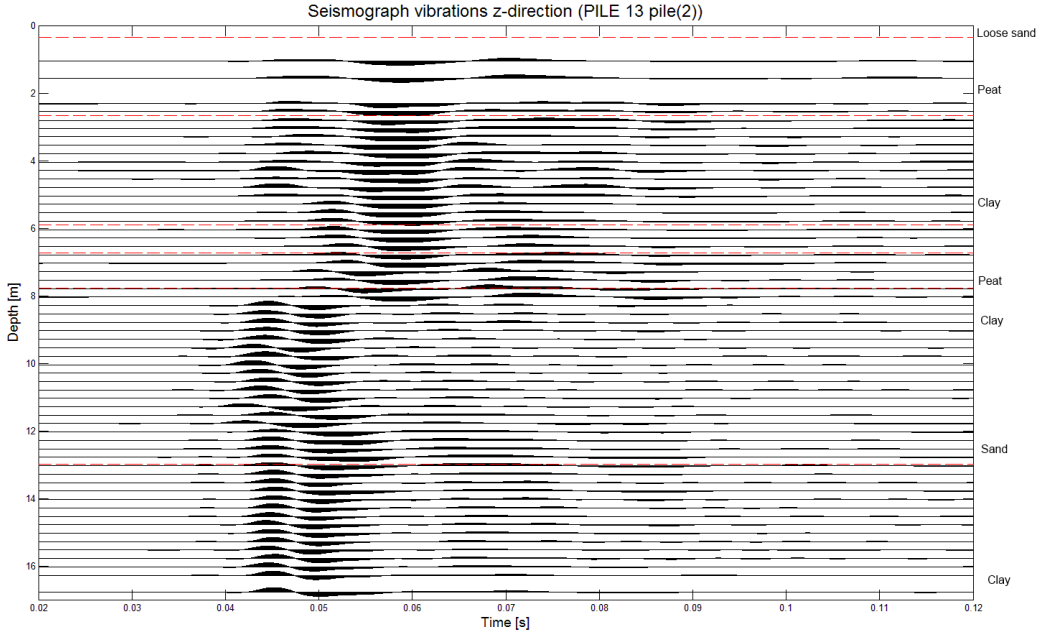

FIGURE E.67: Seismograph for PS test on pile 13, vibration in z-direction. The time axis starts at the point of hammer impact and depth starts at the level of the reinforcement.

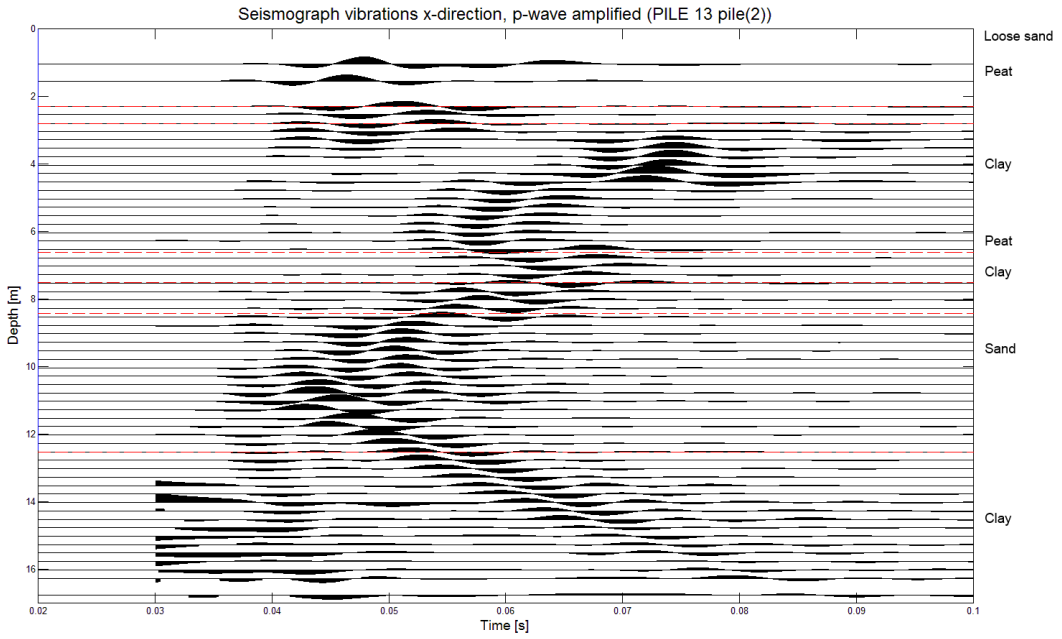

FIGURE E.68: Modified seismograph for PS test on pile 13, vibration in x-direction. The time axis starts at the point of hammer impact and depth starts at the level of the reinforcement.

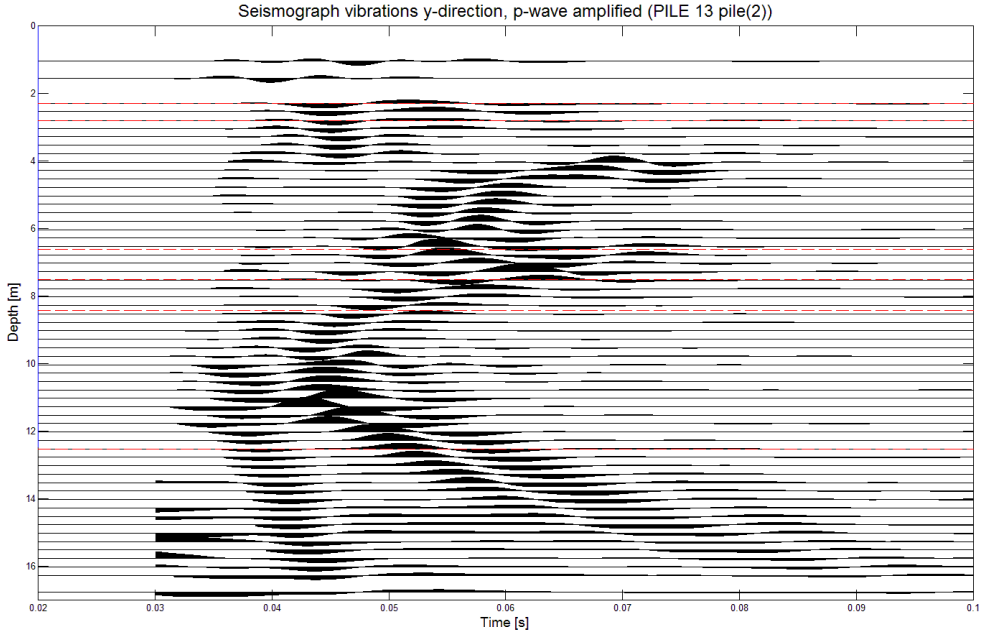

FIGURE E.69: Modified seismograph for PS test on pile 13, vibration in y-direction. The time axis starts at the point of hammer impact and depth starts at the level of the reinforcement.

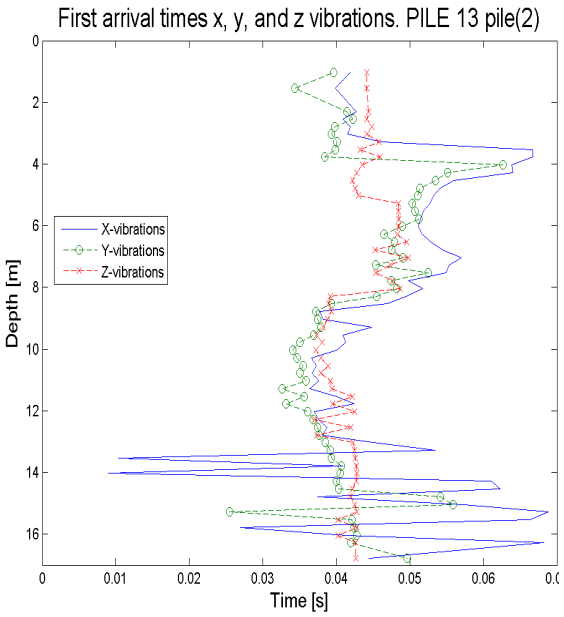

FIGURE E.70: First a.t's for PS test on pile 13. x- is the blue full line, y- is the green broken and circled line, and z- is the red dashed and crossed line.

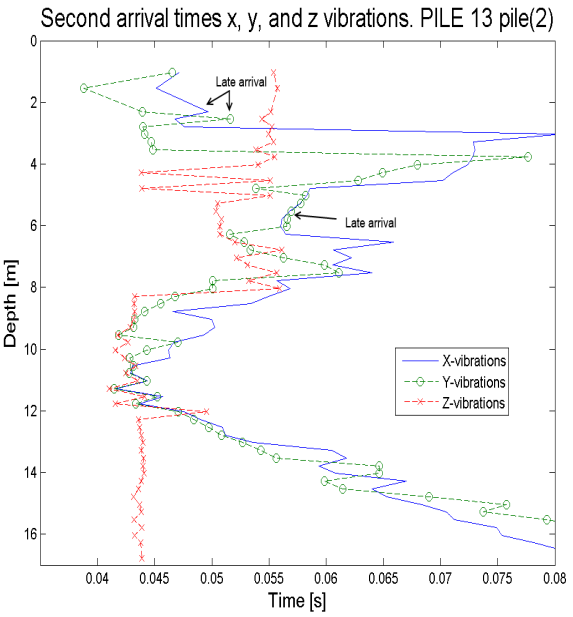

FIGURE E.71: Second a.t's for PS test on pile 13. x- is the blue full line, y- is the green broken and circled line, and z- is the red dashed and crossed line.

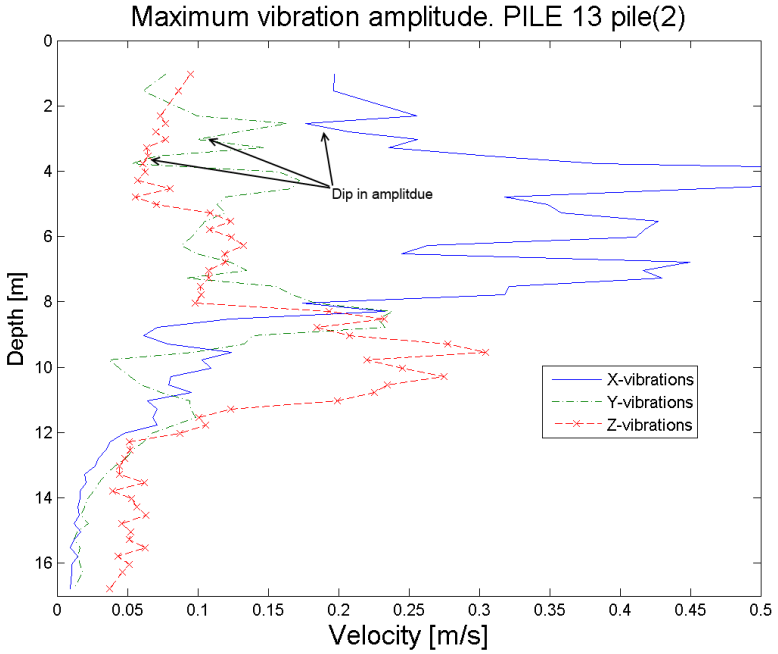

FIGURE E.72: Maximum vibration amplitude for PS test on pile 13. x- is the blue full line, y- is the green broken and circled line, and z- is the red dashed and crossed line.

E.11 Results pile 18 from the second field test

In pile 18 a neck can be detected around $8m$, followed by a bulge below that. Both x- and y-vibration seismographs shows an increase in a.t at $8m$ followed by a decrease in a.t around $9m$. Figures E.78 and E.79 show the changes in a.t.

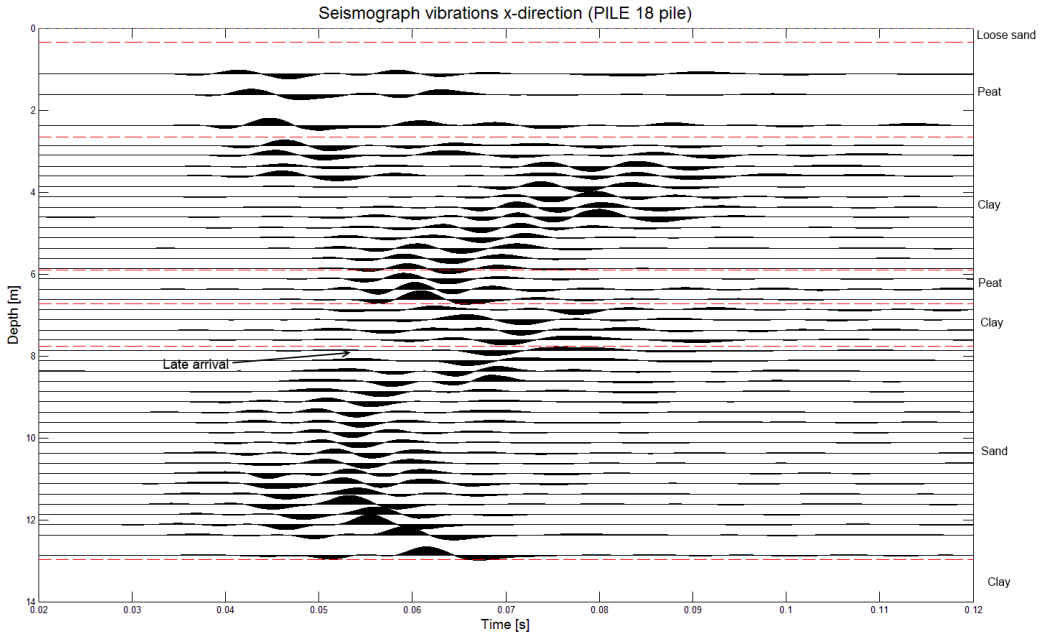

FIGURE E.73: Seismograph for PS test on pile 18, vibration in x-direction. The time axis starts at the point of hammer impact and depth starts at the level of the reinforcement.

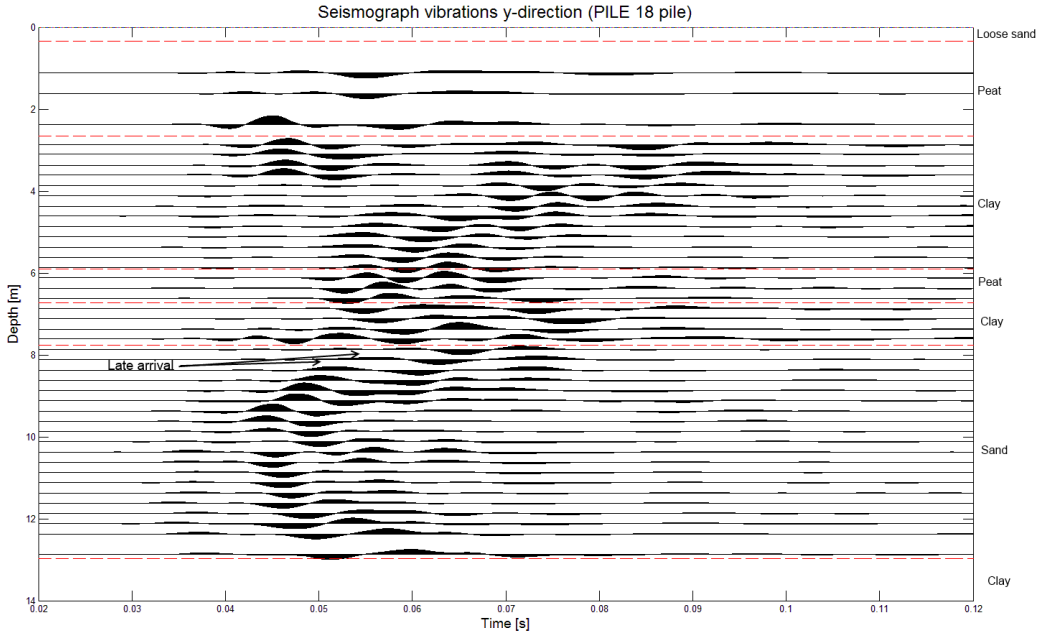

FIGURE E.74: Seismograph for PS test on pile 18, vibration in y-direction. The time axis starts at the point of hammer impact and depth starts at the level of the reinforcement.

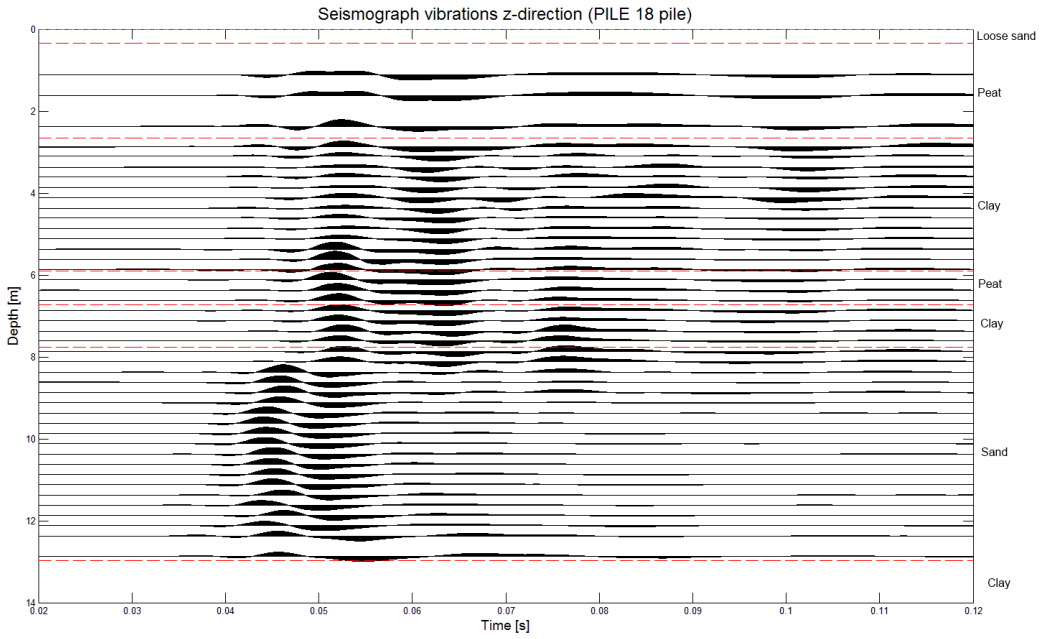

FIGURE E.75: Seismograph for PS test on pile 18, vibration in z-direction. The time axis starts at the point of hammer impact and depth starts at the level of the reinforcement.

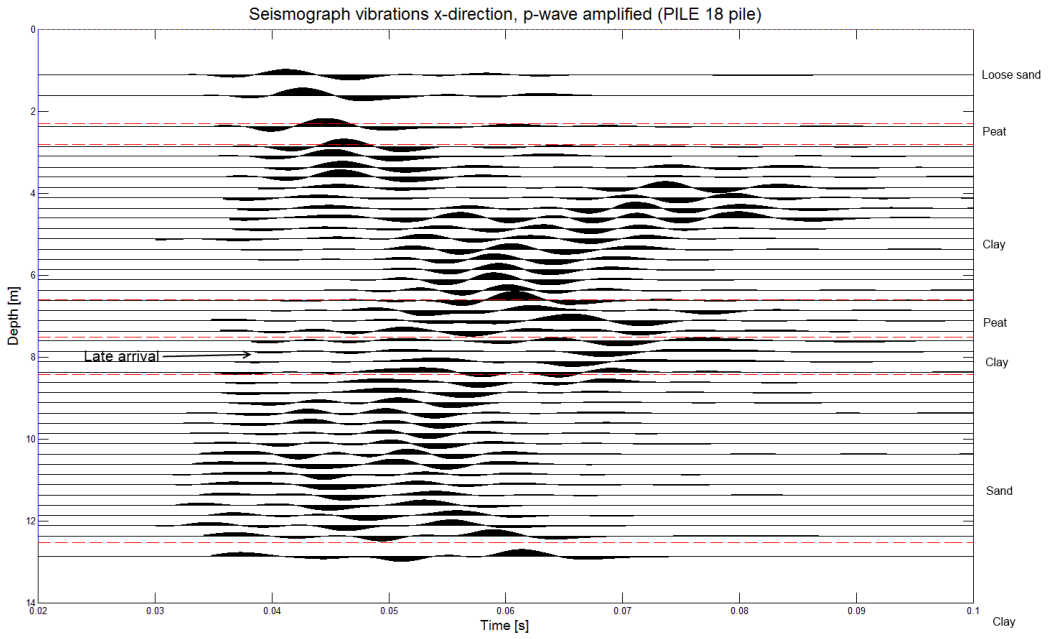

FIGURE E.76: Modified seismograph for PS test on pile 18, vibration in x-direction. The time axis starts at the point of hammer impact and depth starts at the level of the reinforcement.

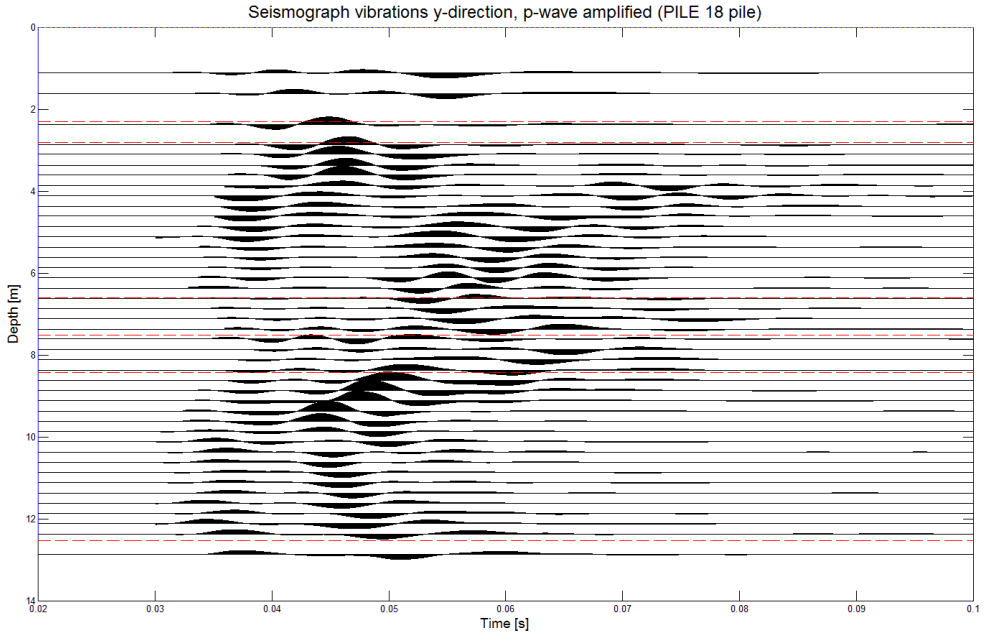

FIGURE E.77: Modified seismograph for PS test on pile 18, vibration in y-direction. The time axis starts at the point of hammer impact and depth starts at the level of the reinforcement.

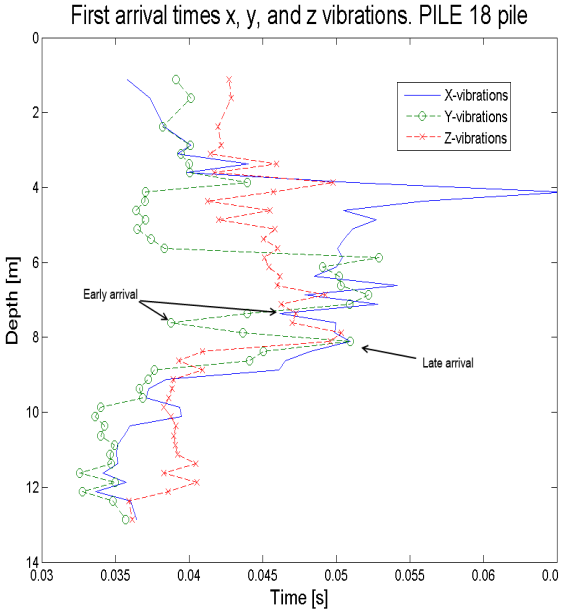

FIGURE E.78: First a.t's for PS test on pile 18. x- is the blue full line, y- is the green broken and circled line, and z- is the red dashed and crossed line.

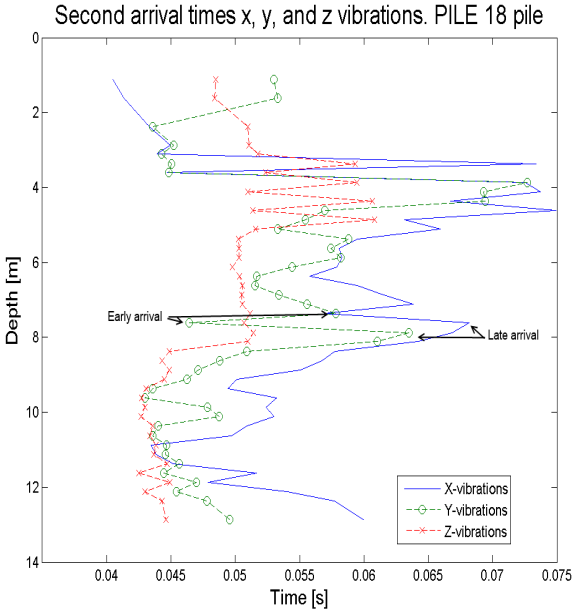

FIGURE E.79: Second a.t's for PS test on pile 18. x- is the blue full line, y- is the green broken and circled line, and z- is the red dashed and crossed line.

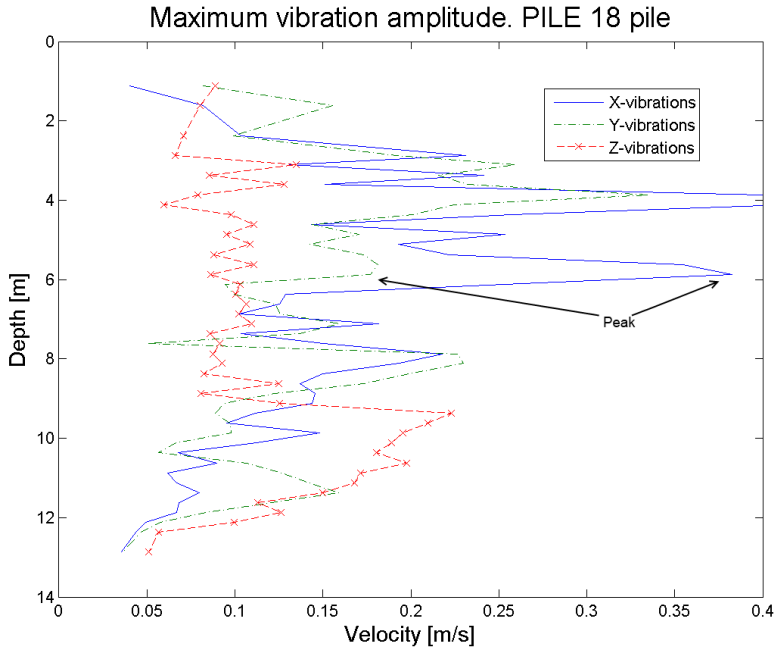

FIGURE E.80: Maximum vibration amplitude for PS test on pile 18. x- is the blue full line, y- is the green broken and circled line, and z- is the red dashed and crossed line.

E.12 Detection of flaws vs. designed flaws

In table 6.1 the detected flaws are compared to the designed flaws. For each pile test this comparison is discussed.

Pile 1: In pile 1 two flaws were detected. One at $3m$ and one at $8m$. The first flaw was mistaken for a crack, based on the reflections seen in the seismograph. In reality the flaw is a bulge which also creates reflections but should result in locally early a.t's. This is very hard to detect due to the many variations in soil properties near the surface.

The second designed flaw is a bulge at $6m$ which was missed, or mistaken for a neck at $8m$. If there is a bulge at $6m$, it cannot be seen in the results. There are no signs of reflections or reductions in a.t. In addition at $8m$ there is a change in soil layer (clay to sand) which could confuse the results.

Pile 2: In the second pile only one flaw was detected, a bulge at $6m$. This prediction matches the designed flaw, and was based on early arrivals around $6m$ and prominent reflections above. Therefore the bulge is probably very big.

Pile 2 also has a crack at $3m$ which was missed. In hindsight there are numerous reflections that might point towards the crack. However these reflections were attributed to soil layering which caused the oversight.

Pile 4: In the fourth pile one flaw was detected, a bulge at $3m$. Again the location of the flaw is correct, but the shape is wrong. The designed flaw is a crack at $3m$. This is hardly visible when compared to the cracks in other piles like pile 1.

The second designed flaw is a neck at $6m$ which is missed. Again this flaw is very hard to spot. There are hardly any reflections and the arrival times follow that of the common pattern attributed to the soil conditions.

Pile 9: In pile 9, instead of missing flaws, ones that should not be there were detected. A bulge at $3m$ should not be present and a crack at $8m$ is actually a non symmetric (NS) bulge.

Mistaking a bulge(NS) for a crack seems reasonable. If the bulge is not in the path of the waves, it will not affect the a.t's. However it will still change the impedance of the pile and cause reflections as a crack would do.

The detected bulge at $3m$ is based on early arrivals and more than average reflections at $3m$ and above. At this depth, these results could be caused by anomalies in the subsurface like stones.

Pile 10: In pile 10 results lead to detection of a neck at $4m$ and a bulge at $8m$. The designed flaws are however a bulge at $3m$ and a neck at $8m$.

As mentioned in chapter 5 it might be common to mistake a neck for a bulge due to the methodology for detection. By comparing a.t's per depth, either an early or late arrival can be constituted. This could explain the error at $8m$. The higher flaw however remains hard to see, even after knowledge of its existence.

Pile 11: Detection in pile 11 resulted in a bulge a $4m$ and one at $8m$. Both predictions do not match the designed flaws; a crack at $3m$ and a bulge(NS) at $6m$.

The early arrivals at $4m$ however remain clear in the results while large reflections above $8m$ could come from the sand layer although they are much larger than when compared to other pile tests.

Reflections that the crack should cause are not visible in the seismographs. The NS bulge also does not leave any trace in the results.

Pile 12: Pile 12 should not have any flaws, yet from the PS test it seems like there is a crack at $3m$ and a bulge at $6m$.

The vibrations at $3m$ look a lot like the results from pile 1 which supposedly has a bulge. Therefore, the reflections at this depth do not particularly mean there is a flaw, which complicates the detection. Furthermore the amplitude of the vibrations change a lot as well, meaning that the amplitude might be less useful than initially hoped.

On the other hand, the bulge at $6m$ is based on early arrival time, yet there are very few reflections. Therefore the presence of reflections seems much more important than the arrival time.

Pile 18: The final pile should have two bulges, one at $3m$ and a NS one at $8m$. Only the second one was detected; although mistaken for a neck.

Above $3m$ depth there are relatively many reflections, so in hindsight it is possible to see some kind of flaw. The reflections however are very subtle. In addition there is no clear change in a.t so the reflections could also be interpreted as a small crack.

At $8m$ there are clear delays in a.t. However at $7.75m$ the a.t is very early hence the bulge might be visible if it is not exactly at $8m$. If this is true the late a.t's could be mistaken for a neck.

Appendix F

Appendix: Validation of the Model

F.1 Introduction

In this appendix the results of the validated model are shown. Amplitude plots for radial and vertical vibrations are plotted for different piles.

F.2 Amplitude radial vibrations

The following plots show the amplitude of radial vibrations.

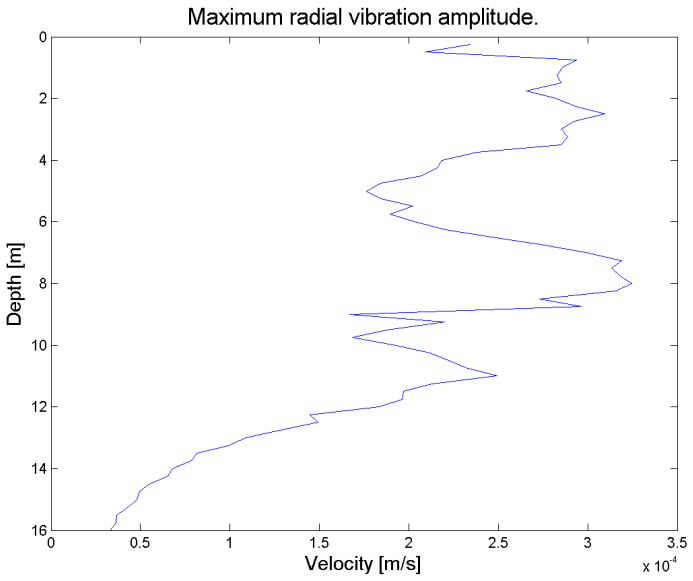

FIGURE F.1: Amplitude of simulated radial vibrations. This pile has no flaws.

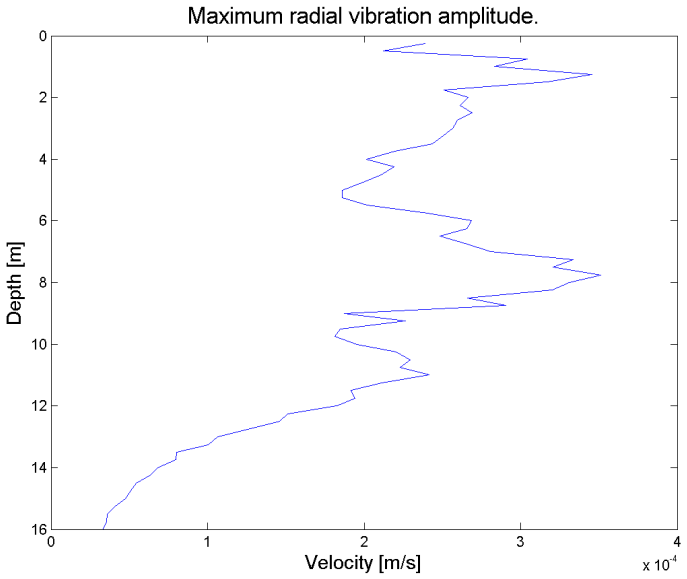

FIGURE F.2: Amplitude of simulated radial vibrations. This pile has a bulge at $6m$.

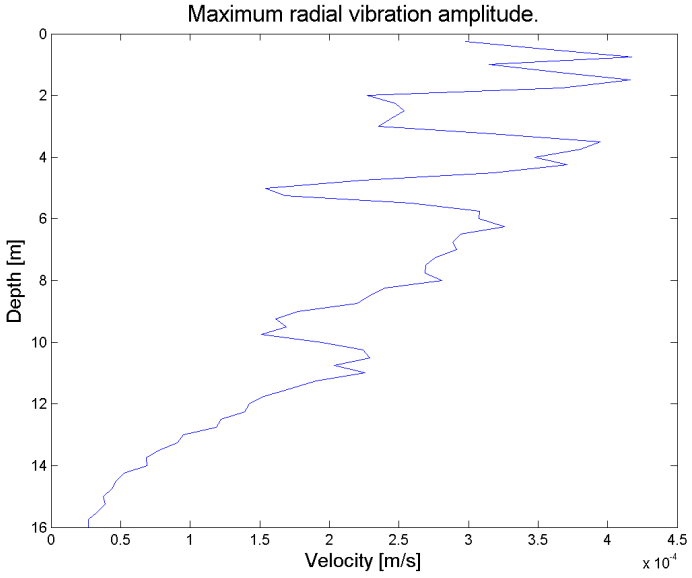

FIGURE F.3: Amplitude of simulated radial vibrations. This pile has a neck at $3m$.

F.3 Amplitude vertical vibrations

The following plots show the amplitude of radial and vertical vibrations.

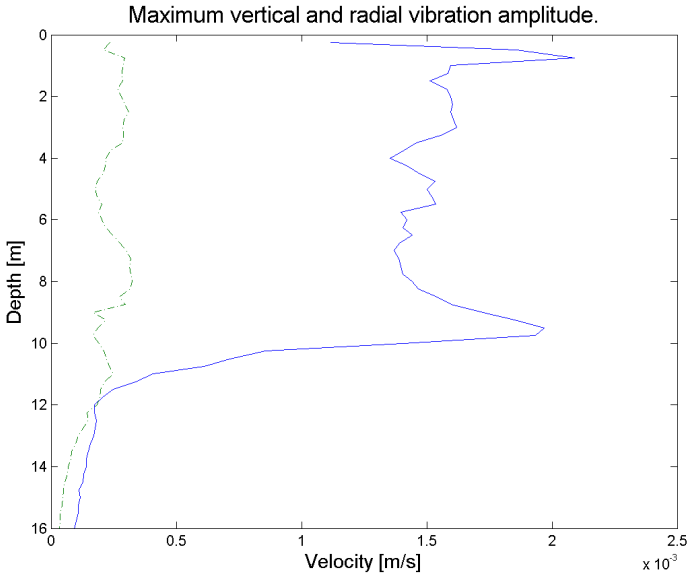

FIGURE F.4: Amplitude of simulated vertical and radial vibrations. This pile has no flaws.

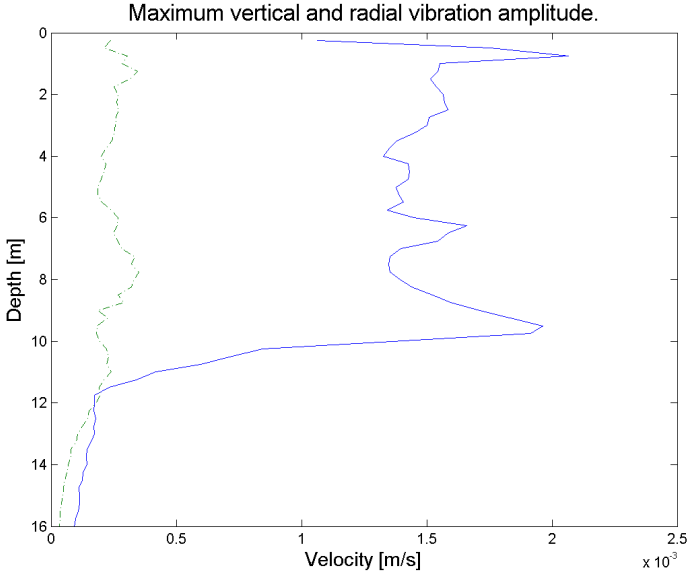

FIGURE F.5: Amplitude of simulated vertical and radial vibrations. This pile has a bulge at $6m$.

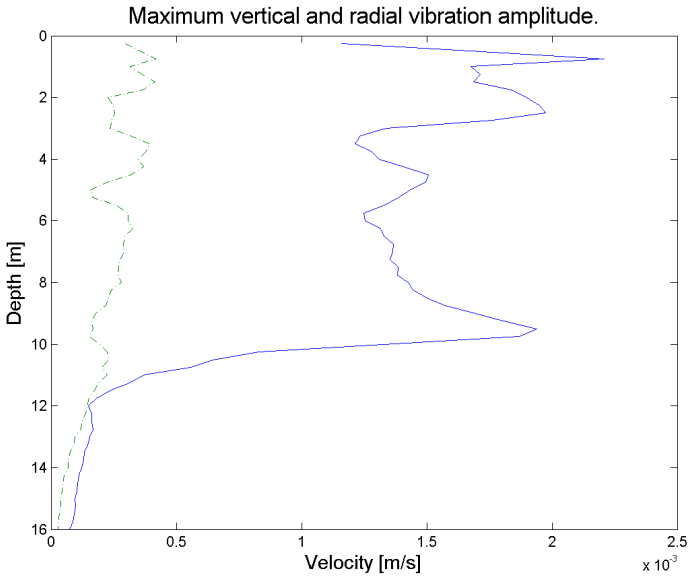

FIGURE F.6: Amplitude of simulated vertical and radial vibrations. This pile has a neck at $3m$.

Bibliography

F. M. Abrabbo and K. E. Gaaver. Installation effects of auger cast-in-place piles. *Alexandria Engineering Journal*, (51):281–292, 2012.

B. M. Das and G. Ramana. *Principles of Soil Dynamics*. Cengage Learning, Stamford, USA, 2011.

A. G. Davis. The nondestructive impulse response test in north america: 1985–2001. *NDT & E International*, 36:185–193, 2003.

R. J. Finno, S. L. Gassman, and P. W. Osborn. Non-destructive evaluation of a deep foundation test section at the northwestern university national geotechnical experimentation site. Technical report, Northwestern University Evanston, Illinois, 1997.

Y. M. Hashash and D. Park. Viscous damping formulation and high frequency motion propagation in non-linear site response analysis. *Soil Dynamics and Earthquake Engineering*, (22): 611–624, 2002.

P. Holscher. Deep acoustic check of piles. Technical report, Deltares, 2012.

P. Holscher. Lectures soil dynamics. Lecture TU Delft, 2013.

Y. Huang and S. Ni. Experimental study for the evaluation of stress wave approaches on a group pile foundation. *NDT & E International*, 47:134–143, 2012.

D. S. Kim and J. S. Lee. Propagation and attenuation characteristics of various ground vibrations. *Soil Dynamics and Earthquake Engineering*, (19):115–126, 2000.

O. Klingmuller and F. Kirsch. A quality and safety issue for cast-in-place piles 25 years of experience with low-strain integrity testing in germany: From scientific peculiarity to day-to-day practice.

S. Liao, J. Tong, C.-H. Chen, and T. Wu. Numerical simulation and experimental study of parallel seismic test for piles. *International Journal of Solids and Structures*, (43):2279–2298, 2005.

Matlab. Ellip, June 2014. URL `http://www.mathworks.nl/help/signal/ref/ellip.html`.

S. Ni, Y. Huang, X. Zhou, and K. Lo. Inclination correction of the parallel seismic test for pile length detection. *Computers and Geotechnics*, (38):127–132, 2010.

E. Niederleithinger. The parallel seismic method for foundation length measurement: Useful also to check pile integrity? Technical report, 2012a.

E. Niederleithinger. Improvement and extension of the parallel seismic method for foundation depth measurement. *Soils and Foundations*, (52):1093–1101, 2012b.

Olson. Parallel seismic. Technical report, Olson Engineering: Experts in nondestructive evaluation.

F. Ostadan, N. Deng, and J. M. Roessetc. Estimating total system damping for soil structure interaction systems. *Proceedings Third UJNR Workshop on Soil-Structure Interaction*, 2004.

P. Robertson. Interpretation of cone penetration tests - a unified approach. *NRC Research Press*, 2009.

L. Tonni and P. Simonini. Shear wave velocity as function of cone penetration test measurements in sand and silt mixtures. *Engineering Geology*, 163:55–67, 2013.

T. van der Poel. The elastodynamic wavefield in horizontally layered media. Master's thesis, TU Delft.

van t' Hek. Hekpaal, June 2014. URL `http://www.vanthek.nl/NL/20/hekpaal.htmll`.

A. Z. E. Wakil and M. Kassim. Bulging as a pile imperfection. *Alexandria Engineering Journal*, (3):387–391, 2010.